

## FUNCTIONAL CELLULOSE AND SILICONES

TUNING THE INTERFACIAL PROPERTIES OF CELLULOSE AND SILICONES  
THROUGH TRIAZINYL AND THIOACETAL CHEMISTRY

By AYODELE TEMITOPE FATONA, M.Sc.

A Thesis

Submitted to the School of Graduate Studies

In Partial Fulfillment of the Requirements for the Degree of

Doctor of Philosophy

McMaster University © Copyright by Ayodele T. Fatona, September 2019

Ayodele Fatona – Ph.D. Thesis McMaster University – Chemistry and Chemical Biology

McMaster University Doctor of Philosophy (2019) Hamilton, Ontario (Chemistry)

TITLE: Tuning the Interfacial Properties of Cellulose and Silicones Through Triazinyl and Thioacetal Chemistry

AUTHOR: Ayodele T. Fatona, M.Sc. (Sheffield Hallam University)

SUPERVISORS: Professor Jose Moran-Mirabal and Professor Michael A. Brook

NUMBER OF PAGES: xiv, 239

## **Abstract**

Interest in the incorporation of renewable, environmentally friendly materials, particularly nanocellulose due to its unique mechanical, optical, electrical and magnetic properties, into consumer products has progressed rapidly because these materials could lead to nanocomposites with enhanced functionality and mechanical properties. However, a well documented challenge that prevents nanocellulose from being widely used is the fact that cellulose is insoluble, relatively inert, and difficult to disperse in non-aqueous solvents and polymeric matrices. Available methods for the surface modification of cellulose to make it dispersible in polar and non-polar systems are complex, cost-prohibitive and difficult to implement on a large scale.

To address these challenges accordingly, the first part of this thesis aims to explore a cost-effective chemistry that is versatile and allows the installation of a broad range of functionalities onto nanocelluloses including cellulose nanocrystals/microfibrils while preserving their individual nature. Chapter 2 demonstrates a simple one-step triazinyl surface modification approach for tuning the interfacial properties of cellulosic materials using cyanuric chloride as a versatile linker to graft aliphatic (C18), polymeric (oligo-polyethylene glycol), alkyne (propargyl) chains and aromatic rings (benzyl) onto nanocelluloses, including CNCs and BMCC. We observed that the crystallinity of all triazine-modified CNCs was preserved, while the thermal stability was slightly enhanced compared to unmodified nanoparticles. CNCs modified with different triazinyl derivatives also formed colloidal suspensions in chloroform, isopropanol, ethanol, and methanol, which were stable over periods of months. In addition, propargyl-modified BMCC was linked to an azido fluorescein dye via a copper-catalyzed Huisgen 1,3-dipolar cycloaddition reaction, demonstrating for the first time the production of triazinyl-based reactive nanocellulose.

Next, a companion study, examines the development of a colorimetric and fluorescent “off-on” cellulose based chemosensors for heavy metal detection in water as a potential lab-on-a-molecule system for biomedical and environmental diagnostics. The use of cyanuric chloride as a covalent linker to install pegylated rhodamine Schiff bases onto cellulose filter paper was explored. The factors required to create on demand selectivity and sensitivity towards specific heavy metals was determined. This resulted into the detection of  $\text{Cu}^{2+}$  and  $\text{Hg}^{2+}$  ions in 100% aqueous environment within 5 seconds of contact with 6.3 ppb and 20 ppb as the limit of colorimetric detection respectively.

Lastly, in addressing the challenges of traditional preparative methods for silicone elastomers largely dependent on several issues associated with current cure strategies mainly cost, toxicity and functional group intolerance of these heavy metal catalyzed reactions (platinum, tin or titanium). Alternative routes based on organic chemistry have been exploited to mitigate these effects. The second part of this thesis introduces organic cure chemistries based on triazinyl and thioacetal linkages as catalyst-free and organic acid catalyzed silicone elastomer preparative methods to control physical properties of silicones while chapter 6 focuses on the preparation of self-driven microfluidic devices tuning the interfacial properties and water wettability of silicones.

## **Acknowledgements**

Without a shadow of doubt, the accomplishment of this milestone would not be possible without the support and guidance of a great deal of persons with whom I have had the pleasure of interacting with throughout my time at McMaster University and Hamilton. First and foremost, I would love to express my sincere gratitude to my co-supervisors- Dr. Jose Moran-Mirabal and Dr. Michael A. Brook for believing in me, providing advice and the freedom to pursue chemistry and research that I found interesting. Their enthusiasm and dedication to good science particularly cellulose and silicone chemistry is inspiring and their synergy in collaborative work ensuring a positive outcome on every research endeavour was very motivating over the years. Indeed, I remain grateful to Mike and Jose for transforming every manuscript of mine into a concise and better scientific communication worthy of reading. I appreciate the fact that Mike and Jose were always there when needed and always willing to provide assistance. I definitely would not have become the researcher and person I am today without their excellent mentorship. Thank you for being such excellent supervisors.

Thanks to my committee member, Dr. Todd Hoare for his advice and insights helping me to think about my research in different ways. I would love to appreciate every member of the Brook and Moran-Mirabal Group past and present as they have contributed to my experience and I enjoyed each friendship especially Dr. Chen Yang, my undergraduate researchers Kajal Bhardwaj and Andrew Osamudiamen who have helped out with some aspects of this thesis.

Finally, my deepest and warmest gratitude goes to my wife, parents and siblings without whom I would be lost in life. They have always been a source of joy, happiness and support during this crucial moment of my life. May your labour of love not be in vain. Hope to make you proud. Thanks

## TABLE OF CONTENTS

<b>CHAPTER 1: INTRODUCTION AND THESIS FOCUS.....</b>	<b>1</b>
1.1 INTRODUCTION .....	1
1.2 SURFACE MODIFICATION OF CELLULOSE .....	3
1.3 HISTORICAL BACKGROUND AND CURRENT USE OF TRIAZINYL CHEMISTRY .....	5
1.4 TRIAZINYL CHEMISTRY FOR CELLULOSE MODIFICATION .....	10
1.4.1 Triazines in dyeing and printing processes .....	10
1.4.2 Triazines for flame retardant treatments .....	16
1.4.3 Triazine Scaffolds for Antibacterial Fabrics.....	20
1.4.4 Triazine Derivatives as Aids in Biomass Conversion.....	23
1.4.5 Triazine-Modified Supports for Affinity Based-Separations .....	25
1.5 FUNCTIONAL NANOCELLULOSES VIA TRIAZINYL CHEMISTRY .....	28
1.6 SUMMARY AND FUTURE OUTLOOK OF TRIAZINYL MODIFICATION OF CELLULOSIC MATERIALS .....	34
1.7 THESIS FOCUS (I, II).....	36
1.8 THE CASE FOR ALTERNATIVE SILICONE CROSSLINK TECHNOLOGY .....	37
1.9 THESIS FOCUS (III, IV) .....	42
1.10 THE INTERFACIAL CONTROL OF SILICONES.....	43
1.11 THESIS FOCUS (V).....	45
1.12 REFERENCE .....	46

<b>CHAPTER 2: VERSATILE SURFACE MODIFICATION OF CELLULOSE FIBRES AND CELLULOSE NANOCRYSTALS THROUGH MODULAR TRIAZINYL CHEMISTRY .....</b>	<b>74</b>
2.1 ABSTRACT .....	74
2.2 INTRODUCTION .....	75
2.3 EXPERIMENTAL SECTION.....	78
2.3.1 Materials .....	78
2.3.2 Characterization .....	78
2.3.3 Synthesis of 4,6-dichloro-n-octadecyl-1,3,5-triazine-2-amine (1, DTC18).....	81
2.3.4 Synthesis of 4,6-dichloro-n-propargyl-1,3,5-triazine-2-amine (2, DTP) .....	82
2.3.5 Synthesis of 4,6-dichloro-n-benzyl-1,3,5-triazine-2-amine (3, DTB) ...	82
2.3.6 Synthesis of 4,6-dichloro-2-poly(ethylene glycol) mono-allyl-1,3,5-triazine-2-ether (4, DTAPEG) .....	83
2.3.7 Chemical Grafting of Dichlorotriazinyl Derivatives onto Nanocellulose.....	83
2.3.8 Fluorescein Labeling of Nanocellulose by an Azide-Alkyne Click Reaction (Scheme 1c).....	84
2.4 RESULTS AND DISCUSSION.....	86
2.4.1 Triazine-Coordinated Chemical Grafting onto Nanocellulose .....	86



2.4.2	Surface Grafting Efficiency of Triazinyl Modified CNCs .....	89
2.4.3	Structural Characterization of Modified Cellulose Nanocrystals .....	93
2.4.4	Thermal Stability of Triazinyl Modified CNCs.....	96
2.4.5	Dispersion of Modified CNCs in Aqueous/Organic Media.....	97
2.4.6	Fluorescent Labeling of DTP-modified Cellulose Fibers through “Click” Reactions .....	100
2.4.7	The Triazinyl Chemistry Cellulose Modification in Context .....	101
2.5	CONCLUSIONS .....	103
2.6	ACKNOWLEDGEMENTS.....	104
2.7	REFERENCES .....	104
2.8	APPENDIX 2: CHAPTER 2 SUPPORTING INFORMATION .....	110
<b>CHAPTER 3: COLORIMETRIC AND FLUORESCENT CELLULOSE-BASED CHEMOSENSOR FOR SELECTIVE DETECTION OF COPPER (II) AND MERCURY (II) IN WATER .....</b>		<b>117</b>
3.1	ABSTRACT .....	117
3.2	INTRODUCTION .....	118
3.3	EXPERIMENTAL SECTION.....	120
3.3.1	Materials .....	120
3.3.2	Characterization .....	121
3.3.3	Synthesis of poly(ethylene glycol)-vanillin-rhodamine derivatives ....	121
3.3.4	Synthesis of 4,6-dichloro-s-triazinyl-poly(ethylene glycol)-	

	vanillin (Triazine-PEG-Vanillin).....	125
3.3.5	Grafting of Triazine-PEG-Vanillin onto cellulose.....	125
3.3.6	Synthesis of PEG-vanillin-rhodamine Schiff base and cellulose-PEG-vanillin-rhodamine Schiff base.....	126
3.4	RESULTS AND DISCUSSION.....	127
3.4.1	Synthesis and characterization of chemosensors .....	127
3.4.2	Spectral response of PEG-Vanillin-Rh6G Schiff base .....	129
3.4.3	Spectral response of cellulose-PEG-vanillin-rhodamine Schiff base ..	131
3.4.4	Fluorescence imaging of cellulose fibres.....	133
3.5	CONCLUSIONS .....	133
3.6	ACKNOWLEDGEMENTS.....	134
3.7	REFERENCES .....	134
<b>CHAPTER 4: CATALYST-FREE SILICONE ELASTOMERS CROSSLINKED USING TRIAZINES.....</b>		<b>142</b>
4.1	ABSTRACT .....	142
4.2	INTRODUCTION .....	143
4.3	EXPERIMENTAL.....	145
4.3.1	Materials .....	145
4.3.2	Characterization .....	145
4.3.3	Silicone elastomer preparation using triazinyl crosslinkers.....	146
4.3.4	Reinforcement of triazinyl crosslinked elastomers.....	150

4.3.5	Hydrolytic stability of amino-triazinyl silicone elastomers.....	151
4.4	RESULTS AND DISCUSSION.....	153
4.4.1	Formation and physical properties of amino-triazinyl silicone elastomers .....	153
4.4.2	Effect of external amino functionality on elastomer properties.....	155
4.4.3	Role of pre-grafted $\alpha,\omega$ -Bis(4,6-dichloro)-s-triazinyl -modified aminosilicone (A11-CC) .....	158
4.4.4	Reinforcing triazinyl-based silicone elastomers .....	159
4.4.5	Hydrolytic and thermal stability of amino-triazinyl elastomers .....	159
4.5	CONCLUSIONS .....	161
4.6	ACKNOWLEDGEMENTS.....	162
4.7	REFERENCES .....	162
4.8	APPENDIX 4: CHAPTER 4 SUPPORTING INFORMATION .....	167
<b>CHAPTER 5: CONTROLLING SILICONE NETWORKS USING DITHIOACETAL CROSSLINKS .....</b>		<b>173</b>
5.1	ABSTRACT .....	173
5.2	INTRODUCTION .....	173
5.3	EXPERIMENTAL SECTION.....	176
5.3.1	Materials .....	176
5.3.2	Characterization .....	176
5.3.3	Elastomer preparation using traditional platinum cure technique .....	178

5.3.4	Elastomer preparation using dithioacetal crosslinked silicones.....	178
5.3.5	The role of silica .....	179
5.4	RESULTS .....	181
5.4.1	Elastomer formation: Stoichiometry controls physical properties.....	183
5.4.2	Role of the aromatic crosslinker .....	184
5.4.3	Role of silica .....	186
5.4.4	Stability of the resulting products .....	187
5.5	DISCUSSION .....	188
5.6	CONCLUSIONS .....	191
5.7	ACKNOWLEDGEMENTS.....	192
5.8	REFERENCES .....	192
5.9	APPENDIX 5: CHAPTER 5 SUPPORTING INFORMATION.....	196
<b>CHAPTER 6: ONE-STEP IN-MOULD MODIFICATION OF PDMS SURFACE AND ITS APPLICATION IN THE FABRICATION OF SELF-DRIVEN MICROFLUIDIC CHANNELS .....</b>		<b>211</b>
6.1	ABSTRACT .....	211
6.2	INTRODUCTION .....	212
6.3	EXPERIMENTAL SECTION.....	213
6.3.1	Materials .....	213
6.3.2	Fabrication of surface functionalized PDMS arrays.....	214

6.3.3	Elastomer preparation using traditional platinum cure technique .....	214
6.3.4	Fabrication of surface-modified microfluidic devices .....	215
6.4	RESULTS AND DISCUSSION.....	215
6.4.1	In-mould modification of PDMS surfaces .....	215
6.4.2	Wettability of modified PDMS surfaces.....	217
6.4.3	Effect of surfactant concentration on wettability .....	220
6.4.4	Surface morphology of functionalized PDMS surfaces.....	221
6.4.5	Fabrication of self driven microfluidic devices .....	224
6.5	CONCLUSIONS .....	228
6.6	ACKNOWLEDGEMENTS.....	229
6.7	REFERENCES .....	229
6.8	APPENDIX 6: CHAPTER 6 SUPPORTING INFORMATION .....	232
	<b>CHAPTER 7: GENERAL CONCLUSIONS .....</b>	<b>235</b>

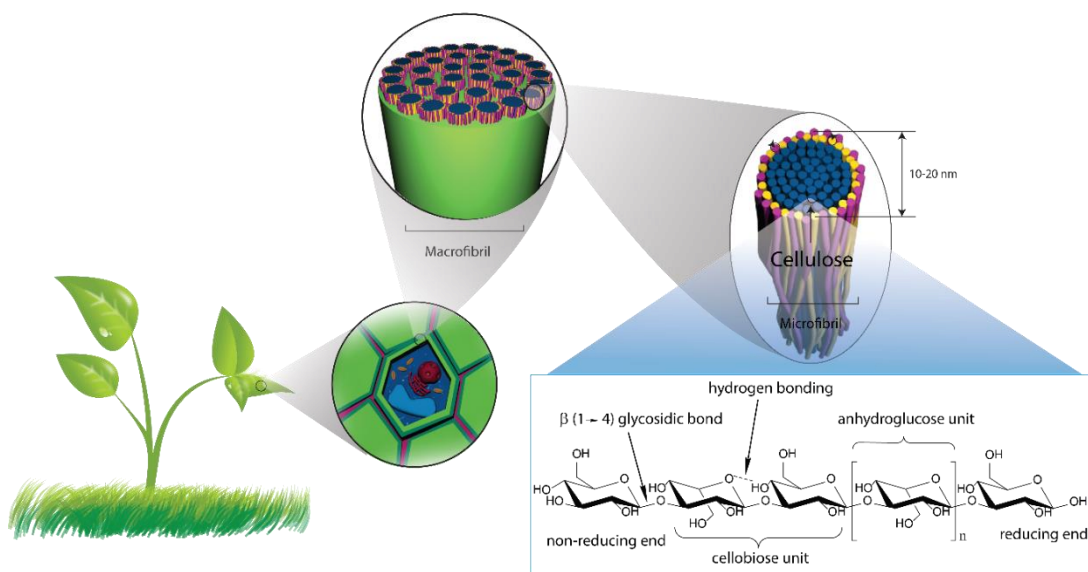
### List of Abbreviations and Symbols

AFM	Atomic force microscope
CNC	Cellulose nanocrystals
BMCC	Bacterial microcrystalline cellulose
LOI	Limiting oxygen index
CA	Contact Angle
MOF	Metal organic framework
COF	Covalent organic framework
XPS	X-ray photoelectron spectroscopy
CMC	Critical Micelle Concentration
CQ	Chloroquine
DS	Degree of substitution
DCM	Dichloromethane
CC	Cyanuric chloride
$M_n$	Number-average Molecular Weight
MW	Molecular Weight
NMR	Nuclear Magnetic Resonance
PDMS	Polydimethylsiloxane
APEG	monoAllyl poly(ethylene glycol)
RTV	Room-temperature vulcanization
SDS	Sodium dodecyl Sulfate
DSC	Differential scanning calorimetry
$T_g$	Glass transition temperature
DTAF	5-([4,6-dichlorotriazin-2-yl]amino)fluorescein
$G'$	Storage modulus
$G''$	Loss modulus

## CHAPTER 1: Introduction and Thesis Focus

### 1.1 Introduction

Cellulose, the main structural component of plant biomass (also found in algae, fungi, bacteria and tunicates), is produced at an estimated  $10^{11}$  to  $10^{12}$  tons per year in the biosphere and remains the most abundant biopolymer for composite processing.<sup>1</sup> Cellulose is a renewable, non-cytotoxic, and biodegradable material made of linear polymers of  $\beta(1\rightarrow4)$  linked anhydroglucose units.<sup>2</sup> These elementary glucan chains strongly associate to form cellulose microfibrils via van der Waals interactions, intra-chain and intermolecular hydrogen bonding. The core of the microfibrils consists of tightly packed crystalline cellulose regions, interrupted by dislocations and/or areas of amorphous cellulose. These microfibrils bundle together to produce macrofibrils that make up the main structural motifs within the plant cell wall (Figure 1.1).

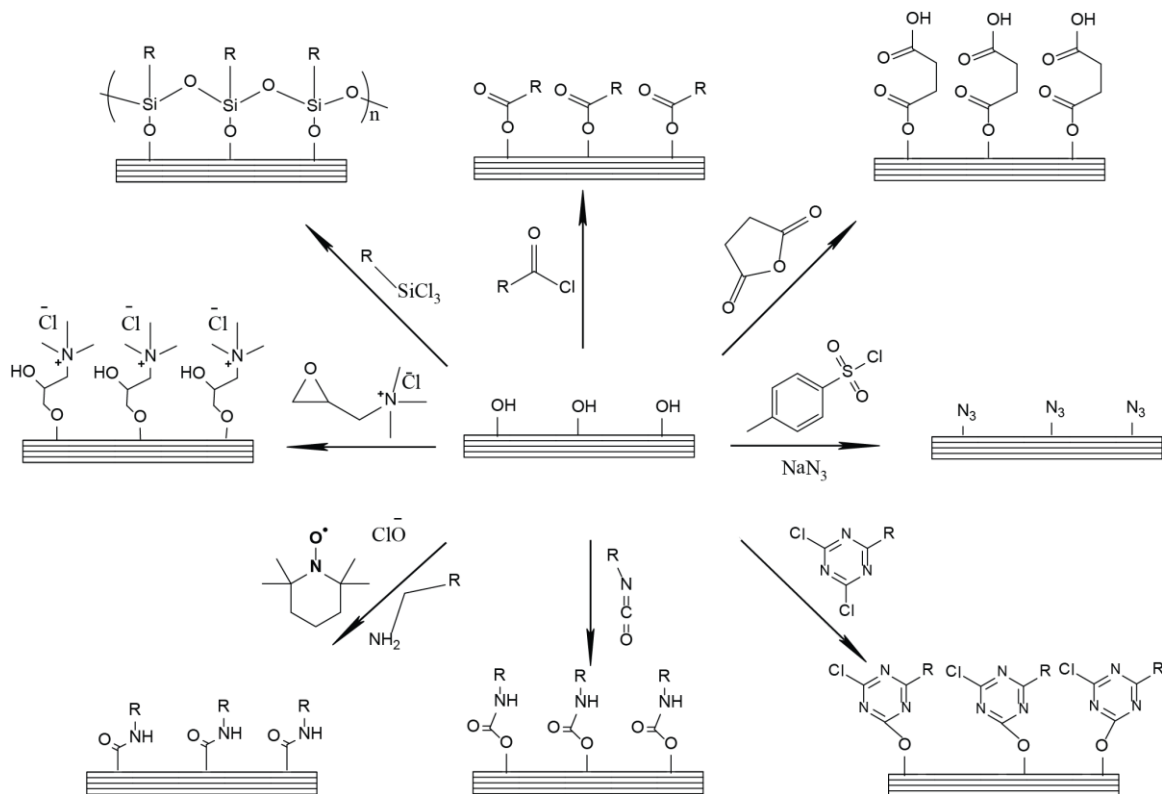


**Figure 1.1:** Schematic representation describing the hierarchical structure of cellulose derived from plant biomass. Modified with permission from reference 136. Copyright 2015 Mary Ann Liebert, Inc.

This hierarchical structure, spanning from the nano- to the macroscale, endows cellulose with unique properties, including very high mechanical strength and flexibility. These properties have been exploited throughout history for a variety of applications, such as construction, textile, and printing materials. Several polymorphs of crystalline cellulose (I, II, III, IV) have been described and are generally accepted, which present different parallel and anti-parallel chain packing depending on the directionality adopted by the 1→4 linkage along the glucan chain length.<sup>3</sup> Naturally sourced crystalline cellulose is solely cellulose I, but this can be converted to celluloses II or III through processing.<sup>4</sup> Cellulose II (regenerated or mercerized) remains the most stable of all allomorphs with high industrial importance,<sup>5</sup> while cellulose IV is obtained from the thermal annealing of cellulose III. In fact, two distinct crystalline arrangements have been discovered for cellulose I that coexist in nature, a triclinic system ( $I_{\alpha}$ ) and a monoclinic system ( $I_{\beta}$ ),<sup>3,4,6,7</sup> and whose proportions ( $I_{\alpha/\beta}$ ) are source dependent. For example, algae<sup>8</sup> and bacteria<sup>9</sup> are  $I_{\alpha}$  dominant whereas higher plant cellulose (e.g., ramie, cotton)<sup>10</sup> and tunicates<sup>9</sup> are  $I_{\beta}$  dominant. The  $I_{\alpha}$  allomorph is metastable and experiences transformation to  $I_{\beta}$  under certain conditions, like hydrothermal saponification<sup>11</sup> and high-temperature treatments in organic solvents or helium gas.<sup>12</sup>

The formation of highly ordered crystalline regions within and the abundance of surface hydroxyl groups results in cellulosic materials that are amphiphilic and moisture responsive but largely insoluble in water and most common organic solvents/polymer matrices. Thus, in order to harness the intrinsic mechanical properties of this hierarchical biobased material and use it to reinforce polymer matrices, the surface modification of cellulose is needed. Several surface modification strategies<sup>2,13</sup> (Figure 1.2) have been used to tune the interfacial properties of cellulose, particularly nanocellulose (CNC), such as controlling its wettability, enhancing its dispersion in non-polar solvents, enhancing its compatibility with polymeric matrices, and providing higher thermal stability or flame retardant properties.





**Figure 1.2:** Schematic representation of various chemistries reported for the surface modification of nanocellulose.

## 1.2 Surface modification of cellulose

The chemical surface modification of cellulose does involve the covalent attachment of chemical entities at the cellulose interface or the transformation of surface hydroxy groups into other chemical functional groups in preparation for further functionalization procedures. The introduction of carboxylic and aldehydic functionalities preferentially at the hydroxymethyl and vicinal diol groups of cellulose through the use of 2,2,6,6-Tetramethylpiperidinyloxy radical (TEMPO) and periodate has been reported.<sup>14,15</sup> With the grafting of polymer demonstrated to tune the dispersion and interfacial adhesion of modified cellulose within polymer matrix to improve stress transfer during nanocomposite processing. Under the polymer grafting regime, two significant strategies are utilized,

namely, the “grafting-onto” and “grafting-from” approaches<sup>16</sup> for the dispersibility and compatibilization of CNC in polymer resin to improve mechanical properties or induce functionality. The “grafting onto” entails attaching pre-synthesized polymer onto CNC surface in the presence of a coupling agent while the “grafting from” involves in situ surface-initiated polymerization of a monomer from active initiator sites localized on the CNC surface. Habibi and Dufresne<sup>17</sup> carried out carbamation (isocyanate-mediated) reaction to graft polycaprolactone (PCL) chains of various molecular weights onto CNCs using a combination of 2,4-diisocyanate (2,4-TDI) and phenylisocyanate in the presence of triethylamine as catalyst. Aliphatic<sup>18</sup> (n-octadecyl isocyanate) and fatty acid<sup>19</sup> (isocyanate-terminated castor oil) chains have also been grafted onto CNC using the same carbamation chemistry. While single-stranded DNA oligonucleotides,<sup>20</sup> polystyrene,<sup>21</sup> poly(*tert*-butylacrylate),<sup>21</sup> polyethers<sup>22</sup> and poly(ethyleneglycol)<sup>23</sup> just to mention a few, have all been successfully grafted onto TEMPO oxidized CNC through the amidation chemistry.

Esterification remains a vital chemistry which has been exploited to graft polymers onto CNCs. Maleated polypropylene<sup>24</sup> has been demonstrated to tune the dispersion and better enhance interfacial adhesion of modified CNCs within polymer matrix which led to improved stress transfer within the nanocomposites. On the other hand, the same chemistry has been utilized to modify CNCs in the “grafting from” approach via ring-opening (stannous octoate/hexanoate or citric acid catalysed)<sup>25,26</sup> and atom transfer radical<sup>27–29</sup> polymerizations (ATRP). Zhang and co-workers<sup>27,28</sup> used Bromoisobutryl bromide (BiB) to modify CNCs which were subsequently utilized in ATRP to grow polystyrene and poly-6-[4-(4-methoxyphenylazo)phenoxy]hexyl methacrylate (PMMAZO) chains from CNCs that exhibited both thermotropic and lyotropic liquid-crystalline behaviors. In contrast, another “grafting from” approach for polymer cationization of CNCs that does not require any pre-polymerization step, have been reported using the ceric-cerous redox system.<sup>30</sup> Poly(4-vinylpyridine) (P4VP) chains were grafted from CNCs to initiate a pH-responsive system with reversible suspension-flocculation capabilities as a result of changing from cationic (hydrophilic) to anionic (hydrophobic) states as pH is altered from less than 5 to

anything above 5. Yet again, another ubiquitous chemistry reported that has been used in the “graft to” approach to modify CNC with polymer chains is etherification as epoxide-terminated PEG chains were successfully grafted onto CNC to achieve steric stabilization that showed chiral nematic phase separation<sup>31</sup> which were later utilized as reinforcing fillers in poly(lactic acid) (PLA) electrospun nanocomposite scaffolds.<sup>32</sup> A range of these modifications could provide the advantage of making nanocellulose suspensions insensitive or stimuli controlled to electrolyte/ionic strength fluctuations. In addition to its dispersion in both aqueous and non-aqueous media or polymer resin as the delay in the onset of glassy phase transition of nanocellulose at high volume fractions is quite possible. However, available methods for the surface modification of cellulose to make it dispersible in polar and non-polar systems are complex, cost-prohibitive and difficult to implement on a large scale or have limitations in the functionalities that can be introduced. Thus, as part of my graduate research work which focused on using triazinyl chemistry as a versatile and low-cost modification approach, the first section of this chapter highlights the use of the triazinyl chemistry as an alternative technology for tuning the interfacial properties of cellulosic materials from macro-to-nanocellulose. Discussing processes for creating dyed, antimicrobial, or flame-retardant cellulose, as well as the development of new functional cellulose-based materials for affinity-based separations, wastewater treatment, and biofuel production. Extending to new bio-based nanomaterials, and describing envisioned new routes that if addressed, can translate to new research and large-scale nanocomposites processing. While the concluding section, focuses more on the need for alternative routes to silicone crosslinking and tuning the interface properties of silicones.

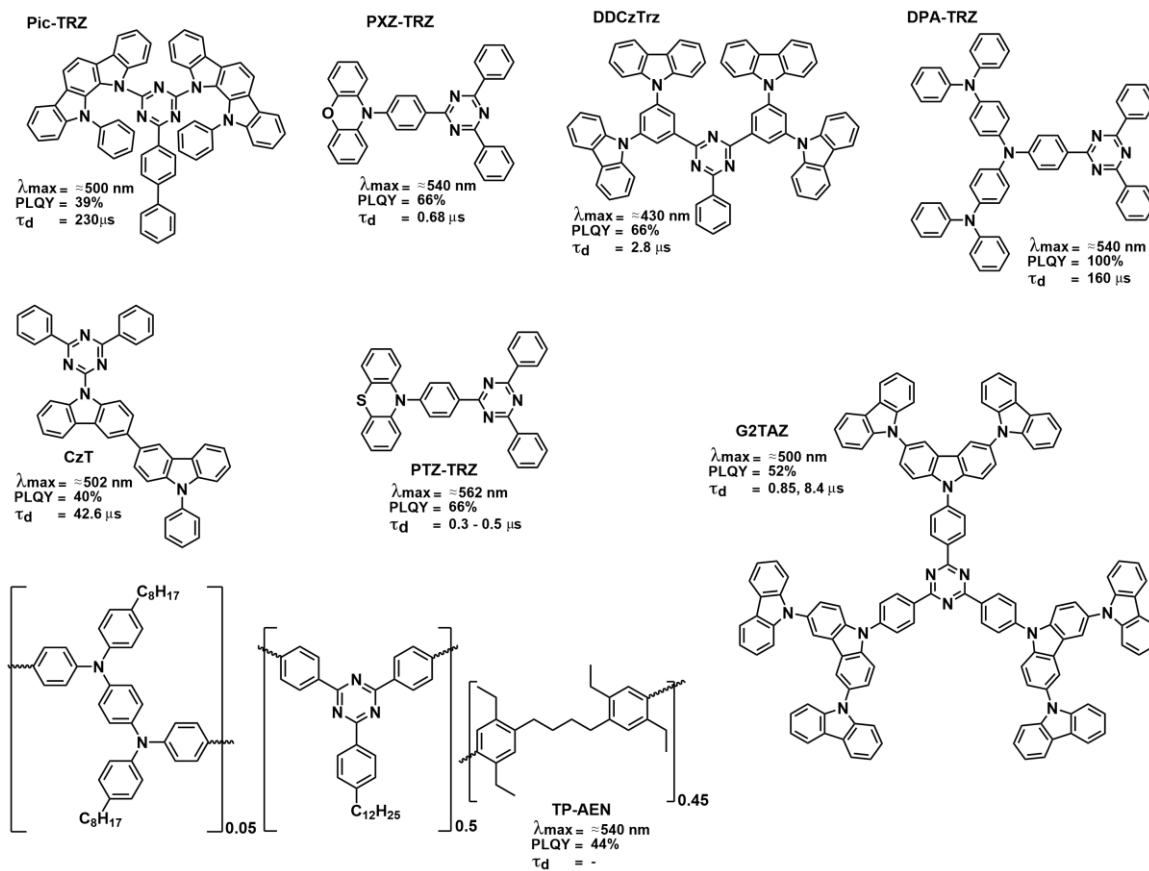
### **1.3 Historical background and current use of triazinyl chemistry**

Heterocyclic compounds make up the largest class of molecules used in the pharmaceutical, agrochemical, textile, plastics and semiconductor industries. They are routinely used to make drugs, pesticides, dyes, UV absorbers and surface-active agents, among many other reagents and products.<sup>33</sup> Within this class of molecules, s-triazine

derivatives are widely used to generate new chemical constructs because of their versatility and ability to yield compounds with a broad range of physicochemical properties. Symmetrical triazines are a popular choice given their long history in organic synthesis, with the first reports dating to 1793 and 1820 when cyanuric acid (1,3,5-triazine-2,4,6(1H,3H,5H)-trione) was obtained by the pyrolysis of uric acid.<sup>34</sup> This process was rapidly improved on with the synthesis of cyanuric chloride (2,4,6-trichloro-1,3,5-triazine) through methods including converting cyanogen chloride in the presence of sunlight in 1828 and the passage of chlorine over dry potassium thiocyanate 1834.<sup>35,36</sup> Melamine (1,3,5-triazine-2,4,6-triamine) was prepared by Justus von Liebig around the same time by fusing potassium thiocyanate with ammonium chloride to give melamine thiocyanate, which upon treatment with a base provided the free melamine.<sup>37,38</sup> Today, the majority of these processes have been replaced by the pyrolysis of urea and the trimerization of halogenated hydrocyanic acid<sup>39</sup> to produce the starting materials for millions of tons of triazine-based products commercialized worldwide.

Cyanuric chloride remains the most important building block used to generate 2,4,6-mono, di- and tri-substituted (symmetric or asymmetric) s-triazines due to its reactivity, selectivity, availability and low cost.<sup>40</sup> One key advantage of cyanuric chloride is the stepwise nature by which chlorine atoms can be displaced by nucleophiles, processes that have been shown to be temperature dependent. In this process, the chemical structure of the nucleophile, base strength, steric bulk, solvent and the substituents already present on the s-triazine ring further determine the temperature required for each substitution. Typically, mono-substitution products can be obtained at temperatures  $\leq 0$  °C, while di- and tri-substitution products are obtained at room temperature and at more elevated temperatures ( $> 60$  °C), respectively. Similar to reactions used with acyl chlorides, triazinyl derivatives starting from cyanuric chloride have been produced using the Friedel-Crafts reaction<sup>41</sup> and Suzuki coupling,<sup>42</sup> among other methods<sup>43-47</sup> in constructing synthetic scaffolds that incorporate the s-triazinyl moiety and other electron-donors/acceptors into a single structure.

One of the most active research areas involving triazines is the production of aryl-s-triazine derivatives, compounds with tunable photochemical and photo-physical properties. Derivatives with these properties are attractive as photo and thermal stabilizers, antioxidants, and organic emitters.<sup>48,49</sup>



**Figure 1.3:** Chemical structures of representative triazine-based organic thermally activated delayed fluorescence emitters. PLOY = photoluminescence quantum yield,  $\tau_d$  = lifetime of delayed fluorescence. Modified with permission from reference 49. Copyright 2017 John Wiley & Sons, Inc.

Since the first report in 2011 of an organic thermally activated delayed fluorescence (TADF) emitter based on the 1,3,5-triazinyl architecture,<sup>50</sup> several new compounds involving this motif have been introduced that display enhanced electroluminescence efficiencies in a broad range of colors (Figure 1.3).<sup>51-56</sup> Additionally, high molecular weight TADF dendrimers<sup>57</sup> and polymers<sup>58</sup> based on a triazine acceptor core have also been shown to improve film processability, enabling the production of solution-processed organic light-emitting diodes with photoluminescence quantum yields of up to 52%.

The properties of triazinyl derivatives can be directly tuned by modulating the substitutions at the C2, C4 and C6 positions of the cyanuric chloride ring to yield asymmetric heterofunctional structures that combine the chemical functionality of the individual moieties. Appropriate substitution patterns in triazines allow one to control molecular responses to various phenomena. For example, substituted triazines have been used to study the behaviour of photoabsorbers, compounds that can mediate radical reactions including polymerization. The synthesis of a polymerizable unsaturated triazinyl light stabilizer bearing 2,2,6,6-tetramethylpiperidine and 2-hydroxybenzo-phenone groups was recently reported, where it was shown that the inclusion of the asymmetric triazine did not affect the polymerization rate, molecular weight or polydispersity of methyl acrylate copolymers while conveying significant stabilization against photodegradation.<sup>59</sup> Protection against radiation has also been widely achieved in sunscreen products containing hydroxyphenyl-s-triazines, which show strong absorption of UV radiation over a broad range of wavelengths and help by protecting other active photosensitive ingredients, making them more stable upon exposure to sunlight.<sup>60,61</sup>

Tri-substituted triazine derivatives have been incorporated into the reticular syntheses used to build metal organic frameworks (MOFs). Triazine-scaffolds have led to architecturally robust crystalline structures with porosities that account for 84 to 88% of the total MOF crystal volume.<sup>62,63</sup> Due to their pore size and the surface availability of free amino groups and triazine nitrogen atoms that provide localized charged densities, these MOF structures have been proposed as suitable materials for the efficient separation and storage of CO<sub>2</sub>

and H<sub>2</sub>.<sup>64,65</sup> Covalent organic frameworks (COF) based on the triazine ring have also been produced and have been used in the form of films on metal surfaces to improve the lubricity in copper and steel systems;<sup>66</sup> they have also been shown to operate as highly efficient green catalysts when formulated as hybrids with metals like palladium,<sup>67,68</sup> ruthenium<sup>69</sup> and platinum.<sup>70</sup>

The ability to attach different functional compounds onto the triazine core structure has also been exploited in the synthesis of biologically active compounds. Metallo-drugs incorporating triazine scaffolds have been used for cancer treatment. A ruthenium(II)-arene aminotriazine complex has been used to selectively target DNA and shown pH dependent activity against human ovarian carcinoma cells,<sup>71</sup> while copper (II) pyridyl-triazine complexes have been reported as apoptosis inducers for breast cancer cells.<sup>72</sup> Di- and tri-substituted or hetero-fused triazinyl derivatives have also been used as efficient kinase inhibitors with promising antitumor properties.<sup>73,74</sup> A series of pyridine, benzimidazolyl, benzenesulfonamide and pyrazolo derivatives bearing the triazine moiety have shown strong inhibition of CDK (cyclin-dependent kinase),<sup>75</sup> mTOR (mammalian target of rapamycin),<sup>76,77</sup> PI3K (phosphoinositide 3-kinase),<sup>78</sup> hCA IX (carbonic anhydrase)<sup>79</sup> and CK2 (casein kinase 2).<sup>80</sup> These compounds had inhibitory and antiproliferative activities against a wide range of cancer cell lines (*in vitro*) or in human xenograft models (*in vivo*).

Heterofunctional triazinyl compounds have shown medicinal and biotechnological importance as bioactive compounds. 6-Naphthyloxy-substituted diaryl-triazines have been used to inhibit HIV-1 replication at nanomolar concentrations, with N-methyl/amine substituents found to be 15-times more potent than the standard drug nevirapine.<sup>81</sup> Triazinyl hybrid drugs including 4-anilinoquinoline triazines<sup>82</sup> and 9-anilinoacridine triazines<sup>83</sup> have been used as potent antimalarial drugs. These triazine derivatives have shown excellent activity against a chloroquine (CQ) sensitive strain of *Plasmodium falciparum*, as well as against CQ-resistant strain of *P. yoelli*, providing viable options for effective long-term strategies for antimalarial chemotherapy. Similarly, atrazine,<sup>84</sup> simetryn,<sup>85</sup> triaziflam<sup>86</sup> and a host of other triazine-based herbicides have been used as

efficient inhibitors of photosystem II electron transport. Despite their ban in Europe, these compounds remain some of the most popular herbicides in the world used in the prevention and post-emergence treatment against broadleaf and grassy weeds. Due to their ability to selectively disrupt photosynthesis to kill weeds, they have cost-effectively increased crop production. Generally, toxicity of these type of triazine compounds have largely been limited to aquatic ecosystem. Where herbicides persistence has been linked to toxicity in fish and bioaccumulation with very low impact on humans.<sup>87,88</sup> Perhaps the area where triazinyl chemistry has historically had the greatest impact is in the chemical modification of cellulosic materials as a versatile route to modify cellulosic materials. This is because cellulose, and polysaccharides in general, present abundant primary hydroxyl groups that can act as nucleophilic sites to displace chlorine atoms in chloro-triazinyl derivatives, resulting in efficient one-step covalent chemical grafting. Nowadays, the need for advanced materials and products that are sustainable and environmentally friendly has spurred intense research into the modification, via triazinyl chemistry for new cellulose-based nanomaterials to produce the next generation of advanced green materials.

## **1.4 Triazinyl chemistry for cellulose modification**

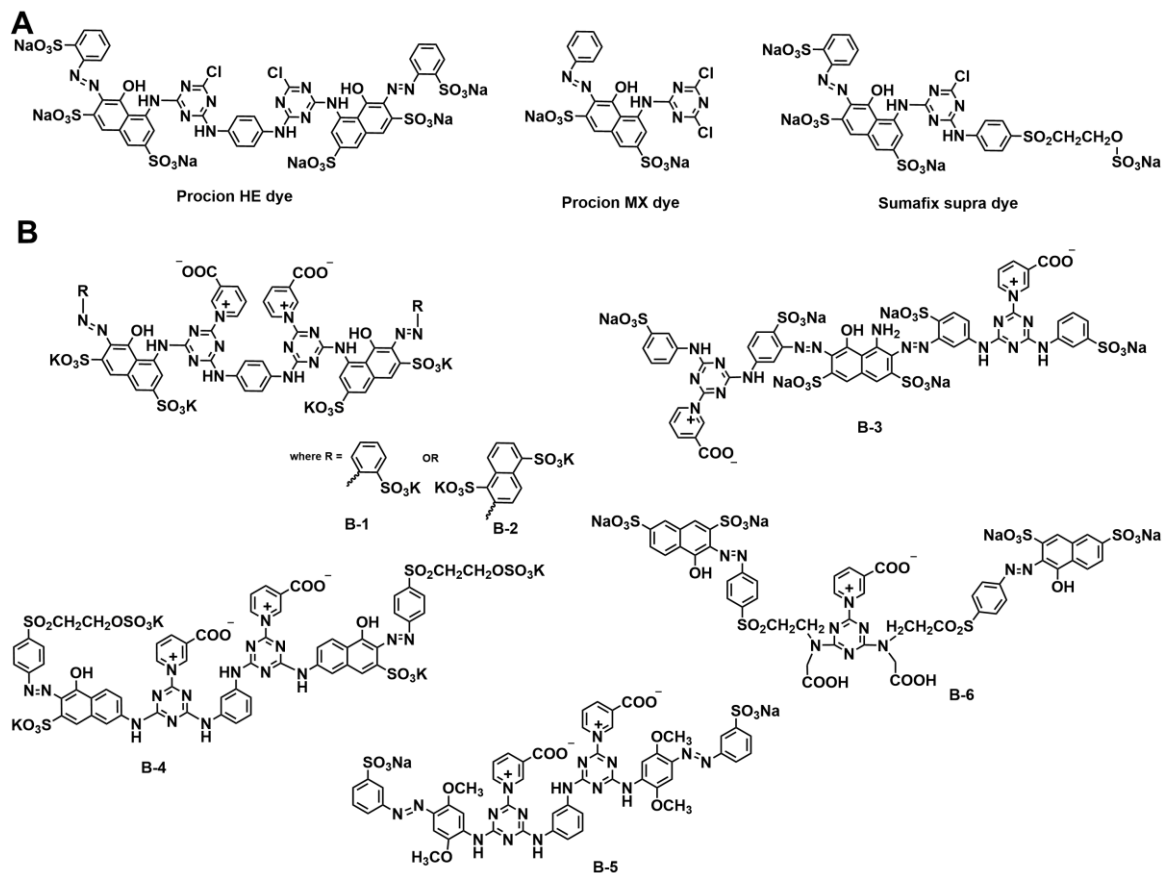
### **1.4.1 Triazines in dyeing and printing processes**

Dyeing and printing are operations of great importance in textile and paper production because adding color, pattern intricacy, or shades can add value to these products.<sup>89</sup> Dyeing is done at different stages of production and it chemically changes the substrate fibers such that they reflect light of a particular color. Cellulosic and polyamide fibers are most commonly treated with reactive dyes that covalently bind to nucleophilic sites already present on the fiber. Reactive dyes result in fibers with excellent wash fastness and color shades, which set them apart from adsorbed and acid dyes. Dyes containing monochloro-s-triazine, dichloro-s-triazine, or monochloro-s-triazine and sulfato-ethylsulfone reactive groups (e.g., Procion MX, H-E, H-EXL and Sumifix Supra dyes, Figure 1.4A) dominated the textile industry from the 1960s to the late 1980s because they offered excellent dye



fixation, reproducibility, substantivity (ability to bind to the target), exhaustion (fraction of the dye bound to the target), migration and easy wash off properties.<sup>90</sup> For example, the triazine reactive dye Cibacron LS (now Novacron LS, a bis-monofluorotriazine) showed very high substantivity under exhaustive dyeing, resulting in reduced electrolyte and moderate fixation temperature requirements for industrial processes.<sup>90</sup>

Recent work on the development of triazine reactive dyes for cellulosic materials has been largely carried out to address economic and environmental concerns over conventional dyeing methods. The main focus has been on designing environmentally friendly triazine dyes with very high exhaustive properties, short dyeing times, and low water and energy requirements. In one approach, reactive dyes containing 3-carboxypyridine-triazine groups were synthesized (B1-B5, Figure 1.4B) and grafted onto cellulose fibers in a neutral dyeing bath at 130°C.<sup>91</sup> The presence of quaternary pyridinium functionalities promoted the reaction of the dyes with the primary hydroxyl groups on cellulose under dyeing conditions typically used for polyester fibers. It was proposed that the high degree of dye exhaustion and dye fixation at relatively low electrolyte concentrations could lead to greener processes for the single-bath and single-stage dyeing of polyester-cellulose blends.



**Figure 1.4:** Chemical structures of representative triazine reactive dyes. (A) monofunctional, homo-bifunctional and hetero-bifunctional commercial dyes, and (B) Cationic homo-bifunctional and hetero-bifunctional dyes for neutral, alkaline and acidic dyeing conditions with low electrolyte requirement. Modified with permission from refs 91 and 93. Copyright 2007 Institute of Biopolymers and Chemical Fibers, and 2006 John Wiley & Sons, Inc.

Subsequent work showed that similar dyes, when grafted onto refined pulp in the presence of a cationic polyamine compound, gave uniform dye penetration into the paper products obtained after web consolidation at 100-130°C.<sup>92</sup> The resulting colored papers showed high wet fastness (did not bleed) and only 3-8% of the dyes could be extracted by a pyridine azeotrope, while the size, strength, optical, and structural properties of the paper remained unchanged. In an effort to increase the substantivity of sulfato-ethylsulfone reactive dyes,

the complementary nature of  $\beta$ -carboxyamino and quaternary pyridinium- groups installed on reactive triazine crosslinkers has also been studied.<sup>93</sup> Bis-ethylsulfone reactive groups bound to a central bis-N-carboxymethylamino-quaternary-triazine core (B6, Figure 1.4B) were grafted onto cotton cellulose using a dyeing method that combined acidic and alkaline steps. Higher exhaustion (88%) and fixation (70%) values were observed for this dye when compared to a model sulfato-ethylsulfone dye applied using conventional alkaline fixation. The improvement was attributed to the presence of positive charges on the quaternary reactive groups which suppressed the electrostatic repulsion between the sulfonated dyes and the anionic groups present on cellulose.

Even with efforts aimed at improving the exhaustion and fixation properties of quaternary reactive dyes, some challenges remain because heavy depths of shade could not readily be obtained using these dyes.<sup>94</sup> Several solutions aimed at increasing dye fixation efficiency have been investigated, including the development of new multifunctional triazine dyes, the chemical modification of the substrate fibers, and new dyeing methods performed in non-aqueous media. For example, a nonpolar reactive dye bound to a dichlorotriazinyl ring has been used to dye cotton cellulose in supercritical carbon dioxide (scCO<sub>2</sub>).<sup>95</sup> This solvent was found to enhance dye permeation and affinity to cellulose when methanol was used to pre-treat cellulose and as the dye carrier solvent, resulting in increased dye fixation and excellent color strength. Surprisingly, changing the dye structure by switching the chlorine-substituents to fluorinated analogs, resulted in increased fixation and a seven-fold increase in color strength when dyeing cellulose in scCO<sub>2</sub>.<sup>96</sup> The reactivity of the fluoro-triazine dyes used in this process allowed a reduction in dyeing time and an increase in the dye concentration used, without showing any damage to the fibers when compared to chlorotriazines.

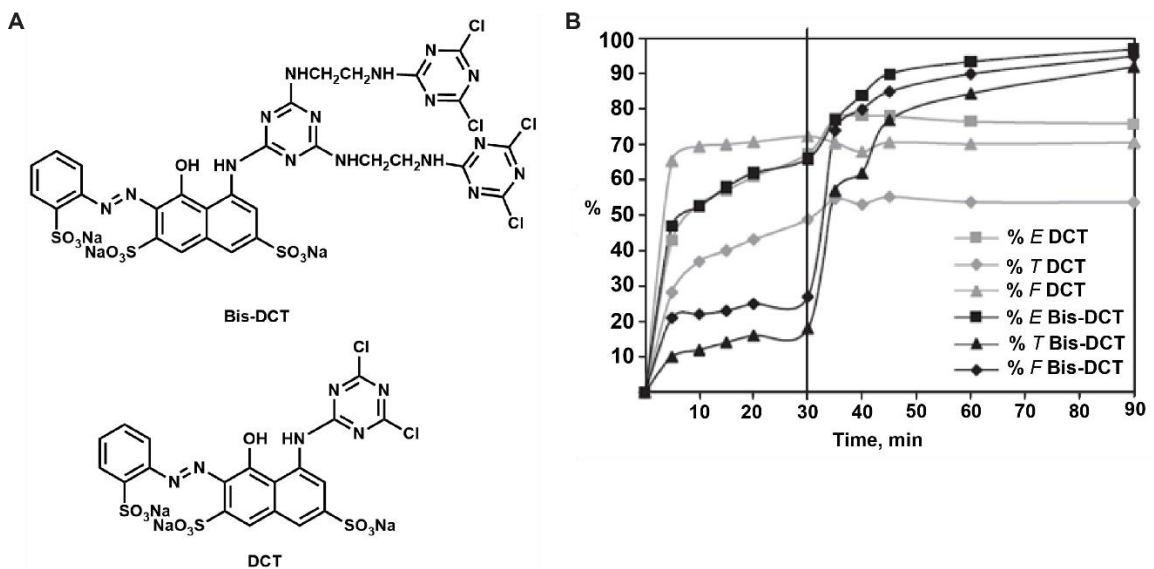
Over the last decade, reverse micelles formed by surfactant molecules in non-polar solvents have been used to dye cotton fibers more efficiently.<sup>97,98</sup> The solubilization of reactive dye molecules in the polar core of the reverse micelles has delivered superior dye substantivity, fixation and exhaustion when compared to aqueous systems.<sup>97-99</sup> Dong and co-workers<sup>99</sup> compared the grafting of the dye CI reactive red 195 onto cotton fabric in Triton X-100

reverse micelles and aqueous systems. They found that reverse micelle dyeing showed stronger dye substantivity without the use of electrolyte, higher dye fixation and better dye diffusion into the fiber. The improvement in dye adsorption capacity was attributed to a reduction in the repulsive force between dye molecules and cellulose due to the reduced ionization of the reactive dyes within the micelles. Additionally, they suggested that cotton fiber swelling by Triton X-100 and the organic solvent enhanced the penetration of the dye during the reverse micelle dyeing. PEG-based reverse micelle dyeing has also been used to graft CI reactive dye violet 2 (in the presence of Span40),<sup>100</sup> as well as a variety of hetero- and mono-functional triazine dyes (with 1-octanol as cosurfactant),<sup>101</sup> onto cotton fibers. These systems have shown similar improvements in color yield, dye substantivity and dye fixation. Despite the success of reverse micelle dyeing, it has been found that the chemical structure of the surfactant molecule chosen is critical in creating a stable dye-cellulose micro-environment, as ionic surfactants result in uneven dyeing.<sup>102,103</sup>

Polyfunctional reactive dyes based on the triazine architecture have been synthesized with the goal of increasing dye efficiency above 95%. Freeman and coworkers<sup>104</sup> synthesized tetrafunctional and bifunctional triazine dyes (bearing cysteine or cysteamine groups) and reported an improvement in dye substantivity and fixation efficiency on cotton fibers with reduced salt requirements. Upon replacing cysteamine with ethylene diamine (Figure 1.5A) the tetrachloro-s-triazine dye (bis-DCT) showed improved efficiency over the starting dichloro-s-triazine (DCT) dye when applied in long-liquor dyeing.<sup>105</sup> The bis-DCT dye gave a total fixation efficiency (T) of 93% whereas the parent DCT dye gave a T of 69% (Figure 1.5B). Differences in the exhaustion/fixation profiles of both dyes (post-alkali addition,  $T \geq 30$  min) were significant as the bis-DCT dye underwent rapid fixation during the first 5 min post-alkali addition, after which the rate slowed down, but fixation continued to increase. In comparison, DCT showed no additional increase of the absorbed dye as the amount of fixed dye plateaued after the initial neutral exhaustion phase.

The chemical modification of cellulose has also been explored as a way to overcome the electrostatic repulsion between dye molecules and cellulose fibers during reactive dye printing. The modification of cellulose fabric with 2,4,6-tri[(2-hydroxy-3-trimethyl-

aminonium)propyl]-1,3,5-triazine revealed improved printing with 3 different reactive dyes without the need for electrolytes.<sup>106</sup> Printing on the modified fibers resulted higher color strength, with increases in color yield of 6-13%, when compared to unmodified fibers.



**Figure 1.5:** Chemical structures of representative multifunctional triazine dyes (A) homo-bifunctional and -tetrafunctional dyes, and (B) Exhaustion/fixation profiles of DCT and Bis-DCT dyes. E = dye exhaustion, F = absorbed dye fixation and T = total dyeing fixation efficiency. Modified with permission from ref 105. Copyright 2008 John Wiley & Sons, Inc.

In this approach, the covalent binding of multiple triazinyl cationic groups onto the cellulose surface promoted electrostatic interactions with the dye, improving substantivity and fixation. Similarly, the grafting of poly(amidoamine) G2 dendrimers pre-modified with cyanuric chloride was discovered to be an effective way of tuning the surface properties of cotton cellulose for single-phase ink-jet printing of reactive dyes.<sup>107</sup> The modified fabrics not only showed excellent color fastness, higher dye fixation and higher thermal stability, but also resulted in antimicrobial properties that were not present in the native fibers.

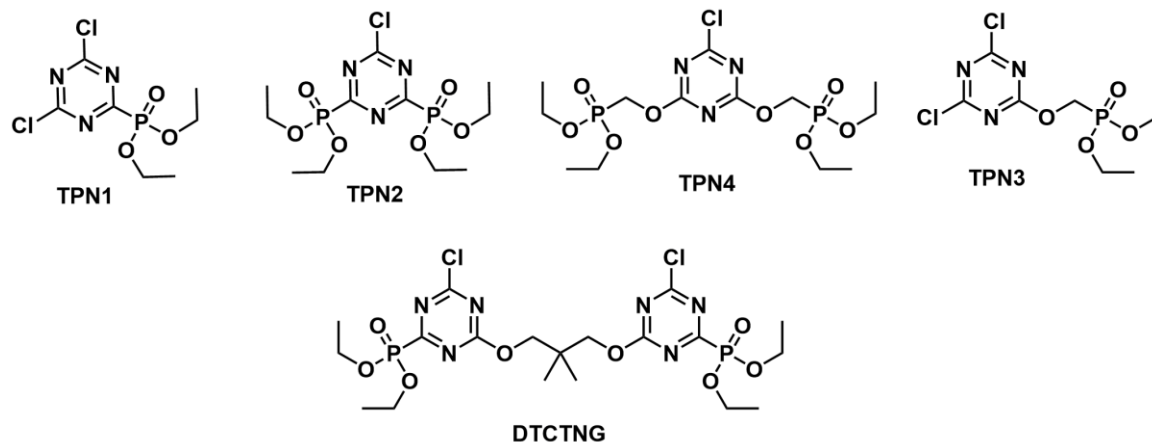
So far, triazine chemistry in the dyeing and printing industry has been used to implement solutions that address the environmental and economic problems of dyehouse effluents. Research has been particularly focused on improving dye-fibre fixation efficiency, cutting down on CO<sub>2</sub> emissions, and lowering water and energy requirements. The reactive dyes based on the triazinyl chemistry and dyeing methodologies discussed above, are promising and capable of delivering excellent color fastness, high dye fixation, high dye efficiency and dye printability. However, in long-liquor dyeing, where the use of large quantities of electrolytes is increasingly viewed as an environmental hazard, there is still a need to develop new systems with no or very low electrolyte requirements, without sacrificing dyeing evenness and reproducibility.

#### **1.4.2 Triazines for flame retardant treatments**

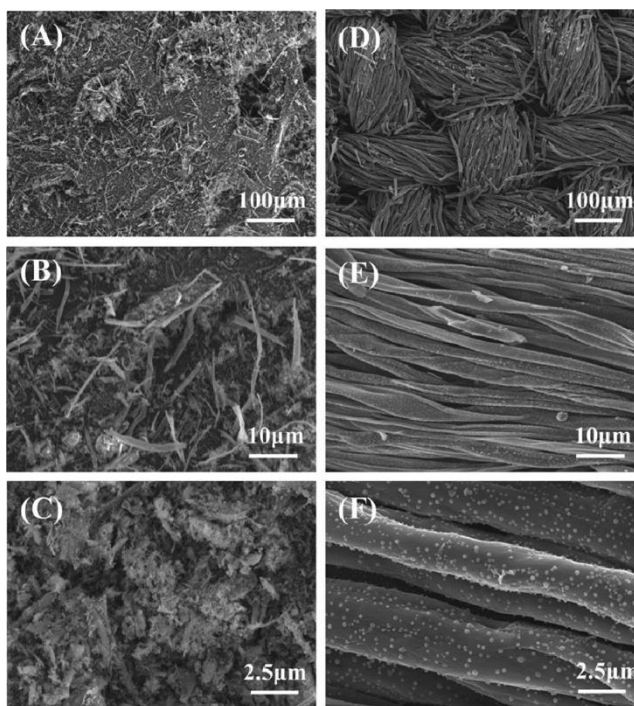
Fabric flammability depends on a variety of factors, such as the source of fibre, its linear density, thread density, fabric construction, environmental oxygen and humidity levels, and even the weave of the fabric.<sup>108,109</sup> Cellulose, the most common textile fiber, burns readily when ignited and undergoes thermal degradation, resulting in combustible volatile compounds that further propagate fire.<sup>108,110</sup> Government regulations aimed to improve consumer safety have stimulated significant research into ways to improve flame retardancy in textiles. In this regards, triazinyl chemistry has been used to attach phosphorous-containing compounds to cotton cellulose fibers to reduce their flammability. In particular, nitrogen-phosphorus flame retardants have demonstrated significant advantages, such as high efficiency, low toxicity during combustion, and low smoke production.<sup>111</sup> Cotton fabrics grafted with tetraethyl 6-chloro-1,3,5-triazine-2,4-diylidiphosphonate showed self-extinguishing properties (char lengths less than a quarter of total sample length) under vertical flammability tests.<sup>112</sup> The treated fabrics yielded >30% char residue under thermogravimetric degradation (air and nitrogen) at 600 °C, much higher than the control cotton fabric that only yielded 1-2%. The limiting oxygen index

(LOI) of treated fabrics at 45% add-on were > 40% (control fabrics averaged 18.5%), which outperformed the LOI benchmark of 26-28% oxygen in nitrogen for flame retardant materials.<sup>113</sup>

Further work into the development of flame-retardant textiles have involved the synthesis of triazinyl compounds incorporating diethylphosphonate (TPN1 and TPN2) and dimethyl-hydroxymethylphosphonate (TPN3 and TPN4) groups covalently bound onto cotton cellulose (Figure 1.6).<sup>114</sup> The LOI data and vertical/45° angle flammability test of treated cotton twill samples at various add-on levels (Tables 1 & 2) show an array of slow burning, self-extinguishing to non-ignitable samples. The grafting of a neopentyl glycol-linked bis-(diethyl phosphonate monochloro-s-triazine) (DTCTNG, Figure 1.6) onto cotton fabric has also been studied as a flame retardant treatment.<sup>115</sup> The use of sodium hypophosphite as catalyst during grafting was found to improve flame resistance of cotton as treated samples reached LOI values >28% and were water resistant. The samples were self-extinguishing, did not show any burning or flame damage, and yielded 92.9% char. The surface of the residual char was uniform, and the structure of fabrics remained relatively intact with the formation of a foam/swollen layer that served as a barrier to prevent heat and flames from damaging the cotton fibers (Figure 1.7). These examples show the promise of triazinyl linkers as cost-effective ways to install multifunctional nitrogen-phosphorus flame retardants onto cellulose.












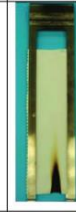


**Figure 1.6:** Chemical structures of representative triazine-based flame-retardants. Modified with permission from references 114 and 115. Copyright 2012 and 2015 American Chemical Society and Elsevier.






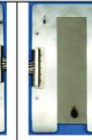
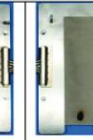





**Figure 1.7:** SEM images of pure cotton fabrics after limiting oxygen index tests (A, B, C) and treated cotton fabrics after limiting oxygen index tests (D, E, F) showing the self-extinguishing and spumescent properties of DTCTNG on cotton. Adapted with permission from reference 115. Copyright 2015 Elsevier.



**Table I. Vertical flammability (ASTM D-6413-08) and limiting oxygen index (LOI) (ASTM D-2863-09) test for different add-ons (wt %) of treated twill fabrics for TPN<sub>1</sub> and TPN<sub>2</sub>. Adapted with permission from reference 114. Copyright 2012 American Chemical Society.**

<b>TPN1 series</b>							
	Add-on (wt %)	control	4	12	17	26	33
	After-flame (sec)	10	18	2	0	0	0
	After-glow (sec)	30	3	0	0	0	0
	Char length (cm)	NA	>30	6.0	5.0	3.5	2.5
	Ave. LOI (%) $[\sigma]$	18[0.12]	28[0.26]	37[0.13]	45[0.26]	38[0]	48[0.20]
<b>TPN2 series</b>							
	Add-on (wt %)	control	4	10	15	24	31
	After-flame (sec)	10	24	0	0	0	0
	After-glow (sec)	30	2	0	0	0	0
	Char length (cm)	NA	>30	8.5	5.0	3.5	2.5
	Ave. LOI (%) $[\sigma]$	18[0.12]	28[0]	36[0]	42[0.20]	45[0.20]	48[0.26]

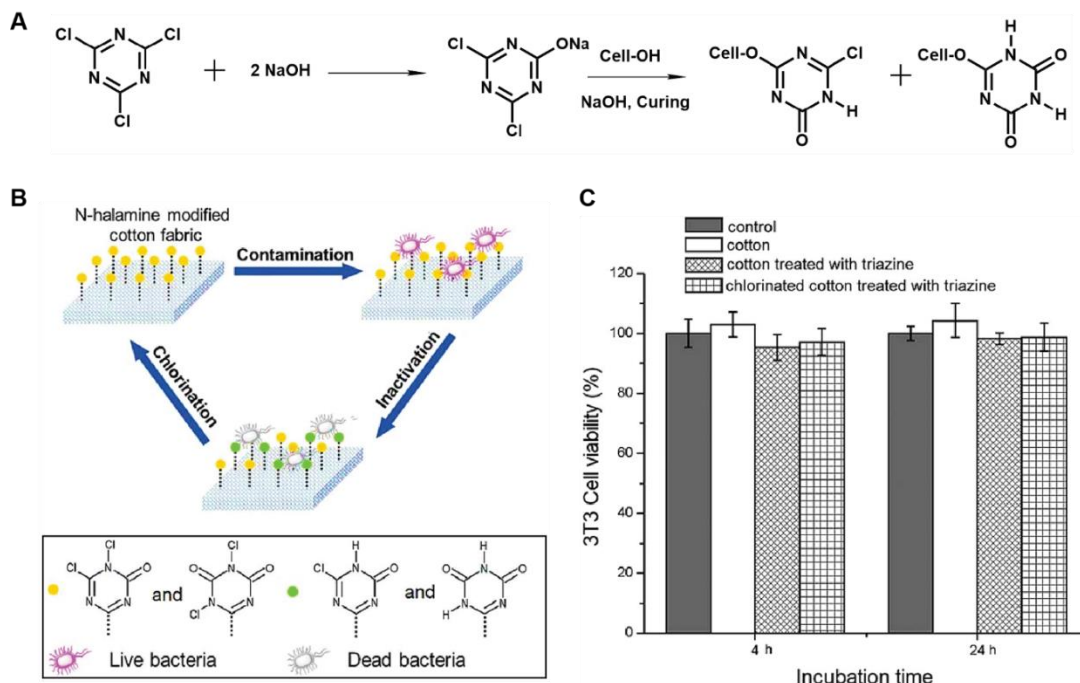
**Table II. 45° angle flammability (ASTM D-1230-01) and limiting oxygen index (LOI) (ASTM D-2863-09) test for different add-ons (wt %) of treated twill fabrics for TPN<sub>3</sub> and TPN<sub>4</sub>. Adapted with permission from reference 114. Copyright 2012 American Chemical Society.**

<b>TPN3 series</b>						
	Add-on (wt %)	control	5	10	16	21
	Flammability (sec)		DNI <sup>a</sup>	DNI	DNI	DNI
	Class	Class III <sup>b</sup>	Class I <sup>c</sup>	Class I	Class I	Class I
Ave. LOI (%) $[\sigma]$	18[0.12]	30.0[0]	32.0[0]	34.2[0.41]	40.2[1.1]	
<b>TPN4 series</b>						
	Add-on (wt %)	control	5	9	14	19
	Flammability (sec)		80 <sup>d</sup>	46 <sup>d</sup>	DNI	DNI
	Class	Class III	Class I	Class I	Class I	Class I
Ave. LOI (%) $[\sigma]$	18[0.12]	19.6[0.55]	22.7[0.52]	31.0[1.0]	36.0[5.03]	

### 1.4.3 Triazine Scaffolds for Antibacterial Fabrics

The growing interest in textile materials with antimicrobial properties that can withstand washing or exposure to cleaning products has made the covalent attachment of biocidal functionalities onto cellulose fibers attractive. The immobilization of neutral, anionic and cationic amino-porphyrins on cellulose fibers through triazinyl chemistry has been recently explored as a way to endow them with antimicrobial properties.<sup>116</sup> This study found photo-bactericidal activity with as little as 10  $\mu\text{mol}$  of active porphyrin per fabric square sample (12  $\text{cm}^2$ ) when tested *in vitro* against *Staphylococcus aureus*. The percentage of live bacteria after 24 h exposure to light (radiant exposure = 9.5  $\text{J}/\text{cm}^2$ ,  $T = 37^\circ\text{C}$ ) were 63%, 6.3% and 0% for anionic, neutral and cationic surfaces, respectively. This highlights the effect of charge on bactericidal activity for Gram-positive cells. The efficacy of the materials was attributed to the generation of singlet oxygen from the photosensitizers, which is known to damage the cell membrane.<sup>117</sup> In addition, the toxicity of the cationic fabric under dark conditions (80%) was linked to the presence of a quaternary ammonium group that is known to disrupt the bacterial cell wall.<sup>118</sup> Consistent with this interpretation, tests carried out against Gram-negative bacteria *Escherichia coli* showed no photoactivity by any of the three aminoporphyrin treated materials.<sup>119</sup> In this case, the lipopolysaccharide coat present in the cell wall of *E. coli* protected the bacteria from extracellular singlet oxygen diffusion. In contrast, increasing the number of cationic centers in the aminoporphyrin grafted onto cellulose from one to three resulted in photo-bactericidal efficacy against both *S. aureus* and *Escherichia coli* bacterial strains with no surviving bacteria after 24h exposure to light.<sup>120</sup>

The preparation of cellulose fabrics with antimicrobial properties that can be regenerated after standard washing and UVA irradiation is another area of significant interest. Ren and coworkers<sup>121</sup> recently developed a method to form N-halamine precursors through the controlled hydrolysis of cyanuric chloride and grafted them onto cellulose via a pad-dry-cure finishing process (Figure 1.8). The N-halamine modified cotton fabrics were rendered antimicrobial upon exposure to dilute household bleach and showed 7-log reduction of colony forming units against *S. aureus* and *E. coli* O157:H7 with contact times of minutes.



**Figure 1.8:** (A) Schematic representation for the alkali hydrolysis of cyanuric chloride and the chemical attachment of triazine rings onto cellulose, (B) Schematic illustration of the biocidal function and regeneration of the N-halamine-modified cotton fabric, and (C) Cell viability of 3T3 fibroblasts on different fabrics and control (tissue culture plates) after 4 and 24 h of incubation. Modified with permission from reference 121. Copyright 2014 John Wiley & Sons, Inc.

The fabrics were stable and regenerable after laundering and UVA irradiation, a significant improvement over cotton fabrics modified with N-halamine siloxanes<sup>122–124</sup> and 1-glycidyl-s-triazine-2,4,6-trione (GTT).<sup>125</sup> Moreover, the treated fibers showed resiliency against mechanical and physical damage under high temperatures due to the good thermal stability of triazines. Other types of N-halamine biocidal agents based on the hydantoin<sup>126,127</sup> and tetramethylpiperidinol<sup>128</sup> groups attached onto the triazinyl framework have also been reported. Hydantoin-benzenesulfonate (HB) treated cotton fabrics were

shown to be superior to dichloro-piperidinol- and monochloro-piperidinol-s-triazine-treated cotton fabrics,<sup>128</sup> since it inactivated all *S. aureus* and *E. coli* O157:H7 bacteria within a contact time of 1 minute.<sup>126</sup> This result was attributed to N-halamines that contain amide N-Cl groups being able to release the halogens more readily than those that contain amine N-Cl groups, thus killing bacteria more rapidly.<sup>129</sup>

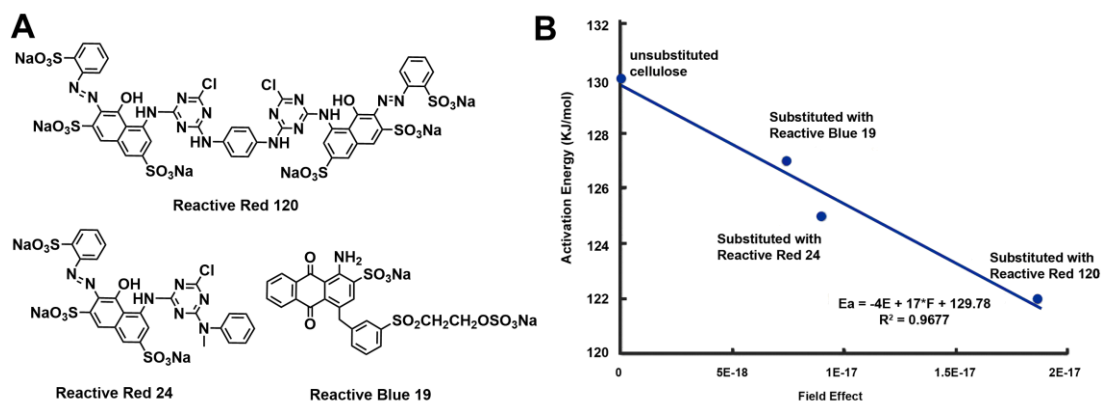
Multi-cationic materials have also been grafted onto cellulose during textile finishing as antibacterial compounds that are biocompatible and non-cytotoxic towards mammalian cells. For example, the incorporation of multi-cationic benzyl groups on the surface of cellulose fibers has been found to impart excellent antibacterial properties.<sup>130</sup> The antibacterial efficacy of these fabrics was shown to be durable, as they inactivated *S. aureus* and resisted growth (~100% inhibition) at zero washing cycle, and retained 91 and 84% inhibition after 10 and 20 cycles of washing, respectively. The mechanism of action was postulated to be purely physical in nature and to rely on the dynamic interaction of the modified cellulose surface with the bacterial cell wall, where once the cell wall was disrupted the bacteria could not resort to any protective response for survival. Cationic N-halamine has similarly been successfully used to provide cellulose with powerful biocidal action against *S. aureus* and *E. coli* O157:H7 through the synergistic antimicrobial effect of a quaternary ammonium and N-halamine.<sup>131</sup> The treated fibers showed inactivation of both bacterial strains with contact time of minutes, and retained approximately 50% of the oxidant chlorine after 50 washing cycles and 30 days of storage. More importantly, any lost active chlorine could be recovered upon exposure to dilute bleach solution. The idea of inactivation of microorganisms on textile fabrics is especially important in places where the risk of infection is high. The triazine chemistry has demonstrated its versatility by enabling the linkage of a wide range of biocidal agents onto cellulose effectively, making it a major player in this area of research.

#### 1.4.4 Triazine Derivatives as Aids in Biomass Conversion

Conversion of renewable plant biomass into biofuels and bio-based products has garnered significant attention because these can replace petroleum-based products and reduce the human environmental footprint.<sup>132–134</sup> Biomass conversion typically involves processes that remove lignins and hemicelluloses from plant material (pretreatment), break down the crystalline cellulose portion into soluble sugars (hydrolysis), and turn these soluble sugars into chemicals of interest (e.g., fermentation). A key bottleneck in the economic production of bio-based products is the low conversion efficiency of crystalline cellulose, which has been linked to the tight intra- and intermolecular hydrogen bonding between glucan chains that results in recalcitrance to chemical and enzymatic breakdown.<sup>135,136</sup> It has been discovered that the chemical modification of crystalline cellulose can improve hydrolysis yields, which is interesting considering that large amounts of chemically-substituted cellulose fibers are already generated as waste (> 1.5 million tons generated annually from dyed textiles alone).<sup>137</sup> Cotton fibers treated with dyes have been found to be more easily hydrolysable than untreated fibers, obviating the need for any pretreatment.<sup>137,138</sup> In particular, the attachment of aromatic compounds onto cellulose has been shown to dramatically increase the hydrolysis of the glycosidic linkages, with the yield correlating with the size of molecule grafted.<sup>138</sup> Additionally, substituents attached to the C6 position of the glucose units within cellulose have been shown to enhance hydrolysis to a greater extent than the same substituents attached to the C2 or C3 positions.<sup>138</sup>

Triazine-based reactive dyes have been commonly used in studies aimed at improving the hydrolysis of cellulose fibers. Reactive Red 120 was shown to give the lowest activation energy for hydrolysis compared to Reactive Blue 19 and Reactive Red 24, experiencing 100% loss in single-end fiber strength after repeated commercial laundering (Figure 1.9).<sup>137,138</sup> The modification of microcrystalline cellulose (MCC) with 2-chloro-4,6-diphenylamino-s-triazine (DACT) was also shown to increase the reducing sugar yield from 78% (MCC) to 89% (DACT-MCC).<sup>139</sup> These improvements arose from changes in the hydrogen bonding between cellulose glucan chains elicited by DACT, which was

reflected in a decrease in the crystallinity index (CI) from 80% (native MCC) to 60% (DACT-MCC). Similarly, the grafting of 5-(4,6-dichlorotriazinyl)-aminofluorescein (DTAF) onto bacterial MCC was found to almost double the hydrolytic activity of *Thermobifida fusca* endocellulase Cel5A, as measured through reducing sugar production.<sup>140</sup> The enhanced activity was attributed to the local changes in cellulose chain arrangement and interstitial spacings as the large DTAF molecules were grafted onto the glucan chains. MCC modified with cyanuric chloride alone also showed a doubling in the hydrolysis yields, which could be traced back to changes in the crystalline structure of cellulose with the CI decreasing from 80% to 56%.<sup>141</sup> The recalcitrant MCC structure was distorted by the covalent attachment of cyanuric chloride at low concentrations (< 3.9%), but it was observed that larger concentrations gave way to the formation of dimers, trimers or oligomers in solution that were too big to attach to glucose residues in the crystalline regions. These sample studies highlight the impact that simple triazine treatments could have on the crystalline structure, accessibility and ability to hydrolyze waste cellulose fibers and textiles, making them attractive processes to improve the reducing sugar yields needed for the production of biofuels and bio-based products.



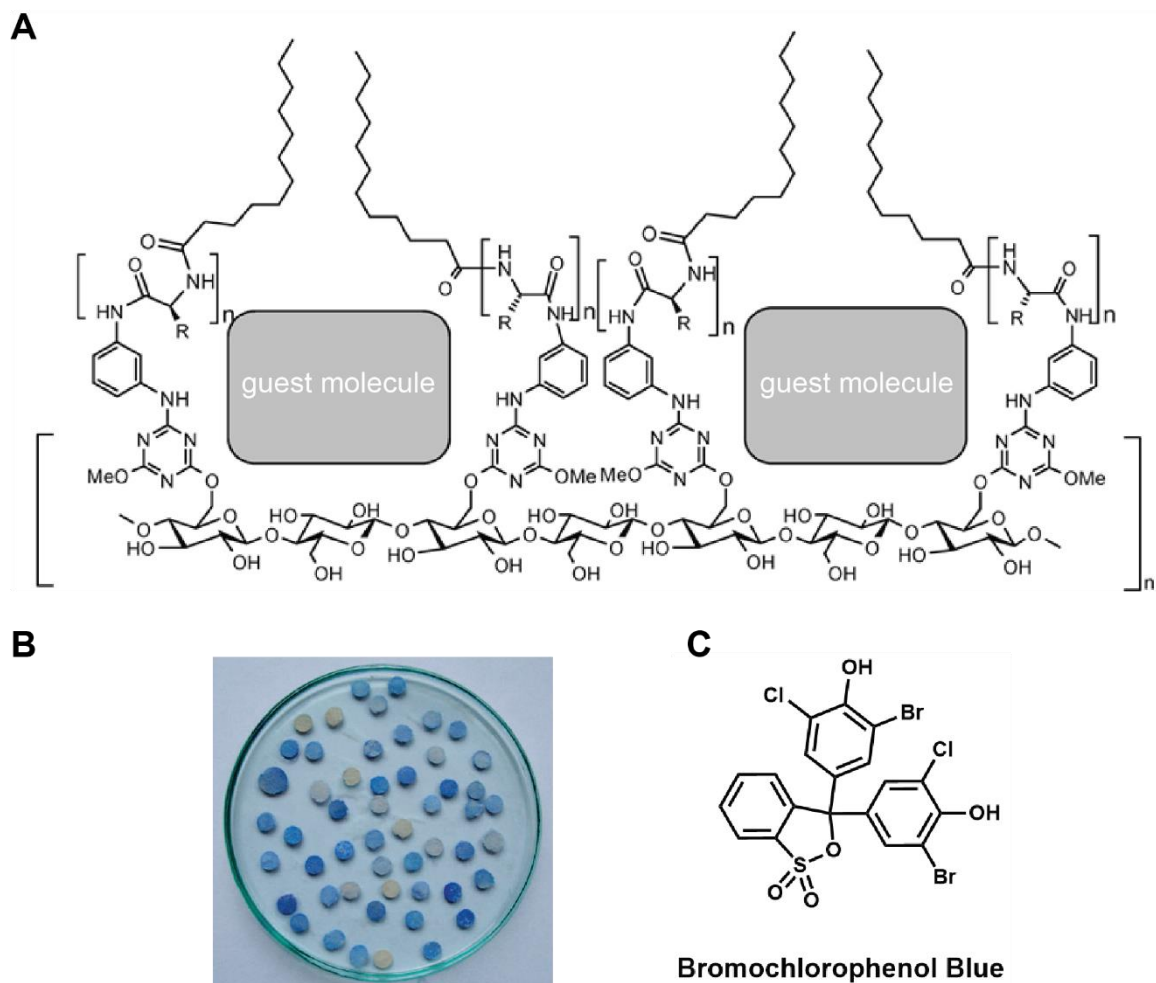
**Figure 1.9:** Chemical structures of representative dyes grafted onto cotton yarn. (A) reactive red 120, reactive red 24 and reactive blue 19, (B) Graph showing the relationship between size/field effect from individual dye substituents and activation energy for the hydrolysis of unsubstituted and substituted cellulose. Modified with permission from ref 137. Copyright 2019 Elsevier.

#### 1.4.5 Triazine-Modified Supports for Affinity Based-Separations

Triazinyl chemistry has been the principal modification method used in the development of activated polysaccharides for use as support materials in affinity-based separations.<sup>142–144</sup> In an effort to make supports that are reproducible, stable and capable of eliminating nonspecific adsorption, early methods were developed to prepare dichloro-s-triazine Sepharose gels under controlled activation conditions.<sup>145</sup> Reaction of these supports with aniline yielded monochloro-activated gels that could be used to quantitatively immobilize small (6-aminocaproic acid) and large (<sup>125</sup>I-labelled fibrinogen, bovine serum albumin,  $\alpha$ -amylase, lactate dehydrogenase, cellulase, trypsin and chymotrypsin) ligands. The activated supports could be lyophilized for later use without loss of molecular sieving properties, as assessed through the separation of blue dextran 2000 from albumin. Sepharose-fibrinogen supports prepared in this way were used to isolate antibodies against human fibrinogen from whole goat serum, and it was observed that triazinyl-linked fibrinogen was more resistant to hydrolysis than the cyanogen bromide-linked one. In another early work, cellulose modified with dichloro-s-triazine was found to reproducibly and efficiently immobilize double stranded DNA.<sup>146</sup> The immobilized DNA was stable in the presence of urea, high salt, and alkaline conditions, with > 85% DNA remaining double-stranded, only 0.65% of DNA being released when treated with 5 M urea and 3 M NaCl, and 1% being released with 0.1 M sodium hydroxide. This DNA-functionalized support was successfully used to fractionate histones and other chromatin proteins.

Interestingly, the use of immobilized reactive dyes as ligands for protein affinity-based chromatography has also been reported.<sup>147,148</sup> Triazine-linked Procion red H-8BN dye immobilized on Sepharose 6B has been used to purify the folate-degrading enzyme carboxypeptidase G<sub>2</sub> from *Pseudomonas sp.* on a large scale.<sup>148</sup> The presence of Zn<sup>2+</sup> ions was found to promote quantitative binding of the enzyme to the immobilized triazine dye through a highly specific ternary coordination complex. Similarly, triazine dyes have been used as chelators for copper ion immobilization in the analysis of protein adsorption on regenerated cellulose membranes. Cibacron-blue 3GA and -red 3BA were found to

outperform iminodiacetic acid and tris(carboxymethyl)ethylenediamine in the percentage of copper ion utilization for protein adsorption.<sup>149</sup>



**Figure 1.10:** (A) Schematic representation of an artificial receptor formed by the self-organization of N-lipo-peptide grafted onto cellulose filter paper binding guest molecules inside its pockets, (B) Ambient light photograph of receptor sub-libraries A and B treated with reporter dye, and (C) Chemical structure of a representative reporter dye. Modified with permission from reference 153. Copyright 2008 American Chemical Society.



More recent studies have seen the use of triazine scaffolds for the development of functional solid supports for affinity-based separations in operations at larger scales, such as wastewater treatment<sup>150,151</sup> or the screening of pharmaceutically-relevant molecules.<sup>152,153</sup> Lu *et al.*<sup>150</sup> synthesized a cobalt tetraaminophthalocyanine-dichlorotriazinyl derivative and grafted it onto cellulose fibers to produce a solid support capable of removing organic dyes from aqueous solutions. This solid support resulted in the rapid catalytic degradation of acid red 1 (AR1) dye upon the addition of hydrogen peroxide. The dye concentration was observed to decrease to ~0% in 40 minutes compared to 75% for the case of homogeneous catalysis in solution. The excellent performance in the phase-transfer catalytic oxidation of AR1 were linked to the controllable surface potential and unique swelling ability of cellulose in aqueous solutions, as well as to the ability to overcome  $\pi$ -stacking and aggregation issues associated with the use of phthalocyanines in solution.<sup>154,155</sup> In a second application for water treatment, triazinyl chemistry was used to graft ligands onto polysaccharide supports for the complexation and removal of heavy metals. Bifunctional calix[4]arenes grafted onto water-soluble dextran have been shown to complex copper(I) via the formation of a tetrahedral bipyridine/Cu(I) complex, resulting in solutions with a stable orange to red coloration.<sup>156</sup> Similarly, calcein immobilized onto powdered cellulose has been used in binding Co(II), Cu(II) and Ni(II) metal ions in water over a range of pH values<sup>157</sup> and anthranilic acid grafted onto microcrystalline cellulose has been used in the chromatographic separation of Co(II), Cu(II) and Ni(II) metal ions.<sup>158</sup> These types of solid supports have been proposed as promising systems for the practical removal of contaminants from wastewater in the presence of typical additives and ions.

In the area of pharmaceutical screening, artificial receptors formed by the self-organization of N-lipopeptides have been grafted onto cellulose filter paper using a triazine scaffold.<sup>152,153</sup> In this approach, amino-functional cellulose fibers were first prepared by the immobilization of 2,4-dichloro-6-methoxy-s-triazine followed by reaction with *m*-phenylenediamine.<sup>153</sup> Acylation of the amino groups with N-protected amino acids, followed by deprotection to free the amine functionality, and coupling of the target carboxylic acids (previously activated with a triazine coupling reagent)<sup>159</sup> resulted in a

library of N-lipopeptides grafted onto cellulose supports. The ability of the grafted lipopeptides to form a monolayer of holes and pockets in dynamic equilibrium, capable of efficiently binding small guest molecules while recognizing the shape, size and polarity of the ligand has been used to selectively capture triphenylmethyl dyes (Figure 1.10). The binding strength and selectivity increased with the length of the alkyl chain of the lipophilic fragment and depended on the structure of the amino acid linker fragments, with the strongest binding reported for fragments containing histidine side groups with imidazole functions. The same solid support technology has also been used to study the binding of N-phenylpiperazine guest molecules to N-lipopeptide receptors.<sup>152</sup> These supports could find application in the development of low cost screening platforms to be used in the discovery of new drugs or as portable sensors.

## **1.5 Functional nanocelluloses via triazinyl chemistry**

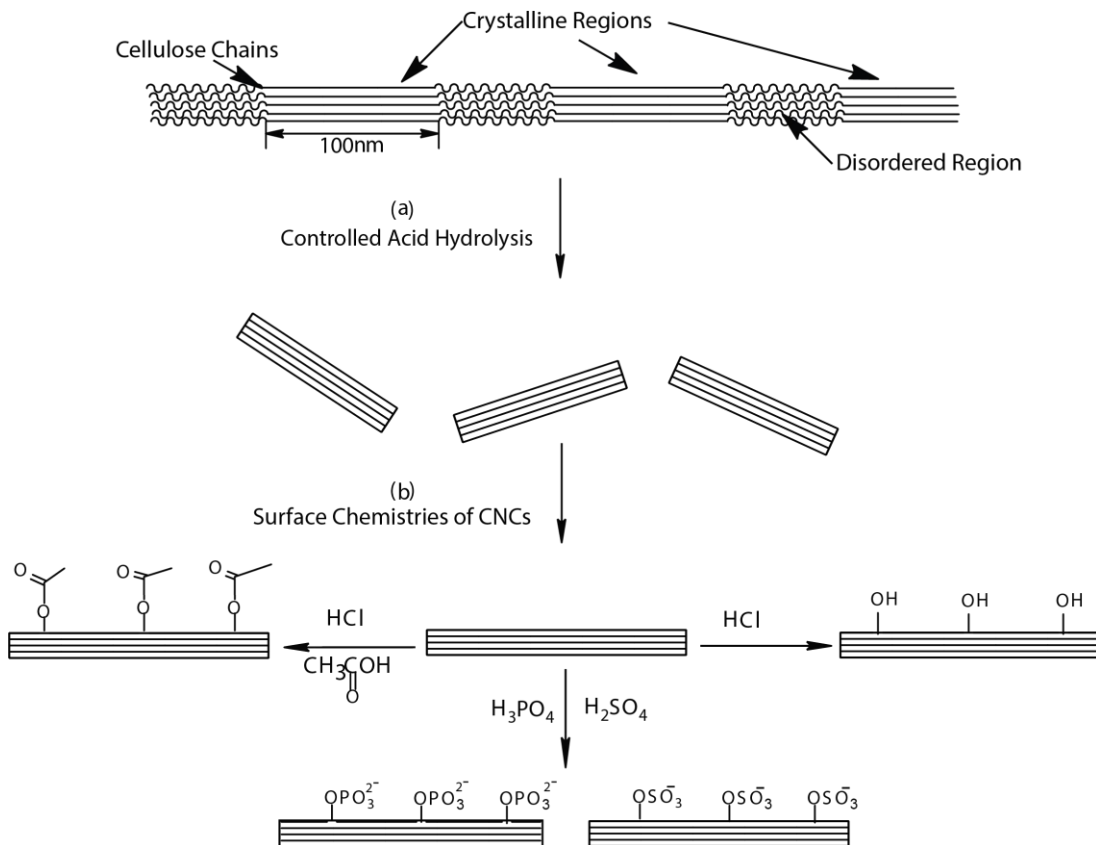
Over the last decades nanocelluloses have emerged as interesting bio-based, renewable and environmentally friendly materials with unique mechanical, optical, electrical and magnetic properties suitable for the development of advanced composites and materials. The term nanocellulose encompasses high aspect ratio nanoparticles (3-5 nm wide, 50-500 nm in length, cellulose nanocrystals – CNCs) and fibrils (5-50 nm wide and micrometers long, microcrystalline cellulose – MCC and cellulose nanofibrils – CNFs). Nanocelluloses are typically isolated from plants, algae, tunicates or bacteria. They are made of parallel arrangements of  $\beta$  (1-4)-linked glucose polymers (glucan chains) and are partially to fully crystalline, with crystallinity indices of 50-95%, dependent on the cellulose source.<sup>2</sup> The intrinsic physical and chemical properties of nanocellulose, including high tensile strength, low cost (relative to other nanoparticles), renewability, light weight, high aspect ratio, and their high surface area-to-volume have made it a prime target for use in applications such as materials reinforcement, drug delivery, foam stabilization, supercapacitor development and rheological property modification, among many others.<sup>13</sup> This potential for development has spurred intense research into ways to functionalize these naturally derived

nanomaterials (for reviews on the different surface modification of nanocelluloses the interested reader is directed to references <sup>2,13,160</sup>), with recent developments focused on the use of triazinyl scaffolds to tune the interfacial properties of nanocelluloses.

Early work on the modification of nanocelluloses with triazinyl scaffolds was done with the intent of monitoring the enzymatic binding to and hydrolysis of crystalline cellulose by fungal and bacterial cellulases. The first report of triazinyl chemistry being applied to nanocellulose was the modification of bacterial microcrystalline cellulose (BMCC) with the fluorescent triazine dye 5-([4,6-dichlorotriazin-2-yl]amino)fluorescein (DTAF) by Helbert and collaborators.<sup>161</sup> In this report, the labeling process was optimized for the labeling of cellulose I<sub>α</sub> and cellulose III<sub>I</sub> allomorphs by varying the dye load, base concentration, and number of labeling steps. The resulting fluorescent microfibrils were used to study the release of soluble sugars during the enzymatic hydrolysis by cellulases derived from the filamentous fungus *Humicola insolens*. Subsequent works by Walker, Moran-Mirabal, and others have used surface immobilized DTAF-labeled BMCC fibrils and a variety of fluorescence microscopy techniques to monitor bacterial and fungal cellulase binding kinetics,<sup>140</sup> binding reversibility,<sup>162</sup> hydrolysis kinetics,<sup>163</sup> single molecule enzyme motion,<sup>164,165</sup> and hydrolysis-induced structural changes in cellulose fibrils.<sup>166,167</sup> Cellulose microfibrils fluorescently tagged with triazine dyes continue to be a valuable asset in the prospecting and characterization of cellulose degrading enzymes for biomass conversion, since the triazinyl linker is stable over time and under a range of pH and ionic strengths and does not appear to hinder enzymatic hydrolysis.

Cellulose nanocrystals have become increasingly relevant for the development of advanced materials, composites, and bio-based products because they are now produced at industrial scales and they can be processed as colloidal nanoparticle suspensions, which preserves their unique nanoscale properties. While sulfuric acid hydrolysis of native or treated cellulose is still the most common process for CNC isolation, hydrochloric, acetic, and phosphoric acid hydrolysis have also been used (Figure 1.11).<sup>168,169</sup> Hydrochloric acid hydrolysis produces uncharged CNCs that form unstable suspensions, leading to aggregation and precipitation in all solvents that do not dissolve cellulose. On the other

hand, sulfuric and phosphoric acid isolation result in CNCs with surface sulfate or phosphate groups (negatively charged) that allow them to form stable electrostatically stabilized colloidal suspensions in aqueous solutions.

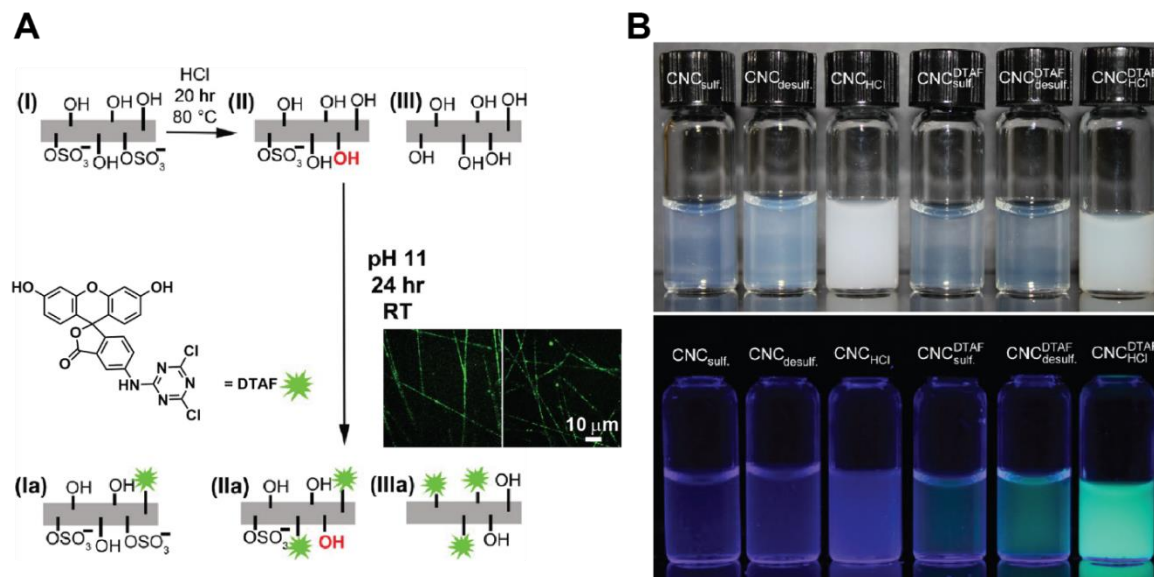


**Figure 1.11:** Schematic representation of cellulose microfibrils (a) Acid hydrolysis targeting the disordered regions (b) Surface chemistries of various isolated CNCs after acid hydrolysis.

Yet, these particles are still unstable in all other polar and organic solvents. The ability to disperse CNCs in polar and non-polar solvents remains the biggest challenge for their widespread utilization. To address this bottleneck and extend the range of applications of CNCs, there have been significant efforts to tune their surface functionality through a variety of covalent modifications, including triazinyl scaffolds.

The first reported application of triazinyl chemistry to modify CNCs was the grafting of DTAF to render them fluorescent by Abitbol and colleagues.<sup>170</sup> In this study, the effect of surface charge on the colloidal stability of DTAF-CNCs in aqueous suspensions and on the degree of fluorescent labeling were evaluated. The use of three CNC samples containing different sulfate contents, based on their pre-and post-isolation treatments, showed that increased negative charge lowered the degree of labeling (Figure 1.12). As expected, colloidal stability was better with higher sulfate contents and was seen to improve with labeling, which reduced the agglomeration of uncharged CNCs (isolated using HCl). These materials were proposed as suitable tracers to evaluate the dispersion of CNCs within hydrophilic polymer composites. As a proof of concept, DTAF-CNCs were doped into aqueous polyvinyl alcohol solutions that were electrospun into microfibers. These exhibited uniform fluorescence, indicating the uniform dispersion of the nanoparticles within the polymer matrix.

Subsequent work by the groups of Cranston and Johnston have used DTAF-labeled CNCs to visualize their distribution at the interface of emulsions<sup>171</sup> and emulsion gels,<sup>172</sup> and to assess the fluorescence stability and labeling efficiency compared to other linking chemistries.<sup>173</sup> In an approach similar to that used for DTAF labeling, AlexaFluor-546 dyes have been modified to contain a monochloro-triazine linker that facilitates the grafting of this dye onto the surface of CNCs.<sup>174</sup> At 1% labeling of the total glucose monomers, fluorescently-labeled CNCs could be spatially localized within microfluidic structures containing homogeneous or heterogeneous porous networks. Solid nanocellulose deposits formed within these networks were then used to visualize the depolymerization of the crystalline cellulose by commercial Celluclast enzyme cocktails, as well as by *Flavobacterium johnsoniae* and *Cytophaga hutchinsonii* bacteria. To date, fluorescent CNCs remain one of the simplest and most direct methods to evaluate the distribution of the nanoparticles within solid, liquid or hydrogel composites, where their reinforcing or stabilizing properties depend on uniform dispersions and reduced aggregation.



**Figure 1.12:** (A) Schematic representation of the DTAF labeling reaction of CNC samples with different surface charge densities: (I) sulfated CNCs (CNC<sub>sulf.</sub>), (II) partially desulfated CNCs (CNC<sub>desulf.</sub>), and (III) unchanged CNCs (CNC<sub>HCl</sub>), and their labeled counterparts (Ia), (IIa), and (IIIa) (B) Ambient light (top) and UV-light (bottom) photographs of initial CNC suspensions and corresponding labeled materials showing improved colloidal stability. Inset shows epifluorescence images of electrospun PVA fibers loaded with DTAF-labeled CNCs homogeneously dispersed within the polymer matrix. Modified with permission from ref 170. Copyright 2013 American Chemical Society.

As recent labeling of azido-Cy5 dyes onto alkyne-triazinyl modified CNCs<sup>175</sup> were used to study the biodistribution and fate of the nanoparticles after being subcutaneously injected into mice either as aqueous solutions or entrapped within CNC-(poly(oligoethylene glycol methacrylate), POEGMA) composite hydrogels. A large initial fluorescence intensity was seen at the site of injection, which persisted over the 28 days of the experiment with some spreading observed in the surrounding subcutaneous space for CNCs injected in aqueous solution. While the analysis of the CNC biodistribution in sacrificed mice over the duration

of the study showed normal nanoparticle clearance with the mass of the hydrogel and concentration of CNCs at the site of injection decreasing over time, but no partitioning to typical nanoparticle clearance organs.

Over the past few years, the use of triazinyl linkers to convey functionality to CNCs has increased significantly, with a number of groups reporting new applications. For example, dodecylamine-modified CNCs (CNC-TCT-DA) have been used as a reinforcing filler for polylactic acid (PLA) bionanocomposites.<sup>176</sup> The triazinyl modification not only increased the compatibility of CNCs with PLA but also improved their thermal stability. The increased interfacial adhesion and polar interactions between PLA chains and CNC-TCT-DA significantly improved the mechanical properties of PLA-CNC composites, where the stress and elongation at break of 1% CNC-TCT-DA doped PLA composites was doubled. In another application, cyanuric chloride has been used as a linker to graft N-halamine to CNCs to produce nanoparticles with excellent biocidal properties.<sup>177</sup> The covalent attachment of 1-hydroxymethyl-5,5-dimethylhydantoin (HDH) onto CNCs followed by chlorination yielded the biocidal nanoparticles (CNC-HDH-Cl), which were mixed with chitosan (CS) and polyvinyl alcohol (PVA) solutions to prepare antibacterial films. Films with 90/10 PVA/CS containing 7 wt% loading of CNC-HDH-Cl exhibited significantly enhanced tensile strength and demonstrated excellent antibacterial efficacy against *S. aureus* and *E. coli* O157:H7, with 6-logs reductions within the contact time of 5 mins. *In vitro* testing showed that the antibacterial films have excellent cytocompatibility towards NIH 3T3 fibroblasts, which suggests their potential use in biomedical and packaging applications.

Similarly,  $\beta$ -cyclodextrin ( $\beta$ -CD) has been grafted onto CNCs using triazine linkers.<sup>178</sup> CD-modified CNCs have been used to bind surfactants (Triton X-100, sodium dodecyl sulfate – SDS, and hexadecyl-trimethylammonium bromide – CTAB) at concentrations below and above their critical micelle concentration (CMC).<sup>179</sup> In this study, the authors found that, at concentrations below the CMC, the formation of CD-SDS inclusion complexes induced the aggregation of SDS-bound CD-CNCs. This behavior was mediated by hydrophobic interactions between the free and partially bound alkyl chains of SDS and disappeared at

higher SDS concentrations. On the other hand, the aggregation of CTAB-bound CD-CNCs could not be avoided, even at concentrations above the CMC. CD-modified CNCs could be incorporated into a variety of hydrogels and other nano-biocomposites to improve the encapsulation and delivery of active compounds in biomedical sciences. These examples, while not exhaustive, show that the availability of CNCs with tunable surface functionalities could open the doors for new applications, given that the compatibility of the triazine-modified CNCs with organic and polar solvents and their reactivity should allow them to be dispersed in and crosslinked to a wide range of polymeric matrices.

## **1.6 Summary and future outlook of triazinyl modification of cellulosic materials**

Given the relevance of the triazinyl chemistry towards the chemical modification of cellulose, many of the material examples described above were developed to add value to macroscopic cellulose fibers and products, such as improving color fastness and shades, or adding flame retardant and antibacterial properties to woven materials for the textile industry. The demonstrated versatility of the triazinyl chemistry holds tremendous promise for the chemical modification of new forms of cellulose and their application in the development of advanced materials

Recent developments have focused on the application of triazinyl chemistry to nanoscale forms of cellulose. These have probed fundamental questions like the impact of crystallinity on the depolymerization of cellulose microfibrils, how cellulases interact with cellulose, or the cytotoxicity and distribution of cellulose nanocrystals. While these applications have provided useful insight into the mechanisms of enzymes and how cellulose nanoparticles are processed in the body, the area where triazinyl chemistry promises to have the largest impact is in controlling the interfacial properties and reactivity of cellulosic materials, and nanocellulose in particular.

There is increasing interest, as evidenced by a large body of work in the literature, in using nanocellulose to tune the structural and functional properties of existing polymer systems



to develop environmentally friendly nanocomposites that can replace petroleum-based materials. Thus, there is an ongoing quest for versatile and cost-effective surface modification approaches to control the interfacial chemistry of nanocellulose and drive cost down for commercial applications. In this context, the grafting of various classes of small molecules or polymer chains onto nanocellulose using cyanuric chloride as a modular linker can be achieved strategically. Creating a library of nanocelluloses grafted with a variety of triazinyl-linked surface functionalities that can be used either as standalone components or as building blocks for secondary modifications via orthogonal chemistries.

There are a number of areas that have not yet been explored where nanocellulose modified with the triazinyl chemistry could be of advantage. This is particularly true in biomedical applications, where the attachment of various classes of biologically active molecules or drugs onto nanocellulose will result in a new class of biocompatible drug delivery vehicles. The surface functionality of nanocellulose could be tuned to enable the on-demand triggered release of repeated and controlled doses of sequestered drugs at targeted sites. These efforts could be aided by the reactivity of triazine chemistry towards nucleophilic substitution where amino-, hydroxy- and thiol-containing drugs with poor bioavailability could be grafted onto hydrophilic nanocellulose. However, efforts in this direction and the knowledge about the long-term biological fate of such nanoscale systems is still lacking and would require further assessment.

Similarly, the synthesis of new triazinyl derivatives amenable to phase-transfer modification of nanocellulose materials is of considerable interest. These methodologies would enable the uniform dispersion of cellulose nanocrystals in aqueous solutions and their partitioning into the second, non-miscible, phase once the functionalities have been grafted. We foresee this will result in better dispersions of modified CNCs in solvents that are not compatible with the native nanocrystals. Additionally, phase-transfer could translate into green methodologies for the production of modified CNCs with a range of polarities that make them compatible and dispersible in a range of polymer matrices suited for large scale nanocomposite processing.

Finally, the incorporation of reactive functionalities onto triazinyl derivatives that allow the modification of nanocellulose post-grafting of triazines remains largely unexplored. This is an attractive route to create cross-linkable nanocellulose structures with tunable mechanical properties and surface functionalities. These could find application in the development of printable materials, hierarchical scaffolds or hydrogels for tissue engineering, cell or drug encapsulation. With the commercial availability of nanocellulose and potential synthesis of a wide gamut of heterofunctional triazinyl derivatives, we anticipate ongoing work will open new application areas in printable electronics, bioremediation, biomedical and packaging materials.

## 1.7 Thesis Focus (I, II)

Given the increasing interest in the use of modified cellulose in consumer products, key priorities when modifying cellulose at large scales are that the chemistries used are cost-effective and that they don't involve processes that are complex. The focus of **Chapter 2** in this thesis is to explore a cost-effective chemistry that is versatile and allows the installation of a broad range of functionalities onto nanocelluloses including cellulose nanocrystals/microfibrils while preserving their individual nature. Whereby it is hypothesized that the installation of both polar and nonpolar molecules that have affinity for organic solvents will improve the dispersion and compatibility of nanocelluloses with different solvents and matrices, and to render them reactive. This work focused on using cyanuric chloride as a versatile linker to graft aliphatic (C18), polymeric (oligo-polyethylene glycol), alkyne (propargyl) chains and aromatic rings (benzyl) onto nanocelluloses, including CNCs and BMCC. We observed that the crystallinity of all triazine-modified CNCs was preserved, while the thermal stability was slightly enhanced compared to unmodified nanoparticles. CNCs modified with different triazinyl derivatives also formed colloidal suspensions in chloroform, isopropanol, ethanol, and methanol, which were stable over periods of months. In addition, propargyl-modified BMCC was

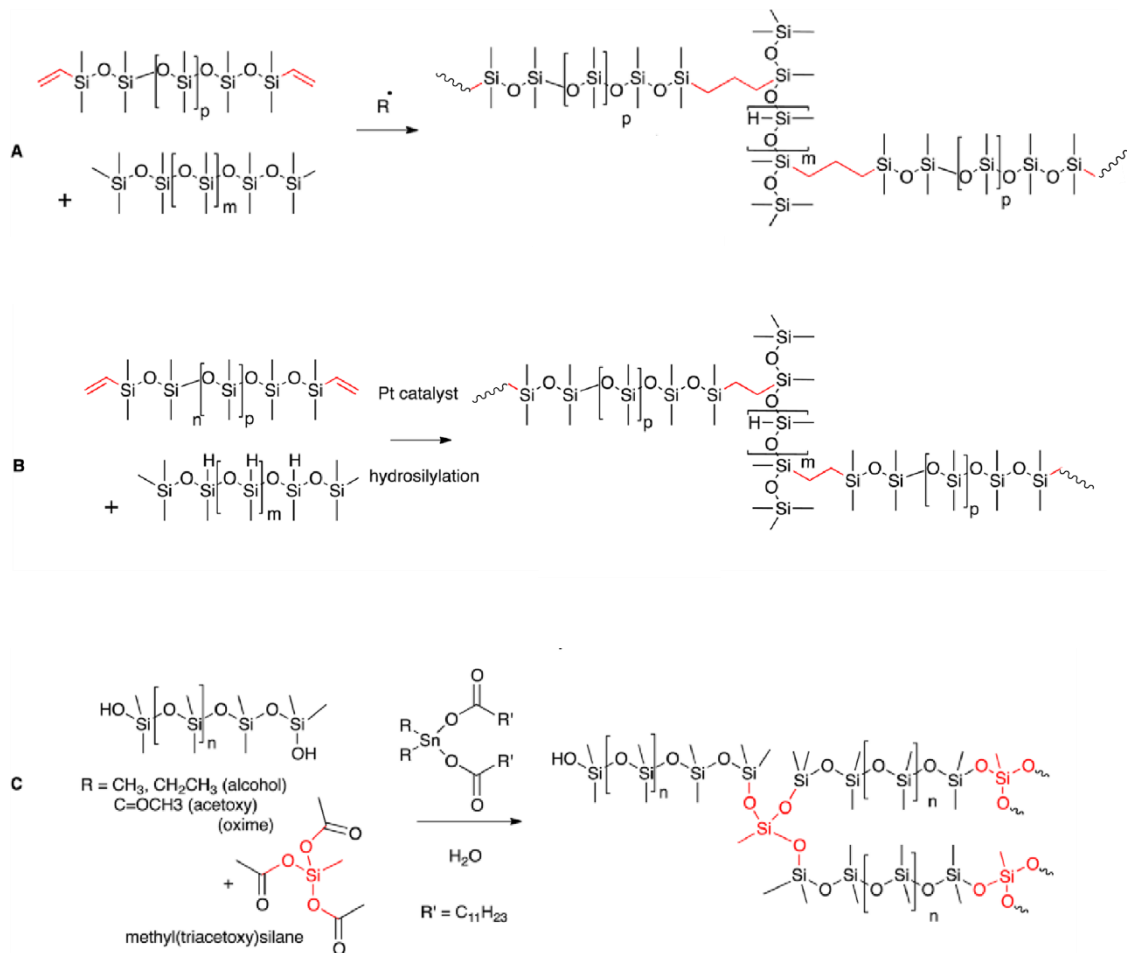
linked to an azido fluorescein dye via a copper-catalyzed Huisgen 1,3-dipolar cycloaddition reaction, demonstrating for the first time the production of triazinyl-based reactive nanocellulose.

In **Chapter 3**, I leveraged the versatility of the triazinyl chemistry to generate a colorimetric and fluorescent cellulose-based chemosensor for selective detection of heavy metals in water. The use of cyanuric chloride as a covalent linker to install pegylated rhodamine Schiff bases onto cellulose filter paper was explored. The factors required to create on demand selectivity and sensitivity towards specific heavy metals was determined. This resulted into the detection of  $\text{Cu}^{2+}$  and  $\text{Hg}^{2+}$  ions in 100% aqueous environment within 5 seconds of contact with 6.3 ppb and 20 ppb as the limit of colorimetric detection respectively. Thus, the use of triazinyl chemistry to install hydrophilic chemical probes onto cellulose creates a unique paper-based lab-on-a-molecule system, which may have use in many applications, including heavy metal sensing and sequestering for biomedical and environmental diagnostics.

## **1.8 The case for alternative silicone crosslink technology**

Silicones and silicone rubbers are widely used in household and industrial products such as lubricants, coatings, sealants, insulators, biomedical devices, cosmetics etc., due to the unique properties they possess which are largely unmatched by their hydrocarbon analogues including low surface energy, low Tg, high thermal stability, chemical inertness, viscoelasticity and biocompatibility.<sup>180</sup> Commercially, 3D silicone network-formation processes have been carried out using three major technologies (Figure 1.13): radical cure under thermal conditioning of silicone oils or vinyl-modified silicone oils; condensation crosslinking of telechelic silanol polymers with moisture sensitive organo-multifunctional silanes (often referred to as room temperature vulcanization-RTV); and hydrosilylation cure between HSi- and vinyl-modified silicones mostly at elevated temperature (or at room temperature, also called RTV) to give a two carbon spacer between silicone chains.<sup>181</sup> As

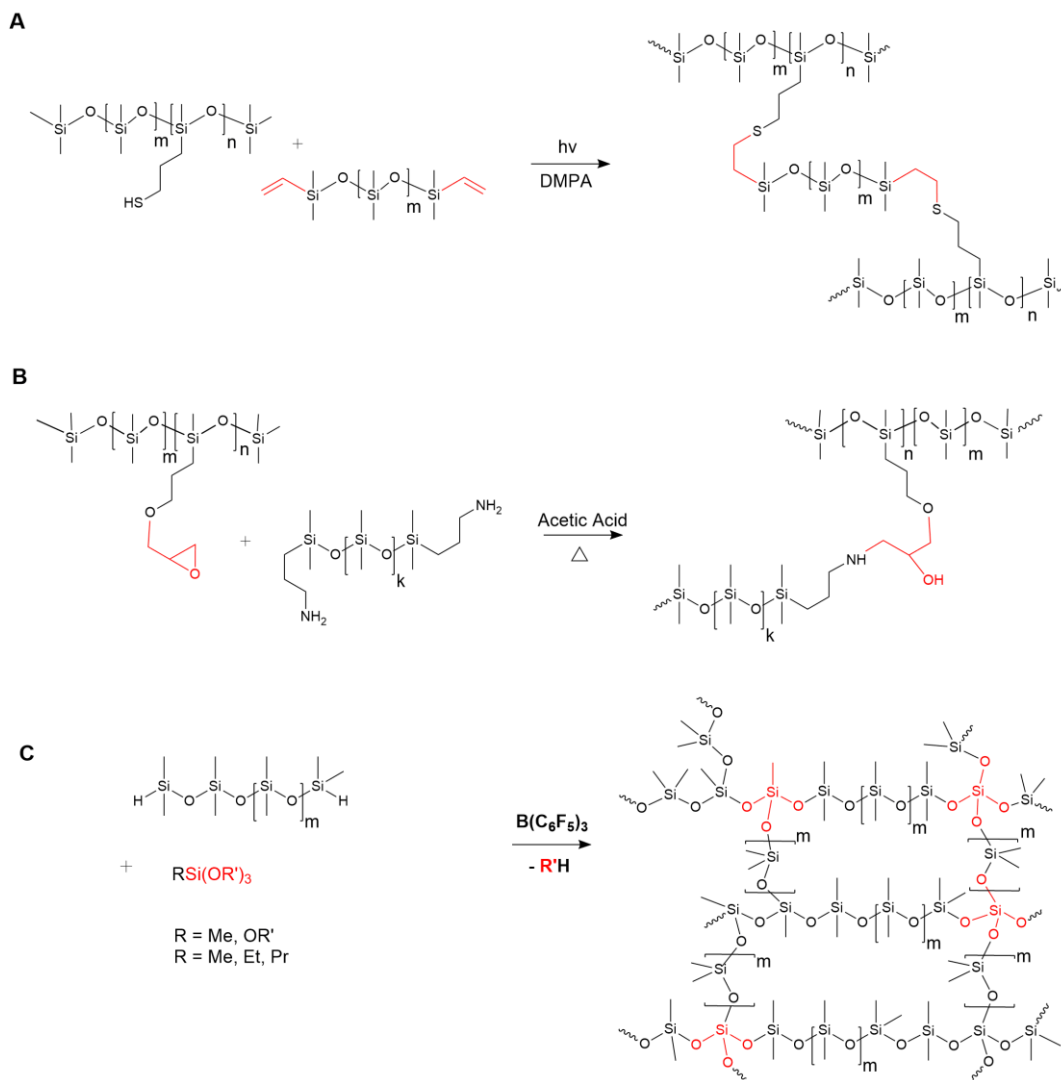
much as these cure technologies have been widely used for large scale processing of silicone elastomers, they all require catalysts. For example, peroxides<sup>182</sup> are used in radical cure, tin or titanium<sup>183,184</sup>-derived catalysts for RTV(moisture) cure and precious metals like platinum, rhodium or palladium in addition to non-precious metals (Fe or Ni) have been used in hydrosilylation cure.<sup>185,186</sup>



**Figure 1.13:** Schematic representation of commercial cure strategies for silicones.

Over the years, the use of these catalysts has been shown to carry with it significant challenges in the removal of unreacted, spent or catalyst by-products from elastomer

postproduction. Of particular concern is leaching and the environmental fate of the catalysts upon release from the products, with a primary example being the well-known toxicity of tin catalysts.<sup>187</sup>

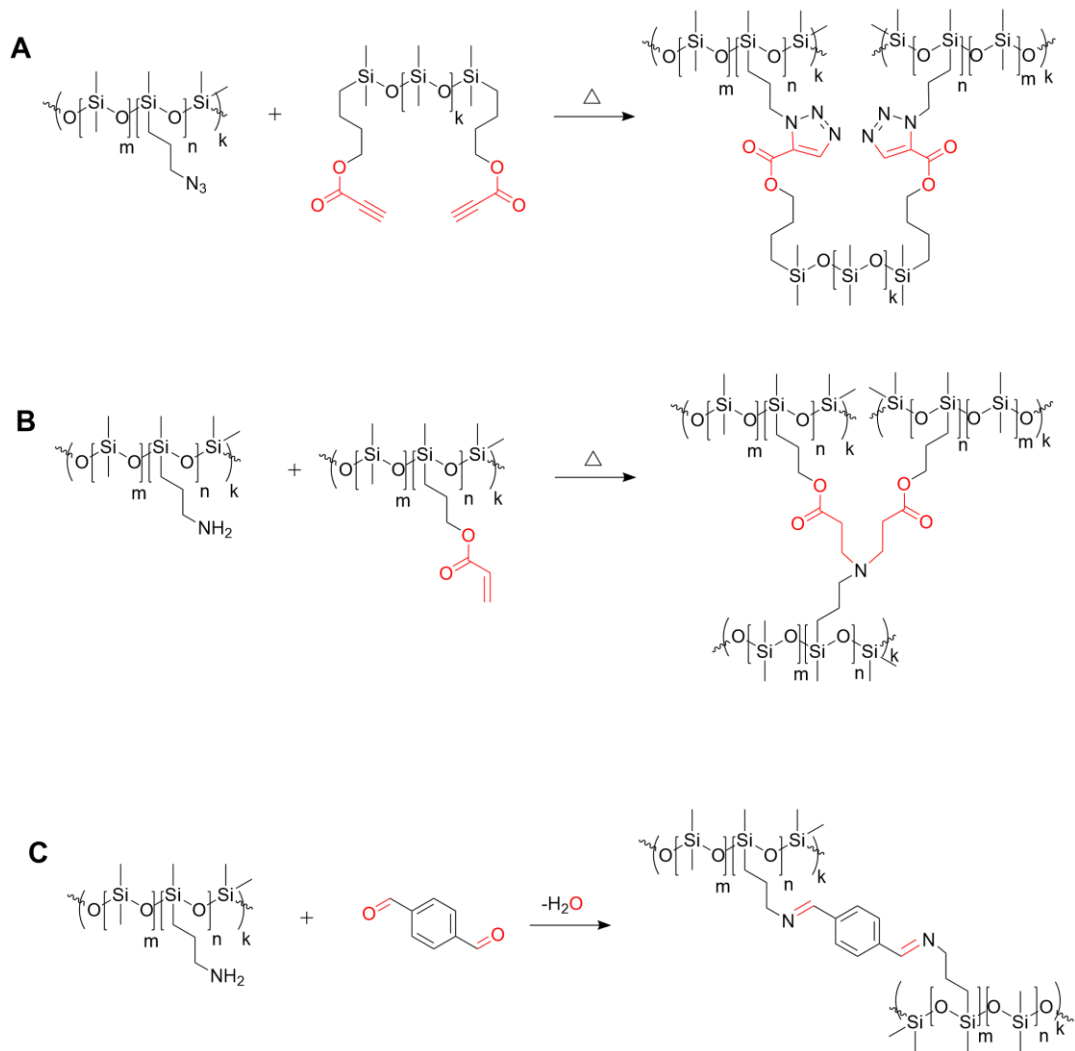


**Figure 1.14:** Schematic representation of catalyzed organic cure strategies for silicones.

Other concerns include the expensive nature of some of these catalysts, as in the case of platinum, and the poisoning of catalysts due to their functional group intolerance in starting materials, leading to premature deactivation and shelf-life limitations.<sup>180</sup> Consequently, a

series of curing strategies based on organic reactions have been developed, aimed at avoiding or reducing the use of conventional catalysts. The majority of these still require non-metal catalysts (Figure 1.14), as radical photoinitiators are used in the case of thiolene<sup>188</sup> and acrylate<sup>189,190</sup> silicone formulations, while acid and base have been utilized in epoxy<sup>191</sup> and isocyanate<sup>192</sup> curing chemistries.

The Piers–Rubinsztajn (Lewis acid boron catalyzed) condensation reaction has been successfully used to make silicone elastomers with well-defined 3D polymer networks.<sup>193</sup> Unfortunately, this chemistry is sensitive to moisture (used as an advantage in living polymerization of hydrosiloxanes<sup>194</sup>) and releases volatiles (typically ethanol, methane or hydrogen gas), that can result in technical and/or safety issues if used on large scale.



**Figure 1.15:** Schematic representation of catalyst free organic cure strategies for silicones.

Alternatively, by taking advantage of organic chemistry to further enhance silicone reactivity, catalyst free systems have been developed. These present greener routes to silicone crosslinking and have allowed the independent manipulation of elastomer properties (Figure 1:15). For example, the Huisgen reaction at high temperature has been used to assemble hybrid silicone elastomers of tunable wettability for low protein fouling applications.<sup>195</sup> Similar hybrid silicones have been entrapped at the surface of silicone elastomers for the fabrication of self-wetting microfluidic devices for bioanalytical

Ayodele Fatona – Ph.D. Thesis McMaster University – Chemistry and Chemical Biology applications.<sup>196</sup> Other chemistries including Dier-Alder<sup>197</sup> and Schiff-base<sup>198</sup> reactions have been used in making thermoplastic silicone elastomers with self-healing capabilities to facilitate the recycling and repurposing of silicones. The aza-Michael reaction also benefits from mild conditions such as no metallic catalyst, no solvent, low temperatures and high yields with no by-product formation.<sup>199</sup> However, the requirement for cost effective processes, reactions with predictable outcomes especially in aza-Michael and the lack of commercially available modified silicone precursors highlights the need to develop alternative catalyst-free silicone crosslinking systems. These should make use of low cost and readily available starting materials, use reactions that are easy to control, and provide elastomers that have properties that are similar to those of traditional silicones.

## 1.9 Thesis Focus (III, IV)

The incorporation of covalent crosslinks between silicone polymer chains leads to subtle changes in material properties. One way to effect such changes is the use of new silicone crosslinking strategies dependent on organic reactions, where the introduction of functionalities can provide a means for both silicone polymer property optimization and reactivity. There could be many advantages associated with combining silicones with organic chemistry, such as physical crosslinks from  $\pi$ -interaction or nucleophilic substitution reaction which would allow the independent manipulation of elastomer properties. **Chapter 4** introduces triazinyl chemistry as a catalyst free, greener and more cost-effective cure technology for making elastomers from aminosilicones. This work describes amino-triazinyl silicone networks, which are readily formed between commercially available aminopropyl silicones and cyanuric chloride or its synthesized, premodified tetrachloro-triazinyl silicone analog without the use of catalyst, optionally in the presence of a solvent. The presence of residual amines and the type of residual amines were utilized to independently manipulate elastomer properties. As the self-neutralizing ability of available amines for the HCl byproduct made it possible to tailor silicone mechanical properties from very soft gels to much more rigid elastomers. In addition, the



neutralization facilitates the maintainance of stability of the products against hydrolytic and thermal oxidative stress. The ability to control the specific concentration of crosslinks between silicone polymers, at any time, to afford novel materials with unique properties was explored. The use of chemoselective nucleophilic aromatic substitution reaction of readily available chloro-s-triazines as an alternative organic cure for aminosilicones provided an attractive route to greener and cost-effective silicone elastomers.

**Chapter 5** examines covalently crosslinked silicone networks using a novel thioacetalization reaction to create a variety of functional silicone materials. Dithioacetal silicone networks were formed between readily available aromatic aldehydes and thiopropylsilicones in the presence of a catalytic amount of toluene sulfonic acid. This chapter describes the unprecedented stability of the resulting products despite the presence of acid trapped within the polymer networks, which is contrary to the general experience of silicone depolymerization under acidic conditions. While the oxidative stress resistant of such dithioacetal silicone networks is another surprising outcome of the cure chemistry. In addition, to the synergistic effect between the covalent crosslinks and the physical interactions provided by aryl association in the thioacetal-crosslinked silicone shown to lead to materials with improved mechanical properties and stability. Therefore, the use of thioacetalization reaction as an alternative organic cure for thiopropylsilicones results into cost-effective elastomers with advanced modulus while avoiding the need for heavy metal catalysts.

### **1.10 The interfacial control of silicones**

Poly(dimethylsiloxane) (PDMS) has been widely used as a soft elastomer material for the cost-effective prototyping of microfluidic channels for Lab-on-a-Chip and micro total analysis system applications. The hydrophobic nature of silicones has been considered a disadvantage, especially when used for biomedical applications. In particular, the hydrophobicity of PDMS prevents aqueous solutions from filling micron-sized channels

resulting into sample loss,<sup>200</sup> and promotes the non-specific adsorption of proteins<sup>201</sup> leading to biofouling. Additionally, the tethering of tubes to externally powered pumps and micro valves makes microfluidic device fabrication and operation complicated, which limits their use as they cannot be deployed as independent hand-held devices. Therefore, the controlled surface modification of silicone elastomers to make them more hydrophilic without changing their bulk properties has been widely used in the development of Lab-on-a-Chip system for biomedical applications.<sup>202–206</sup>

Surface-active molecules, such as surfactants, amphiphilic copolymers or charged polymers, have been used as dynamic coatings that can be deposited in situ onto PDMS surfaces through hydrogen bonding or hydrophobic-hydrophilic interactions. In particular, the addition of surfactants to silicone prepolymer mixtures prior to cure allows tuning of the interfacial properties of the elastomers and can result in significant improvements in wettability. For example, in the work of Yao and Fang<sup>207</sup> PDMS prepolymer mixture was blended with PDMS-b-PEO surfactant to create hydrophilic microfluidic devices having controlled water contact angles ranging from 21.5 - 80.9°. Another method by Yu and Han<sup>208</sup> utilized a solvent swelling process to create openings within cured elastomers through which the hydrophobic tail of a PDMS-b-PEO surfactant could interact with the PDMS elastomer network. Upon deswelling, the surfactant was trapped forming a tethered layer of hydrophilic molecules at the silicone-air interface shown to be stable when treated with water over 16 h.

However, despite the myriad of strategies for PDMS surface modification, one of the key challenges is the stability of the modified surface which undergoes the process of hydrophobic recovery often referred to as surface reversion. From the standpoint of PDMS being an elastomer polymer, there is the ability of PDMS chains with low  $T_g$  value (~ -120 °C) and low surface energy to migrate past any form of hydrophilic groups introduced at its surface to get to the air interface where it is favored thermodynamically.<sup>205</sup> Migration of both tethered and free oligomer chains bury the functional/hydrophilic layer and this lead to surface loss over time. While challenges of reproducibility<sup>209</sup>, modification spatial resolution<sup>209</sup>, non-homogeneity<sup>209</sup>, surface defects<sup>205,210–212</sup> and loss of optical

Ayodele Fatona – Ph.D. Thesis McMaster University – Chemistry and Chemical Biology  
transparency<sup>205,207,208,210–212</sup> still remains unaddressed in literature and most of these strategies are difficult to carry out within a microfluidic channels hence limits PDMS LOC commercialization applications. This stands as the motivation for Chapter 6 and highlights its importance.

### **1.11 Thesis Focus (V)**

**Chapter 6** describes a new method for tuning the interfacial properties of silicone elastomers using a series of surfactants with different chemical properties. This method used thin films of ionic and non-ionic surfactants patterned on moulds, onto which a silicone pre-polymer mixture was cast. The subsequent curing of the elastomer entrapped the surfactants at the PDMS interface. This method allows us to directly compare small molecule and block copolymer surfactant modifications on PDMS surfaces. It was determined that while all surfactants tested could render PDMS surfaces hydrophilic, only those modified with silicone-based triblock copolymer surfactants capped with small hydrophobes were stable over two wetting cycles. In a proof-of-concept experiment, the in-mould modification approach was further used to fabricate self-driven microfluidic devices that exhibited steady capillary flow rates that could be tuned by changing the device geometry. The key contributions from this work are: (i) a one-step method to achieve spatially controlled modification of PDMS surfaces, (ii) a thorough characterization that compares the performance of a variety of surfactants with the one-step modification method, (iii) the demonstration of the applicability of the method to produce microfluidic devices that can be filled by capillarity alone.

## 1.12 Reference

- (1) Zhao, H.; Kwak, J. H.; Conrad Zhang, Z.; Brown, H. M.; Arey, B. W.; Holladay, J. E. Studying Cellulose Fiber Structure by SEM, XRD, NMR and Acid Hydrolysis. *Carbohydrate Polymers* **2007**, *68* (2), 235–241.
- (2) Moon, R. J.; Martini, A.; Nairn, J.; Simonsen, J.; Youngblood, J. Cellulose Nanomaterials Review: Structure, Properties and Nanocomposites. *Chem. Soc. Rev.* **2011**, *40* (7), 3941–3994.
- (3) Nishiyama, Y. Structure and Properties of the Cellulose Microfibril. *J Wood Sci* **2009**, *55* (4), 241–249.
- (4) O’SULLIVAN, A. C. Cellulose: The Structure Slowly Unravels. *Cellulose* **1997**, *4* (3), 173–207.
- (5) Klemm, D.; Heublein, B.; Fink, H.-P.; Bohn, A. Cellulose: Fascinating Biopolymer and Sustainable Raw Material. *Angewandte Chemie International Edition* **2005**, *44* (22), 3358–3393.
- (6) Azizi Samir, M. A. S.; Alloin, F.; Dufresne, A. Review of Recent Research into Cellulosic Whiskers, Their Properties and Their Application in Nanocomposite Field. *Biomacromolecules* **2005**, *6* (2), 612–626.
- (7) Habibi, Y.; Lucia, L. A.; Rojas, O. J. Cellulose Nanocrystals: Chemistry, Self-Assembly, and Applications. *Chem. Rev.* **2010**, *110* (6), 3479–3500.
- (8) Yamamoto, H.; Horn, F. In Situ Crystallization of Bacterial Cellulose I. Influences of Polymeric Additives, Stirring and Temperature on the Formation Celluloses I $\alpha$  and I $\beta$ s Revealed by Cross Polarization/Magic Angle Spinning (CP/MAS)<sup>13</sup>C NMR Spectroscopy. *Cellulose* **1994**, *1* (1), 57–66.

- (9) Belton, P. S.; Tanner, S. F.; Cartier, N.; Chanzy, H. High-Resolution Solid-State Carbon-13 Nuclear Magnetic Resonance Spectroscopy of Tunicin, an Animal Cellulose. *Macromolecules* **1989**, *22* (4), 1615–1617.
- (10) Horii, F.; Hirai, A.; Kitamaru, R. CP/MAS Carbon-13 NMR Spectra of the Crystalline Components of Native Celluloses. *Macromolecules* **1987**, *20* (9), 2117–2120.
- (11) Watanabe, A.; Morita, S.; Ozaki, Y. Temperature-Dependent Changes in Hydrogen Bonds in Cellulose I $\alpha$  Studied by Infrared Spectroscopy in Combination with Perturbation-Correlation Moving-Window Two-Dimensional Correlation Spectroscopy: Comparison with Cellulose I $\beta$ . *Biomacromolecules* **2007**, *8* (9), 2969–2975.
- (12) Debzi, E. M.; Chanzy, H.; Sugiyama, J.; Tekely, P.; Excoffier, G. The I $\alpha$   $\rightarrow$  I $\beta$  Transformation of Highly Crystalline Cellulose by Annealing in Various Mediums. *Macromolecules* **1991**, *24* (26), 6816–6822.
- (13) Eyley, S.; Thielemans, W. Surface Modification of Cellulose Nanocrystals. *Nanoscale* **2014**, *6* (14), 7764–7779.
- (14) Pérez, S.; Samain, D. Structure and Engineering of Celluloses. In *Advances in Carbohydrate Chemistry and Biochemistry*; Horton, D., Ed.; Academic Press, 2010; Vol. 64, pp 25–116.
- (15) Bunton, C. A.; Shiner, V. J. 321. Periodate Oxidation of 1,2-Diols, Diketones, and Hydroxy-Ketones: The Use of Oxygen-18 as a Tracer. *J. Chem. Soc.* **1960**, No. 0, 1593–1598.
- (16) Zhao, B.; Brittain, W. J. Polymer Brushes: Surface-Immobilized Macromolecules. *Progress in Polymer Science* **2000**, *25* (5), 677–710.
- (17) Habibi, Y.; Dufresne, A. Highly Filled Bionanocomposites from Functionalized Polysaccharide Nanocrystals. *Biomacromolecules* **2008**, *9* (7), 1974–1980.

- (18) Siqueira, G.; Bras, J.; Dufresne, A. Cellulose Whiskers versus Microfibrils: Influence of the Nature of the Nanoparticle and Its Surface Functionalization on the Thermal and Mechanical Properties of Nanocomposites. *Biomacromolecules* **2009**, *10* (2), 425–432.
- (19) Shang, W.; Huang, J.; Luo, H.; Chang, P. R.; Feng, J.; Xie, G. Hydrophobic Modification of Cellulose Nanocrystal via Covalently Grafting of Castor Oil. *Cellulose* **2013**, *20* (1), 179–190.
- (20) Mangalam, A. P.; Simonsen, J.; Benight, A. S. Cellulose/DNA Hybrid Nanomaterials. *Biomacromolecules* **2009**, *10* (3), 497–504.
- (21) Harrison, S.; Drisko, G. L.; Malmström, E.; Hult, A.; Wooley, K. L. Hybrid Rigid/Soft and Biologic/Synthetic Materials: Polymers Grafted onto Cellulose Microcrystals. *Biomacromolecules* **2011**, *12* (4), 1214–1223.
- (22) Azzam, F.; Heux, L.; Putaux, J.-L.; Jean, B. Preparation By Grafting Onto, Characterization, and Properties of Thermally Responsive Polymer-Decorated Cellulose Nanocrystals. *Biomacromolecules* **2010**, *11* (12), 3652–3659.
- (23) Araki, J.; Wada, M.; Kuga, S. Steric Stabilization of a Cellulose Microcrystal Suspension by Poly(Ethylene Glycol) Grafting. *Langmuir* **2001**, *17* (1), 21–27.
- (24) Ljungberg, N.; Bonini, C.; Bortolussi, F.; Boisson, C.; Heux, L.; Cavaillé. New Nanocomposite Materials Reinforced with Cellulose Whiskers in Atactic Polypropylene: Effect of Surface and Dispersion Characteristics. *Biomacromolecules* **2005**, *6* (5), 2732–2739.
- (25) Habibi, Y.; Goffin, A.-L.; Schiltz, N.; Duquesne, E.; Dubois, P.; Dufresne, A. Bionanocomposites Based on Poly( $\epsilon$ -Caprolactone)-Grafted Cellulose Nanocrystals by Ring-Opening Polymerization. *J. Mater. Chem.* **2008**, *18* (41), 5002–5010.

- (26) Labet, M.; Thielemans, W. Citric Acid as a Benign Alternative to Metal Catalysts for the Production of Cellulose-Grafted-Polycaprolactone Copolymers. *Polym. Chem.* **2012**, *3* (3), 679–684.
- (27) Yi, J.; Xu, Q.; Zhang, X.; Zhang, H. Chiral-Nematic Self-Ordering of Rodlike Cellulose Nanocrystals Grafted with Poly(Styrene) in Both Thermotropic and Lyotropic States. *Polymer* **2008**, *49* (20), 4406–4412.
- (28) Xu, Q.; Yi, J.; Zhang, X.; Zhang, H. A Novel Amphotropic Polymer Based on Cellulose Nanocrystals Grafted with Azo Polymers. *European Polymer Journal* **2008**, *44* (9), 2830–2837.
- (29) Morandi, G.; Heath, L.; Thielemans, W. Cellulose Nanocrystals Grafted with Polystyrene Chains through Surface-Initiated Atom Transfer Radical Polymerization (SI-ATRP). *Langmuir* **2009**, *25* (14), 8280–8286.
- (30) Kan, K. H. M.; Li, J.; Wijesekera, K.; Cranston, E. D. Polymer-Grafted Cellulose Nanocrystals as PH-Responsive Reversible Flocculants. *Biomacromolecules* **2013**, *14* (9), 3130–3139.
- (31) Kloser, E.; Gray, D. G. Surface Grafting of Cellulose Nanocrystals with Poly(Ethylene Oxide) in Aqueous Media. *Langmuir* **2010**, *26* (16), 13450–13456.
- (32) Zhang, C.; Salick, M. R.; Cordie, T. M.; Ellingham, T.; Dan, Y.; Turng, L. S. Incorporation of Poly(Ethylene Glycol) Grafted Cellulose Nanocrystals in Poly(Lactic Acid) Electrospun Nanocomposite Fibers as Potential Scaffolds for Bone Tissue Engineering. *Mater Sci Eng C Mater Biol Appl* **2015**, *49*, 463–471.
- (33) Katritzky, A. R.; Rees, C. W. Introduction. In *Comprehensive Heterocyclic Chemistry*; Katritzky, A. R., Rees, C. W., Eds.; Pergamon: Oxford, 1984; pp 1–6.

- (34) Scheele, C. W. *Sämmtliche physische und chemische Werke*; Hermbstädt, S. F., Ed.; Mayer & Müller: Berlin, 1793; Vol. II.
- (35) von Angerer, S. 1,3,5-Triazines and Phosphorus Analogues. In *Category 2, Heteroarenes and Related Ring Systems*; Weinreb, S. M., Schaumann, E., Eds.; Science of Synthesis; Georg Thieme Verlag: Stuttgart, 2004; Vol. 17.
- (36) Smolin, E. M.; Rapoport, L. *S-Triazines and Derivatives*; Interscience Publishers Inc: New York, 1959; Vol. 13.
- (37) Quirke, J. M. E. 1,3,5-Triazines. In *Comprehensive Heterocyclic Chemistry*; Katritzky, A. R., Rees, C. W., Eds.; Pergamon: Oxford, 1984; pp 457–530.
- (38) Crews, G. M.; Ripperger, W.; Kersebohm, D. B.; Güthner, T.; Mertschenk, B. Melamine and Guanamines. In *Ullmann's Encyclopedia of Industrial Chemistry*; Wiley-VCH: Weinheim, 2006.
- (39) Huthmacher, K.; Most, D. Cyanuric Acid and Cyanuric Chloride. In *Ullmann's Encyclopedia of Industrial Chemistry*; Wiley-VCH: Weinheim, 2000.
- (40) Blotny, G. Recent Applications of 2,4,6-Trichloro-1,3,5-Triazine and Its Derivatives in Organic Synthesis. *Tetrahedron* **2006**, 62 (41), 9507–9522.
- (41) Brunetti, H.; Lüthi, C. E. Die Synthese von Asymmetrisch Substituierten O-Hydroxyphenyl-s-Triazinen. *Helvetica Chimica Acta* **1972**, 55 (5), 1566–1595.
- (42) Shu, W.; Valiyaveetil, S. Intramolecular Hydrogen Bond Assisted Planarization and Self-Assembly of Simple Disc-Shaped Molecules in Mesophases. *Chem. Commun.* **2002**, 0 (13), 1350–1351.
- (43) Berger, D.; Wilhelm, P.; Neuenschwander, M. Synthese von Gestapelten 'Push-Pull'-Acetylenen. *Helvetica Chimica Acta* **1999**, 82 (3), 326–337.



- (44) Pitts, W. J.; Guo, J.; Dhar, T. G. M.; Shen, Z.; Gu, H. H.; Watterson, S. H.; Bednarz, M. S.; Chen, B.-C.; Barrish, J. C.; Bassolino, D.; et al. Rapid Synthesis of Triazine Inhibitors of Inosine Monophosphate Dehydrogenase. *Bioorganic & Medicinal Chemistry Letters* **2002**, *12* (16), 2137–2140.
- (45) Arvanitis, A. G.; Gilligan, P. J.; Chorvat, R. J.; Cheeseman, R. S.; Christos, T. E.; Bakthavatchalam, R.; Beck, J. P.; Cocuzza, A. J.; Hobbs, F. W.; Wilde, R. G.; et al. Non-Peptide Corticotropin-Releasing Hormone Antagonists: Syntheses and Structure–Activity Relationships of 2-Anilinopyrimidines and -Triazines. *J. Med. Chem.* **1999**, *42* (5), 805–818.
- (46) Menicagli, R.; Samaritani, S.; Gori, S. 2-(Alk-1'-Ynyl)-4,6-Dimethoxy-1,3,5-Triazines via Pd-Mediated Alkynylation of 2-Chloro-4,6-Dimethoxy-1,3,5-Triazine. *Tetrahedron Letters* **1999**, *40* (48), 8419–8422.
- (47) Menicagli, R.; Samaritani, S.; Signore, G.; Vaglini, F.; Dalla Via, L. In Vitro Cytotoxic Activities of 2-Alkyl-4,6-Diheteroalkyl-1,3,5-Triazines: New Molecules in Anticancer Research. *J. Med. Chem.* **2004**, *47* (19), 4649–4652.
- (48) Borovik, V. P.; Shkurko, O. P. Properties and Application of Aryl-Substituted Azines (Review). *Chem Heterocycl Compd* **1997**, *33* (8), 883–897.
- (49) Wong, M. Y.; Zysman-Colman, E. Purely Organic Thermally Activated Delayed Fluorescence Materials for Organic Light-Emitting Diodes. *Advanced Materials* **2017**, *29* (22), 1605444.
- (50) Endo, A.; Sato, K.; Yoshimura, K.; Kai, T.; Kawada, A.; Miyazaki, H.; Adachi, C. Efficient Up-Conversion of Triplet Excitons into a Singlet State and Its Application for Organic Light Emitting Diodes. *Appl. Phys. Lett.* **2011**, *98* (8), 083302.

- (51) Serevičius, T.; Nakagawa, T.; Kuo, M.-C.; Cheng, S.-H.; Wong, K.-T.; Chang, C.-H.; Kwong, R. C.; Xia, S.; Adachi, C. Enhanced Electroluminescence Based on Thermally Activated Delayed Fluorescence from a Carbazole–Triazine Derivative. *Phys. Chem. Chem. Phys.* **2013**, *15* (38), 15850–15855.
- (52) Kim, M.; Jeon, S. K.; Hwang, S.-H.; Lee, J. Y. Stable Blue Thermally Activated Delayed Fluorescent Organic Light-Emitting Diodes with Three Times Longer Lifetime than Phosphorescent Organic Light-Emitting Diodes. *Advanced Materials* **2015**, *27* (15), 2515–2520.
- (53) Tanaka, H.; Shizu, K.; Miyazaki, H.; Adachi, C. Efficient Green Thermally Activated Delayed Fluorescence (TADF) from a Phenoxazine–Triphenyltriazine (PXZ–TRZ) Derivative. *Chem. Commun.* **2012**, *48* (93), 11392–11394.
- (54) Tanaka, H.; Shizu, K.; Nakanotani, H.; Adachi, C. Dual Intramolecular Charge-Transfer Fluorescence Derived from a Phenothiazine-Triphenyltriazine Derivative. *J. Phys. Chem. C* **2014**, *118* (29), 15985–15994.
- (55) Shizu, K.; Uejima, M.; Nomura, H.; Sato, T.; Tanaka, K.; Kaji, H.; Adachi, C. Enhanced Electroluminescence from a Thermally Activated Delayed-Fluorescence Emitter by Suppressing Nonradiative Decay. *Phys. Rev. Applied* **2015**, *3* (1), 014001.
- (56) Hung, W.-Y.; Fang, G.-C.; Chang, Y.-C.; Kuo, T.-Y.; Chou, P.-T.; Lin, S.-W.; Wong, K.-T. Highly Efficient Bilayer Interface Exciplex For Yellow Organic Light-Emitting Diode. *ACS Appl. Mater. Interfaces* **2013**, *5* (15), 6826–6831.
- (57) Albrecht, K.; Matsuoka, K.; Fujita, K.; Yamamoto, K. Carbazole Dendrimers as Solution-Processable Thermally Activated Delayed-Fluorescence Materials. *Angewandte Chemie International Edition* **2015**, *54* (19), 5677–5682.

(58) Nikolaenko, A. E.; Cass, M.; Bourcet, F.; Mohamad, D.; Roberts, M. Thermally Activated Delayed Fluorescence in Polymers: A New Route toward Highly Efficient Solution Processable OLEDs. *Advanced Materials* **2015**, *27* (44), 7236–7240.

(59) Bojinov, V.; Grabchev, I. Synthesis and Application of New Combined 2,2,6,6-Tetramethylpiperidine–2-Hydroxybenzophenone 1,3,5-Triazine Derivatives as Photostabilizers for Polymer Materials. *Journal of Photochemistry and Photobiology A: Chemistry* **2002**, *146* (3), 199–205.

(60) Couteau, C.; Pommier, M.; Paparis, E.; Coiffard, L. J. M. Study of the efficacy of 18 sun filters authorized in European Union tested in vitro. *Pharmazie*. **2007**, *62* (6), 449-452.

(61) Chatelain, E.; Gabard, B. Photostabilization of Butyl Methoxydibenzoylmethane (Avobenzon) and Ethylhexyl Methoxycinnamate by Bis-Ethylhexyloxyphenol Methoxyphenyl Triazine (Tinosorb S), a New UV Broadband Filter¶. *Photochemistry and Photobiology* **2001**, *74* (3), 401–406.

(62) Furukawa, H.; Go, Y. B.; Ko, N.; Park, Y. K.; Uribe-Romo, F. J.; Kim, J.; O’Keeffe, M.; Yaghi, O. M. Isorecticular Expansion of Metal–Organic Frameworks with Triangular and Square Building Units and the Lowest Calculated Density for Porous Crystals. *Inorg. Chem.* **2011**, *50* (18), 9147–9152.

(63) Wang, X.-S.; Ma, S.; Sun, D.; Parkin, S.; Zhou, H.-C. A Mesoporous Metal–Organic Framework with Permanent Porosity. *J. Am. Chem. Soc.* **2006**, *128* (51), 16474–16475.

(64) Luebke, R.; Eubank, J. F.; Cairns, A. J.; Belmabkhout, Y.; Wojtas, L.; Eddaoudi, M. The Unique Rht-MOF Platform, Ideal for Pinpointing the Functionalization and CO<sub>2</sub> Adsorption Relationship. *Chem. Commun.* **2012**, *48* (10), 1455–1457.

- (65) Ma, S.; Sun, D.; Ambrogio, M.; Fillinger, J. A.; Parkin, S.; Zhou, H.-C. Framework-Catenation Isomerism in Metal–Organic Frameworks and Its Impact on Hydrogen Uptake. *J. Am. Chem. Soc.* **2007**, *129* (7), 1858–1859.
- (66) Wen, P.; Zhang, C.; Yang, Z.; Dong, R.; Wang, D.; Fan, M.; Wang, J. Triazine-Based Covalent–Organic Frameworks: A Novel Lubricant Additive with Excellent Tribological Performances. *Tribology International* **2017**, *111*, 57–65.
- (67) Chan-Thaw, C. E.; Villa, A.; Katekomol, P.; Su, D.; Thomas, A.; Prati, L. Covalent Triazine Framework as Catalytic Support for Liquid Phase Reaction. *Nano Lett.* **2010**, *10* (2), 537–541.
- (68) Lin, S.; Hou, Y.; Deng, X.; Wang, H.; Sun, S.; Zhang, X. A Triazine-Based Covalent Organic Framework/Palladium Hybrid for One-Pot Silicon-Based Cross-Coupling of Silanes and Aryl Iodides. *RSC Adv.* **2015**, *5* (51), 41017–41024.
- (69) Chang, F.; Guo, J.; Wu, G.; Liu, L.; Zhang, M.; He, T.; Wang, P.; Yu, P.; Chen, P. Covalent Triazine-Based Framework as an Efficient Catalyst Support for Ammonia Decomposition. *RSC Adv.* **2014**, *5* (5), 3605–3610.
- (70) Palkovits, R.; Antonietti, M.; Kuhn, P.; Thomas, A.; Schüth, F. Solid Catalysts for the Selective Low-Temperature Oxidation of Methane to Methanol. *Angewandte Chemie International Edition* **2009**, *48* (37), 6909–6912.
- (71) Busto, N.; Valladolid, J.; Martínez-Alonso, M.; Lozano, H. J.; Jalón, F. A.; Manzano, B. R.; Rodríguez, A. M.; Carrión, M. C.; Biver, T.; Leal, J. M.; et al. Anticancer Activity and DNA Binding of a Bifunctional Ru(II) Arene Aqua-Complex with the 2,4-Diamino-6-(2-Pyridyl)-1,3,5-Triazine Ligand. *Inorg. Chem.* **2013**, *52* (17), 9962–9974.

(72) Salimi, M.; Abdi, K.; Kandelous, H. M.; Hadadzadeh, H.; Azadmanesh, K.; Amanzadeh, A.; Sanati, H. Antiproliferative Effects of Copper(II)–Polypyridyl Complexes in Breast Cancer Cells through Inducing Apoptosis. *Biometals* **2015**, 28 (2), 267–278.

(73) Shah, D. R.; Modh, R. P.; Chikhahia, K. H. Privileged S-Triazines: Structure and Pharmacological Applications. *Future Medicinal Chemistry* **2014**, 6 (4), 463–477.

(74) Cascioferro, S.; Parrino, B.; Spanò, V.; Carbone, A.; Montalbano, A.; Barraja, P.; Diana, P.; Cirrincione, G. 1,3,5-Triazines: A Promising Scaffold for Anticancer Drugs Development. *European Journal of Medicinal Chemistry* **2017**, 142, 523–549.

(75) Kuo, G.-H.; DeAngelis, A.; Emanuel, S.; Wang, A.; Zhang, Y.; Connolly, P. J.; Chen, X.; Gruninger, R. H.; Rugg, C.; Fuentes-Pesquera, A.; et al. Synthesis and Identification of [1,3,5]Triazine-Pyridine Biheteroaryl as a Novel Series of Potent Cyclin-Dependent Kinase Inhibitors. *J. Med. Chem.* **2005**, 48 (14), 4535–4546.

(76) Peterson, E. A.; Andrews, P. S.; Be, X.; Boezio, A. A.; Bush, T. L.; Cheng, A. C.; Coats, J. R.; Colletti, A. E.; Copeland, K. W.; DuPont, M.; et al. Discovery of Triazine-Benzimidazoles as Selective Inhibitors of MTOR. *Bioorganic & Medicinal Chemistry Letters* **2011**, 21 (7), 2064–2070.

(77) Verheijen, J. C.; Richard, D. J.; Curran, K.; Kaplan, J.; Yu, K.; Zask, A. 2-Arylureidophenyl-4-(3-Oxa-8-Azabicyclo[3.2.1]Octan-8-Yl)Triazines as Highly Potent and Selective ATP Competitive MTOR Inhibitors: Optimization of Human Microsomal Stability. *Bioorganic & Medicinal Chemistry Letters* **2010**, 20 (8), 2648–2653.

(78) Yaguchi, S.; Fukui, Y.; Koshimizu, I.; Yoshimi, H.; Matsuno, T.; Gouda, H.; Hirono, S.; Yamazaki, K.; Yamori, T. Antitumor Activity of ZSTK474, a New Phosphatidylinositol 3-Kinase Inhibitor. *J Natl Cancer Inst* **2006**, 98 (8), 545–556.

- (79) Garaj, V.; Puccetti, L.; Fasolis, G.; Winum, J.-Y.; Montero, J.-L.; Scozzafava, A.; Vullo, D.; Innocenti, A.; Supuran, C. T. Carbonic Anhydrase Inhibitors: Novel Sulfonamides Incorporating 1,3,5-Triazine Moieties as Inhibitors of the Cytosolic and Tumour-Associated Carbonic Anhydrase Isozymes I, II and IX. *Bioorganic & Medicinal Chemistry Letters* **2005**, *15* (12), 3102–3108.
- (80) Nie, Z.; Perretta, C.; Erickson, P.; Margosiak, S.; Almasy, R.; Lu, J.; Averill, A.; Yager, K. M.; Chu, S. Structure-Based Design, Synthesis, and Study of Pyrazolo[1,5-a][1,3,5]Triazine Derivatives as Potent Inhibitors of Protein Kinase CK2. *Bioorganic & Medicinal Chemistry Letters* **2007**, *17* (15), 4191–4195.
- (81) Xiong, Y.-Z.; Chen, F.-E.; Balzarini, J.; De Clercq, E.; Pannecouque, C. Non-Nucleoside HIV-1 Reverse Transcriptase Inhibitors. Part 11: Structural Modulations of Diaryltriazenes with Potent Anti-HIV Activity. *European Journal of Medicinal Chemistry* **2008**, *43* (6), 1230–1236.
- (82) Kumar, A.; Srivastava, K.; Raja Kumar, S.; Siddiqi, M. I.; Puri, S. K.; Sexana, J. K.; Chauhan, P. M. S. 4-Anilinoquinoline Triazines: A Novel Class of Hybrid Antimalarial Agents. *European Journal of Medicinal Chemistry* **2011**, *46* (2), 676–690.
- (83) Kumar, A.; Srivastava, K.; Raja Kumar, S.; Puri, S. K.; Chauhan, P. M. S. Synthesis of 9-Anilinoacridine Triazines as New Class of Hybrid Antimalarial Agents. *Bioorganic & Medicinal Chemistry Letters* **2009**, *19* (24), 6996–6999.
- (84) Wackett, L.; Sadowsky, M.; Martinez, B.; Shapir, N. Biodegradation of Atrazine and Related S-Triazine Compounds: From Enzymes to Field Studies. *Appl Microbiol Biotechnol* **2002**, *58* (1), 39–45.
- (85) Waseem, A.; Yaqoob, M.; Nabi, A. Photodegradation and Flow-Injection Determination of Simetryn Herbicide by Luminol Chemiluminescence Detection. *Analytical Sciences* **2008**, *24* (8), 979–983.

(86) Grossmann, K.; Tresch, S.; Plath, P. Triaziflam and Diaminotriazine Derivatives Affect Enantioselectively Multiple Herbicide Target Sites. *Z. Naturforsch., C, J. Biosci.* **2001**, *56* (7–8), 559–569.

(87) Josef Velisek. The Effects of Pyrethroid and Triazine Pesticides on Fish Physiology. In *Pesticides in the Modern World*; Alzbeta Stara, Ed.; Zdenka Svobodova ED1 - Margarita Stoytcheva, Series Ed.; IntechOpen: Rijeka, 2011; pp 377–402.

(88) JOWA, L.; HOWD, R. Should Atrazine and Related Chlorotriazines Be Considered Carcinogenic for Human Health Risk Assessment? *Journal of Environmental Science and Health, Part C* **2011**, *29* (2), 91–144.

(89) Shang, S. M. 13 - Process Control in Dyeing of Textiles. In *Process Control in Textile Manufacturing*; Majumdar, A., Das, A., Alagirusamy, R., Kothari, V. K., Eds.; Woodhead Publishing Series in Textiles; Woodhead Publishing, 2013; pp 300–338.

(90) Lewis, D. M. Developments in the Chemistry of Reactive Dyes and Their Application Processes. *Coloration Technology* **2014**, *130* (6), 382–412.

(91) Blus, K.; Paluszkiewicz, J.; Czajkowski, W. Reactive Dyes for Single-Bath and Single-Stage Dyeing of Polyester-Cellulose Blends. *FIBRES & TEXTILES in Eastern Europe* **2005**, No. 6(54), 75–78.

(92) Blus, K.; Czechowski, J.; Koziróg, A. New Eco-Friendly Method for Paper Dyeing. *FIBRES & TEXTILES in Eastern Europe* **2014**, *22* (5(107)), 121–125.

(93) Lewis, D. M.; Siddique, A. A. Synthesis of Reactive Dyes Based on the Bis-(N-Carboxymethylamino)Monoquaternary-Triazine-Bis-Ethylsulphone Reactive Group. Part 1: Application to Cotton Cellulose. *Coloration Technology* **2006**, *122* (4), 217–226.

(94) Bone, J. A.; Le, T. T.; Phillips, D. a. S.; Taylor, J. A. One-Bath Dyeing of Polyester/Cotton with Disperse and Bis-3-Carboxypyridinium-s-Triazine Reactive Dyes.

Part 1: Factors Limiting Production of Heavy Shades. *Coloration Technology* **2007**, *123* (3), 152–162.

(95) Fernandez Cid, M. V.; Gerstner, K. N.; van Spronsen, J.; van der Kraan, M.; Veugelers, W. J. T.; Woerlee, G. F.; Witkamp, G. J. Novel Process to Enhance the Dyeability of Cotton in Supercritical Carbon Dioxide. *Textile Research Journal* **2007**, *77* (1), 38–46.

(96) Fernandez Cid, M. V.; van Spronsen, J.; van der Kraan, M.; Veugelers, W. J. T.; Woerlee, G. F.; Witkamp, G. J. A Significant Approach to Dye Cotton in Supercritical Carbon Dioxide with Fluorotriazine Reactive Dyes. *The Journal of Supercritical Fluids* **2007**, *40* (3), 477–484.

(97) Sawada, K.; Ueda, M. Adsorption and Fixation of a Reactive Dye on Cotton in Non-Aqueous Systems. *Coloration Technology* **2003**, *119* (3), 182–186.

(98) Tang, A. Y.; Lee, C.; Wang, Y.; Kan, C. Octane-Assisted Reverse Micellar Dyeing of Cotton with Reactive Dyes. *Polymers* **2017**, *9* (12), 678.

(99) Yi, S.; Dong, Y.; Li, B.; Ding, Z.; Huang, X.; Xue, L. Adsorption and Fixation Behaviour of CI Reactive Red 195 on Cotton Woven Fabric in a Nonionic Surfactant Triton X-100 Reverse Micelle. *Coloration Technology* **2012**, *128* (4), 306–314.

(100) Yi, S.; Tong, X.; Sun, S.; Dai, F. Dyeing Properties of CI Reactive Violet 2 on Cotton Fabric in Non-Ionic TX-100/Span40 Mixed Reverse Micelles. *Fibers Polym* **2015**, *16* (8), 1663–1670.

(101) Tang, A. Y. L.; Lee, C. H.; Wang, Y. M.; Kan, C. W. A Study of PEG-Based Reverse Micellar Dyeing of Cotton Fabric: Reactive Dyes with Different Reactive Groups. *Cellulose* **2019**, *26* (6), 4159–4173.



- (102) Sawada, K.; Ueda, M. Enzyme Processing of Wool Fabrics in a Non-ionic Surfactant Reverse Micellar System. *Journal of Chemical Technology & Biotechnology* **2004**, 79 (4), 376–380.
- (103) Sawada, K.; Ueda, M. Characteristics of Aqueous Microenvironments in Non-ionic Surfactant Reverse Micelles and Their Use for Enzyme Reactions in Non-aqueous Media. *Journal of Chemical Technology & Biotechnology* **2004**, 79 (4), 369–375.
- (104) Smith, B.; Berger, R.; Freeman, H. S. High Affinity, High Efficiency Fibre-Reactive Dyes. *Coloration Technology* **2006**, 122 (4), 187–193.
- (105) Morris, K. F.; Lewis, D. M.; Broadbent, P. J. Design and Application of a Multifunctional Reactive Dye Capable of High Fixation Efficiency on Cellulose. *Coloration Technology* **2008**, 124 (3), 186–194.
- (106) Xie, K.; Liu, H.; Wang, X. Surface Modification of Cellulose with Triazine Derivative to Improve Printability with Reactive Dyes. *Carbohydrate Polymers* **2009**, 78 (3), 538–542.
- (107) Soleimani-Gorgani, A.; Najafi, F.; Karami, Z. Modification of Cotton Fabric with a Dendrimer to Improve Ink-Jet Printing Process. *Carbohydr Polym* **2015**, 131, 168–176.
- (108) Lam, Y.-L.; Kan, C.-W.; Yuen, C.-W. M. Developments in Functional Finishing of Cotton Fibres – Wrinkle-Resistant, Flame-Retardant and Antimicrobial Treatments. *Textile Progress* **2012**, 44 (3–4), 175–249.
- (109) Mikučionienė, D.; Milasiute, L.; Baltušnikaite, J.; Milašius, R. Influence of Plain Knits Structure on Flammability and Air Permeability. *FIBRES & TEXTILES in Eastern Europe*. **2012**, 20, 5 (94), 66-69.

(110) Kandola, B. K.; Horrocks, A. R.; Price, D.; Coleman, G. V. Flame-Retardant Treatments of Cellulose and Their Influence on the Mechanism of Cellulose Pyrolysis. *Journal of Macromolecular Science, Part C* **1996**, *36* (4), 721–794.

(111) Horacek, H.; Grabner, R. Advantages of Flame Retardants Based on Nitrogen Compounds. *Polymer Degradation and Stability* **1996**, *54* (2), 205–215.

(112) Chang, S.; Condon, B.; Graves, E.; Uchimiya, M.; Fortier, C.; Easson, M.; Wakelyn, P. Flame Retardant Properties of Triazine Phosphonates Derivative with Cotton Fabric. *Fibers Polym* **2011**, *12* (3), 334–339.

(113) Bajaj, P. 10 - Heat and Flame Protection. In *Handbook of Technical Textiles*; Horrocks, A. R., Anand, S. C., Eds.; Woodhead Publishing Series in Textiles; Woodhead Publishing, 2000; pp 223–263.

(114) Chang, S.; Condon, B.; Nguyen, T.-M.; Graves, E.; Smith, J. Antiflammable Properties of Capable Phosphorus–Nitrogen-Containing Triazine Derivatives on Cotton. In *Fire and Polymers VI: New Advances in Flame Retardant Chemistry and Science*; ACS Symposium Series; American Chemical Society, 2012; Vol. 1118, pp 123–137.

(115) Li, X.; Chen, H.; Wang, W.; Liu, Y.; Zhao, P. Synthesis of a Formaldehyde-Free Phosphorus–Nitrogen Flame Retardant with Multiple Reactive Groups and Its Application in Cotton Fabrics. *Polymer Degradation and Stability* **2015**, *120*, 193–202.

(116) Ringot, C.; Saad, N.; Granet, R.; Bressollier, P.; Sol, V.; Krausz, P. Meso-Functionalized Aminoporphyrins as Efficient Agents for Photo-Antibacterial Surfaces. *J. Porphyrins Phthalocyanines* **2010**, *14* (11), 925–931.

(117) Dahl, T.; RobertMiddenand, W.; Hartman, P. Pure Singlet Oxygen Cytotoxicity for Bacteria. *Photochemistry and Photobiology* **1987**, *46* (3), 345–352.

(118) Gerba, C. P. Quaternary Ammonium Biocides: Efficacy in Application. *Appl. Environ. Microbiol.* **2015**, *81* (2), 464–469.

(119) Ringot, C.; Sol, V.; Barrière, M.; Saad, N.; Bressollier, P.; Granet, R.; Couleaud, P.; Frochot, C.; Krausz, P. Triazinyl Porphyrin-Based Photoactive Cotton Fabrics: Preparation, Characterization, and Antibacterial Activity. *Biomacromolecules* **2011**, *12* (5), 1716–1723.

(120) Mbakidi, J.-P.; Herke, K.; Alvès, S.; Chaleix, V.; Granet, R.; Krausz, P.; Leroy-Lhez, S.; Ouk, T.-S.; Sol, V. Synthesis and Photobiocidal Properties of Cationic Porphyrin-Grafted Paper. *Carbohydrate Polymers* **2013**, *91* (1), 333–338.

(121) Ma, K.; Xie, Z.; Jiang, Q.; Li, J.; Li, R.; Ren, X.; Huang, T.-S.; Zhang, K.-Q. Cytocompatible and Regenerable Antimicrobial Cellulose Modified by N-Halamine Triazine Ring. *Journal of Applied Polymer Science* **2014**, *131* (16).

(122) Ren, X.; Kou, L.; Liang, J.; Worley, S. D.; Tzou, Y.-M.; Huang, T. S. Antimicrobial Efficacy and Light Stability of N-Halamine Siloxanes Bound to Cotton. *Cellulose* **2008**, *15* (4), 593–598.

(123) Kocer, H. B.; Akdag, A.; Worley, S. D.; Acevedo, O.; Broughton, R. M.; Wu, Y. Mechanism of Photolytic Decomposition of N-Halamine Antimicrobial Siloxane Coatings. *ACS Appl Mater Interfaces* **2010**, *2* (8), 2456–2464.

(124) Kocer, H. B.; Worley, S. D.; Broughton, R. M.; Acevedo, O.; Huang, T. S. Effect of Phenyl Derivatization on the Stabilities of Antimicrobial N-Chlorohydantoin Derivatives. *Ind. Eng. Chem. Res.* **2010**, *49* (22), 11188–11194.

(125) Ma, K.; Liu, Y.; Xie, Z.; Li, R.; Jiang, Z.; Ren, X.; Huang, T.-S. Synthesis of Novel N-Halamine Epoxide Based on Cyanuric Acid and Its Application for Antimicrobial Finishing. *Ind. Eng. Chem. Res.* **2013**, *52* (22), 7413–7418.

(126) Jiang, Z.; Liu, Y.; Li, R.; Ren, X.; Huang, T. S. Preparation of Antibacterial Cellulose with a Monochloro-s-Triazine-Based N-Halamine Biocide. *Polymers for Advanced Technologies* **2016**, 27 (4), 460–465.

(127) Lee, J.; Broughton, R. M.; Akdag, A.; Worley, S. D.; Huang, T. S. Preparation and Application of Ans-Triazine-Based Novel N-Halamine Biocide for Antimicrobial Fibers. *Fibers Polym* **2007**, 8 (2), 148–154.

(128) Jiang, Z.; Ma, K.; Du, J.; Li, R.; Ren, X.; Huang, T. S. Synthesis of Novel Reactive N-Halamine Precursors and Application in Antimicrobial Cellulose. *Applied Surface Science* **2014**, 288, 518–523.

(129) Akdag, A.; Okur, S.; McKee, M. L.; Worley, S. D. The Stabilities of N–Cl Bonds in Biocidal Materials. *J. Chem. Theory Comput.* **2006**, 2 (3), 879–884.

(130) Hou, A.; Zhou, M.; Wang, X. Preparation and Characterization of Durable Antibacterial Cellulose Biomaterials Modified with Triazine Derivatives. *Carbohydrate Polymers* **2009**, 75 (2), 328–332.

(131) Jiang, Z.; Qiao, M.; Ren, X.; Zhu, P.; Huang, T.-S. Preparation of Antibacterial Cellulose with S-Triazine-Based Quaternarized N-Halamine. *Journal of Applied Polymer Science* **2017**, 134 (26).

(132) Rahman, Q. M.; Wang, L.; Zhang, B.; Xiu, S.; Shahbazi, A. Green Biorefinery of Fresh Cattail for Microalgal Culture and Ethanol Production. *Bioresource Technology* **2015**, 185, 436–440.

(133) Lewis, A. J.; Ren, S.; Ye, X.; Kim, P.; Labbe, N.; Borole, A. P. Hydrogen Production from Switchgrass via an Integrated Pyrolysis–Microbial Electrolysis Process. *Bioresource Technology* **2015**, 195, 231–241.

(134) Farrell, A. E.; Plevin, R. J.; Turner, B. T.; Jones, A. D.; O'Hare, M.; Kammen, D. M. Ethanol Can Contribute to Energy and Environmental Goals. *Science* **2006**, *311* (5760), 506–508.

(135) Alvira, P.; Tomás-Pejó, E.; Ballesteros, M.; Negro, M. J. Pretreatment Technologies for an Efficient Bioethanol Production Process Based on Enzymatic Hydrolysis: A Review. *Bioresource Technology* **2010**, *101* (13), 4851–4861.

(136) Rose, M.; Babi, M.; Moran-Mirabal, J. The Study of Cellulose Structure and Depolymerization Through Single-Molecule Methods. *Industrial Biotechnology* **2015**, *11* (1), 16–24.

(137) Mu, B.; Xu, H.; Li, W.; Yang, Y. Quantitation of Fast Hydrolysis of Cellulose Catalyzed by Its Substituents for Potential Biomass Conversion. *Bioresource Technology* **2019**, *273*, 305–312.

(138) Karst, D.; Yang, Y. Effect of Structure of Large Aromatic Molecules Grafted onto Cellulose on Hydrolysis of the Glycosidic Linkages. *Macromolecular Chemistry and Physics* **2007**, *208* (7), 784–791.

(139) Tian, X.; Liu, L.; Sun, Y.; Gu, J.; Jiang, X.; Yu, W.; Huang, D. Mechanism of Increasing the Reducing Sugar Yield in Cellulose Hydrolysis via Modification with 2,4-Dianilino-6-Chloro-s-Triazine. *Iran Polym J* **2014**, *23* (1), 79–86.

(140) Moran-Mirabal, J. M.; Santhanam, N.; Corgie, S. C.; Craighead, H. G.; Walker, L. P. Immobilization of Cellulose Fibrils on Solid Substrates for Cellulase-Binding Studies through Quantitative Fluorescence Microscopy. *Biotechnology and Bioengineering* **2008**, *101* (6), 1129–1141.

(141) Jiang, X.; Gu, J.; Tian, X.; Li, Y.; Huang, D. Modification of Cellulose for High Glucose Generation. *Bioresource Technology* **2012**, *104*, 473–479.

(142) Smith, N. L.; Lenhoff, H. M. Covalent Binding of Proteins and Glucose-6-Phosphate Dehydrogenase to Cellulosic Carriers Activated with s-Triazine Trichloride. *Analytical Biochemistry* **1974**, *61* (2), 392–415.

(143) Kay, G.; Crook, E. M. Coupling of Enzymes to Cellulose Using Chloro- s - Triazines. *Nature* **1967**, *216* (5114), 514.

(144) Kay, G.; Lilly, M. D. The Chemical Attachment of Chymotrypsin to Water-Insoluble Polymers Using 2-Amino-4,6-Dichloro-s-Triazine. *Biochimica et Biophysica Acta (BBA) - Enzymology* **1970**, *198* (2), 276–285.

(145) Finlay, T. H.; Troll, V.; Levy, M.; Johnson, A. J.; Hodgins, L. T. New Methods for the Preparation of Biospecific Adsorbents and Immobilized Enzymes Utilizing Trichloro-s-Triazine. *Analytical Biochemistry* **1978**, *87* (1), 77–90.

(146) Biagioni, S.; Sisto, R.; Ferraro, A.; Caiafa, P.; Turano, C. A New Method for the Preparation of DNA-Cellulose. *Analytical Biochemistry* **1978**, *89* (2), 616–619.

(147) Baird, J. K.; Sherwood, R. F.; Carr, R. J. G.; Atkinson, A. Enzyme Purification by Substrate Elution Chromatography from Procion Dye—Polysaccharide Matrices. *FEBS Letters* **1976**, *70* (1–2), 61–66.

(148) Sherwood, R. F.; Melton, R. G.; Alwan, S. M.; Hughes, P. Purification and Properties of Carboxypeptidase G2 from *Pseudomonas* Sp. Strain RS-16. *European Journal of Biochemistry* **1985**, *148* (3), 447–453.

(149) Wu, C.-Y.; Suen, S.-Y.; Chen, S.-C.; Tzeng, J.-H. Analysis of Protein Adsorption on Regenerated Cellulose-Based Immobilized Copper Ion Affinity Membranes. *Journal of Chromatography A* **2003**, *996* (1), 53–70.

- (150) Gao, M.; Lu, W.; Li, N.; Chen, W. Enhanced Removal of Acid Red 1 with Large Amounts of Dyeing Auxiliaries: The Pivotal Role of Cellulose Support. *Cellulose* **2014**, *21* (3), 2073–2087.
- (151) Gao, M.; Li, N.; Lu, W.; Chen, W. Role of Cellulose Fibers in Enhancing Photosensitized Oxidation of Basic Green 1 with Massive Dyeing Auxiliaries. *Applied Catalysis B: Environmental* **2014**, *147*, 805–812.
- (152) Fraczyk, J.; Kolesinska, B.; Czarnecka, A.; Malawska, B.; Wieckowska, A.; Bajda, M.; Kaminski, Z. J. Application of a Library of Artificial Receptors Formed by Self-Organization of N-Lipidated Peptides Immobilized on Cellulose for Preliminary Studies of Binding of N-Phenylpiperazines. *QSAR & Combinatorial Science* **2009**, *28* (6–7), 728–736.
- (153) Fraczyk, J.; Kaminski, Z. J. Design, Synthesis, and Application of a Library of Supramolecular Structures Formed by N-Lipidated Peptides Immobilized on Cellulose. Artificial Receptors. *J. Comb. Chem.* **2008**, *10* (6), 934–940.
- (154) Bıyıkliođlu, Z.; Saka, E. T.; Gökçe, S.; Kantekin, H. Synthesis, Characterization and Investigation of Homogeneous Oxidation Activities of Peripherally Tetra-Substituted Co(II) and Fe(II) Phthalocyanines: Oxidation of Cyclohexene. *Journal of Molecular Catalysis A: Chemical* **2013**, *378*, 156–163.
- (155) Gouloumis, A.; González-Rodríguez, D.; Vázquez, P.; Torres, T.; Liu, S.; Echegoyen, L.; Ramey, J.; Hug, G. L.; Guldi, D. M. Control Over Charge Separation in Phthalocyanine–Anthraquinone Conjugates as a Function of the Aggregation Status. *J. Am. Chem. Soc.* **2006**, *128* (39), 12674–12684.
- (156) Engrand, P.; Regnouf-de-Vains, J.-B. A Bifunctional Calixarene Designed for Immobilisation on a Natural Polymer and for Metal Complexation. *Tetrahedron Letters* **2002**, *43* (49), 8863–8866.

(157) Saari, L. A.; Seitz, W. R. Immobilized Calcein for Metal Ion Preconcentration. *Anal. Chem.* **1984**, *56* (4), 810–813.

(158) Trivedi, C. P.; Jain, D.; Kapoor, P. Analytical Separation of Copper(II), Cobalt(II) and Nickel(II) Using Polymer Bound Anthranic Acid. *Analytical Letters* **1989**, *22* (8), 2021–2031.

(159) Kamiński, Z. J.; Kolesińska, B.; Kolesińska, J.; Sabatino, G.; Chelli, M.; Rovero, P.; Błaszczak, M.; Głowska, M. L.; Papini, A. M. N-Triazinylammonium Tetrafluoroborates. A New Generation of Efficient Coupling Reagents Useful for Peptide Synthesis. *J. Am. Chem. Soc.* **2005**, *127* (48), 16912–16920.

(160) Mishra, R. K.; Sabu, A.; Tiwari, S. K. Materials Chemistry and the Futurist Eco-Friendly Applications of Nanocellulose: Status and Prospect. *Journal of Saudi Chemical Society* **2018**, *22* (8), 949–978.

(161) Helbert, W.; Chanzy, H.; Husum, T. L.; Schülein, M.; Ernst, S. Fluorescent Cellulose Microfibrils As Substrate for the Detection of Cellulase Activity. *Biomacromolecules* **2003**, *4* (3), 481–487.

(162) Moran-Mirabal, J. M.; Bolewski, J. C.; Walker, L. P. Reversibility and Binding Kinetics of *Thermobifida fusca* Cellulases Studied through Fluorescence Recovery after Photobleaching Microscopy. *Biophysical Chemistry* **2011**, *155* (1), 20–28.

(163) Luterbacher, J. S.; Walker, L. P.; Moran-Mirabal, J. M. Observing and Modeling BMCC Degradation by Commercial Cellulase Cocktails with Fluorescently Labeled *Trichoderma reesei* Cel7A through Confocal Microscopy. *Biotechnology and Bioengineering* **2013**, *110* (1), 108–117.



(164) Moran-Mirabal, J. M.; Bolewski, J. C.; Walker, L. P. Thermobifida Fusca Cellulases Exhibit Limited Surface Diffusion on Bacterial Micro-Crystalline Cellulose. *Biotechnology and Bioengineering* **2013**, *110* (1), 47–56.

(165) Jung, J.; Sethi, A.; Gaiotto, T.; Han, J. J.; Jeoh, T.; Gnanakaran, S.; Goodwin, P. M. Binding and Movement of Individual Cel7A Cellobiohydrolases on Crystalline Cellulose Surfaces Revealed by Single-Molecule Fluorescence Imaging. *J. Biol. Chem.* **2013**, *288* (33), 24164–24172.

(166) Santa-Maria, M.; Jeoh, T. Molecular-Scale Investigations of Cellulose Microstructure during Enzymatic Hydrolysis. *Biomacromolecules* **2010**, *11* (8), 2000–2007.

(167) Jeoh, T.; Santa-Maria, M. C.; O’Dell, P. J. Assessing Cellulose Microfibrillar Structure Changes Due to Cellulase Action. *Carbohydrate Polymers* **2013**, *97* (2), 581–586.

(168) Lemke, C. H.; Dong, R. Y.; Michal, C. A.; Hamad, W. Y. New Insights into Nano-Crystalline Cellulose Structure and Morphology Based on Solid-State NMR. *Cellulose* **2012**, *19* (5), 1619–1629.

(169) Camarero Espinosa, S.; Kuhnt, T.; Foster, E. J.; Weder, C. Isolation of Thermally Stable Cellulose Nanocrystals by Phosphoric Acid Hydrolysis. *Biomacromolecules* **2013**, *14* (4), 1223–1230.

(170) Abitbol, T.; Palermo, A.; Moran-Mirabal, J. M.; Cranston, E. D. Fluorescent Labeling and Characterization of Cellulose Nanocrystals with Varying Charge Contents. *Biomacromolecules* **2013**, *14* (9), 3278–3284.

(171) Hu, Z.; Ballinger, S.; Pelton, R.; Cranston, E. D. Surfactant-Enhanced Cellulose Nanocrystal Pickering Emulsions. *Journal of Colloid and Interface Science* **2015**, *439*, 139–148.

(172) Hu, Z.; Patten, T.; Pelton, R.; Cranston, E. D. Synergistic Stabilization of Emulsions and Emulsion Gels with Water-Soluble Polymers and Cellulose Nanocrystals. *ACS Sustainable Chem. Eng.* **2015**, *3* (5), 1023–1031.

(173) Leng, T.; Jakubek, Z. J.; Mazloumi, M.; Leung, A. C. W.; Johnston, L. J. Ensemble and Single Particle Fluorescence Characterization of Dye-Labeled Cellulose Nanocrystals. *Langmuir* **2017**, *33* (32), 8002–8011.

(174) Grate, J. W.; Mo, K.-F.; Shin, Y.; Vasdekis, A.; Warner, M. G.; Kelly, R. T.; Orr, G.; Hu, D.; Dehoff, K. J.; Brockman, F. J.; et al. Alexa Fluor-Labeled Fluorescent Cellulose Nanocrystals for Bioimaging Solid Cellulose in Spatially Structured Microenvironments. *Bioconjugate Chem.* **2015**, *26* (3), 593–601.

(175) De France, K. J.; Badv, M.; Dorogin, J.; Siebers, E.; Panchal, V.; Babi, M.; Moran-Mirabal, J.; Lawlor, M.; Cranston, E. D.; Hoare, T. Tissue Response and Biodistribution of Injectable Cellulose Nanocrystal Composite Hydrogels. *ACS Biomater. Sci. Eng.* **2019**, *5* (5), 2235–2246.

(176) Yin, Y.; Zhao, L.; Jiang, X.; Wang, H.; Gao, W. Cellulose Nanocrystals Modified with a Triazine Derivative and Their Reinforcement of Poly(Lactic Acid)-Based Bionanocomposites. *Cellulose* **2018**, *25* (5), 2965–2976.

(177) Zhang, Y.; Liu, Y.; Li, R.; Ren, X.; Huang, T.-S. Preparation and Characterization of Antimicrobial Films Based on Nanocrystalline Cellulose. *Journal of Applied Polymer Science* **2019**, *136* (8), 47101.

- (178) Chen, L.; Berry, R. M.; Tam, K. C. Synthesis of  $\beta$ -Cyclodextrin-Modified Cellulose Nanocrystals (CNCs)@Fe<sub>3</sub>O<sub>4</sub>@SiO<sub>2</sub> Superparamagnetic Nanorods. *ACS Sustainable Chem. Eng.* **2014**, 2 (4), 951–958.
- (179) Zhang, F.; Islam, M. S.; Berry, R. M.; Tam, K. C.  $\beta$ -Cyclodextrin-Functionalized Cellulose Nanocrystals and Their Interactions with Surfactants. *ACS Omega* **2019**, 4 (1), 2102–2110.
- (180) Wang, D.; Klein, J.; Mejía, E. Catalytic Systems for the Cross-Linking of Organosilicon Polymers. *Chemistry – An Asian Journal* **2017**, 12 (11), 1180–1197.
- (181) Brook, M. A. Chapter 9. In. In *Silicon in Organic, Organometallic, and Polymer Chemistry*; A Wiley-Interscience publication; John Wiley & Sons, Inc: New York, 2000; p 256.
- (182) Moretto, H.-H.; Schulze, M.; Wagner, G. Silicones. In *Ullmann's Encyclopedia of Industrial Chemistry*; American Cancer Society, 2000.
- (183) Cervantes, J.; Zárraga, R.; Salazar-Hernández, C. Organotin Catalysts in Organosilicon Chemistry. *Applied Organometallic Chemistry* **2012**, 26 (4), 157–163.
- (184) Weij, F. W. van D. The Action of Tin Compounds in Condensation-Type RTV Silicone Rubbers. *Die Makromolekulare Chemie* **1980**, 181 (12), 2541–2548.
- (185) Putzien, S.; Nuyken, O.; Kühn, F. E. Functionalized Polysilalkylene Siloxanes (Polycarbosiloxanes) by Hydrosilylation—Catalysis and Synthesis. *Progress in Polymer Science* **2010**, 35 (6), 687–713.
- (186) Wang, C.; Nair, S. S.; Veeravalli, S.; Moseh, P.; Wynne, K. J. Sticky or Slippery Wetting: Network Formation Conditions Can Provide a One-Way Street for Water Flow on Platinum-Cured Silicone. *ACS Appl. Mater. Interfaces* **2016**, 8 (22), 14252–14262.

- (187) Boyer, I. J. Toxicity of Dibutyltin, Tributyltin and Other Organotin Compounds to Humans and to Experimental Animals. *Toxicology* **1989**, *55* (3), 253–298.
- (188) Zheng, S.; Zlatin, M.; Selvaganapathy, P. R.; Brook, M. A. Multiple Modulus Silicone Elastomers Using 3D Extrusion Printing of Low Viscosity Inks. *Additive Manufacturing* **2018**, *24*, 86–92.
- (189) Müller, U.; Timpe, H.-J.; Neuenfeld, J. Photocrosslinking of Silicones—5. Photo-Induced Polymerization of Silicone with Pendant Acrylate Groups in the Presence of Oxygen. *European Polymer Journal* **1991**, *27* (7), 621–625.
- (190) Choi, K. M.; Rogers, J. A. A Photocurable Poly(Dimethylsiloxane) Chemistry Designed for Soft Lithographic Molding and Printing in the Nanometer Regime. *J. Am. Chem. Soc.* **2003**, *125* (14), 4060–4061.
- (191) Jin, F.-L.; Li, X.; Park, S.-J. Synthesis and Application of Epoxy Resins: A Review. *Journal of Industrial and Engineering Chemistry* **2015**, *29*, 1–11.
- (192) Silva, A. L.; Bordado, J. C. Recent Developments in Polyurethane Catalysis: Catalytic Mechanisms Review. *Catalysis Reviews* **2004**, *46* (1), 31–51.
- (193) Fawcett, A. S.; Grande, J. B.; Brook, M. A. Rapid, Metal-Free Room Temperature Vulcanization Produces Silicone Elastomers. *Journal of Polymer Science Part A: Polymer Chemistry* **2013**, *51* (3), 644–652.
- (194) Liao, M.; Schneider, A. F.; Laengert, S. E.; Gale, C. B.; Chen, Y.; Brook, M. A. Living Synthesis of Silicone Polymers Controlled by Humidity. *European Polymer Journal* **2018**, *107*, 287–293.
- (195) Rambarran, T.; Gonzaga, F.; Brook, M. A.; Lasowski, F.; Sheardown, H. Amphiphilic Thermoset Elastomers from Metal-Free, Click Crosslinking of PEG-Grafted

Silicone Surfactants. *Journal of Polymer Science Part A: Polymer Chemistry* **2015**, *53* (9), 1082–1093.

(196) Rambarran, T.; Gonzaga, F.; Fatona, A.; Coulson, M.; Saem, S.; Moran-Mirabal, J.; Brook, M. A. Bonding and In-Channel Microfluidic Functionalization Using the Huisgen Cyclization. *Journal of Polymer Science Part A: Polymer Chemistry* **2018**, *56* (6), 589–597.

(197) Zhao, J.; Xu, R.; Luo, G.; Wu, J.; Xia, H. A Self-Healing, Re-Moldable and Biocompatible Crosslinked Polysiloxane Elastomer. *J. Mater. Chem. B* **2016**, *4* (5), 982–989.

(198) Bui, R.; Brook, M. A. Dynamic Covalent Schiff-Base Silicone Polymers and Elastomers. *Polymer* **2019**, *160*, 282–290.

(199) Genest, A.; Binauld, S.; Pouget, E.; Ganachaud, F.; Fleury, E.; Portinha, D. Going beyond the Barriers of Aza-Michael Reactions: Controlling the Selectivity of Acrylates towards Primary Amino-PDMS. *Polym. Chem.* **2017**, *8* (3), 624–630.

(200) Boxshall, K.; Wu, M.-H.; Cui, Z.; Cui, Z.; Watts, J. F.; Baker, M. A. Simple Surface Treatments to Modify Protein Adsorption and Cell Attachment Properties within a Poly(Dimethylsiloxane) Micro-Bioreactor. *Surface and Interface Analysis* **2006**, *38* (4), 198–201.

(201) Bartzoka, V.; Brook, M. A.; McDermott, M. R. Protein–Silicone Interactions: How Compatible Are the Two Species? *Langmuir* **1998**, *14* (7), 1887–1891.

(202) Vickers, J. A.; Caulum, M. M.; Henry, C. S. Generation of Hydrophilic Poly(Dimethylsiloxane) for High-Performance Microchip Electrophoresis. *Anal. Chem.* **2006**, *78* (21), 7446–7452.

- (203) Zhao, B.; Brittain, W. J. Polymer Brushes: Surface-Immobilized Macromolecules. *Progress in Polymer Science* **2000**, *25* (5), 677–710.
- (204) Wong, I.; Ho, C.-M. Surface Molecular Property Modifications for Poly(Dimethylsiloxane) (PDMS) Based Microfluidic Devices. *Microfluid Nanofluid* **2009**, *7* (3), 291.
- (205) Zhang, J.; Chen, Y.; Brook, M. A. Facile Functionalization of PDMS Elastomer Surfaces Using Thiol–Ene Click Chemistry. *Langmuir* **2013**, *29* (40), 12432–12442.
- (206) Xu, J.; Gleason, K. K. Conformal, Amine-Functionalized Thin Films by Initiated Chemical Vapor Deposition (ICVD) for Hydrolytically Stable Microfluidic Devices. *Chem. Mater.* **2010**, *22* (5), 1732–1738.
- (207) Yao, M.; Fang, J. Hydrophilic PEO-PDMS for Microfluidic Applications. *J. Micromech. Microeng.* **2012**, *22* (2), 025012.
- (208) Yu, K.; Han, Y. A Stable PEO-Tethered PDMS Surface Having Controllable Wetting Property by a Swelling–Deswelling Process. *Soft Matter* **2006**, *2* (8), 705–709.
- (209) Hu, S.; Ren, X.; Bachman, M.; Sims, C. E.; Li, G. P.; Allbritton, N. Surface Modification of Poly(Dimethylsiloxane) Microfluidic Devices by Ultraviolet Polymer Grafting. *Anal. Chem.* **2002**, *74* (16), 4117–4123.
- (210) Mikhail, A. S.; Ranger, J. J.; Liu, L.; Longenecker, R.; Thompson, D. B.; Sheardown, H. D.; Brook, M. A. Rapid and Efficient Assembly of Functional Silicone Surfaces Protected by PEG: Cell Adhesion to Peptide-Modified PDMS. *Journal of Biomaterials Science, Polymer Edition* **2010**, *21* (6–7), 821–842.
- (211) Alauzun, J. G.; Young, S.; D’Souza, R.; Liu, L.; Brook, M. A.; Sheardown, H. D. Biocompatible, Hyaluronic Acid Modified Silicone Elastomers. *Biomaterials* **2010**, *31* (13), 3471–3478.

(212) Hu, S.; Ren, X.; Bachman, M.; Sims, C. E.; Li, G. P.; Allbritton, N. L. Surface-Directed, Graft Polymerization within Microfluidic Channels. *Anal. Chem.* **2004**, *76* (7), 1865–1870.

## **CHAPTER 2: Versatile Surface Modification of Cellulose Fibres and Cellulose Nanocrystals through Modular Triazinyl Chemistry †**

### **2.1 Abstract**

The ability to tune the interfacial and functional properties of cellulose nanomaterials has been identified as a critical step for the full utilization of nanocellulose in the development of new materials. Here, we use triazine chemistry in a modular approach to install various functionalities and chemistries onto cellulose fibres and cellulose nanocrystals (CNCs). The surface modification is demonstrated in aqueous and organic media. Octadecyl, mono-allyl-PEG, benzyl and propargyl triazinyl derivatives were grafted onto cellulose/CNCs via aromatic nucleophilic substitution in the presence of base as hydrochloric acid scavenger. The covalent nature and degree of substitution of grafted aliphatic, polymeric, alkyne chains and aromatic rings were characterized through Fourier transform infrared spectroscopy, X-ray photoelectron spectroscopy, elemental analysis, and thermogravimetric analysis. In addition, AFM and DLS analysis showed minimal change in the geometry and individualized character of CNCs after surface modification. X-ray diffraction analysis confirmed that the modification happened only at the CNC surface, while the bulk crystalline core remained unmodified. Modified cellulose/CNCs showed

---

†This chapter is reproduced from A. Fatona, R. M. Berry, M. A. Brook and J. M. Moran-Mirabal, *Chemistry of Materials*, 2018, 30, 7, 2424-2435 with permission from the American Chemical Society, Copyright 2018 American Chemical Society. Fatona and Moran-Mirabal designed the experiments and analyzed the data. Fatona performed all experiments using cellulose nanocrystals provided by Richard M. Berry. Fatona wrote the manuscript with additions, edits and guidance from both Brook and Moran-Mirabal.



hydrophilic or hydrophobic, properties depending on the grafted functionality, which resulted in stable colloidal suspensions of CNCs in polar and non-polar organic solvents. Furthermore, the reactive nature of propargyl modified cellulose was demonstrated by the successful grafting of an azido-fluorescein dye via copper-catalysed Huisgen 1,3-dipolar cycloaddition. The triazinyl chemistry thus presents a versatile route for tuning the interfacial properties of nanocellulose, with the possibility of post-modification for applications that require the conjugation of molecules onto cellulose through bio-orthogonal chemistries.

## **2.2 Introduction**

Cellulose is an attractive green material due to its intrinsic mechanical and chemical properties, which can be used to build hierarchical structures that enhance the performance of traditional polymeric materials.<sup>1-3</sup> The partial hydrolysis of the networks of cellulose microfibrils in plant cell walls with strong acids, which attack preferentially the disordered or para-crystalline regions of the microfibrils, allows the isolation of highly crystalline rod-like nanoparticles, called cellulose nanocrystals (CNCs). These environmentally friendly and non-cytotoxic<sup>4</sup> nanoparticles have unique characteristics, including very high surface area (150-300 m<sup>2</sup>/g),<sup>5,6</sup> high tensile strength (7.5-7.7 GPa),<sup>7</sup> high elastic modulus (110-220 GPa),<sup>7</sup> high aspect ratio (~20-70),<sup>5</sup> and interesting optical and electrical properties.<sup>8</sup> Such characteristics make them attractive for a broad range of applications, including materials reinforcement, drug delivery, foam stabilization, super-capacitor development, rheological property modification, among many others. However, a major hurdle to the widespread application and utilization of CNCs, and nanocellulose in general, is their inability to form stable suspensions in a range of organic solvents or be compatible with polymer matrices. Thus, the effective use of CNCs in select applications, such as materials reinforcement, depends strongly on our ability to tune their interfacial properties to enhance dispersion or introduce reactive functional groups that can form covalent bonds with the host matrix.

The surface chemistry of isolated CNCs is dependent on the acid used during hydrolysis. Sulfuric acid hydrolysis of cellulose is still the most common process for CNC isolation and results in the grafting of sulfate half ester groups onto the surface of the isolated CNCs. While these negatively charged groups allow the colloidal stabilization of CNCs in aqueous media through electrostatic repulsion, they, along with the abundant hydroxyl groups on the CNC surface, prevent their suspension/dispersion in most organic solvents and polymer systems.<sup>5, 9</sup> This limits the reinforcement capabilities of CNCs as well as their processability for new nanotechnological applications.

Efforts have been made to convert electrostatically stabilized CNCs into sterically stabilized CNCs through the modification of the surface reactive hydroxyl groups along the cellulose backbone. This would permit the CNCs to be dispersed in non-aqueous solvents and enhance their compatibility with a wide range of hydrophobic polymer matrices. Esterification,<sup>10</sup> cationization,<sup>11</sup> carbamination,<sup>12-14</sup> silylation,<sup>15</sup> amidation,<sup>16, 17</sup> polymer grafting<sup>18, 19</sup> and etherification<sup>20</sup> have all been successfully used to modify the surface of CNCs. However, such approaches are rarely suitable for large scale implementation or have limitations in the functionalities that can be introduced. The present work explores triazine chemistry – a well-known technology in the textile, agriculture, polymer, and paper industries for the production of dyes,<sup>21</sup> herbicides,<sup>22</sup> optical brighteners,<sup>23</sup> and dendrimers<sup>24</sup> – as a simple, versatile, and mild approach to carry out the modular surface modification of cellulose, especially CNCs, with potential for large scale implementation. Haller and Heckendorn<sup>21</sup> pioneered the triazine chemistry for affixing amino-reactive dyes onto cellulose fibres for coloration. Helbert et al.,<sup>25</sup> Ringot et al.,<sup>26</sup> and Walczak et al.<sup>27</sup> further extended this process for the grafting of fluorescent dyes, porphyrin, and *N*-lipidated oligopeptides onto cellulose fibres, for applications involving the study of cellulase activity, endowing cellulose with antibacterial properties, and for metabolite profiling, respectively.

Our choice of 2,4,6-trichloro-1,3,5-triazine (cyanuric chloride) as a linker molecule derives not only from its commercial availability and low cost, but also from the ease of derivatizing cyanuric chloride with nucleophiles to generate a myriad of mono- or di-

substituted 1,3,5-triazines. In our approach, the surface functionality of CNCs is strategically tuned by first grafting the targeted molecules (small or polymeric) onto the cyanuric chloride linker, and then grafting the resulting triazinyl derivatives onto CNCs in a single step. In this way, the triazinyl linker can be used either as a standalone modification or as a building block for secondary modifications with biorthogonal chemistries. An additional advantage of this chemistry is that the selective chlorine substitution of cyanuric chloride can be controlled with moderate temperatures, making it a highly predictable procedure for nanocellulose modification. More importantly, to the best of our knowledge, this is the first article detailing the use of triazine chemistry in tuning the interfacial properties of nanocellulose.

We report the grafting of four different triazinyl derivatives onto crystalline cellulose fibres or CNCs. These consist of non-polar aliphatic chains (octadecylamine, C18), polymer chains (poly(ethylene glycol) mono allyl ether, APEG), aromatic rings (benzylamine) and alkyne functionalities (propargylamine). Depending on the chemical moiety coupled to cyanuric chloride, the surface modification of CNCs was carried out in polar or non-polar solvents. With this chemistry, the polarity of the CNC surface has been tuned to enable their dispersion in a range of solvents to form homogenous colloidal suspensions that are stabilized through electrostatic and steric interactions. In addition, two triazine derivatives are amenable to further addition chemistries such as click reactions. Thus, as proof-of-concept, nanocellulose modified with propargyl-triazine derivatives was further modified with fluorescein through an azide-alkyne click reaction.

Our intention is to leverage the triazine chemistry as a versatile and low-cost technique for surface modification of CNCs. It is anticipated that this surface chemistry will aid in the production of functional CNCs that can be deployed in high volume nanocomposite processing, rheological modification, cosmetics, and sensing applications.

## 2.3 Experimental section

### 2.3.1 Materials

Octadecylamine (C18), benzylamine, propargylamine, cyanuric chloride, triethylamine, *N,N*-diisopropylethylamine (DIPEA), sodium hydroxide (NaOH), Whatman grade 1 cellulose filter paper (10 mm) and potassium carbonate (K<sub>2</sub>CO<sub>3</sub>) were purchased from Sigma-Aldrich (Oakville, ON, Canada). Poly(ethylene glycol) monoallyl ether (MW 388 g/mol) was a gift from EnRoute Interfaces, Inc. (Hamilton, ON, Canada). 5-Fluorescein azide (5-FAM-Azide) was purchased from Lumiprobe Corp. (Hunt Valley, MD, USA). Spray-dried cellulose nanocrystals hydrogen sulphate sodium salt (CNCs) were provided by CelluForce Inc. (Montreal, QC, Canada). All solvents including dichloromethane (DCM), acetone, ethanol, *N,N*-dimethylformamide (DMF), tetrahydrofuran (THF) and chloroform were purchased from Caledon Laboratories (ON, Canada) and used as received. Bacterial microcrystalline cellulose (BMCC) was isolated in house from the commercial foodstuff Nata de Coco.

### 2.3.2 Characterization

**Nuclear Magnetic Resonance (NMR).** (<sup>1</sup>H and <sup>13</sup>C NMR) spectra were obtained on a Bruker AV600-600 MHz NMR spectrometer using deuterated CDCl<sub>3</sub> and CD<sub>2</sub>Cl<sub>2</sub> as solvents.

**Mass Spectrometry (MS).** Mass spectra of synthesized dichlorotriazinyl derivatives were recorded on a Micromass Ultima (LC-ESI/APCI) Triple Quadrupole Mass spectrometer and Micromass Global Ultima ESI Quadrupole Time of Flight (Q-TOF) Mass spectrometer.

**Fourier Transform Infrared Spectroscopy (FTIR).** FTIR spectra of unmodified and modified CNCs were recorded on a Thermo Nicolet 6700 FTIR spectrometer in transmission mode using KBr disks loaded with 1 wt % sample dried under vacuum overnight at 60 °C.

**X-ray Photoelectron Spectroscopy (XPS).** Spectra were recorded with a Thermo Scientific Theta Probe XPS spectrometer with monochromatic Al K $\alpha$  radiation (50 W) at a takeoff angle of 45 $^{\circ}$  and a spot size of 200  $\mu\text{m}$ . Survey and high-resolution spectra were collected with pass energies of 280 eV and 26 eV respectively, and data were analysed with the software provided with the instrument. Unmodified and modified CNC samples, 1 wt%, were deposited via drop casting onto clean silicon wafers and air dried at room temperature before analysis.

**Elemental Analysis.** Mass fractions of carbon, hydrogen, nitrogen, and sulfur were determined for vacuum-dried unmodified and modified CNCs by Micro Analysis Inc. (Wilmington, DE). The samples were combusted in a pure oxygen environment where product gases were separated and detected by thermal conductivity. Triplicates were measured for each sample, and averages are reported. The results obtained from this technique were used to determine the degree of substitution (DS), given by the number of hydroxyl groups substituted by dichlorotriazinyl derivatives per unit of anhydroglucose. The DS was calculated using equation (1) below; as reported,<sup>28</sup>

$$(DS) = \frac{72.07 - C \times 162.14}{M_g \times C - M_{C_g}} \dots \dots \dots (1)$$

where C is the relative carbon content in the sample; the numbers 72.07 and 162.14 correspond to the carbon mass of the anhydroglucose unit (C<sub>6</sub>H<sub>10</sub>O<sub>5</sub>) and the molecular weight of anhydroglucose, respectively; M<sub>g</sub> and M<sub>C<sub>g</sub></sub> correspond to the molecular weight of the dichlorotriazinyl derivatives (*i.e.*, compounds 1, 2, 3 & 4) linked to the anhydroglucose unit, and their carbon masses, respectively. Experimental values were corrected by a conversion factor of 1.077 considering unmodified CNCs as pure cellulose, which correlates with a relative carbon content of 44.44%, following a previously reported procedure.<sup>29</sup>

**Thermogravimetric Analysis (TGA).** Analyses were carried out on a TA instruments Q50 thermogravimetric analyser. Data was collected after placing *ca.* 10 mg of a vacuum

dried sample in a clean platinum pan and heating from ambient temperature to 800 °C under argon atmosphere (heating rate of 20 °C min<sup>-1</sup>).

**Fluorescence Microscopy.** Fluorescence images of BMCC labeled using triazine-alkyne/azide click chemistry were taken using a Nikon-Eclipse LV100N POL microscope, equipped with excitation and emission filters for fluorescein dye, a Retiga 2000R CCD monochromatic camera (QImaging, Surrey, BC, Canada), and CFI LU P 10x/0.25 NA and 40x/0.65 NA objectives (Nikon Canada Inc., Mississauga, ON, Canada).

**Dynamic Light Scattering (DLS).** The apparent hydrodynamic size was measured for native and surface modified CNCs in 0.025 wt% dispersions in water (except for DTC18 modified CNCs, where the measurements were done in 1:1 chloroform:DMSO) using a Malvern Zetasizer Nano particle analyzer. Triplicate samples were measured 15 times each, and the average hydrodynamic size is reported. The standard deviation from the triplicate samples is reported as the error for the measurements.

**Atomic Force Microscopy (AFM).** AFM images were obtained using an Asylum Research MFP-3D Classic™ Scanning Probe Microscope (Santa Barbara, CA, USA). Images were acquired in tapping mode with aluminum reflex coated silicon cantilevers (FMR, Nanoworld AG, Neuchâtel, Switzerland) with nominal spring constant of 2.8 Nm<sup>-1</sup> and resonant frequency of 75 kHz. Samples were prepared by spin coating solutions containing 0.001 wt % unmodified CNCs or 0.01 wt% modified CNCs samples onto piranha cleaned silicon wafers (for unmodified CNCs, the substrates were pretreated by spin coating with a 0.1% PAH solution) at 4000 rpm for 30 seconds and air dried at room temperature before analysis. CNC lengths were measured for individual particles within the images, and an average was calculated for n > 50 measurements. The error associated with the CNC lengths is reported as the standard deviation of the measurements.

**X-ray Diffraction (XRD).** Two-dimensional diffraction patterns were collected using a D8 Davinci diffractometer (Bruker, Billerica, MA, USA) equipped with a sealed tube cobalt source. Analysis of the resulting patterns was conducted using the Bruker TOPAS software and Matlab scripts. The beam was collimated to a diameter of 0.5 mm (35 mA,

45 kV). Cellulose samples were drop-cast and oven dried onto clean Si wafer pieces for the analysis. A still frame of a blank piece of Si was initially examined to correct for background. The background intensity was subtracted from each sample frame prior to integration of the data. A  $2\theta$  range of  $13\text{--}42^\circ$  was used for the crystallinity index (CrI) analysis. Integration along relative angle  $\chi$  for every  $2\theta$  value was performed to obtain one-dimensional diffraction plots of intensity versus  $2\theta$ . The background corrected intensity vs.  $2\theta$  plots were fitted to five symmetric Lorentzian peaks; four peaks corresponding to the (100), (010), (002), and (040) crystalline planes,<sup>30</sup> and one broad amorphous peak fixed at  $24.1^\circ$ . The CrI was calculated by the peak deconvolution method as the ratio of the area for the crystalline peaks over the total area for the diffraction plots.

**Contact Angle Measurements.** The wettability of modified cellulose fibres (Whatman filter paper) were assessed by static contact angle measurement through sessile drop method via OCA 20 Future Digital Scientific system (Garden City, NY, USA) equipped with a CCD camera. Water ( $1\ \mu\text{l}$  of  $18.2\ \text{M}\Omega\ \text{cm}^{-1}$ , A10-Merck-Millipore system, Darmstadt, Germany) was dropped onto modified cellulose paper while digital images were captured. The average of 3 replicate filter paper samples is reported as the contact angle.

### 2.3.3 Synthesis of 4,6-dichloro-*n*-octadecyl-1,3,5-triazine-2-amine (1, DTC18)

To a stirred solution of cyanuric chloride (5.0 g, 0.027 mol) in dry THF (50 mL) cooled to  $0\ ^\circ\text{C}$ , was added  $\text{Na}_2\text{CO}_3$  (2.86 g, 0.027 mol). After 20 minutes of stirring, a solution containing *n*-octadecylamine (7.28 g, 0.027 mol) in dry THF (100 mL) was added dropwise over a period of 45 min. The end of reaction – complete disappearance of starting material - was monitored via TLC (silica gel, DCM). The reaction mixture was filtered and THF was removed under vacuum to yield a white precipitate which was suspended in water for 1 h to remove any remaining  $\text{Na}_2\text{CO}_3$ . This suspension was filtered, and the filtrate was dried at room temperature to give the final product (white precipitate, 10.9 g, 97% yield).  $^1\text{H}$  NMR (600 MHz,  $\text{CD}_2\text{Cl}_2$ , ppm)  $\delta$ : 5.96 (s, 1H), 3.51-3.38 (m, 2H), 1.69-1.58 (m, 2H), 1.43-1.23(m, 31H), 0.90 (t,  $J=7.0\ \text{Hz}$ , 3H).  $^{13}\text{C}$  NMR (151 MHz,  $\text{CD}_2\text{Cl}_2$ , ppm)  $\delta$ : 170.20,

166.53, 41.94, 32.32, 30.44, 27.01, 23.08, 14.26. HRMS (ESI-QTOF): Calcd for  $C_{21}H_{38}Cl_2N_4$  as 417.46, Found 417.2543 ( $M^+$ ).

### 2.3.4 Synthesis of 4,6-dichloro-*n*-propargyl-1,3,5-triazine-2-amine (2, DTP)

To a stirred solution of cyanuric chloride (2.00 g, 10.85 mmol) in dry THF (25 mL) cooled to  $-20\text{ }^\circ\text{C}$ , was added a mixture of propargyl amine (0.59 g, 0.69 ml, 10.76 mmol). DIPEA (1.54 g, 2.08 ml, 11.94 mmol) in dry THF (5 mL) was then added dropwise over a period of 2 h with the help of a syringe pump. Thereafter, reaction mixture was stirred for another 3 h maintaining the reaction temperature between  $-20 - 0\text{ }^\circ\text{C}$ . After this time, THF was removed under vacuum to yield a residue that was dissolved in EtOAc (50 ml) in a separating funnel and washed with water (3 x 15 ml), followed by brine solution (30 ml) and finally dried over solid anhydrous  $Na_2SO_4$  to yield a pure product (white precipitate) in quantitative yield (2.18 g, 99%) under reduced pressure.  $^1H$  NMR (600 MHz,  $CDCl_3$ , ppm)  $\delta$ : 6.00 (s, 1H), 4.23 (dd,  $J=5.7, 2.5$  Hz, 2H), 2.26 (t,  $J=2.5$  Hz, 1H).  $^{13}C$  NMR (151 MHz,  $CD_2Cl_2$ , ppm)  $\delta$ : 170.62, 166.10, 78.16, 72.73, 31.61. MS (ESI): Calcd for  $C_6H_4Cl_2N_4$  203.03, Found 203.0 ( $M^+$ ).

### 2.3.5 Synthesis of 4,6-dichloro-*n*-benzyl-1,3,5-triazine-2-amine (3, DTB)

To a stirred solution of cyanuric chloride (1.00 g, 5.4 mmol) in dry THF (20 mL) cooled to  $-20\text{ }^\circ\text{C}$ , was added  $Na_2CO_3$  (0.58 g, 5.4 mmol). After 20 min of stirring, a solution containing benzylamine (0.58 g, 5.5 mmol) in dry THF (10 mL) was added dropwise over a period of 60 min. The end of reaction was monitored via TLC (silica gel, DCM). The product was isolated by centrifugation followed by filtration of the supernatant, and evaporation under vacuum to yield a pure product (white precipitate) in quantitative yield (1.35 g, 98%).  $^1H$  NMR (600 MHz,  $CDCl_3$ , ppm)  $\delta$ : 7.45-7.28 (m, 5H), 6.10 (s, 1H), 4.67 (d,  $J=6.0$  Hz, 2H).  $^{13}C$  NMR (151 MHz,  $CDCl_3$ , ppm)  $\delta$ : 169.81, 165.50, 136.07, 129.03, 128.25, 127.76, 45.52. MS (ESI): Calcd for  $C_{10}H_8Cl_2N_4$  255.10, Found 255.3 ( $M^+$ ).



### 2.3.6 Synthesis of 4,6-dichloro-2-poly(ethylene glycol) mono-allyl-1,3,5-triazine-2-ether (4, DTAPEG)

To a stirred solution of cyanuric chloride (2.00 g, 10.85 mmol) in DCM (30 mL) cooled to -20 °C, was added poly(ethylene glycol) mono-allyl ether (4.21 g, 10.85 mmol) dissolved in DCM (20 mL). After 20 min of stirring, a NaOH solution (50%, 1 g in 2 mL of water) was added dropwise over 30 min with constant stirring. After 2 h of stirring while keeping temperature near 0 °C, the organic layer was separated and washed twice with water (2 x 10 ml), dried over Na<sub>2</sub>SO<sub>4</sub> and concentrated under vacuum, resulting in an oily product (5.0 g, 86% yield). <sup>1</sup>H NMR (600 MHz, CDCl<sub>3</sub>, ppm) δ: 5.99-5.84 (m, 1H), 5.31-5.12 (dd, 2H), 4.72-4.54 (m, 2H), 4.03 (d, *J*=5.5 Hz, 2H), 3.91-3.81 (m, 2H), 3.78-3.5 (m, 29H). <sup>13</sup>C NMR (151 MHz, CDCl<sub>3</sub>, ppm) δ: 172.50, 171.06, 134.78, 117.07, 72.36, 71.32, 69.40, 68.42.

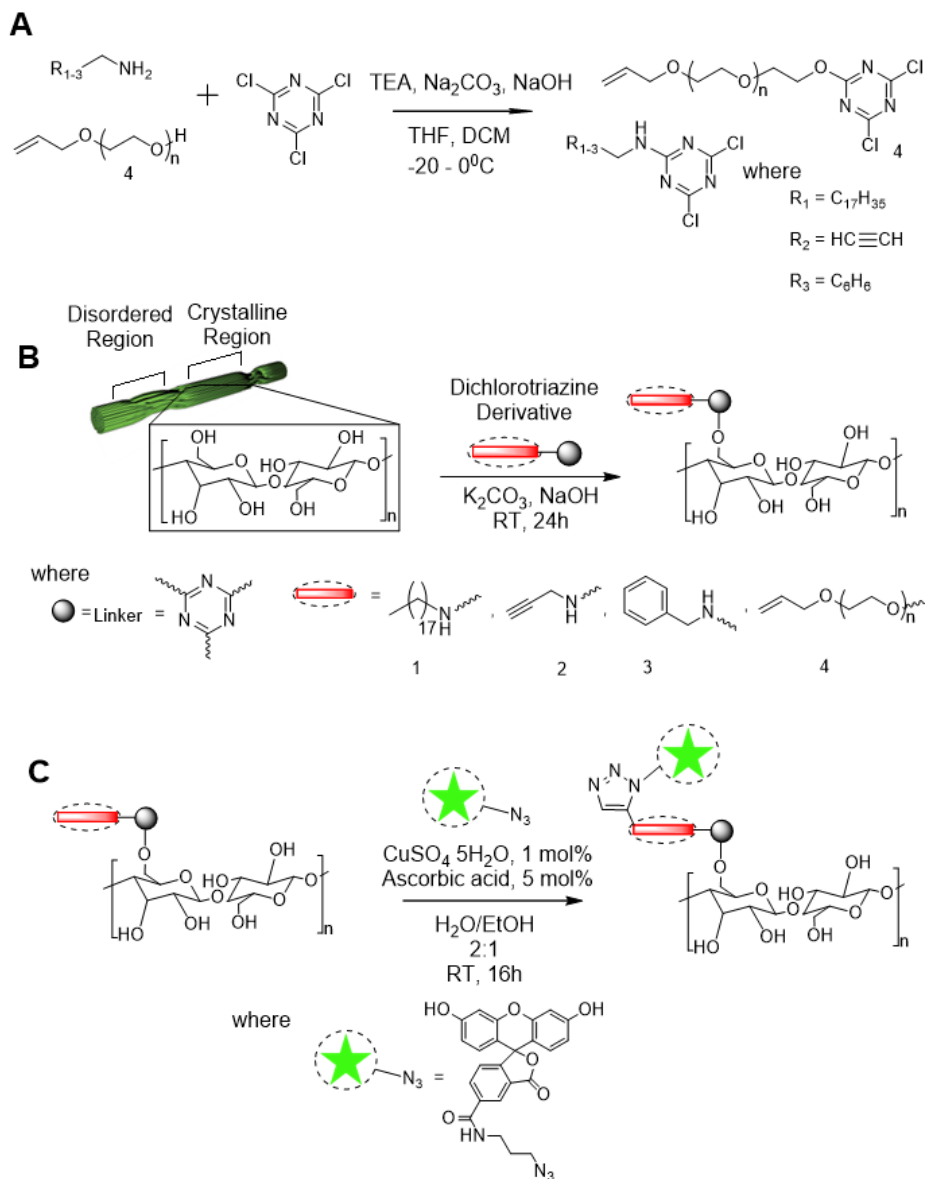
### 2.3.7 Chemical Grafting of Dichlorotriazinyl Derivatives onto Nanocellulose

Two methods were used in the grafting of dichlorotriazinyl derivatives onto CNCs (Scheme 1b); **Method 1**: An aqueous suspension of CNCs (20 mL, 1 wt%) in a 100-ml round-bottomed flask was solvent-exchanged into DMF (30 mL) by vacuum-assisted rotary evaporation removing small portion of water (10 mL). This was followed by successive centrifugation (10,000 g, 5 °C, 10 min) and resuspension in acetone and then dry DCM, with sonication (10 min, 5 °C) in between each solvent exchange step to prevent CNC aggregation. To a stirred suspension containing CNCs in dry DCM (0.5 g, 1 wt%) was added K<sub>2</sub>CO<sub>3</sub> (0.25 g, 1.81 mmol). After 20 min, 5 mmol of **1**, **2** or **3** (10:1 excess to the surface OH per g of CNCs) in dry DCM (10 ml) were added and left to stir at room temperature for 24 h. Modified CNCs were then subjected to 3 successive centrifugation and sonication steps in DCM to remove excess dichlorotriazinyl derivatives. This was followed by stirred cell dialysis to remove inorganic base and any leftover unbound derivatives in the presence of acetone (3 cycle runs), acetone-water (50%, 3 cycle runs) and water (14 cycle runs). **Method 2**: Since compound **4** is hydrophilic in nature, the solvent exchange procedure in method 1 was not necessary and the grafting reaction was

carried in a 70% water/acetone system. Compound **4** (5 mmol) in acetone (20 mL) was added to a stirred suspension containing CNCs in milliQ water (0.5 g, 1 wt%). Then, NaOH (10 mL, 0.2 N) was added to the mixture drop-wise over 30 min and left to react under continuous stirring at room temperature for 24 h. A similar cleanup procedure as method 1 above, was utilized for DTAPEG-modified CNCs.

### **2.3.8 Fluorescein Labeling of Nanocellulose by an Azide-Alkyne Click Reaction (Scheme 1c)**

An aqueous suspension of BMCC (10 ml 0.3 wt%) was solvent-exchanged by successive centrifugation (10,000 g, 5 °C, 5 min) and resuspension in acetone and then dry DCM, with sonication (10 min, 5 °C) in between each solvent exchange step to prevent BMCC aggregation. To a stirred suspension containing BMCC (30 mg, 0.3 wt%) in dry DCM (10 mL), K<sub>2</sub>CO<sub>3</sub> was added (15 mg, 0.11 mmol). After 20 min, compound **2** (30 mg, 0.15 mmol) in dry DCM (2 mL) was added and left to stir at room temperature for 24 h. Modified BMCC was then subjected to 3 successive centrifugation and sonication steps in DCM to remove excess DTP derivatives. This was followed by stirred cell dialysis to remove inorganic base and any leftover unbound derivatives in the presence of acetone (3 cycle runs), acetone-water (50%, 3 cycle runs) and water (14 cycle runs). The modified BMCC was then used in the azide-alkyne click reaction as follows. A solution containing 5-FAM-azide (2 mg, 4.36 µmol) in ethanol (1 mL) was added to a stirred suspension



**Scheme 1.** (a) Synthesis of 4,6-dichloro-1,3,5-triazine derivatives; (b) chemical grafting of 4,6-dichloro-1,3,5-triazine derivatives onto cellulose; and (c) fluorescein azide click grafting onto alkyne-modified nanocellulose.

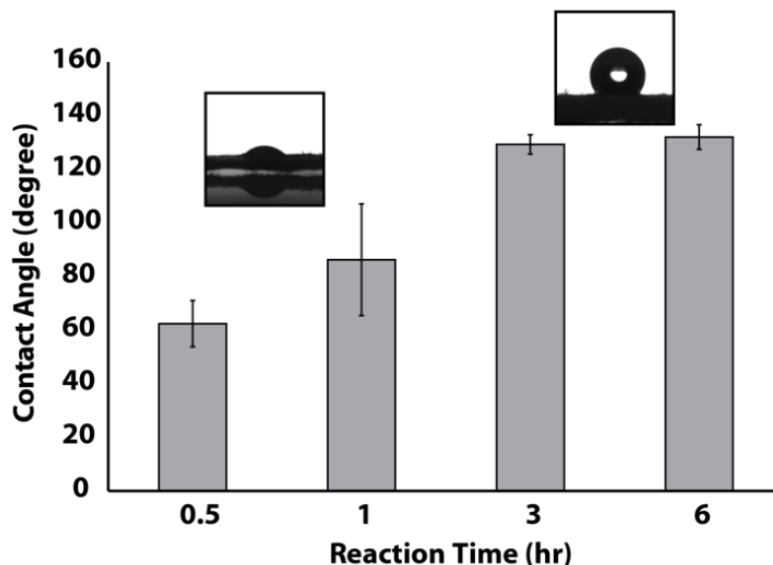
containing DTP-modified BMCC (6 mg) in milliQ H<sub>2</sub>O (2 mL), followed by the addition of a solution containing CuSO<sub>4</sub> × 5H<sub>2</sub>O (0.2 mg) and ascorbic acid (0.6 mg) in milliQ H<sub>2</sub>O (100 μL). The reaction mixture was stirred overnight in the dark at room temperature. The

fluorescently labelled BMCC was cleaned-up with milliQ water through stirred-cell dialysis until the effluent gave a UV absorbance value similar to that of water.

## **2.4 Results and Discussion**

### **2.4.1 Triazine-Coordinated Chemical Grafting onto Nanocellulose**

Cyanuric chloride was utilized as a linker to tune the interfacial properties of nanocellulose in a modular fashion. In the synthetic approach, one of the three chlorine atoms of cyanuric chloride was substituted with octadecylamine (DTC18, 1), propargylamine (DTP, 2), benzylamine (DTB, 3), or poly(ethylene glycol) mono-allyl ether (DTAPEG, 4), to yield four distinct triazinyl derivatives (Scheme 1a) with different physicochemical characteristics. After thorough characterization of the derivatives (NMR and MS spectra presented in Figures S2.1-S2.4, Appendix 2), the triazine chemistry on cellulose was first demonstrated by grafting DTC18 onto filter paper. This one-step reaction proceeded rapidly at room temperature and allowed us to tune the hydrophilicity of the cellulose surface (Figure 2.1). Under the reaction conditions selected for the triazine substitution, the filter paper presented water contact angles of  $\sim 125^\circ$  after 3 hrs. The contact angle did not increase even after doubling the reaction time, which points to a saturation of the cellulose surface with DTC18. Furthermore, it was observed that the water droplets remained intact on the surface of the modified paper even after prolonged incubation, indicating that the surface functionalization turned the filter paper into an effective water barrier. However, plasma oxidation of the modified cellulose surface returned the filter paper to a hydrophilic state, allowing full penetration of the water droplet into the filter lumen. These results show that the triazine chemistry can be used to tune the interfacial properties of cellulosic materials, where a DTC18-based modification can be used to define hydrophilic/hydrophobic areas, with application in the fabrication of channels for paper-based micro-analytical devices.



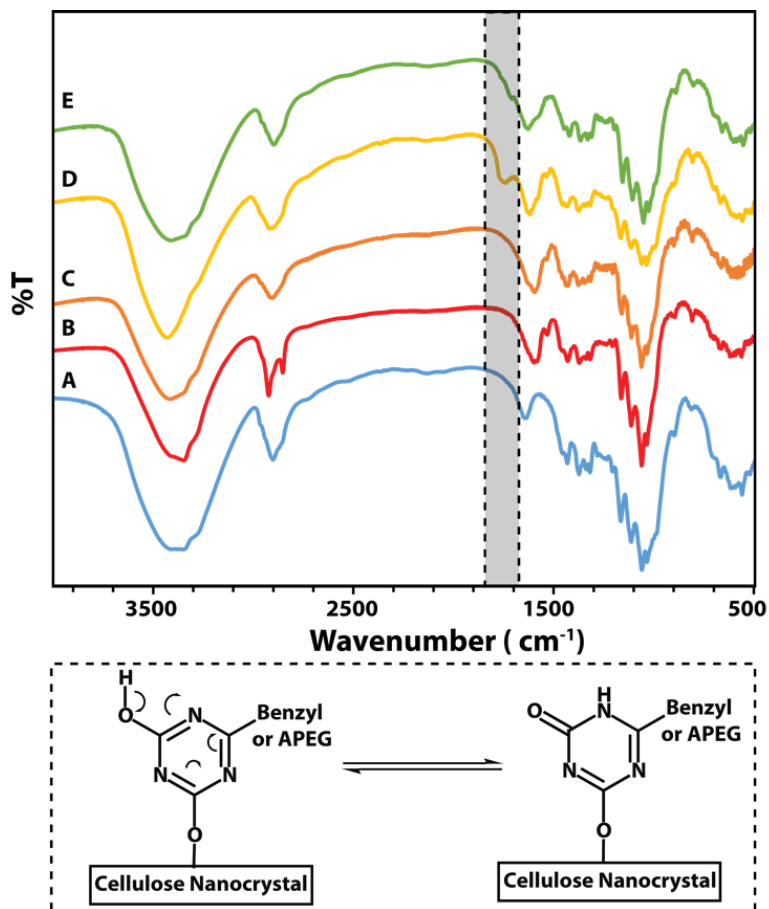
**Figure 2.1** Tunable hydrophobization of filter paper through the controlled grafting of **DTC18** derivatives. Insets show the sessile water droplet contact angle measured on the filter paper after treatment. Error bars represent the standard deviation,  $n = 3$ .

Having demonstrated the triazine-mediated grafting for macroscopic cellulosic materials, we focused our attention on the surface modification of CNCs. The chemical modification of CNCs with non-polar moieties presents a challenge, due to the charge imparted by the sulfate half-ester groups introduced during the production of CNCs via sulfuric acid hydrolysis.<sup>9, 28</sup> Therefore, for the successful grafting of **DTC18**, **DTP**, and **DTB** onto CNCs, an initial solvent exchange was performed from an aqueous suspension to dichloromethane (DCM). This enabled the chemical modification of CNCs without aggregation using non-polar triazinyl derivatives **1**, **2** & **3** at ambient temperature in the presence of solid potassium carbonate as a hydrochloric acid scavenger (Scheme 1b). Conversely, the chemical grafting of **4** (a polar triazinyl derivative) onto CNCs was carried out in a straight-forward fashion in aqueous solutions, where sodium hydroxide was used as the base. The etherification of CNCs by the triazinyl derivatives involved the nucleophilic aromatic substitution of the chlorine atoms present in compounds **1-4** by the

numerous surface hydroxyl groups along the crystalline cellulose backbone. It has been reported that the ether linkages are stable, as shown by the imaging of bacterial cellulose microfibrils and CNCs fluorescently labeled with DTAF (dichlorotriazinyl-aminofluorescein).<sup>25,32, 33</sup> To ensure that no unbound triazinyl derivatives were non-specifically adsorbed onto the CNCs after the modification reactions, they were subjected to a rigorous cleanup procedure involving several washing steps through centrifugation (to remove the bulk of the unreacted material and base), followed by several cycles of stirred-cell dialysis. This cleanup procedure has been previously shown as an effective way to obtain reproducible and predictable DTAF grafting results.<sup>33</sup>

FITR spectroscopy was used to confirm the covalent grafting of the triazinyl derivatives onto CNCs. Figure 2.2 shows a comparison between the FTIR spectra of unmodified and chemically modified CNCs, demonstrating the successful grafting of C18, APEG, propargyl and benzyl functionalities onto CNCs. The data shows the appearance of distinct and unique absorption bands around 1630 - 1560  $\text{cm}^{-1}$  in each modified sample, which correspond to the C=N and C-N  $\text{sp}^2$  vibrations present in the triazine rings chemically grafted onto CNCs. The modified CNCs also exhibit a narrower OH stretching band (3360  $\text{cm}^{-1}$ ) with broad shoulders (overlapping N-H, C $\equiv$ C-H and C=C-H stretching vibrations 3300 – 3010  $\text{cm}^{-1}$ ) due to the depletion of hydroxyl groups and the introduction of new chemical bonds at the cellulose surface. In addition, the appearance of characteristic aliphatic C-H stretching absorption bands (2960-2850  $\text{cm}^{-1}$ ) in modified CNCs (most prominent in C18) further confirms chemical grafting of the different triazinyl derivatives onto CNCs. It is also worth noting that a tautomeric shift within the triazine ring is observed in both benzyl (prominent) and APEG (minor) modified CNCs, which corresponds to the formation of amide bonds (1725  $\text{cm}^{-1}$ , new C=ONH vibrations) with  $\alpha,\beta$ -unsaturation. This results from the substitution of the last chlorine atom (6-Cl) in the 4,6-dichlorotriazinyl derivatives by a hydroxyl group after initial chemical grafting onto the CNCs that, in turn, involves the shift of a proton from the introduced OH (enol form) to one of the adjacent nitrogen atoms. The outcome is a delocalization of the  $\pi$ -electrons within the triazine ring to form amide bonds (keto form, Figure 2.2). This phenomenon was found to occur while

drying the modified CNCs at elevated temperatures, as any bound water molecule can force the substitution of the third chlorine atom. Hence, the tautomeric shift into its most stable form.<sup>34,35</sup>



**Figure 2.2** FTIR spectra of (A) unmodified CNC and (B-E) modified CNCs. The modified CNCs bear (B) **DTC18**, (C) **DTP**, (D) **DTB**, and (E) **DTAPEG** moieties. Inset shows the triazine ring tautomeric shift in **DTB** and **DTAPEG** modified CNCs.

#### 2.4.2 Surface Grafting Efficiency of Triazinyl Modified CNCs

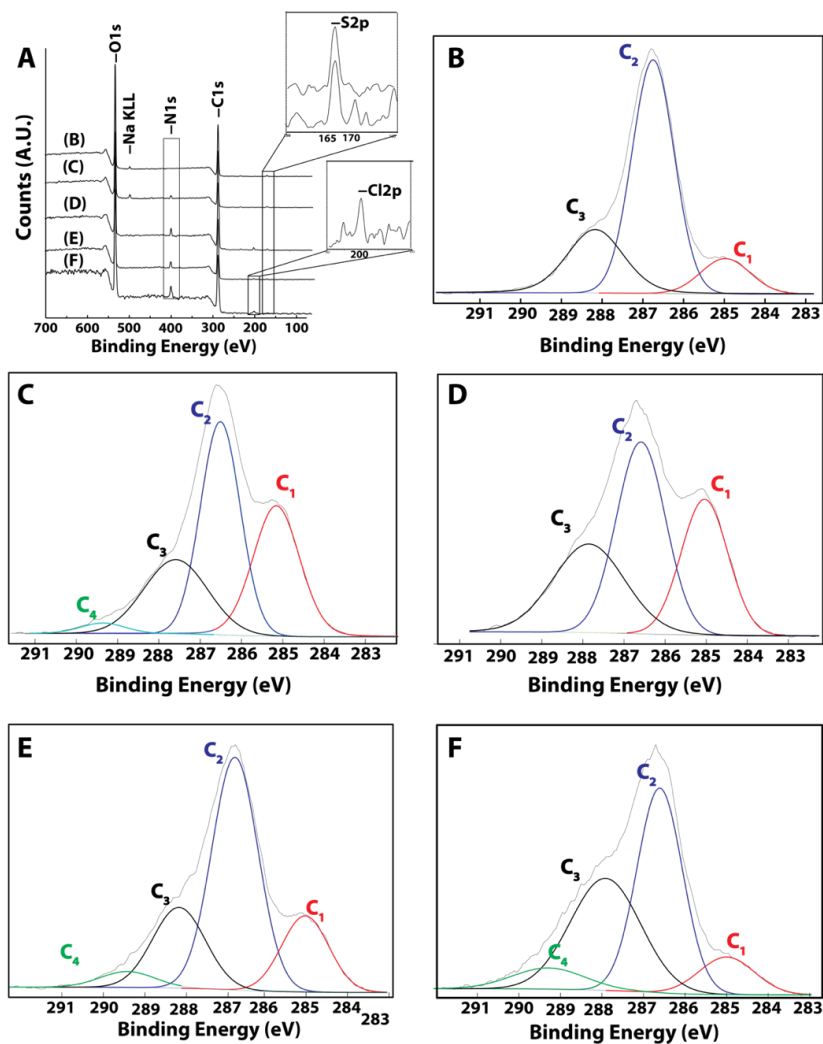
The surface modification efficiency of the triazine chemistry was established using X-ray photoelectron spectroscopy (XPS) and elemental analysis (EA), while X-ray diffraction

(XRD) measurements were used to establish the retention of the crystallinity of unmodified and modified CNCs. Full scan low-resolution XPS spectra are shown in Figure 2.3a, highlighting the characteristic peaks observed around binding energies 287 and 534 eV, which correspond to carbon and oxygen atoms, respectively, as the main components in the anhydroglucose units of cellulose. The value of 0.80 oxygen-to-carbon (O/C) ratio (Table S1, Appendix 2) for unmodified CNCs is close to those reported for pure cellulose.<sup>36</sup> As expected, the O/C ratios for all triazinyl-modified CNCs decreased in comparison to unmodified CNCs, a clear demonstration of the increase in carbon content as chemical modification was carried out. A small amount of sulfur was also detected at ~168 eV, which arose from sulfate half-ester groups grafted onto CNCs during production via sulphuric acid hydrolysis. In addition, modified CNCs exhibited distinct peaks at 400 and 200 eV, corresponding to nitrogen (N) and chlorine (Cl) atoms, respectively, that are non-native to cellulose. These new chemical signatures arise from the successful grafting of triazinyl derivatives and were consistently seen in all modified CNCs, with the exception of **DTAPEG**-CNCs where chlorine was not present in a detectable amount. This finding can be explained by the displacement of all chlorine atoms on the triazine ring when the grafting reaction was performed under basic conditions in an aqueous environment. Under these conditions, the last remaining chlorine atom could be displaced via hydrolysis after the initial **DTAPEG** grafting. The low-resolution XPS results thus confirmed the surface grafting of triazinyl derivatives onto CNCs.

An additional advantage of XPS analysis is that detailed information about the surface chemistry of modified CNC can be retrieved from the deconvolution of high resolution (surface) C1s signals. The high-resolution C1s spectra from unmodified and modified CNCs were deconvolved into the various carbon peaks, which reflect their local environments. The C1, C2, C3 and C4 peaks with corresponding bond energies of 285.0, 286.3, 287.7, and 288.9 eV, were assigned to C-C/C-H aliphatic linkages, C-O linkages in alcohols and ethers, O-C-O/C=O linkages in acetals, and O-C=O linkages in esters, respectively.<sup>28, 36</sup> Changes in the intensities of the C1s signals (Figure 2.3) reflect changes in the relative proportions of the (surface) chemical bonds involving carbon atoms



(including new types of bonds) associated with the grafted triazinyl derivative. A marked increase in



**Figure 2.3** Low-resolution XPS spectra (a) and high-resolution C 1s peak deconvolution of (b) unmodified CNC and CNCs modified with (c) **DTAPEG**, (d) **DTC18**, (e) **DTB**, and (f) **DTP**. Insets in panel (a) show the (S2p) and Cl (Cl2p) signals respectively indicating the presence of sulfur and chlorine.

C1 intensity was observed for **DTC18**-CNCs and **DTAPEG**-CNCs, confirming the successful grafting of aliphatic/ethylene chains onto CNCs through the triazine chemistry. On the other hand, only a small increase was recorded for benzyl- and propargyl-grafted CNCs, since their aliphatic/C-C bond contribution is minimal. All modified CNCs showed an expected increase in C3 peak intensity, which results from the new O-C=N or N-C=N bonds introduced by the covalent linkage between the triazinyl derivatives and the CNC surface.

While the low resolution XPS results corroborate the presence of nitrogen and chlorine on modified CNCs, it was impossible to reliably determine the degree of surface substitution from the high-resolution data since the binding energies of the newly introduced O-C=O and N-C=N bonds overlap with those of acetal groups present in unmodified CNCs. Thus, elemental analysis was carried out to determine the degree of substitution (DS) in modified CNCs. DS values were calculated for modified CNCs from their relative atomic compositions (C, H, N and S presented in Table 1) according to Equation 1. A corrected carbon content was used in the calculation to account for the difference between the theoretical value (44.44%) and the experimentally obtained value (41.28%) for unmodified CNCs, which is in line with reported values.<sup>28, 29</sup> The difference between theoretical and experimental values is ascribed to organic impurities adsorbed onto the surface of CNCs during storage or processing. A significant increase in nitrogen content over the baseline of unmodified CNCs was observed in all modified materials, as expected from the introduction of the triazinyl moiety. In addition, small amounts of sulfur from sulfate half ester groups were observed in all samples, indicating that no significant desulfation occurred during the grafting procedure. The relative decrease in %S for modified CNCs, most noticeable in those bearing the bulkier **DTC18** and **DTAPEG** derivatives, was expected as a result of the proportional increase in C, H, and N content from the grafted triazinyl derivatives. The number of triazinyl derivatives grafted per 100 anhydroglucose units, as calculated from the carbon elemental analysis data, were 11, 18, 16 and 6 for **DTC18**, **DTP**, **DTB** and **DTAPEG** grafted CNCs, respectively. These numbers correspond to 4-6% of the hydroxyl groups bearing triazine ether linkages in **DTC18**, **DTP**

and **DTB**-modified CNCs, and 2% in the case of **DTAPEG** grafting. The DS values reported here correspond to a high grafting efficiency, and are comparable to values reported for other chemistries used in the surface modification of CNCs.<sup>37, 38</sup> Furthermore, the DS could be tuned by modifying the grafting conditions to tune the surface energy of CNCs, since only a small number of grafted molecules are needed to modify the interfacial properties of CNCs.<sup>39</sup>

**Table 1.** CNC characterization<sup>a</sup>

Sample	%C (corrected)	%H	%N	%S	DS	CI (%)	Length (nm)	AHPR (nm)
CNCs	41.28 (44.44)	6.07	0.05	0.72	–	95 ± 1	150 ± 40	90 ± 40
<b>DTAPEG-CNCs</b>	42.41 (45.67)	6.37	1.88	0.65	0.06 ± 0.01	90 ± 4	150 ± 30	130 ± 40
<b>DTB-CNCs</b>	44.26 (47.67)	5.95	2.50	0.70	0.16 ± 0.01	87 ± 1	140 ± 30	140 ± 50
<b>DTP-CNCs</b>	42.49 (45.76)	5.81	3.70	0.73	0.18 ± 0.04	87 ± 3	170 ± 30	240 ± 120
<b>DTC18-CNCs</b>	46.13 (49.68)	7.08	2.54	0.59	0.110 ± 0.003	78 ± 4	280 ± 80	300 ± 100

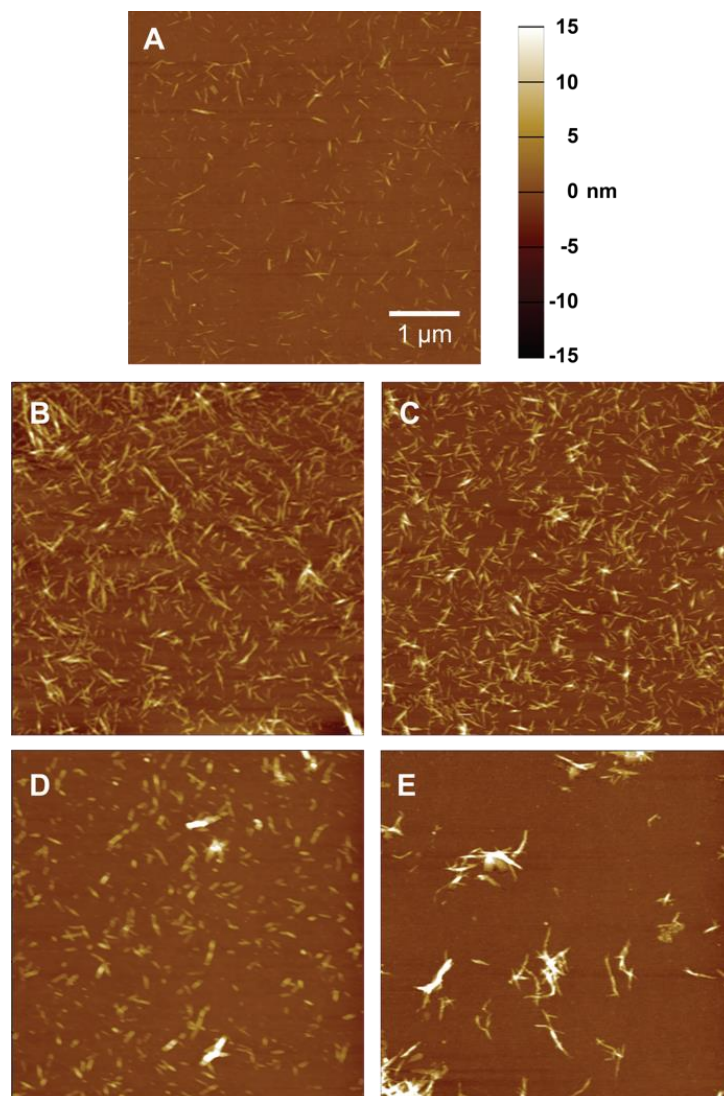
<sup>a</sup>The composition of all CNC materials was determined by elemental analysis (corrected values in parenthesis), CNC crystallinity index (CI) was quantified by X-ray diffraction, CNC lengths were obtained from AFM images (histograms shown in Figure S2.5, Appendix 2), and the apparent hydrodynamic particle radius (AHPR) was obtained from DLS measurements (representative measurements shown in Figure S2.5, Appendix 2). Values for all measurements are means of  $n > 3$  replicate samples, except for AFM, where  $n > 50$  particles were measured. Errors represent standard deviations.

### 2.4.3 Structural Characterization of Modified Cellulose Nanocrystals

X-ray diffraction (XRD) measurements were performed to assess the crystallinity of native and modified CNCs. The crystallinity index (CI) was determined using 2-dimensional diffraction intensity patterns (Figure S2.6, Appendix 2). Integration along the relative angle  $\chi$  for every  $2\theta$  value was performed to obtain one-dimensional plots of intensity versus  $2\theta$ . Background corrected intensity vs.  $2\theta$  plots for native CNCs were then fitted to five

symmetric Lorentzian peaks, four peaks corresponding to the (100), (010), (002), and (040) crystalline planes,<sup>30</sup> and one broad amorphous peak fixed at 24.1°. The four crystalline peaks were used to create a base crystalline cellulose scattering function, and the CI was calculated as the ratio of the area of this scattering function to the total area under the curve. This methodology has been previously validated against CNC-polymer mixtures with well defined compositions.<sup>40</sup> This method yielded a CI value of 95% for unmodified CNCs (Table 1), which is in agreement with previous measurements.<sup>40, 41</sup>

The scattering plots for CNCs modified with triazinyl derivatives (Figure S2.6, Appendix 2) were then fit to the base crystalline scattering function, where only the overall amplitude of the function was allowed to vary. This allowed the crystalline signal to be fitted keeping the relative proportion of each of the four crystalline peaks found in native CNCs constant. This practice was important because the triazinyl modifications could introduce signals that overlapped with the crystalline peaks and could bias the calculated crystallinity if each one of the crystalline peaks was fitted independently. The CI for the modified materials was then calculated as the ratio of the area under the crystalline scattering function over the total area under the curve. In all cases, it was observed that the introduced triazinyl modification moderately lowered the CI value (Table 1), since the grafted materials contributed to the signal considered amorphous. The changes in crystallinity were dependent not only on the degree of substitution, but also the size of the grafted molecule, as evidenced by the largest decrease for **DTC18**-grafted CNCs. A quick calculation using published values for CNC length and width (130 and 8 nm, respectively),<sup>41</sup> and crystalline cellulose density (1.5 g/cm<sup>3</sup>),<sup>42</sup> and using the degree of substitution obtained from elemental analysis (Table 1), indicated that the mass of the crystalline cellulose core would represent ~79% of the total mass of the **DTC18**-modified nanoparticles. This is in good agreement with the CI values obtained from XRD, suggesting the crystallinity of the core CNCs was not affected by the modification, and that the changes in the scattering intensity arise solely from the surface grafting of the triazinyl derivatives.



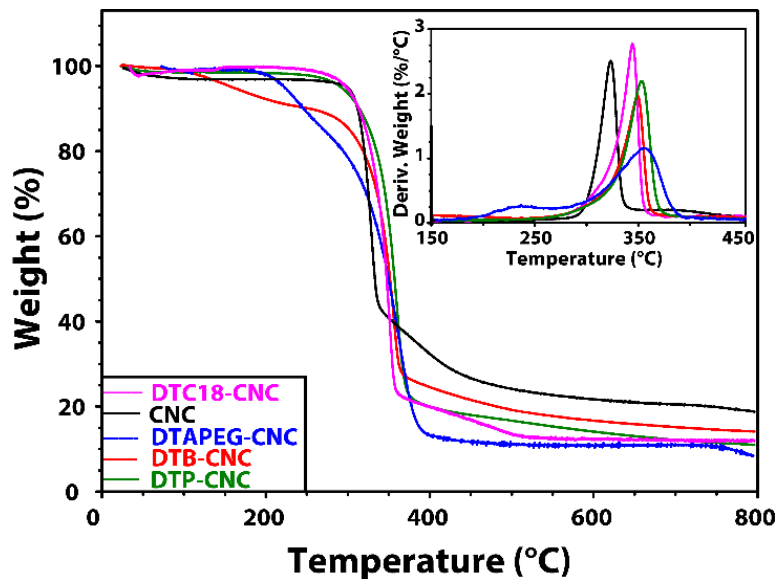
**Figure 2.4** AFM height images of (A) unmodified CNC and CNCs modified with (B) **DTAPEG**, (C) **DTB**, (D) **DTP**, and (E) **DTC18**. All images acquired at the same magnification.

AFM imaging was performed on dilute spin coated samples of the unmodified and modified CNCs to confirm the individual nature of the nanoparticles. Figure 2.4 shows that the native CNCs, as well as those modified with DTAPEG, DTB, and DTP appear well dispersed and can be identified as individual particles, with only a few aggregates appearing in the modified materials, and being more predominant in the DTP sample. On the other hand, CNCs modified with DTC18 showed a proportion of the sample in the form

of sub-micron aggregates, where multiple individual particles could be visualized. Quantification of the length of the particles in the AFM images confirmed the visual observations, and yielded histograms with narrow dispersions for CNCs bearing DTAPEG, DTB and DTP, and a wider distribution of sizes for those modified with DTC18 (Figure S2.5, Appendix 2). The averages and standard deviations for samples measuring  $n > 50$  particles are presented in Table 1.

#### 2.4.4 Thermal Stability of Triazinyl Modified CNCs

The thermal degradation of CNCs during nanocomposite processing can severely limit their applicability. Thus, maintaining thermal stability after surface modification is a key requirement for the use of modified CNCs. Thermogravimetric analysis (TGA) was performed on unmodified and modified CNCs to study the effect that the chemically grafted triazinyl derivatives have on stability. The unmodified CNCs showed a thermal degradation profile characteristic to commercial CNCs<sup>41</sup> (sodium salt form) with the onset of degradation occurring at  $\sim 300$  °C and the fastest degradation at  $\sim 330$  °C (Figure 2.5). We observed that all modified materials had a similar onset, but showed a slight enhancement in thermal stability, as evidenced by the fastest degradation of the cellulose core observed at  $\sim 350$ ,  $355$ ,  $360$ , and  $365$  °C for **DTC18**, **DTB**, **DTP** and **DTAPEG** grafted CNCs, respectively (Figure 2.5, inset). This indicates that the sulfate half-ester groups on the backbone of the crystalline cellulose are further protected by the surface modification with the triazinyl derivatives. Nevertheless, the **DTAPEG** modified particles showed partial degradation at lower temperatures, which is ascribed to the degradation of the grafted polymer chain, whose thermal stability is lower.

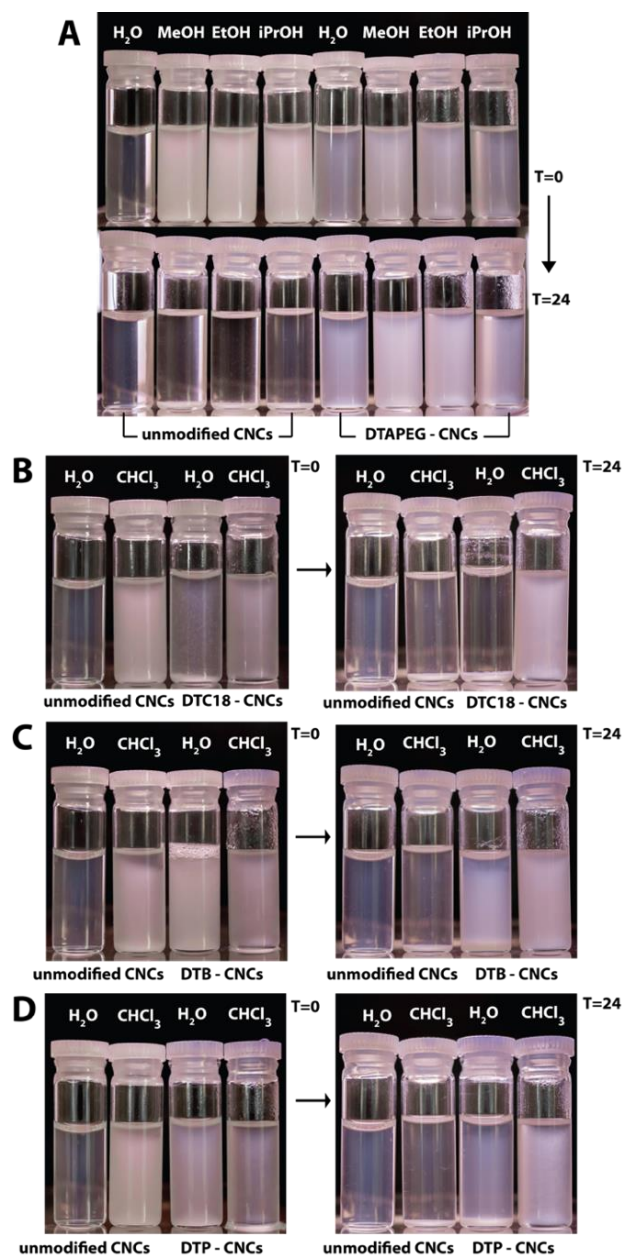


**Figure 2.5** TGA thermograms and derivative curves (Inset) of unmodified and modified CNCs.

#### 2.4.5 Dispersion of Modified CNCs in Aqueous/Organic Media

One of the goals of this work was to enhance the dispersion and stability of CNCs in a wide range of solvents through their modification with triazinyl derivatives. The blending of CNCs into materials for the formation of nanocomposites benefits from the compatibilization of the CNC surface chemistry with the receiving matrix, which ensures reduced aggregation, more uniform dispersion, and better transfer of the intrinsic CNC properties to the composite. To demonstrate this, the modified CNCs were dispersed in aqueous and organic media and the suspensions were followed over time to investigate the impact of the introduced surface functionalities on the stability of the suspensions. Unmodified and modified CNCs were dispersed in solvents at a concentration of 0.5 wt% through 15-minute point probe sonication in an ice bath. Figure 2.6 shows pictures of the suspensions obtained immediately after sonication ( $T = 0$  h) and after being left undisturbed on the benchtop for 24 h. It was observed that **DTAPEG-CNCs** were dispersible in aqueous and polar organic solvents (methanol, ethanol and isopropyl alcohol), and yielded

homogeneous suspensions that remained stable over time through electrostatic and steric interactions. In contrast, unmodified CNCs almost immediately aggregated and crashed out



**Figure 2.6** Photographs of unmodified and modified CNCs suspensions (0.5 wt %) in aqueous and organic media at T= 0 and T = 24 hours after sonication. (a) **DTAPEG**-CNCs (b) **DTC18**-CNCs (c) **DTB**-CNCs and (d) **DTP**-CNCs.

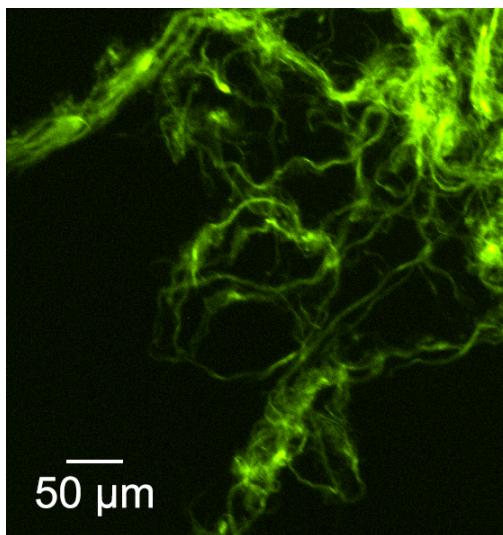


of all polar solvents, with the exception of water. Further characterization through DLS (Table 1 and Figure S2.5, Appendix 2) showed that unmodified CNCs and APEG-modified CNCs remained suspended as individual particles, with average hydrodynamic radii of 90 and 140 nm, respectively. The lack of noticeable aggregation from DLS and AFM measurements, support the notion of colloidal stabilization through steric and electrostatic repulsion. Thus, the introduction of polar polyether chains in the **DTAPEG** derivative made the CNCs stable and compatible with water and polar organic solvents.

Similarly, the grafting of **DTC18**, **DTB** and **DTP** introduced alkyl, benzyl and propargyl moieties, respectively, that rendered the CNCs hydrophobic. Consequently, CNCs modified with such triazinyl derivatives were dispersible and remained stable in chloroform, while unmodified CNCs immediately aggregated and crashed out of this solvent. On the other hand, when suspended in water, **DTC18**-CNCs rapidly crashed out of solution, while **DTB**-CNCs and **DTP**-CNCs showed moderate stability and slow sedimentation. Further characterization through DLS showed that DTB showed similar characteristics to unmodified CNCs and DTAPEG modified CNCs. On the other hand, the average apparent hydrodynamic radii of DTP and DTC18 were 2-3-fold larger than those of unmodified CNCs, which suggests short-range clustering of the modified CNCs over time. This confirmed the observations from AFM images of DTC18-CNCs (Figure 2.4E), where small clusters were easily discernible. Despite the short-range clustering observed, the introduction of **DTB**, **DTP** and **DTC18** modifications made the CNCs compatible with non-polar organic solvents. It must be highlighted that those suspensions exhibiting stability after 24 hours, were found to remain stable even after months of storage in appropriately sealed containers. The compatibilization of modified CNCs with a range of organic solvents could open the door for their use as fillers and reinforcing agents in a range of polymeric and non-polymeric matrices.

#### 2.4.6 Fluorescent Labeling of DTP-modified Cellulose Fibers through “Click” Reactions

Finally, as proof-of-concept, we aimed to demonstrate the versatility of the triazine chemistry by using it as a modular platform for the secondary modification of crystalline cellulose through “click” chemistry. To this end, we first grafted **DTP** onto bacterial microcrystalline cellulose (BMCC) fibrils to introduce alkyne functionalities and carried out a secondary azide-alkyne cycloaddition reaction with azido-fluorescein (Scheme 1c). This yielded uniformly and brightly labeled BMCC fibrils that could be readily imaged through fluorescence microscopy (Figure 2.7). This procedure not only demonstrates the ability to use the triazinyl chemistry as a building block for secondary modifications, but also opens the possibility of designing hetero-bifunctional triazinyl derivatives where one functionality can be used for solvent compatibilization and the second for targeted reactions. Our group is currently pursuing a number of cellulose modification routes along this direction.



**Figure 2.7** DTP-grafted BMCC fibrils labeled through a secondary azide-alkyne cycloaddition reaction with fluorescein derivatives.

### 2.4.7 The Triazinyl Chemistry Cellulose Modification in Context

The discussion so far has focused on the effectiveness of the triazinyl chemistry approach to modify the interfacial properties of cellulose with a range of functional moieties. However, to place this chemistry into proper context, one must compare it with other available surface modification approaches. Table 2 compares some of the cellulose modification strategies reported to date, detailing process considerations and reaction conditions obtained from the cited references. While this comparison does not aim to be exhaustive, it provides representative examples, and highlights some of the advantages of the triazinyl chemistry. In particular, the surface modification of cellulose through the triazinyl chemistry is carried out under mild conditions that do not negatively impact the native structure of cellulose, is versatile in the types of functional groups that can be grafted onto the surface – ranging from polar to non-polar and from small molecules to polymers, and can be carried out with inexpensive reagents. These considerations render the triazinyl chemistry a simple, versatile, and low-cost approach to carry out surface modification of nanocellulose with potential for large-scale implementation.

**Table 2.** Comparison of different chemistries used in the modification of nanocellulose surfaces.

Strategy	Process Considerations	Reaction Conditions	Refs.
<b>Acetylation</b>	Reaction involves low cost reagents and products are stable. However, reaction conditions highly susceptible to “peeling effect” of CNCs, where the CNS crystalline structure/morphology is adversely affected. Reaction/degree of substitution are difficult to control. Only acetylated CNCs are produced, no route for selective post-modification.	94 °C, inert atmosphere, DMF, K <sub>2</sub> CO <sub>3</sub> , 1-24 h	43
<b>Esterification (ring-opening &amp; ATRP)</b>	Reaction involves high cost reagents (alkenyl succinic anhydrides) and involves a freezing drying step before modification. Approach available for the modification of CNCs with alkenyl succinic anhydrides.	105 °C for 2 mins	44

<b>polymerization)</b>	Reaction involves high cost reagents (lactide, tin catalyst), and requires solvent exchange and distillation. The reaction allows grafting of polymer chains through ROP from CNCs.	80 °C, inert atmosphere, dry Toluene, 24 h	45
	Reaction involves a laborious two-step process that uses high cost reagents (2-bromoisobutyryl bromide, Cu(I)Br, Styrene, MMAZO, etc.) and involves freeze-thaw cycles before modification. The resulting materials can be used to graft polymer chains from the CNC surface through ATRP.	RT, DMAP, TEA, dry THF, 24 h 110 °C, HMTETA, Neat, 12 h 90 °C, Chlorobenzene, HMTETA, 24 h	18,19
	Simple and versatile procedure, with many potential functionalities through commercially available silanes. Reaction involve very costly reagents (chloro/alkoxy silanes) that could make it prohibitive for large scale applications. Solvent exchange is required when using chlorosilanes and a freeze-drying step in addition to an annealing process is necessary when using alkoxy silanes. Cellulose crystallinity could be modified during the silylation process.	RT, dry Toluene, Imidazole, 16 h	46, 47
<b>Silylation</b>		RT, H <sub>2</sub> O, 2-4 h, 110 °C, 8 h	48, 49
	Reaction involves a laborious two-step process, where the CNC is first oxidized and then EDC coupling is performed. The process involves high cost reagents (TEMPO, NaClO, EDC, NHS etc.), and the degree of oxidation must be carefully controlled. Depending on the functionality introduced, the CNC may require solvent exchange before modification.	RT, H <sub>2</sub> O, DMF, pH=7.5-8 2-4 h	16, 17
<b>Amidation / Carbamination</b>	Reaction involves a laborious one/three-step process. The process involves costly reagents (isocyanates-phNCO, diisocyanates-2,4-TDI). The procedure requires solvent exchange before CNC modification. Allows grafting well-defined, amine-terminated polymers onto CNCs without modification of the CNC crystallinity.	80-110 °C, Inert atm., TEA, 30 mins - 7 days	12- 14
<b>Etherification</b>	The reaction is simple to implement, but the cost depends on the epoxide used for modification. Complete activation of surface hydroxyl groups with basic solutions required for efficient	65 °C, H <sub>2</sub> O, NaOH, 5 – 6.5 h	11,20

	functionalization. Base content used needs to be carefully controlled to avoid loss of crystallinity. May require a desulfation step before modification reaction.	
<b>Triazinyl</b>	The reaction is simple, performed under mild conditions, involves low cost reagents (cyanuric chloride < \$ 10/kg), and the resulting products are stable. The process is highly tunable, and the resulting modified cellulose/CNCs can either be polar or non-polar and amenable to post-functionalization. Depending on the functionality introduced, the CNC may require solvent exchange before modification.	Room temp, H <sub>2</sub> O/Acetone, NaOH, 24 h Room temp, DCM, K <sub>2</sub> CO <sub>3</sub> , 24 h This work

## 2.5 Conclusions

In this work, we have introduced triazinyl chemistry as a versatile modular approach for tuning the interfacial properties of cellulosic materials using both “grafting to” and “grafting from” reactions. Cyanuric chloride, a relatively inexpensive chemical, was deployed as a linker molecule for the grafting of aliphatic (octadecylamine), polymeric (mono-allyl PEG), aromatic (benzylamine), and alkyne (propargyl) functionalities onto CNCs, forming stable cellulose ether derivatives. Depending on the functionality introduced, the triazine grafting technique was conducted in either aqueous or organic media. Colloidal suspensions of modified CNCs were easily generated and sterically stabilized in polar or non-polar organic solvents. The ability to tune the polarity of the CNC surface is promising for their dispersion into hydrophilic and hydrophobic polymer matrices, and for their use as fillers and reinforcing agents for the generation of nanocomposites with unique mechanical, optical and electrical properties. Finally, the post-modification of alkynyl-grafted CNCs was demonstrated through an azide-alkyne cycloaddition reaction, which was used to fluorescently label the modified cellulose nanofibers. This showcases the ability to use the triazinyl group as a modular building block for such bio-orthogonal reactions, and opens the way for the future development of

Ayodele Fatona – Ph.D. Thesis McMaster University – Chemistry and Chemical Biology  
hetero-bifunctional molecules for the incorporation of nanocellulose into a wide range of materials.

## 2.6 Acknowledgements

We thank Prof. E. Cranston and Prof. Alex Adronov for access to equipment and useful discussions, and V. Jarvis (McMaster Analytical X-Ray Diffraction Facility) and D. Covelli (Biointerfaces Institute) for assistance with sample analysis. This research was supported through the Natural Sciences and Engineering Research Council and a Canada Foundation for Innovation Leaders Opportunity Fund. A. Fatona was partially supported by the BioInterfaces CREATE grant. J. Moran-Mirabal is the recipient of an Early Researcher Award from the Ontario Ministry for Research and Innovation, and the Canada Research Chair on Micro and Nanostructured Materials. We thank EnRoute Interfaces Inc. for providing poly(ethylene glycol) monoallyl ether.

## 2.7 References

- (1) Peponi, L.; Puglia, D.; Torre, L.; Valentini, L.; Kenny, J. M., Processing of nanostructured polymers and advanced polymeric based nanocomposites. *Mater. Sci. Eng., R* **2014**, 85, 1-46.
- (2) Miao, C.; Hamad, W. Y., Cellulose reinforced polymer composites and nanocomposites: a critical review. *Cellulose* **2013**, 20, 2221-2262.
- (3) Moon, R. J.; Martini, A.; Nairn, J.; Simonsen, J.; Youngblood, J., Cellulose nanomaterials review: structure, properties and nanocomposites. *Chem. Soc. Rev.* **2011**, 40, 3941-3994.
- (4) Roman, M., Toxicity of Cellulose Nanocrystals: A Review. *Ind. Biotechnol.* **2015**, 11, 25-33.

- (5) Azzam, F.; Heux, L.; Putaux, J.-L.; Jean, B., Preparation By Grafting Onto, Characterization, and Properties of Thermally Responsive Polymer-Decorated Cellulose Nanocrystals. *Biomacromolecules* **2010**, 11, 3652-3659.
- (6) Dufresne, A., Processing of Polymer Nanocomposites Reinforced with Polysaccharide Nanocrystals. *Molecules* **2010**, 15, 4111-4128.
- (7) Yang, J.; Han, C.-R.; Duan, J.-F.; Ma, M.-G.; Zhang, X.-M.; Xu, F.; Sun, R.-C., Synthesis and characterization of mechanically flexible and tough cellulose nanocrystals-polyacrylamide nanocomposite hydrogels. *Cellulose* **2013**, 20, 227-237.
- (8) Azizi Samir, M. A. S.; Alloin, F.; Dufresne, A., Review of Recent Research into Cellulosic Whiskers, Their Properties and Their Application in Nanocomposite Field. *Biomacromolecules* **2005**, 6, 612-626.
- (9) Kan, K. H. M.; Li, J.; Wijesekera, K.; Cranston, E. D., Polymer-Grafted Cellulose Nanocrystals as pH-Responsive Reversible Flocculants. *Biomacromolecules* **2013**, 14, 3130-3139.
- (10) Ljungberg, N.; Bonini, C.; Bortolussi, F.; Boisson, C.; Heux, L.; Cavallé, New Nanocomposite Materials Reinforced with Cellulose Whiskers in Atactic Polypropylene: Effect of Surface and Dispersion Characteristics. *Biomacromolecules* **2005**, 6, 2732-2739.
- (11) Hasani, M.; Cranston, E. D.; Westman, G.; Gray, D. G., Cationic surface functionalization of cellulose nanocrystals. *Soft Matter* **2008**, 4, 2238-2244.
- (12) Habibi, Y.; Dufresne, A., Highly Filled Bionanocomposites from Functionalized Polysaccharide Nanocrystals. *Biomacromolecules* **2008**, 9, 1974-1980.
- (13) Siqueira, G.; Bras, J.; Dufresne, A., Cellulose Whiskers versus Microfibrils: Influence of the Nature of the Nanoparticle and its Surface Functionalization on the Thermal and Mechanical Properties of Nanocomposites. *Biomacromolecules* **2009**, 10, 425-432.
- (14) Shang, W.; Huang, J.; Luo, H.; Chang, P. R.; Feng, J.; Xie, G., Hydrophobic modification of cellulose nanocrystal via covalently grafting of castor oil. *Cellulose* **2013**, 20, 179-190.

- (15) Yu, H.-Y.; Chen, R.; Chen, G.-Y.; Liu, L.; Yang, X.-G.; Yao, J.-M., Silylation of cellulose nanocrystals and their reinforcement of commercial silicone rubber. *J. Nanopart. Res.* **2015**, *17*, 1-13.
- (16) Mangalam, A. P.; Simonsen, J.; Benight, A. S., Cellulose/DNA Hybrid Nanomaterials. *Biomacromolecules* **2009**, *10*, 497-504.
- (17) Harrison, S.; Drisko, G. L.; Malmström, E.; Hult, A.; Wooley, K. L., Hybrid Rigid/Soft and Biologic/Synthetic Materials: Polymers Grafted onto Cellulose Microcrystals. *Biomacromolecules* **2011**, *12*, 1214-1223.
- (18) Yi, J.; Xu, Q.; Zhang, X.; Zhang, H., Chiral-nematic self-ordering of rodlike cellulose nanocrystals grafted with poly(styrene) in both thermotropic and lyotropic states. *Polymer* **2008**, *49*, 4406-4412.
- (19) Xu, Q.; Yi, J.; Zhang, X.; Zhang, H., A novel amphotropic polymer based on cellulose nanocrystals grafted with azo polymers. *Eur. Polym. J.* **2008**, *44*, 2830-2837.
- (20) Kloser, E.; Gray, D. G., Surface Grafting of Cellulose Nanocrystals with Poly(ethylene oxide) in Aqueous Media. *Langmuir* **2010**, *26*, 13450-13456.
- (21) Tappe, H.; Helmling, W.; Mischke, P.; Rebsamen, K.; Reiher, U.; Russ, W.; Schläfer, L.; Vermehren, P., Reactive Dyes. In *Ullmann's Encyclopedia of Industrial Chemistry*, Wiley-VCH Verlag GmbH & Co. KGaA: 2000.
- (22) Müller, F.; Applebyki, A. P., Weed Control, 2. Individual Herbicides. In *Ullmann's Encyclopedia of Industrial Chemistry*, Wiley-VCH Verlag GmbH & Co. KGaA: 2000.
- (23) Siegrist, A. E.; Eckhardt, C.; Kaschig, J.; Schmidt, E., Optical Brighteners. In *Ullmann's Encyclopedia of Industrial Chemistry*, Wiley-VCH Verlag GmbH & Co. KGaA: 2000.
- (24) Chouai, A.; Simanek, E. E., Kilogram-Scale Synthesis of a Second-Generation Dendrimer Based on 1,3,5-Triazine Using Green and Industrially Compatible Methods with a Single Chromatographic Step. *J. Org. Chem.* **2008**, *73*, 2357-2366.



(25) Helbert, W.; Chanzy, H.; Husum, T. L.; Schüle, M.; Ernst, S., Fluorescent Cellulose Microfibrils As Substrate for the Detection of Cellulase Activity. *Biomacromolecules* **2003**, 4, 481-487.

(26) Ringot, C.; Sol, V.; Barrière, M.; Saad, N.; Bressollier, P.; Granet, R.; Couleaud, P.; Frochot, C.; Krausz, P., Triazinyl Porphyrin-Based Photoactive Cotton Fabrics: Preparation, Characterization, and Antibacterial Activity. *Biomacromolecules* **2011**, 12, 1716-1723.

(27) Walczak, M.; Frączyk, J.; Kamiński, Z. J.; Wietrzyk, J.; Filip-Psurska, B., Preliminary studies on application of library of artificial receptors for differentiation of metabolites in urine of healthy and cancer bearing mice. *Acta Pol. Pharm.* **2014**, 71, 941-953.

(28) Siqueira, G.; Bras, J.; Dufresne, A., New Process of Chemical Grafting of Cellulose Nanoparticles with a Long Chain Isocyanate. *Langmuir* **2010**, 26, 402-411.

(29) Ly, B.; Thielemans, W.; Dufresne, A.; Chaussy, D.; Belgacem, M. N., Surface functionalization of cellulose fibres and their incorporation in renewable polymeric matrices. *Compos. Sci. and Technol.* **2008**, 68, 3193-3201.

(30) Briois, B.; Saito, T.; Pétrier, C.; Putaux, J.-L.; Nishiyama, Y.; Heux, L.; Molina-Boisseau, S.,  $\alpha \rightarrow \beta$  transition of cellulose under ultrasonic radiation. *Cellulose* **2013**, 20, 597-603.

(31) Jasmani, L.; Eyley, S.; Wallbridge, R.; Thielemans, W., A facile one-pot route to cationic cellulose nanocrystals. *Nanoscale* **2013**, 5, 10207-10211.

(32) Moran-Mirabal, J. M.; Santhanam, N.; Corgie, S. C.; Craighead, H. G.; Walker, L. P., Immobilization of cellulose fibrils on solid substrates for cellulase-binding studies through quantitative fluorescence microscopy. *Biotechnol. Bioeng.* **2008**, 101, 1129-1141.

(33) Abitbol, T.; Palermo, A.; Moran-Mirabal, J. M.; Cranston, E. D., Fluorescent Labeling and Characterization of Cellulose Nanocrystals with Varying Charge Contents. *Biomacromolecules* **2013**, 14, 3278-3284.

- (34) Mur, V. I.; Levin, E. S.; Vinogradova, N. P., Synthesis and reactions of some substituted 1, 3, 5-triazines. *Chem. Heterocycl. Compd. (N.Y., NY, U. S.)* **1967**, 3, 589-594.
- (35) Bailey, J.; Kettle, L. J.; Cherryman, J. C.; Mitchell, J. B. O., Triazinone tautomers: solid phase energetics. *CrystEngComm* **2003**, 5, 498-502.
- (36) Zoppe, J. O.; Habibi, Y.; Rojas, O. J.; Venditti, R. A.; Johansson, L.-S.; Efimenko, K.; Österberg, M.; Laine, J., Poly(N-isopropylacrylamide) Brushes Grafted from Cellulose Nanocrystals via Surface-Initiated Single-Electron Transfer Living Radical Polymerization. *Biomacromolecules* **2010**, 11, 2683-2691.
- (37) de Mesquita, J. P.; Donnici, C. L.; Teixeira, I. F.; Pereira, F. V., Bio-based nanocomposites obtained through covalent linkage between chitosan and cellulose nanocrystals. *Carbohydr. Polym.* **2012**, 90, 210-217.
- (38) Lin, N.; Dufresne, A., Surface chemistry, morphological analysis and properties of cellulose nanocrystals with gradiented sulfation degrees. *Nanoscale* **2014**, 6, 5384-5393.
- (39) Peydecastaing, J.; Vaca-Garcia, C.; Borredon, E., Accurate determination of the degree of substitution of long chain cellulose esters. *Cellulose* **2008**, 16, 289-297.
- (40) Gill, U.; Sutherland, T.; Himbert, S.; Zhu, Y.; Rheinstadter, M. C.; Cranston, E. D.; Moran-Mirabal, J. M., Beyond buckling: humidity-independent measurement of the mechanical properties of green nanobiocomposite films. *Nanoscale* **2017**, 9, 7781-7790.
- (41) Reid, M. S.; Villalobos, M.; Cranston, E. D., Benchmarking Cellulose Nanocrystals: From the Laboratory to Industrial Production. *Langmuir* **2017**, 33, 1583-1598.
- (42) Dufresne, A., Nanocellulose: a new ageless bionanomaterial. *Mater. Today* **2013**, 16, 220-227.
- (43) Çetin, N. S.; Tingaut, P.; Özmen, N.; Henry, N.; Harper, D.; Dadmun, M.; Sèbe, G., Acetylation of Cellulose Nanowhiskers with Vinyl Acetate under Moderate Conditions. *Macromol. Biosci.* **2009**, 9, 997-1003.

(44) Yuan, H.; Nishiyama, Y.; Wada, M.; Kuga, S., Surface Acylation of Cellulose Whiskers by Drying Aqueous Emulsion. *Biomacromolecules* **2006**, 7, 696-700.

(45) Goffin, A.-L.; Raquez, J.-M.; Duquesne, E.; Siqueira, G.; Habibi, Y.; Dufresne, A.; Dubois, P., From Interfacial Ring-Opening Polymerization to Melt Processing of Cellulose Nanowhisker-Filled Polylactide-Based Nanocomposites. *Biomacromolecules* **2011**, 12, 2456-2465.

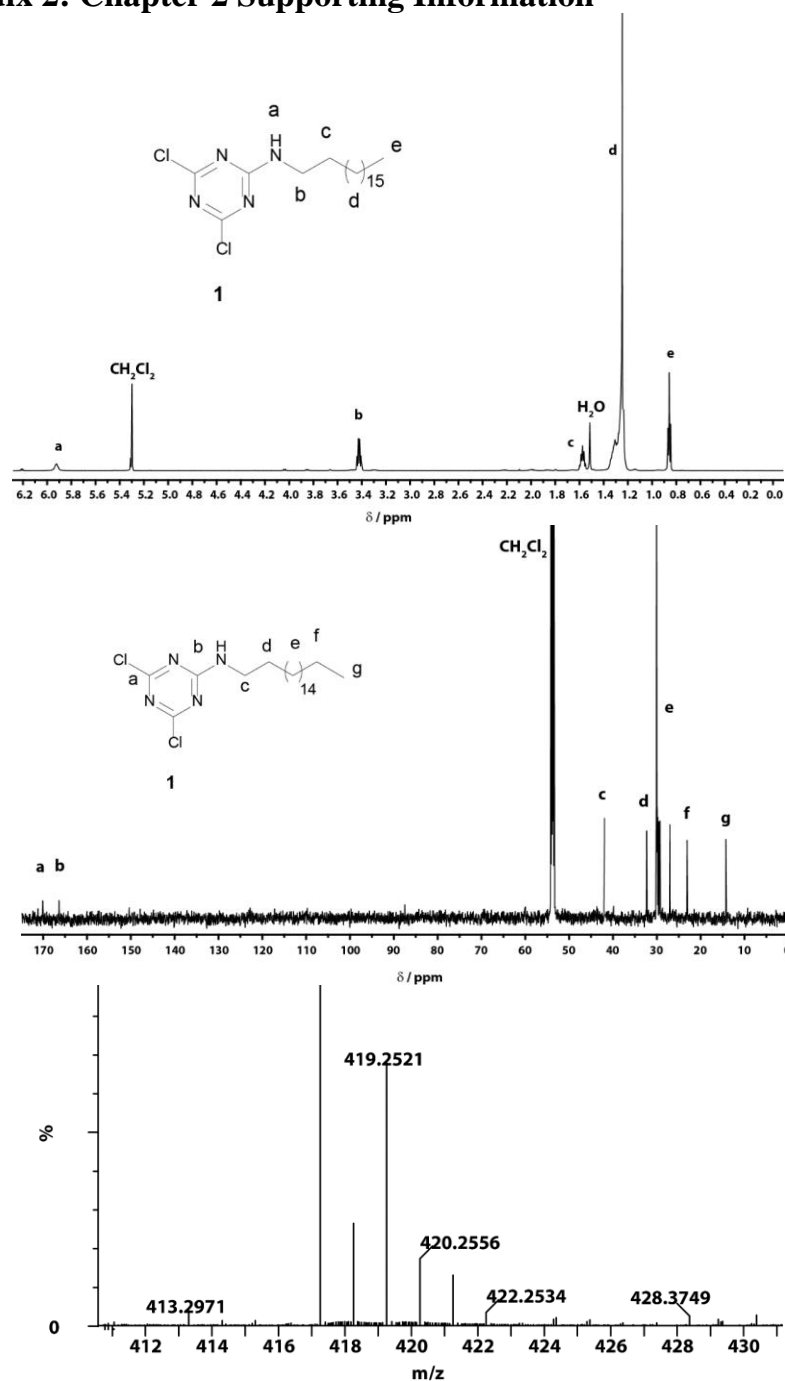
(46) Pei, A.; Zhou, Q.; Berglund, L. A., Functionalized cellulose nanocrystals as biobased nucleation agents in poly(l-lactide) (PLLA) – Crystallization and mechanical property effects. *Compos. Sci. Technol.* **2010**, 70, 815-821.

(47) Goussé, C.; Chanzy, H.; Excoffier, G.; Soubeyrand, L.; Fleury, E., Stable suspensions of partially silylated cellulose whiskers dispersed in organic solvents. *Polymer* **2002**, 43, 2645-2651.

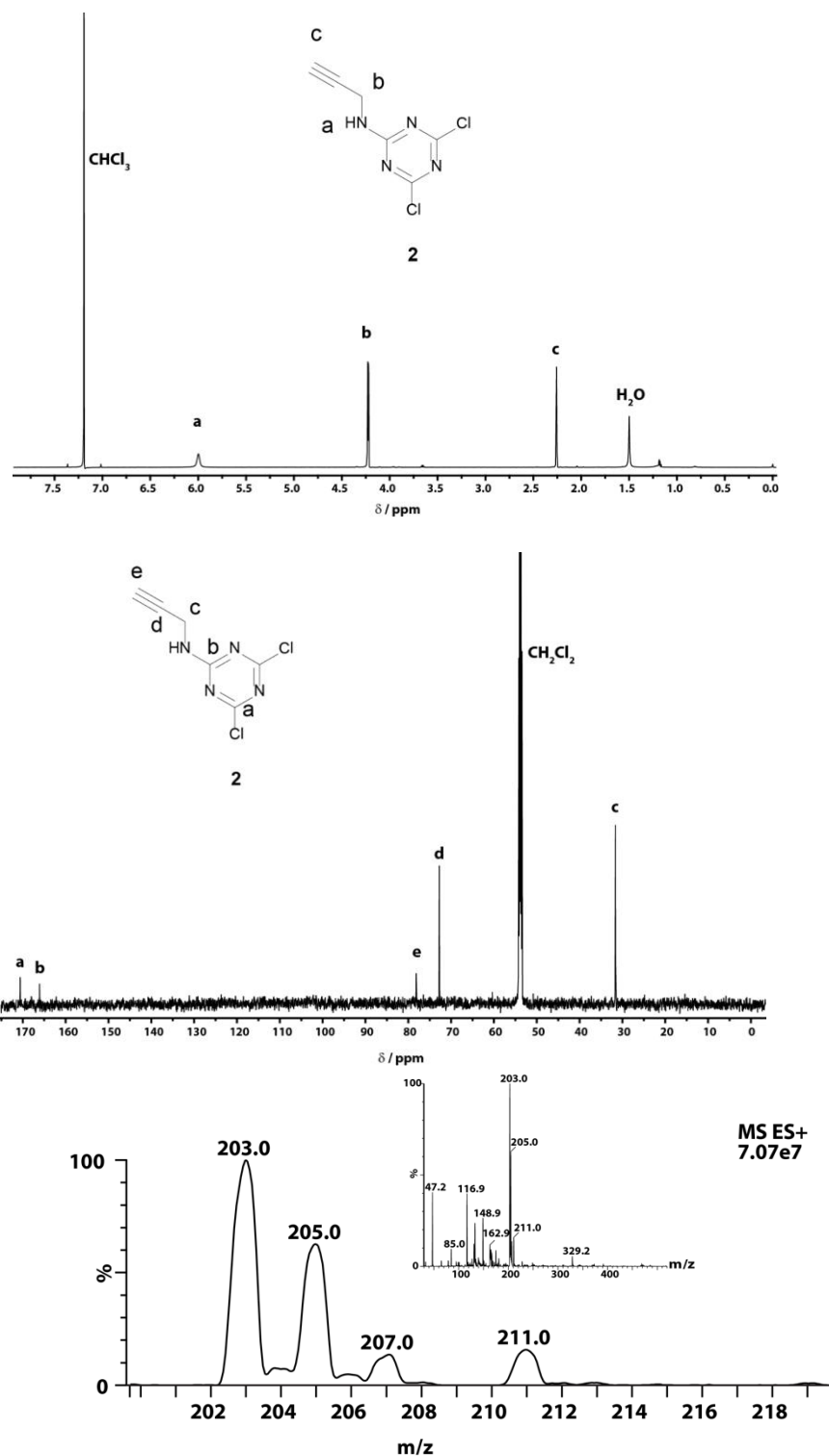
(48) Raquez, J. M.; Murena, Y.; Goffin, A. L.; Habibi, Y.; Ruelle, B.; DeBuyl, F.; Dubois, P., Surface-modification of cellulose nanowhiskers and their use as nanoreinforcers into polylactide: A sustainably-integrated approach. *Compos. Sci. Technol.* **2012**, 72, 544-549.

(49) Huang, J.-L.; Li, C.-J.; Gray, D. G., Functionalization of cellulose nanocrystal films via "thiol-ene" click reaction. *RSC Adv.* **2014**, 4, 6965-6969.

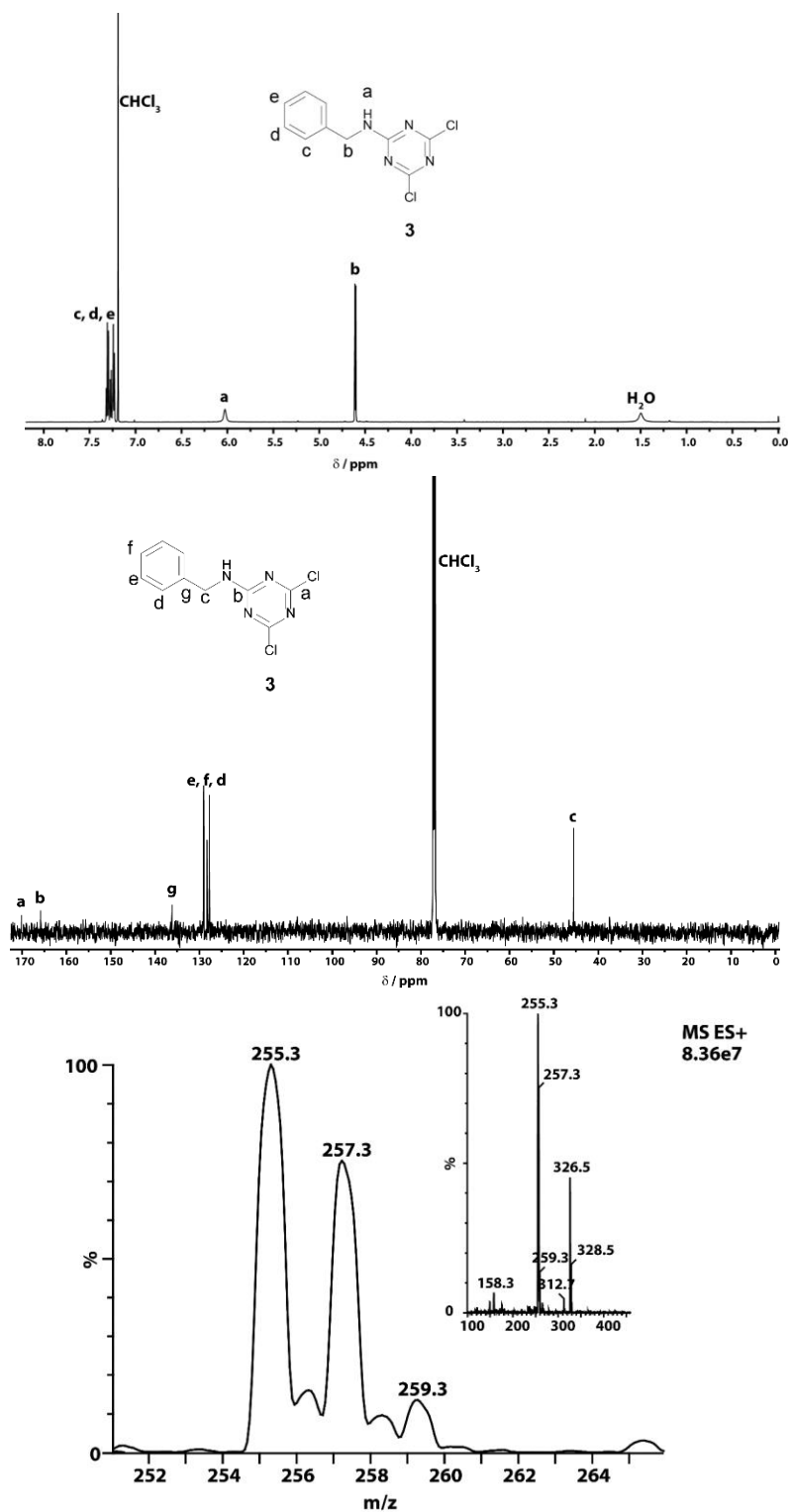
## 2.8 Appendix 2: Chapter 2 Supporting Information



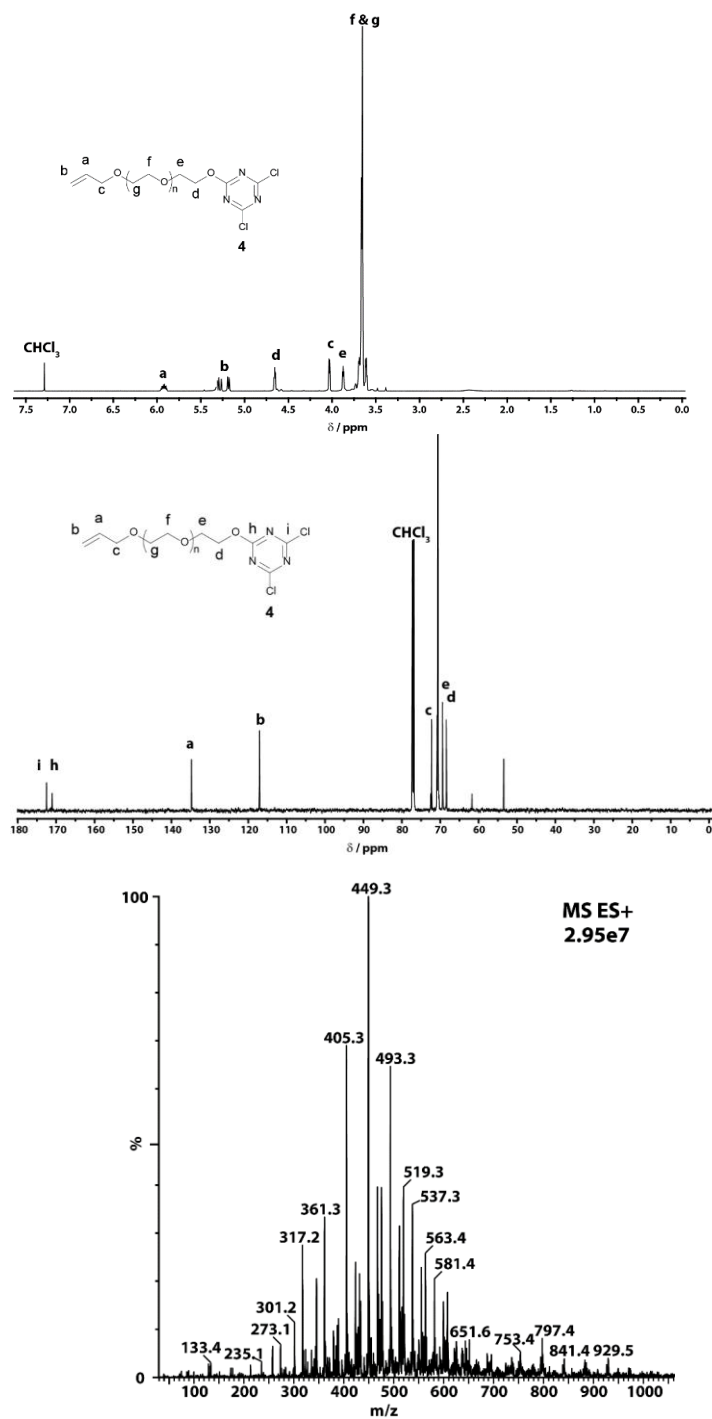
**Figure S2.1** Characterization of 4,6-dichloro-n-octadecyl-1,3,5-triazine-2-amine (1, DTC18). Top:  $^1\text{H}$  NMR spectrum; Middle:  $^{13}\text{C}$  NMR spectrum; Bottom: High-resolution ESI-Q-TOF mass spectrum.



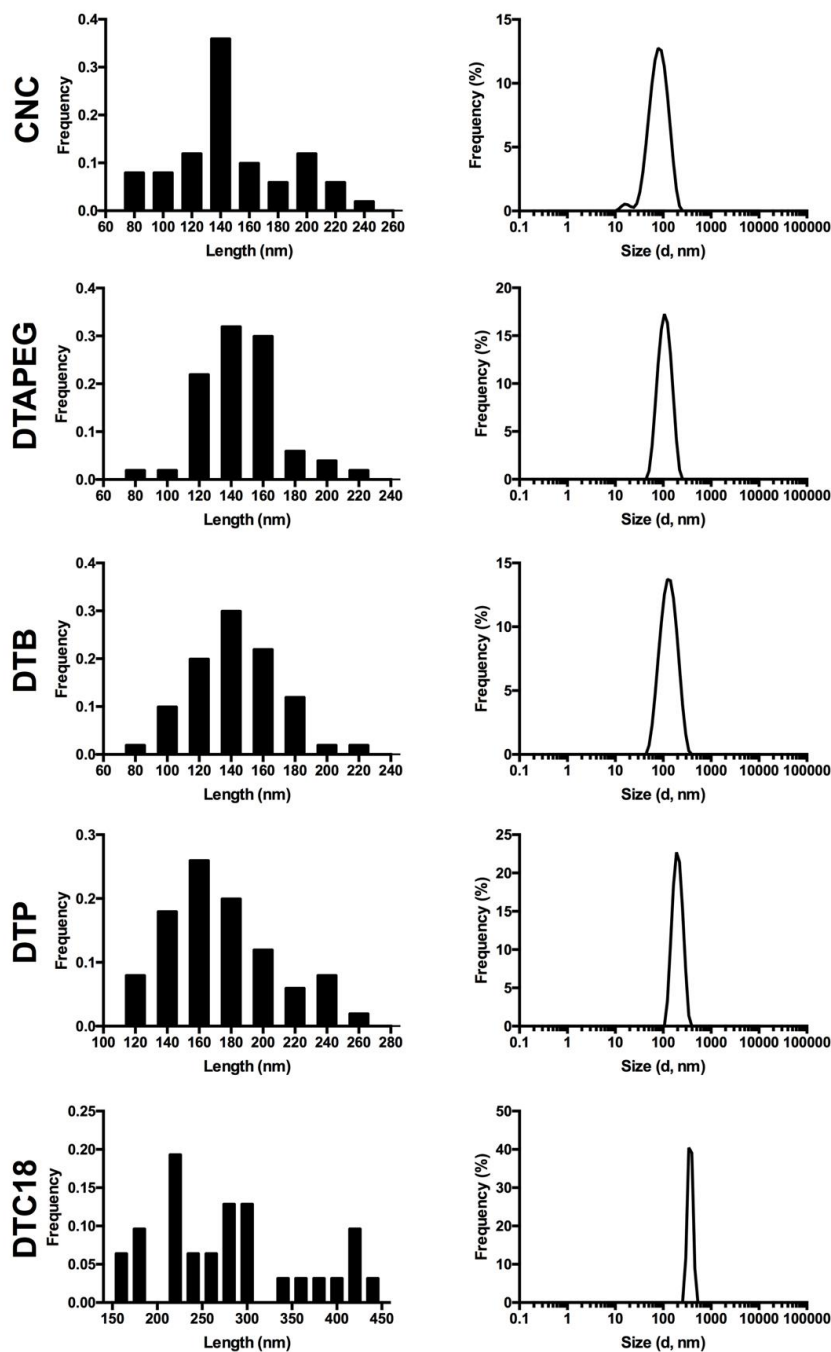
**Figure S2.2** Characterization of 4,6-dichloro-n-propargyl-1,3,5-triazine-2-amine (**2**, **DTP**). Top:  $^1\text{H}$  NMR spectrum; Middle:  $^{13}\text{C}$  NMR spectrum; Bottom: High-resolution ESI-Q-TOF mass spectrum.



**Figure S2.3** Characterization of 4,6-dichloro-n-benzyl-1,3,5-triazine-2-amine (3, DTB). Top:  $^1\text{H}$  NMR spectrum; Middle:  $^{13}\text{C}$  NMR spectrum; Bottom: High-resolution ESI-Q-TOF mass spectrum.



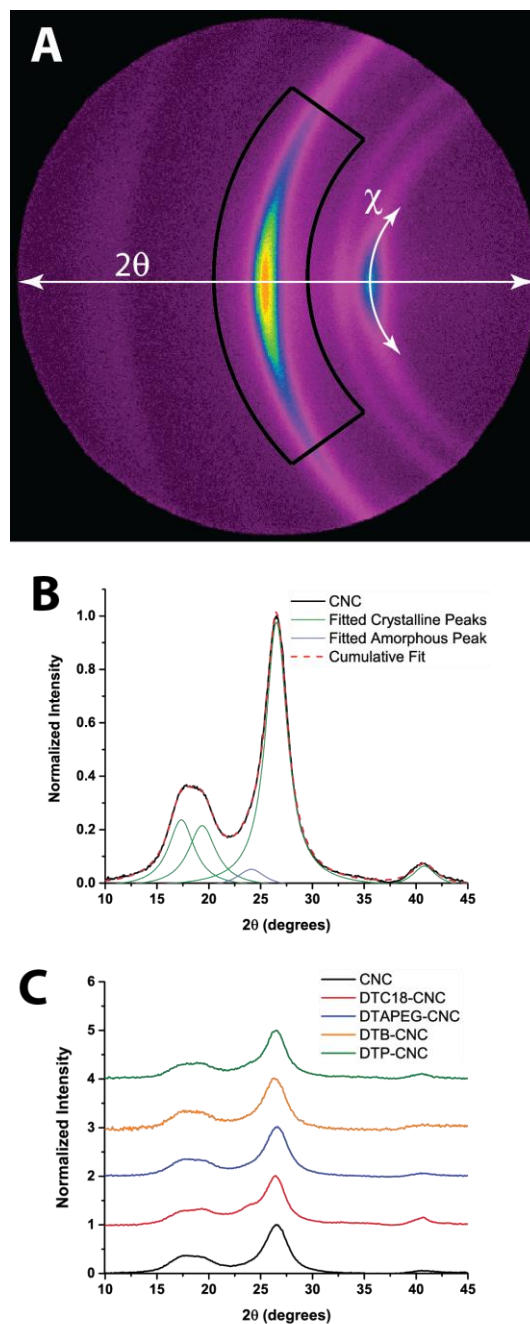
**Figure S2.4 Characterization of 4,6-dichloro-2-poly(ethylene glycol)mono-allyl-1,3,5-triazine-2-ether (4, DTAPEG).** Top:  $^1\text{H}$  NMR spectrum; Middle:  $^{13}\text{C}$  NMR spectrum; Bottom: High-resolution ESI-Q-TOF mass spectrum.



**Figure S2.5 Characterization of the dispersion of unmodified and modified CNCs.**

Left: Frequency histograms of AFM measurements of the particle length for CNCs spin coated onto a silicon substrate. Right: DLS measurements of the apparent hydrodynamic particle size for CNC dispersions at 0.025 wt% in water, with exception of DTC18-modified CNCs, which were measured in DCM.





**Figure S2.6 XRD characterization of unmodified and modified CNCs.** (a) 2D diffraction plots with  $\theta$  and  $\chi$  angles shown. Highlighted area exemplified arc for integration. (b) One-dimensional normalized intensity plot for unmodified CNCs, showing the four crystalline and one amorphous peak fitted. The four crystalline peaks were used to define the crystalline base function. (c) One-dimensional intensity plot comparing unmodified and modified CNCs.

**Table S1:** XPS Atomic percentages and O/C ratios for unmodified and modified CNCs.

	<b>%O</b>	<b>%C</b>	<b>%N</b>	<b>%S</b>	<b>Cl</b>	<b>Na</b>	<b>O/C</b>
	<b>1s</b>	<b>1s</b>	<b>1s</b>	<b>2p</b>	<b>2p</b>	<b>1s</b>	
<b>CNC</b>	44.48	55.17	0	0.35	0	0	0.81
<b>DTC18-CNC</b>	33.06	62.74	3.32	0.29	0.59	0	0.53
<b>DTP-CNC</b>	39.23	53.75	6.22	0.25	0.55	0	0.73
<b>DTB-CNC</b>	39.04	56.67	3.76	0.27	0.26	0	0.69
<b>DTAPEG-CNC</b>	38.74	58.12	2.23	0.39	0	0.52	0.67

### **CHAPTER 3: Colorimetric and Fluorescent Cellulose-Based Chemosensor for Selective Detection of Copper (II) and Mercury (II) in Water<sup>‡</sup>**

#### **3.1 Abstract**

Sensors based on colorimetric and fluorescent probes have gained much attention for analytical applications due to their high sensitivity, fast response time, and technical simplicity. To date, several chemical probes have been developed to detect heavy metals with high selectivity and specificity. Chemosensors based on the rhodamine scaffold are of particular interest because they are efficient in chelating metal species and have fluorescence switching properties that could be useful in mapping the biodistribution of the target species within living cells. In this work, we present a rhodamine chemosensor that can be directly grafted onto cellulose as a promising scaffold for the development of paper-based microanalytical devices for biomedical and environmental diagnostics. We have used triazine chemistry as a linker to covalently attach vanillin-PEG onto cellulose filter paper. Rhodamine 6G hydrazide and thiooxorhodamine 6G hydrazide sensing molecules were then grafted onto the modified paper. The resulting chemosensing papers exhibited hydrophilic properties and produced a colorimetric response to  $\text{Cu}^{2+}$  and  $\text{Hg}^{2+}$  in aqueous solutions within 5 seconds of contact. These paper-based chemosensors yielded limits of detection of 6.3 and 20 ppb for  $\text{Cu}^{2+}$  and  $\text{Hg}^{2+}$ , respectively.

---

<sup>‡</sup> This chapter is in preparation for submission as: A. Fatona, K. Bhardwaj, M. A. Brook and J. M. Moran-Mirabal. Fatona and Moran-Mirabal designed the experiments and analyzed the data. Fatona performed all synthesis and characterization while Bhardwaj helped with heavy metal assay under the supervision of Fatona. Fatona wrote the manuscript with additions, edits and guidance from Brook and Moran-Mirabal.

### 3.2 Introduction

The importance of minimizing the release of heavy metals during industrial and agricultural activities can't be overemphasized. Anthropogenic activities can release large amounts of heavy metals that are harmful to aquatic organisms and toxic to humans. Elevated levels of copper and mercury ions have been found to cause neurodegenerative diseases such as Alzheimer's, Parkinson's, Wilson's and Minamata diseases.<sup>1,2</sup> In addition, liver damage, digestive and kidney diseases have been linked to the overloading of copper or mercury ions in the human body due to overexposure.<sup>3</sup> Thus, the development of selective, sensitive, and robust sensors for heavy metal detection has increased in recent years and seems imperative for the assessment of heavy metal contamination in environmental and biological samples.<sup>4,5</sup>

Given that conventional techniques (e.g., atomic emission spectroscopy) demand complex and expensive sample pre-treatment and instrumentation, the development of probes capable of translating molecular recognition into measurable optical signals have been actively pursued and reported in literature.<sup>6</sup> The design and synthesis of this type of optical probes is mainly driven by the need to detect heavy metals with high sensitivity and selectivity, but at low cost. Sensors based on chromophore frameworks such as coumarin, BODIPY, naphthalimide, pyrene, and rhodamine are becoming increasingly important in this area due to their ease of readout, low cost, and high efficiency.<sup>7-11</sup> In fluorescent chemosensors, metal binding can elicit changes in the fluorescence signal due to enhancement, quenching, or a shift in the emission spectrum. Turn-on chemosensors with fluorescence enhancement properties have been reported to yield colorimetric and fluorescence changes that make qualitative and quantitative detection more reliable.<sup>6</sup> Rhodamine is a popular fluorophore for the development of heavy metal turn-on chemosensors because it has a high quantum yield, excellent photo-stability and long emission wavelengths. Rhodamine derivatives in the spirolactam form (off state, Figure 3.1) are colourless and non-fluorescent due to the disruption of the  $\pi$ -electron conjugation within the aromatic rings. When Rhodamine is approached by a suitable metal ion, it undergoes spirolactam ring opening (due to metal ion complexation) that gives rise to a strong fluorescence emission or color change due to the restoration of the  $\pi$ -conjugation.

In one implementation, Wu *et al.*<sup>12</sup> reported a multifunctional nanosensor based on silica nanoparticles bearing thiooxorhodamine B hydrazone derivatives that acted both as metal binding site and hydrogen bond donor. Under optimized conditions, the reported detection limit for Hg<sup>2+</sup> ions was 60 nM (12 ppb), which according to the author was sufficient to sense Hg<sup>2+</sup> and a variety of anions in aqueous environment. Similarly, Orriach-Fernandez *et al.*<sup>13</sup> reported an irreversible (chemodosimeter) approach for selectively sensing Hg<sup>2+</sup> using a film composed of a novel hydrophilic water-insoluble MMA-co-HEMA copolymer that incorporated spirocyclic phenylthiosemicarbazide rhodamine 6G derivatives. This chemodosimeter relied on a three-step desulphurization process that provided selectivity and sensitivity towards Hg<sup>2+</sup> and methylmercury, which was tested in water and yielded a detection limit of 300 nM (60 ppb).

While copper is considered as part of the essential elements for biological function, transitions between its oxidized (Cu<sup>2+</sup>) and reduced (Cu<sup>+</sup>) state have been shown to generate superoxide and hydroxyl radicals that can mediate adverse effects such as cellular and tissue damage. Cupric ion (Cu<sup>2+</sup>), the most bioavailable and toxic form of copper, is soluble in water and has high bioconcentration potential in plants, marine animals (particularly bottom dwellers) and shellfish. It has been found that fish and crustaceans are 10 to 100 times more sensitive to the toxic effects of copper than mammals. Similarly, algae (especially blue-green algae species) are 1,000 times more sensitive to the toxic effects of copper than mammals.<sup>14</sup> Therefore, monitoring the levels of copper in waterbodies has gained much attention. Rhodamine hydrazone derivatives have been shown to be efficient in the determination of Cu<sup>2+</sup> in aqueous environments. Recently, a dimeric rhodamine B Schiff base synthesized by Shi *et. al.*<sup>15</sup> as an “off-on” fluorescent probe for the detection of Cu<sup>2+</sup> ions in solution was shown to be efficient, with detection limits as low as 38 nM (2.4 ppb). These probes exhibited low cytotoxicity as observed by (MTT) assays and were suitable as imaging probes to monitor heavy metal biodistribution in living cells.

However, despite efforts made at developing reliable and cost efficient chemosensors for heavy metal detection, there remain technological challenges that need to be addressed. A key barrier is the non-polar nature of the synthesized fluorescent probes, which means that assays need to be done in a mixture of aqueous and organic solvents, leading to limited in-

Ayodele Fatona – Ph.D. Thesis McMaster University – Chemistry and Chemical Biology field heavy-metal testing or monitoring of environmental samples.<sup>16,17</sup> The limited probe solubility in aqueous solutions has been reported to limit assay sensitivity due to the restricted availability of sensing probes in the test solution. Other issues such as the cytotoxicity/biocompatibility of the sensing probes remain a challenge that need to be overcome for sensing in live biological samples.<sup>12</sup>

In this work, we present a polyethylene glycol-vanillin-rhodamine fluorescent chemosensor that can be used directly in aqueous solutions or grafted onto cellulose as a scaffold for paper-based microanalytical devices for biomedical and environmental diagnostics. We have used triazine chemistry as a linker to covalently attach vanillin-PEG onto cellulose filter paper. Rhodamine 6G hydrazide and thiooxorhodamine 6G hydrazide sensing molecules were then grafted onto the modified paper. The obtained hydrophilic rhodamine Schiff bases were used as “off-on” sensing probes for the detection of  $\text{Cu}^{2+}$  and  $\text{Hg}^{2+}$  in water, where they exhibited high selectivity and sensitivity.

### **3.3 Experimental section**

#### **3.3.1 Materials**

Hydrazine monohydrate (64-65%), rhodamine 6G (95%), cyanuric chloride (99%), chloroacetyl chloride (99%), 3-methoxy-4-hydroxybenzaldehyde (99%), Lawesson reagent (97%) and 2,4,6-trimethylpyridine (99%) were purchased from Millipore-Sigma (Oakville, ON). Polyethylene glycol ( $M_w$  1050g/mol) was procured from Acros Organic. All metal salts used in the spectroscopic experiments were obtained from Millipore-Sigma (Oakville, ON). Stock solutions of single metal ions (1 mM) were prepared from chloride salts ( $\text{Hg}^{2+}$ ,  $\text{Zn}^{2+}$ ,  $\text{Fe}^{2+}$ ,  $\text{Ca}^{2+}$ ,  $\text{Fe}^{3+}$ ,  $\text{Mn}^{2+}$  and  $\text{Cd}^{2+}$ ), nitrate salts ( $\text{Pb}^{2+}$  and  $\text{Ag}^+$ ), sulfate salts ( $\text{Cu}^{2+}$ ,  $\text{Mg}^{2+}$ ) or perchlorate salts ( $\text{Ni}^{2+}$ ) using ultrapure water as solvent. The stock solution of PEG-vanillin-rhodamine (1 mM) was prepared in ultrapure water while two sets of the assay working solutions were prepared by diluting both metal ion and probe stock solution to 1  $\mu\text{M}$  respectively using ultrapure water. All solvents including dichloromethane (DCM), tetrahydrofuran, anhydrous acetone, anhydrous dimethylformamide, petroleum ether,

diethyl ether, methanol, anhydrous ethanol, chloroform and NaCl were purchased from Caledon Laboratories and used as gotten or dried (passed through activated alumina column) before use.

### 3.3.2 Characterization

**Nuclear Magnetic Resonance (NMR).**  $^1\text{H}$  and  $^{13}\text{C}$  NMR spectra were obtained on a Bruker AV600-600 MHz NMR spectrometer using deuterated  $\text{CDCl}_3$  and  $\text{DMSO-d}_6$  as solvents.

**Mass Spectrometry (MS).** Mass spectra of synthesized rhodamine derivatives were recorded on a Micromass Ultima (LC-ESI/APCI) Triple Quadrupole Mass spectrometer and Micromass Global Ultima ESI Quadrupole Time of Flight (Q-TOF) Mass spectrometer.

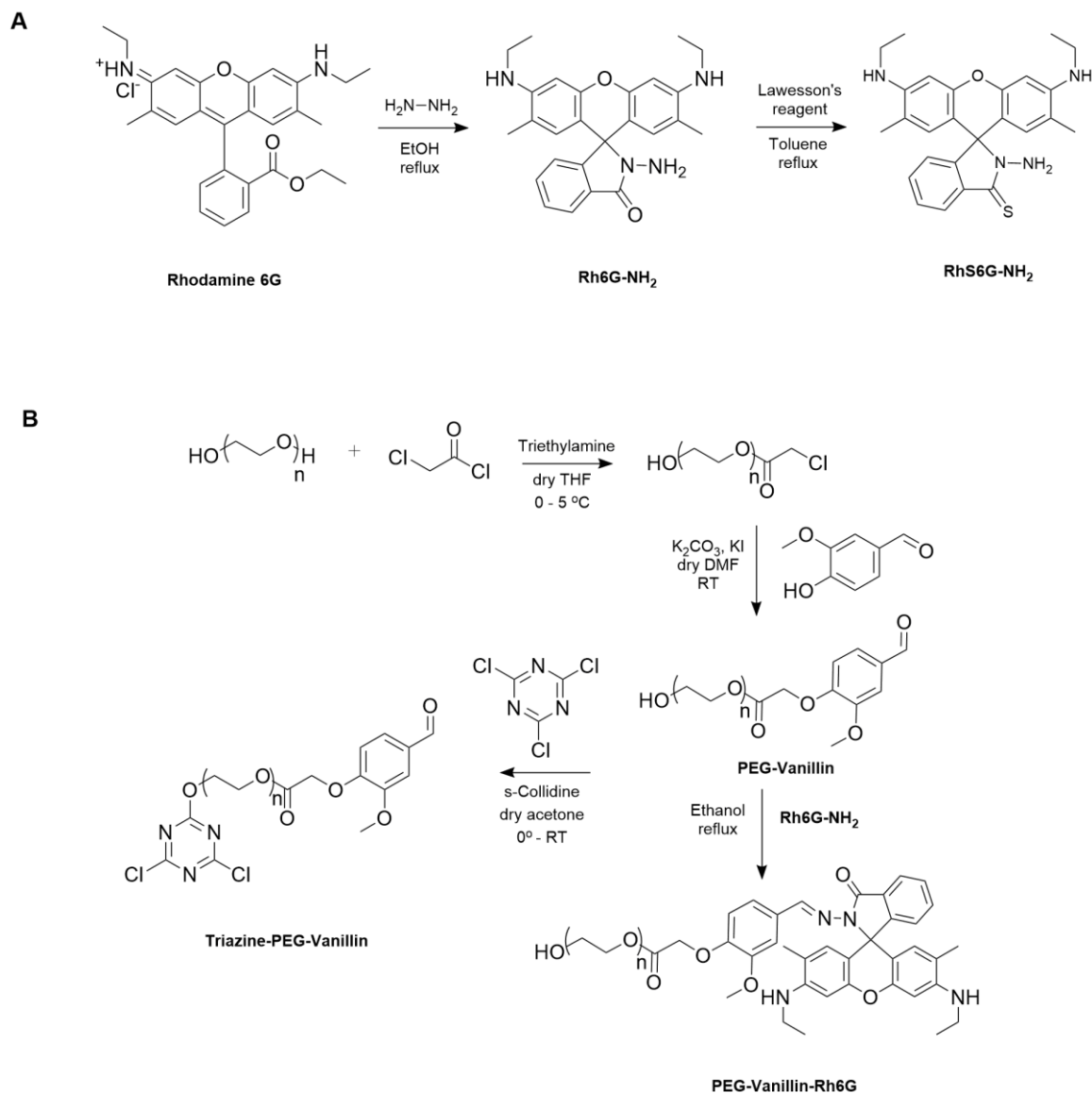
**Fourier Transform Infrared Spectroscopy (FTIR).** FTIR-ATR spectra of modified cellulose fibres were recoded on a Thermo Nicolet 6700 FTIR spectrometer equipped with a SmartiTX attenuated total relectance (ATR) attachment.

**Fluorescence Spectroscopy.** Fluorescence spectra were determined using Biotek<sup>TM</sup> Citation 5<sup>TM</sup> multi-mode reader with a 10 nm excitation and emission slits. The excitation wavelength was fixed at 500 nm, and the emission collected from 550 to 650 nm. All measurements were conducted at room temperature using a Molecular Probes 96-well microplates (ThermoFisher Scientific).

### 3.3.3 Synthesis of poly(ethylene glycol)-vanillin-rhodamine derivatives

A hydrophilic fluorescent chemosensor was synthesized to mitigate the sensitivity and bioavailability limitations of hydrophobic rhodamine chemosensors currently used as probes in metal ion monitoring. A modular approach was adopted according to scheme 1 comprising of two synthetic procedures involving; (a) the synthesis of rhodamine hydrazide derivatives in order to confer selectivity (scheme 1a) and (b) the synthesis of poly(ethylene glycol)-vanillin as the hydrophilic linker to increase sensitivity and bioavailability of the chemosensor (scheme 1b). In addition, with the terminal hydroxyl group in hand, the use

of cyanuric chloride as a linker molecule to graft the pegylated rhodamine Schiff bases onto cellulose filter paper through triazine chemistry was exploited according to Scheme 2.



**Scheme 1.** Synthesis of hydrophilic fluorescent chemosensors. (A) synthesis of rhodamine hydrazide derivatives; and (B) synthesis of **PEG-VA-Rh6G** and **triazinyl-PEG-Va** derivatives.



### 3.3.3.1 Synthesis of rhodamine 6G hydrazide (Rh6G-NH<sub>2</sub>)

Rhodamine 6G hydrazide (Rh6G-NH<sub>2</sub>) was synthesized using a modification of a previously reported protocol.<sup>18</sup> Briefly, to a stirred solution of rhodamine 6G (1 g, 2.09 mmol) dissolved in 20 mL of absolute ethanol, hydrazine monohydrate (64%, 2 mL (excess)) was added dropwise with vigorous stirring at room temperature over a period of 30 min. The resulting mixture was heated to reflux in an oil bath for 8 hours. After cooling, the solid precipitate was filtered off, washed with excess ultrapure water under vacuum and dried to give 0.87 g (97% yield) of **Rh6G-NH<sub>2</sub>** as pale pink crystals used in later reactions without further purification. <sup>1</sup>H-NMR: (600 MHz, DMSO-d<sub>6</sub>, ppm) δ: 7.76 (m, 1H, ArH), 7.46 (m, 2H, ArH), 6.93 (m, 1H, ArH), 6.27 (s, 2H, xanthene-H), 6.10 (s, 2H, xanthene-H), 5.00 (s, 2H, NH<sub>2</sub>), 4.22 (br.s, 2H, 2 x NH), 3.14 (q, 4H, J=3.5 Hz, 2 x CH<sub>2</sub>CH<sub>3</sub>), 1.87 (s, 6H, 2 x Ar-CH<sub>3</sub>), 1.21 (t, 6H, J=7.1 Hz, 2 x CH<sub>2</sub>CH<sub>3</sub>). MS: (ESI, m/z): 429.2 for [M + H]<sup>+</sup>, calc. for C<sub>26</sub>H<sub>28</sub>N<sub>4</sub>O<sub>2</sub> = 428.54.

### 3.3.3.2 Synthesis of thiooxorhodamine 6G hydrazide (RhS6G-NH<sub>2</sub>)

Rhodamine 6G hydrazide (Rh6G-NH<sub>2</sub>) (0.5 g, 1.16 mmol) and Lawesson's reagent (0.47 g, 1.16 mmol) were dissolved in dry toluene (15 mL) and the reaction mixture was refluxed for 24 h under N<sub>2</sub>. Thereafter, reaction mixture was concentrated by evaporation under vacuum and the resulting solid was stirred with K<sub>2</sub>CO<sub>3</sub> (1g) for 2 h before extraction with DCM (30 mL). After removal of DCM, the crude product was purified through silica gel column chromatography using DCM/petroleum ether (4/1, v/v) as eluent to afford **RhS6G-NH<sub>2</sub>** as a magenta red solid (0.19 g, 36.8% yield). <sup>1</sup>H-NMR: (600 MHz, CDCl<sub>3</sub>, ppm) δ: 8.12 (d, J = 7.1 Hz, 1H, ArH), 7.59–7.38 (m, 3H, ArH), 7.08 (s, 2H, xanthene-H), 6.41 (s, 2H, NH<sub>2</sub>), 6.13 (s, 2H, xanthene-H), 4.83 (s, 2H, 2 x NH), 3.22 (dd, J = 13.6, 6.6 Hz, 4H, 2 x CH<sub>2</sub>CH<sub>3</sub>), 1.90 (s, 6H, 2 x Ar-CH<sub>3</sub>), 1.26 (s, 6H, 2 x CH<sub>2</sub>CH<sub>3</sub>). ESI-MS: m/z 445.2 for [M + H]<sup>+</sup>, calc. for C<sub>26</sub>H<sub>28</sub>N<sub>4</sub>OS = 444.60.

### 3.3.3.3 Synthesis of poly(ethylene glycol)-g-vanillin (PEG-Vanillin)

To a stirred solution of polyethylene glycol (3 g, 3 mmol) and triethylamine (0.152 g, 1.5 mmol) dissolved in dry THF (50 mL) cooled to 0 °C, was added chloroacetyl chloride (0.17 g, 1.5 mmol) in dry THF (5 mL) dropwise over a period of 1 h. The reaction mixture was then allowed to slowly warm up to room temperature and stirred for 24 h. After this time, the resulting precipitate was filtered, solvent removed under vacuum and the residue dissolved in chloroform (50 mL) in a separating funnel. The light brown solution was then extracted with NaHCO<sub>3</sub> solution (2%, 2 x 10 mL) and brine solution (5%, 2 x 10 mL). The organic layer was collected and dried with anhydrous Na<sub>2</sub>SO<sub>4</sub> overnight. The solution was concentrated and added dropwise to a large excess of cold diethyl ether to give chloro-PEG (2.5 g, inclusive the monochloro-product) as the intermediate product used in making **PEG-Vanillin** without any further purification.

To a stirred solution of 4-hydroxy-3-methoxybenzaldehyde (vanillin, 0.274 g, 1.8 mmol) dissolved in dry DMF (10 mL) was added K<sub>2</sub>CO<sub>3</sub> (0.249 g, 1.8 mmol), KI (3.32 mg, 0.02 mmol) and chloro-PEG (2 g, 1.8 mmol). The solution was allowed to react at room temperature under N<sub>2</sub> atmosphere for 72 hrs (tracked with the help of TLC). After this time, activated charcoal was added and stirred for another 3 hrs. Then, the reaction mixture was filtered through a bed of celite and the solvent was removed under vacuum. The residue was dissolved in chloroform (50 mL) in a separating funnel. This was followed by extraction with ultrapure water 3 x 20 mL, brine solution (5%, 2 x 10 mL) and drying with anhydrous Na<sub>2</sub>SO<sub>4</sub> overnight. The solution was concentrated, and the crude product was purified through silica gel column chromatography using DCM/MeOH (10/0.5, v/v) as eluent to afford **PEG-Vanillin** as a light-yellow oil (1.8 g, 81.5 % yield). ATR-FTIR  $\nu$  cm<sup>-1</sup>: 3542 (OH), 2870 (sp<sup>3</sup> C-H Aliphatic), 1756, 1682 (C=O for ester and aldehyde groups), 1600, 1586, 1509 (Ar=CH) and 1120-1087 ( $\nu_{as}$  and  $\nu_s$  C-O-C). <sup>1</sup>H-NMR: (600 MHz, CDCl<sub>3</sub>, ppm)  $\delta$ : 9.85 (s, 1H, ArCHO), 7.54 (dd, 1H, J= 8.2, 1.8 Hz, ArH), 7.35 (s, 1H, ArH), 7.04 (d, 1H, J= 8.3 Hz, ArH), 4.81 (s, 2H, OCH<sub>2</sub>COO), 4.38 (m, 2H, OCOCH<sub>2</sub>), 3.99 (s, 3H, OCH<sub>3</sub>), 3.45-3.79 (m, 147H, OCH<sub>2</sub>CH<sub>2</sub>O), 2.00 (s, 1H, OH). <sup>13</sup>C NMR (125 MHz, CDCl<sub>3</sub>, ppm)  $\delta$ : 190.45 (ArCHO), 168.18 (COO), 154.81 (C-OCH<sub>2</sub>COO-Ar), 147.70 (C-OCH<sub>3</sub>-Ar), 129.87 (C-CHO-Ar), 127.40 (C-CH-CHO-Ar), 111.63 (C-C-O-CH<sub>2</sub>-Ar), 111.10 (C-

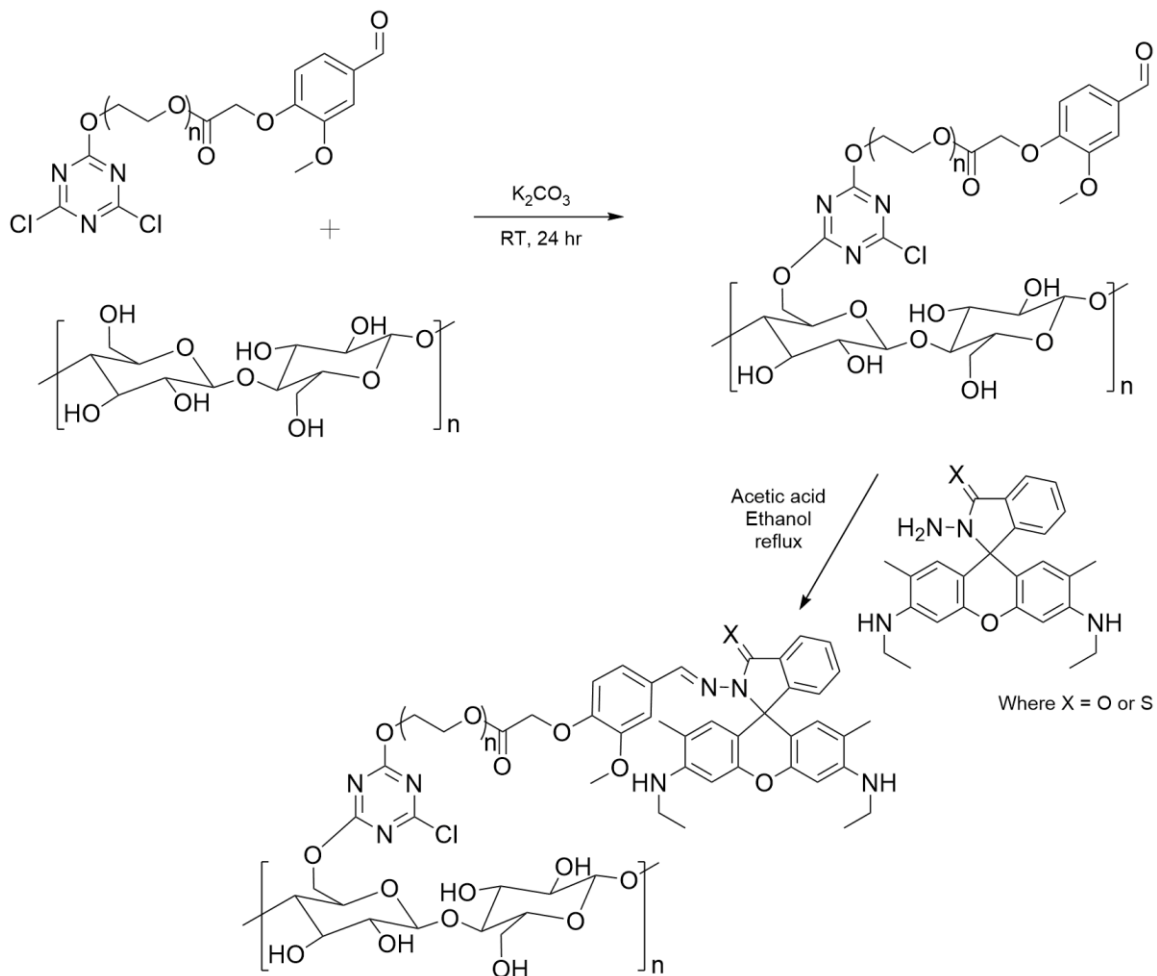
C-O-CH<sub>3</sub>-Ar), 72.57 – 70.27 (OCH<sub>2</sub>CH<sub>2</sub>O), 68.87 (O-CH<sub>2</sub>COO), 61.66 (OCOCH<sub>2</sub>CH<sub>2</sub>), 56.16 (OCH<sub>3</sub>-Ar).

### 3.3.4 Synthesis of 4,6-dichloro-s-triazinyl-poly(ethylene glycol)-vanillin (Triazine-PEG-Vanillin)

To a stirred solution of poly(ethylene glycol)-vanillin (1 g, 0.84 mmol) and 2,4,6-trimethylpyridine (0.102 g, 0.84 mmol) dissolved in dry acetone (15 mL) cooled to 0 °C, was added cyanuric chloride (0.155g, 0.84 mmol) dissolved in dry acetone (5 mL) dropwise over a period of 20 min. The resulting reaction mixture was allowed to slowly warm up to room temperature and stirred for another 24 h. Thereafter, the precipitate was filtered, solvent concentrated and added dropwise to a large excess of cold diethyl ether (resolved in 1 mL of acetone and added to fresh cold ether again) to yield **Triazine-PEG-Vanillin** as a faint yellow solid (0.98 g, 87.3 % yield). ATR-FTIR  $\nu$  cm<sup>-1</sup>: 2922-2870 (sp<sup>3</sup> C-H Aliphatic), 1756, 1684 (C=O for ester and aldehyde groups), 1600, 1570, (Ar=CH), 1635 and 1543 (C=N, C-N), 1120-1087 ( $\nu_{as}$  and  $\nu_s$  C-O-C) and 745.36 (C-Cl). <sup>13</sup>C NMR (125 MHz, CDCl<sub>3</sub>, ppm)  $\delta$ : 190.67 (ArCHO), 172.49 (Cl-C=N), 171.06 (O-C=N), 167.36 (COO), 157.63 (C-OCH<sub>2</sub>COO-Ar), 153.08 (C-OCH<sub>3</sub>-Ar), 127.34 (C-CHO-Ar), 125.07 (C-CH-CHO-Ar), 111.52 (C-C-O-CH<sub>2</sub>-Ar), 111.19 (C-C-O-CH<sub>3</sub>-Ar), 72.57 – 70.27 (OCH<sub>2</sub>CH<sub>2</sub>O), 65.22 (O-CH<sub>2</sub>COO), 61.66 (OCOCH<sub>2</sub>CH<sub>2</sub>), 56.26 (OCH<sub>3</sub>-Ar).

### 3.3.5 Grafting of Triazine-PEG-Vanillin onto cellulose

To a stirred suspension of Whatman No. 1 filter paper (0.75 g, 1 x 1 cm, 15 pieces) in dry acetone (20 mL) at room temperature, was added K<sub>2</sub>CO<sub>3</sub> (0.3 g). After 20 minutes, **Triazine-PEG-Vanillin** (0.5 g, 0.374 mmol) dissolved in dry acetone (10 mL) was added dropwise and left to stir for 24 hr. Then, the modified cellulose filter paper was removed from the reaction solution, dried and subjected to three successive sonication steps (10 min, 5 °C) switching solvent from acetone-to-DCM-to-isopropyl alcohol before finally rinsing in water to remove any bound base.



**Scheme 2.** Chemical grafting of triazinyl-PEG-rhodamine Schiff base onto cellulose

### 3.3.6 Synthesis of PEG-vanillin-rhodamine Schiff base and cellulose-PEG-vanillin-rhodamine Schiff base

A representative procedure for the synthesis of rhodamine Schiff base chemosensors based on PEG-vanillin and cellulose-PEG-vanillin, is provided, as shown in Schemes 1 and 2. Briefly, to a stirred solution of poly(ethylene glycol)-vanillin (0.2 g, 0.15 mmol) dissolved in absolute ethanol (5 mL), was added rhodamine 6g hydrazide (70 mg, 0.6163 mmol) and refluxed under  $\text{N}_2$  for 24 hr in the presence of sodium sulphate (0.2 g). The resulting reaction mixture was cooled, diluted with DCM (10 mL), filtered and concentrated to give a dark red solid. This was redissolved in acetone (5 mL) and kept in the freezer overnight

to generate red precipitates, filtered and oven dried to give pegylated rhodamine Schiff base (0.195 g, 81% yield).  $^1\text{H-NMR}$ : (600 MHz, DMSO- $d_6$ , ppm)  $\delta$ : 8.59 (s, 1H, ArCH=N), 7.88 (m, 1H, ArH), 7.54 (dd, 1H,  $J= 8.2, 1.8$  Hz, ArH), 7.56 (m, 2H, ArH), 7.04 (d, 1H,  $J= 8.3$  Hz, ArH), 6.98 (m, 1H, ArH), 6.93 (m, 1H, ArH), 6.27 (s, 2H, xanthene-H), 6.10 (s, 2H, xanthene-H), 5.01 (br.s, 2H, 2 x NH), 4.73 (s, 2H, OCH<sub>2</sub>COO), 4.38 (m, 2H, OCOCH<sub>2</sub>), 3.75 (s, 3H, OCH<sub>3</sub>), 3.35-3.65 (m, 147H, OCH<sub>2</sub>CH<sub>2</sub>O), 3.12 (q, 4H,  $J=3.5$  Hz, 2 x CH<sub>2</sub>CH<sub>3</sub>), 1.87 (s, 6H, 2 x Ar-CH<sub>3</sub>), 1.21 (t, 6H,  $J=7.1$  Hz, 2 x CH<sub>2</sub>CH<sub>3</sub>).

In the case of cellulose-PEG-vanillin, both rhodamine 6g and thiooxorhodamine 6g hydrazides were used in the Schiff base formation reaction under similar conditions mentioned above except modified cellulose-PEG-Schiff base filter papers were subjected to three successive sonication steps (10 min, 5 °C) switching solvent from DCM-to-isopropyl alcohol-to-water before use.

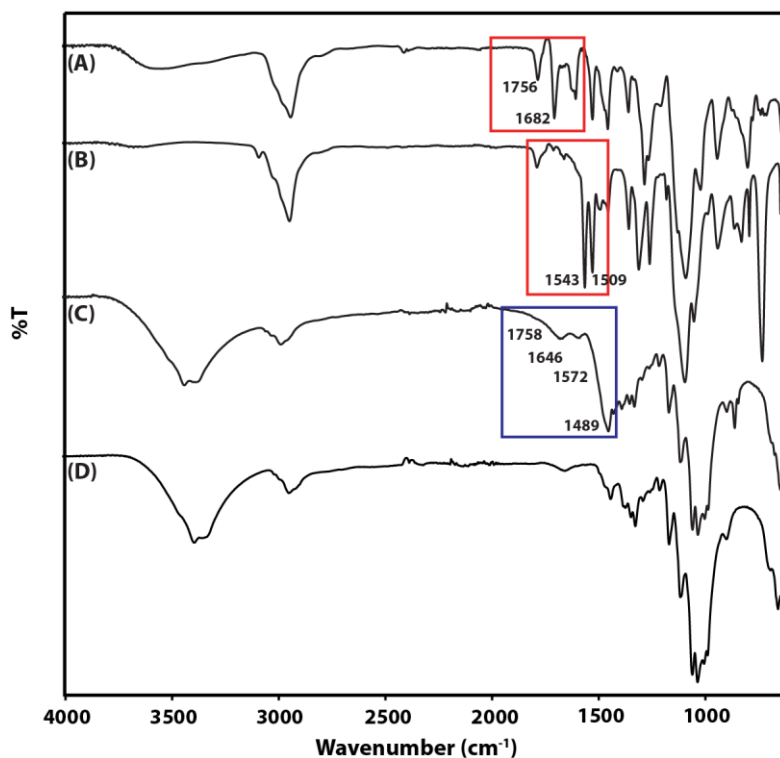
### 3.4 Results and Discussion

#### 3.4.1 Synthesis and characterization of chemosensors

The reactions in schemes 1 and 2 describe the synthesis of rhodamine-based hydrophilic fluorescent chemosensor probes as either free or immobilized compounds for heavy metal detection and monitoring. Cyanuric chloride was utilized as a linker molecule to immobilize PEG-rhodamine probes onto cellulose, which resulted in paper-based chemosensors suitable for on-field testing and with potential for heavy metal sequestration. The PEG spacer was used to tune the molecular properties of the chemosensors making them hydrophilic. This was aimed at increasing the interaction between metal ions and the probe molecules in purely aqueous samples, which would result in enhanced sensitivity.

A combination of esterification and O-alkylation reactions were first used to synthesize **PEG-Vanillin** as a template molecule that was either linked to rhodamine 6G hydrazide to afford the water soluble chemosensor **PEG-Vanillin-Rh6G** or to cyanuric chloride to afford the **Triazine-PEG-Vanillin** precursor, which was grafted onto cellulose filter paper. The modified paper was then subjected to a secondary reaction with **Rh6G-NH<sub>2</sub>** or **RhS6G-NH<sub>2</sub>** to afford paper-based chemosensors for Cu<sup>2+</sup> and Hg<sup>2+</sup>, respectively. After

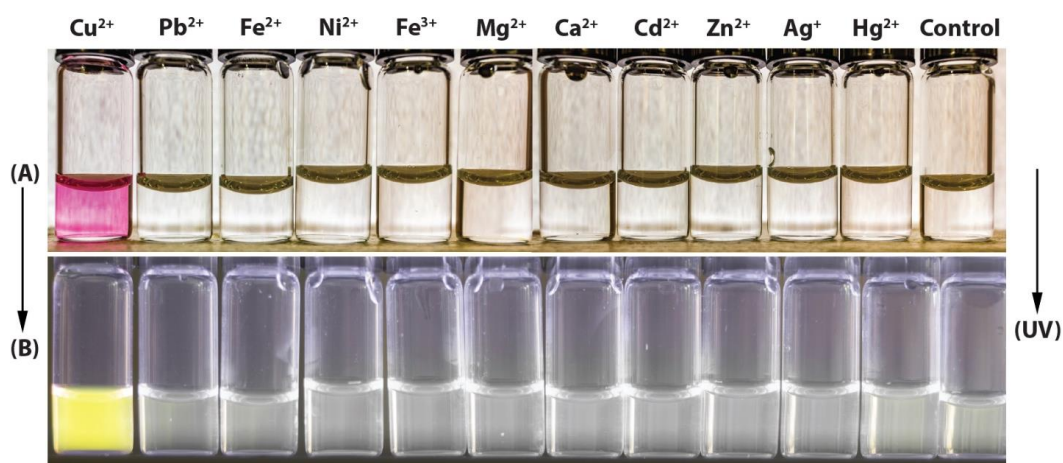
thorough characterization of the rhodamine derivatives (NMR and MS spectra presented in Figures S3.1-S3.5, Appendix 3), FTIR spectroscopy was used to confirm the covalent grafting of the **Triazine-PEG-Vanillin** derivative onto paper. Figure 3.1 shows a comparison between the FTIR spectra of **PEG-Vanillin**, **Triazine-PEG-Vanillin** and cellulose grafted with **Triazine-PEG-Vanillin**, demonstrating the successful attachment of PEG-vanillin functionalities onto cellulose. The data shows the appearance of distinct and unique chemical vibrations non-native to cellulose after grafting **Triazine-PEG-Vanillin** onto it. We observed the appearance of chemical vibrations for carbonyls, C=N and C-N  $sp^2$  bonds ( $\nu = 1758, 1646, 1572$  and  $1489 \text{ cm}^{-1}$  blue box in Figure 3.1C), which are characteristic of the ester, aldehyde and triazinyl groups present in **PEG-Vanillin** and **Triazine-PEG-Vanillin** ( $\nu = 1756, 1682, 1543$  and  $1509 \text{ cm}^{-1}$  red boxes in Figure 3.1A and 3.1B). These results confirmed the successful synthesis of the materials necessary to demonstrate the use of PEG-Vanillin-Rhodamine probes as water soluble or cellulose-bound chemosensors for heavy metal detection.



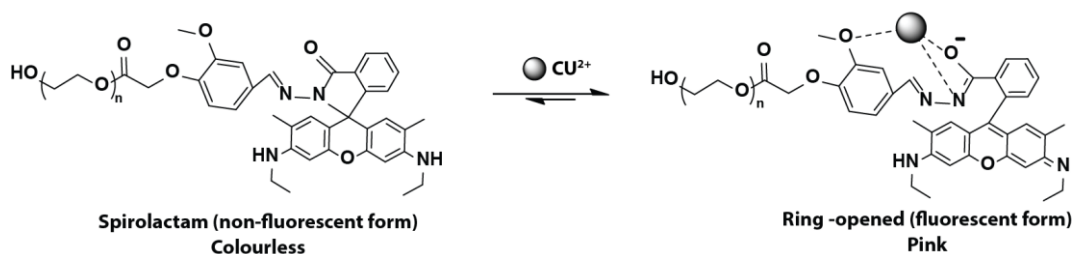
**Figure 3.1** FTIR spectra of (A) HO-PEG-Vanillin, (B) Triazinyl-PEG-Vanillin, (C) Cellulose-PEG-Vanillin and (D) unmodified Cellulose.

### 3.4.2 Spectral response of PEG-Vanillin-Rh6G Schiff base

To address the limitations of hydrophobic fluorescent chemosensors, we tested the ability of **PEG-Vanillin-Rh6G** probe to selectively detect heavy-metal ions in ultrapure water. The optical response of solutions of **PEG-Vanillin-Rh6G** (10  $\mu\text{M}$ ) was examined by mixing it with an equivalent amount of various metal ions (10  $\mu\text{M}$ ) in ultrapure water. We examined the selectivity of **PEG-Vanillin-Rh6G** towards  $\text{Cu}^{2+}$  over  $\text{Hg}^{2+}$ ,  $\text{Zn}^{2+}$ ,  $\text{Fe}^{2+}$ ,  $\text{Ca}^{2+}$ ,  $\text{Fe}^{3+}$ ,  $\text{Mn}^{2+}$ ,  $\text{Cd}^{2+}$ ,  $\text{Pb}^{2+}$ ,  $\text{Ag}^+$ ,  $\text{Mg}^{2+}$  and  $\text{Ni}^{2+}$  metal ions. Figure 3.2 shows that the selectivity of **PEG-Vanillin-Rh6G** towards  $\text{Cu}^{2+}$  ions is high, compared to other metal ions, since there is a rapid transition of the solution from colorless to pink only upon the addition of  $\text{Cu}^{2+}$  ions. While observing same solutions under UV irradiation a similar response was recorded, where only the solution containing  $\text{Cu}^{2+}$  ions displayed fluorescence. This result showcases the ability of  $\text{Cu}^{2+}$  ions to induce the ring opening of the spirolactam rhodamine ring by a metal ion complexation reaction. This is due to the interaction between  $\text{Cu}^{2+}$  ions, the  $\text{sp}^2$  carbonyl oxygen, the methoxy oxygen and the lone pair of electrons on the amide nitrogen which leads to C-N  $\text{Sp}^3$  spiranic bond rupture (Scheme 3) as electronic delocalization takes place. Similar behaviour has been reported for other rhodamine chemosensors used in  $\text{Cu}^{2+}$  ion sensing.<sup>15,19,20</sup> These results show that **PEG-Vanillin-Rh6G** is a highly selective and sensitive colorimetric chemosensor that can be used in-field for copper sensing in all-aqueous solutions.



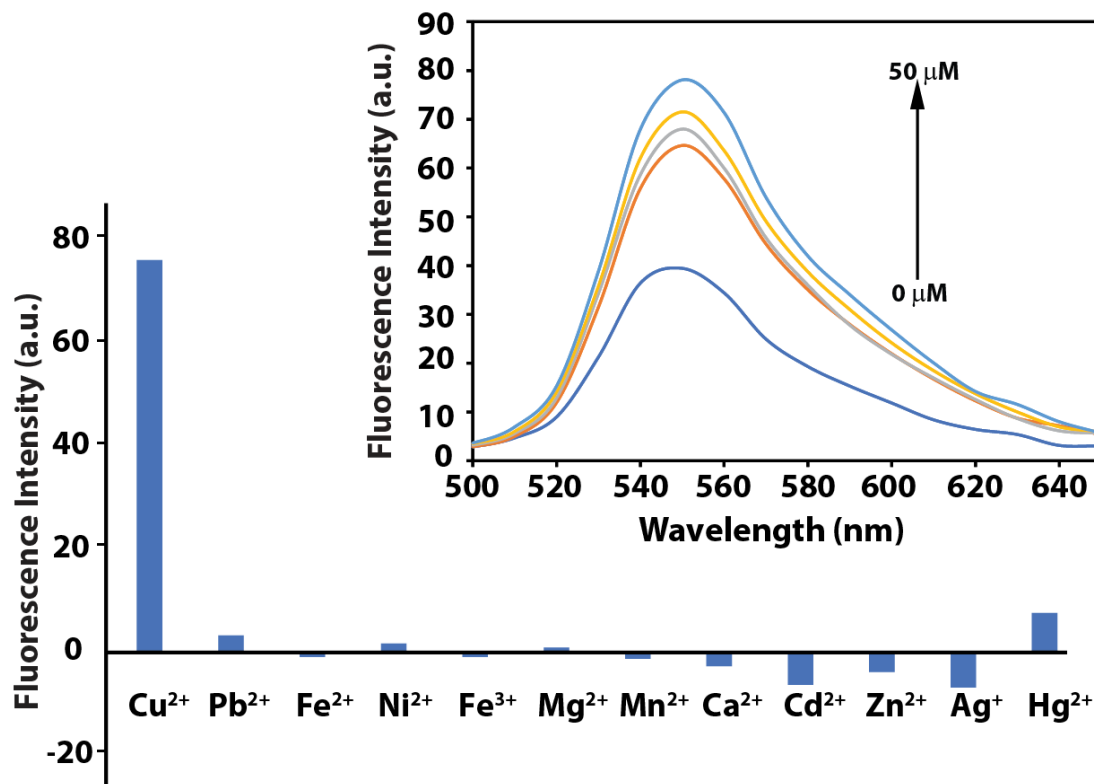
**Figure 3.2** Photographs of the response of **PEG-Vanillin-Rh6G** (10  $\mu\text{M}$ ) probe in water upon addition of metal ions. The assay was monitored (A) colorimetrically and (B) via fluorescence under UV excitation ( $\lambda = 256 \text{ nm}$ ).



**Scheme 3.** Proposed binding mechanism of **PEG-Vanillin-Rh6G** with  $\text{Cu}^{2+}$

To evaluate the selectivity of the **PEG-Vanillin-Rh6G** probe to free  $\text{Cu}^{2+}$  over other ions, the fluorescence signal in water was monitored using excitation and emission wavelengths of 500 nm and 550 nm, respectively. For this experiment, the probe concentration was kept at 1  $\mu\text{M}$ , and  $\text{Cu}^{2+}$  was tested at 1  $\mu\text{M}$  while the other ions were tested at concentrations up to a hundred-fold higher. The fluorescence of solutions exposed to  $\text{Cu}^{2+}$  ions (1  $\mu\text{M}$ ) showed strong enhancement in emission intensity, while the other tested metal ion solutions showed minimal change (Figure 3.3). As a matter of fact, 6 out of the 12 tested metal ions showed slight fluorescence quenching, which is expected when working at a hundred-fold excess of metal ions compared to the probe concentration.<sup>21</sup> The response of the **PEG-vanillin-Rh6G** probe to different  $\text{Cu}^{2+}$  concentrations was also investigated (inset, Figure 3.3). It was found that the intensity enhancement of the probe increased as the  $\text{Cu}^{2+}$  ion concentration was increased. These results indicate that the **PEG-vanillin-Rh6G** probe might be used in quantitative assays for the determination of copper concentration in all-aqueous samples.



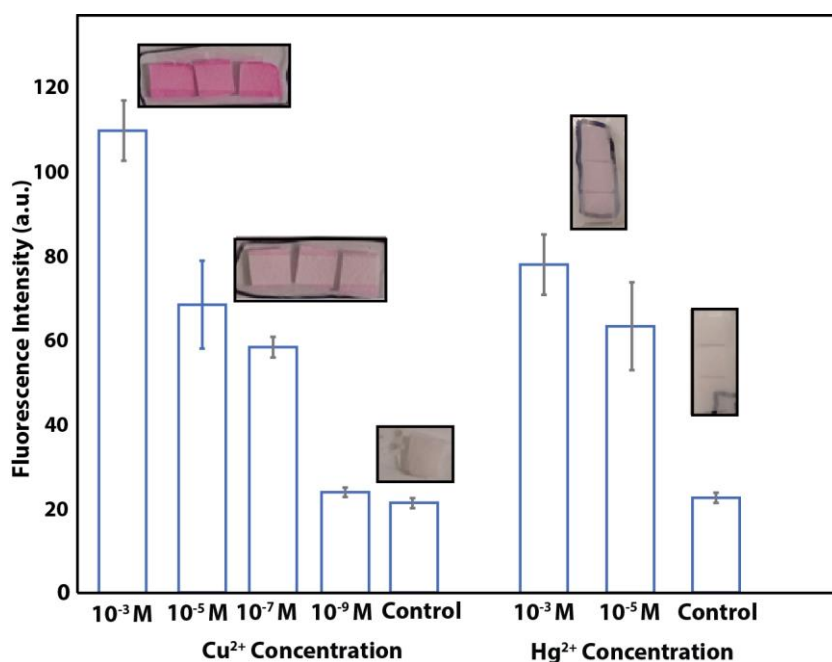


**Figure 3.3** Selectivity of the PEG-vanillin-Rh6G probe ( $10^{-6}$  M) in water to  $\text{Cu}^{2+}$  ( $10^{-6}$  M) and other metal ions ( $10^{-4}$  M). Inset: PEG-vanillin rhodamine fluorescence response to changes in  $\text{Cu}^{2+}$  concentration.

### 3.4.3 Spectral response of cellulose-PEG-vanillin-rhodamine Schiff base

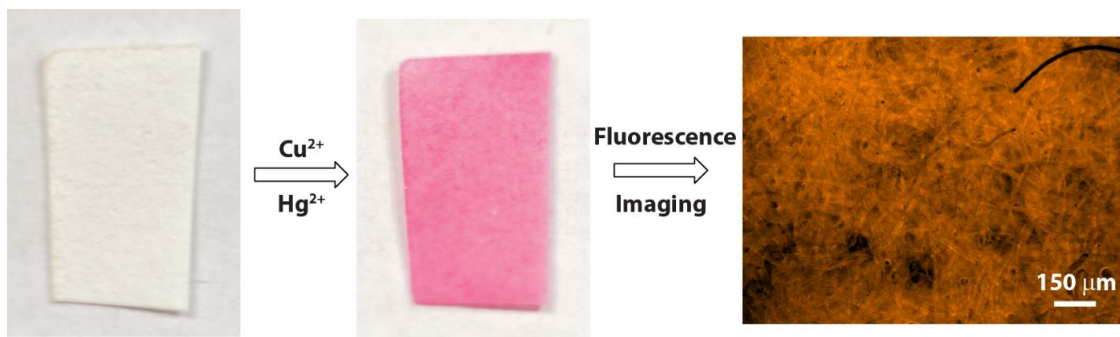
Based on the sensitivity and selectivity demonstrated by the free **PEG-vanillin-Rh6G**, our attention next shifted into testing the response of rhodamine-based probes immobilized on cellulose surfaces to the same panel of metal ions. The paper-based chemosensors grafted with **PEG-vanillin-Rh6G** and **PEG-vanillin-RhS6G** showed strong colorimetric and fluorescent responses only upon exposure to  $\text{Cu}^{2+}$  and  $\text{Hg}^{2+}$  ions (Figure 3.4), respectively. The selectivity of the surface grafted probes mirrors that of the free rhodamine 6G and thioxorhodamine 6G analogs, where the substitution of the spirolactam  $\text{sp}^2$  carbonyl oxygen in Rh6G with sulphur in RhS6G conveys strong selectivity for mercury ions and organic mercury to the latter probe.<sup>17</sup> Exposure to high concentrations of  $\text{Cu}^{2+}$  ions caused the cellulose filter paper modified with the PEG-Rh6G Schiff base to go from colorless to

intense pink rapidly (in a matter of seconds) as the spirolactam ring-opening process took place. The intensity in the shade of pink presented by the cellulose paper showed some direct correlation to the variation in  $\text{Cu}^{2+}$  ion concentrations from  $10^{-3}$  to  $10^{-9}$  M in water (Figure 3.4), highlighting the ability of the cellulose-based chemosensor to give both qualitative and semi-quantitative information about the presence of copper. This trend is similar to that observed with the free PEG-vanillin-rhodamine probe, showing the retention of the photophysical properties of the probe despite its immobilization onto cellulose. Similarly, when exposed to  $\text{Hg}^{2+}$  ions in concentrations ranging from  $10^{-3}$  to  $10^{-5}$  M in water, cellulose modified with PEG thiooxorhodamine Schiff base went from colorless to pink, although with a less intense tint. Nevertheless, the response was still directly proportional to  $\text{Hg}^{2+}$  ion concentration. These results altogether show the potential to use this new type of paper-based chemosensors as a chemical probe for heavy metal detection or as adsorbent for the removal of heavy metals from wastewater and the environment.



**Figure 3.4** Colorimetric response of Cellulose-PEG-vanillin-Rh6G and Cellulose-PEG-vanillin-RhS6G probes in ultrapure water to varying concentrations of  $\text{Cu}^{2+}$  and  $\text{Hg}^{2+}$  ions, respectively.

### 3.4.4 Fluorescence imaging of cellulose fibres



**Figure 3.5** Photograph of paper-based chemosensor and fluorescence image of triazinyl-PEG-vanillin-rhodamine labelled cellulose fibres.

The ability to chemically graft triazinyl-PEG-rhodamine Schiff bases onto cellulose for heavy metal detection afforded us with a tool to carry out fluorescence imaging of cellulose fibre after the spiro lactam ring opening reaction (Figure 3.5). In this case, the homogeneity of the surface modification reaction carried out on cellulose filter paper via the triazinyl chemistry was highlighted by the observation of uniformly labelled cellulose fibres. This provides further proof of the hydrophilicity of the substrate, which allowed the full surface to come into contact with the metal ions.

### 3.5 Conclusions

Hydrophilic colorimetric and fluorescent chemosensors based on the grafting of vanillin and rhodamine 6G hydrazide onto poly(ethylene glycol) chains were designed and synthesized for the first time. Free chemosensor probes were sensitive and selective towards copper and mercury ions in solution, with limits of detection in the ppb range. PEGylated vanillin-rhodamine derivatives were successfully grafted onto cellulose and retained the sensitivity and selectivity of the free probes towards  $\text{Cu}^{2+}$  and  $\text{Hg}^{2+}$  ions in 100% aqueous solution over a host of other metal ions tested.

The selectivity of the cellulose-based chemosensors was linked to the grafted rhodamine hydrazide derivative. The emission intensity enhancement recorded for free and

immobilized probes is directly proportional to  $\text{Cu}^{2+}/\text{Hg}^{2+}$  ion concentrations. With, limits of detection based on colorimetric assays for  $\text{Cu}^{2+}$  and  $\text{Hg}^{2+}$  ions recorded as 6.3 and 20 ppb, respectively. These results make PEG-vanillin-rhodamine and cellulose-PEG-vanillin-rhodamine very promising probes for the colorimetric and fluorescent detection of for heavy metals in all-aqueous solutions for environmental monitoring and remediation applications.

### 3.6 Acknowledgements

We thank Prof. Ryan Wylie for access to equipment and useful discussions. This research was supported through the Natural Sciences and Engineering Research Council and a Canada Foundation for Innovation Leaders Opportunity Fund. A. Fatona was partially supported by the BioInterfaces CREATE grant. J. Moran-Mirabal is the recipient of an Early Researcher Award from the Ontario Ministry for Research and Innovation and is the Tier 2 Canada Research Chair on Micro and Nanostructured Materials.

### 3.7 References

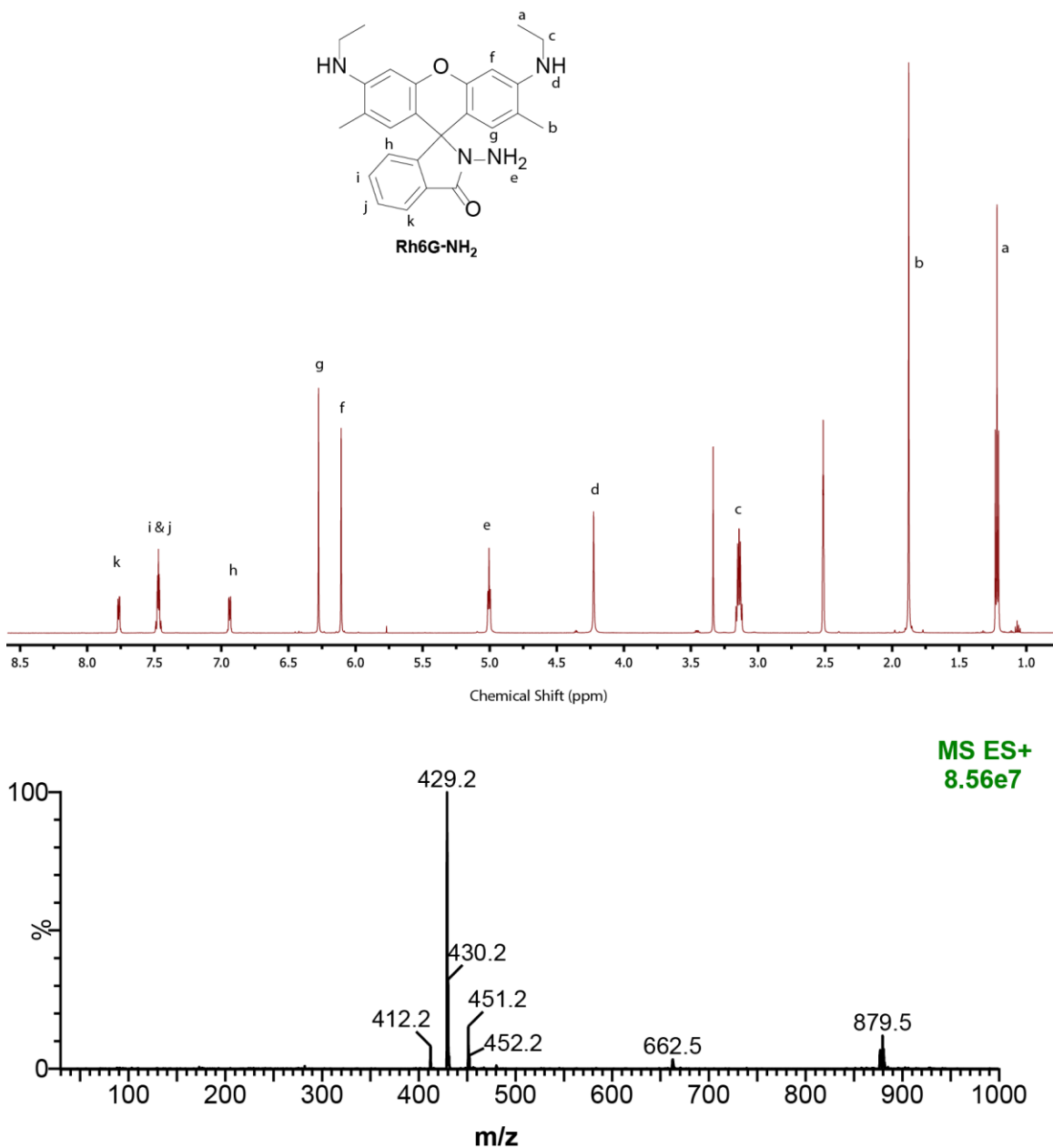
- (1) Multhaup, G.; Schlicksupp, A.; Hesse, L.; Beher, D.; Ruppert, T.; Masters, C. L.; Beyreuther, K. The Amyloid Precursor Protein of Alzheimer's Disease in the Reduction of Copper(II) to Copper(I). *Science* **1996**, *271* (5254), 1406–1409.
- (2) Gaggelli, E.; Kozlowski, H.; Valensin, D.; Valensin, G. Copper Homeostasis and Neurodegenerative Disorders (Alzheimer's, Prion, and Parkinson's Diseases and Amyotrophic Lateral Sclerosis). *Chem. Rev.* **2006**, *106* (6), 1995–2044.
- (3) Tchounwou, P. B.; Yedjou, C. G.; Patlolla, A. K.; Sutton, D. J. Heavy Metal Toxicity and the Environment. In *Molecular, Clinical and Environmental Toxicology: Volume 3: Environmental Toxicology*; Luch, A., Ed.; Experientia Supplementum; Springer Basel: Basel, 2012; pp 133–164.

- (4) Amendola, V.; Fabbrizzi, L.; Foti, F.; Licchelli, M.; Mangano, C.; Pallavicini, P.; Poggi, A.; Sacchi, D.; Taglietti, A. Light-Emitting Molecular Devices Based on Transition Metals. *Coord. Chem. Rev.* **2006**, *250* (3), 273–299.
- (5) Ojida, A.; Nonaka, H.; Miyahara, Y.; Tamaru, S.; Sada, K.; Hamachi, I. Bis(Dpa-ZnII) Appended Xanthone: Excitation Ratiometric Chemosensor for Phosphate Anions. *Angew. Chem. Int. Ed.* **2006**, *45* (33), 5518–5521.
- (6) Culzoni, M. J.; Peña, A. M. de la; Machuca, A.; Goicoechea, H. C.; Babiano, R. Rhodamine and BODIPY Chemodosimeters and Chemosensors for the Detection of Hg<sup>2+</sup>, Based on Fluorescence Enhancement Effects. *Anal. Methods* **2012**, *5* (1), 30–49.
- (7) Xu, H.; Wang, X.; Zhang, C.; Wu, Y.; Liu, Z. Coumarin-Hydrazone Based High Selective Fluorescence Sensor for Copper(II) Detection in Aqueous Solution. *Inorg. Chem. Commun.* **2013**, *34*, 8–11.
- (8) Li, Z.; Chen, Q.-Y.; Wang, P.-D.; Wu, Y. Multifunctional BODIPY Derivatives to Image Cancer Cells and Sense Copper(II) Ions in Living Cells. *RSC Adv.* **2013**, *3* (16), 5524–5528.
- (9) Fan, J.; Zhan, P.; Hu, M.; Sun, W.; Tang, J.; Wang, J.; Sun, S.; Song, F.; Peng, X. A Fluorescent Ratiometric Chemodosimeter for Cu<sup>2+</sup> Based on TBET and Its Application in Living Cells. *Org. Lett.* **2013**, *15* (3), 492–495.
- (10) Padghan, S. D.; Puyad, A. L.; Bhosale, R. S.; Bhosale, S. V.; Bhosale, S. V. A Pyrene Based Fluorescent Turn-on Chemosensor: Aggregation-Induced Emission Enhancement and Application towards Fe<sup>3+</sup> and Fe<sup>2+</sup> Recognition. *Photochem. Photobiol. Sci.* **2017**, *16* (11), 1591–1595.
- (11) Ge, F.; Ye, H.; Luo, J.-Z.; Wang, S.; Sun, Y.-J.; Zhao, B.-X.; Miao, J.-Y. A New Fluorescent and Colorimetric Chemosensor for Cu(II) Based on Rhodamine Hydrazone and Ferrocene Unit. *Sens. Actuators B Chem.* **2013**, *181*, 215–220.
- (12) Wu, W.; Sun, Z.; Zhang, Y.; Xu, J.; Yu, H.; Liu, X.; Wang, Q.; Liu, W.; Tang, Y. A Multifunctional Nanosensor Based on Silica Nanoparticles and Biological Applications in Living Cells. *Chem. Commun.* **2012**, *48* (89), 11017–11019.

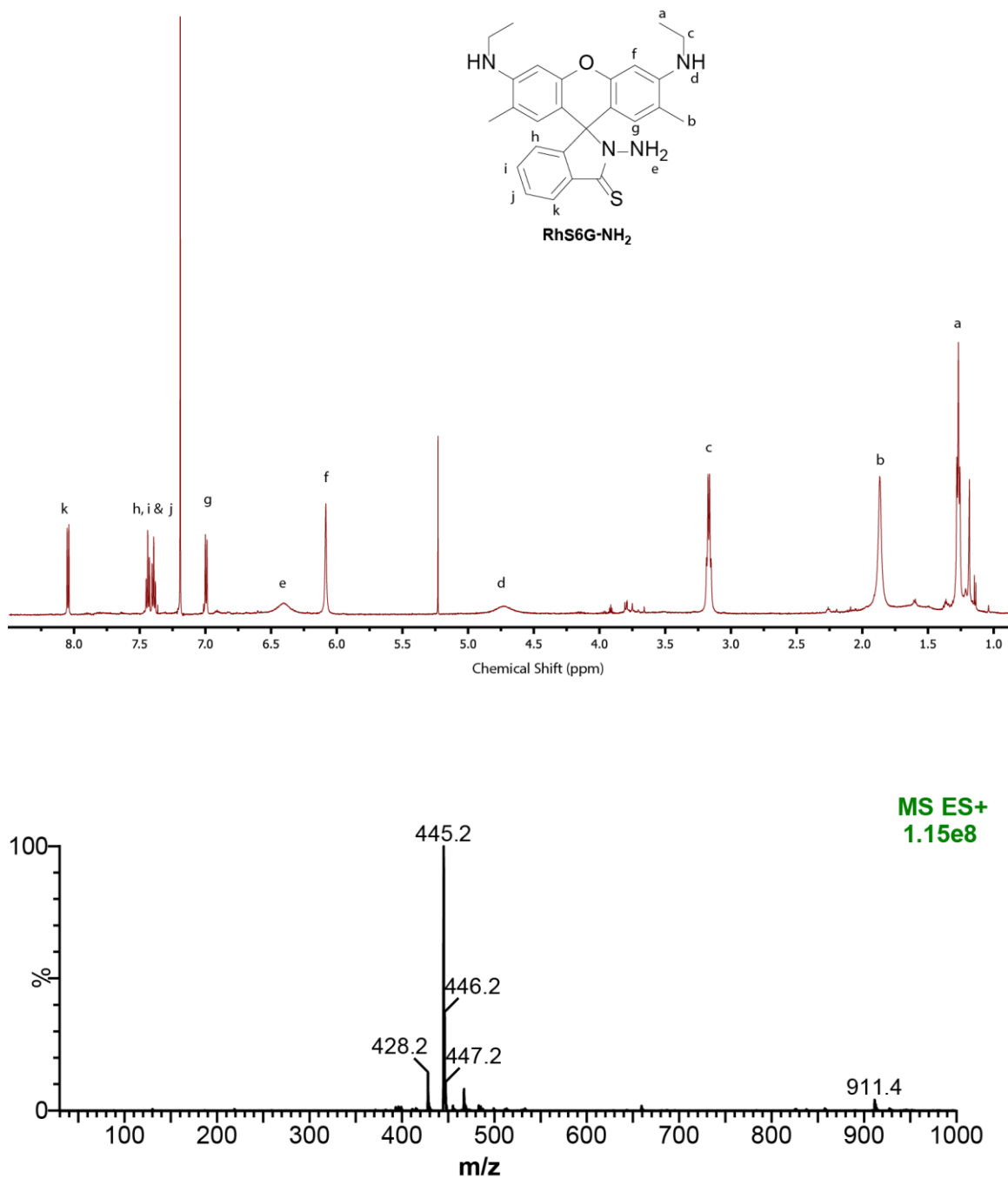
- (13) Orriach-Fernández, F. J.; Medina-Castillo, A.; Fernández-Sánchez, J. F.; Peña, A. M. de la; Fernández-Gutiérrez, A. Hg<sup>2+</sup>-Selective Sensing Film Based on the Incorporation of a Rhodamine 6G Derivative into a Novel Hydrophilic Water-Insoluble Copolymer. *Anal. Methods* **2013**, 5 (23), 6642–6648.
- (14) Solomon, F. Impacts of Copper on Aquatic Ecosystems and Human Health. *Env. Commun* **2009**, 25–28.
- (15) Meng, X.; Xu, Y.; Liu, J.; Sun, L.; Shi, L. A New Fluorescent Rhodamine B Derivative as an “off-on” Chemosensor for Cu<sup>2+</sup> with High Selectivity and Sensitivity. *Anal. Methods* **2016**, 8 (5), 1044–1051.
- (16) Dai, K.; Xu, B.; Chen, J. A Rhodamine-Based “Off-On” Colorimetric and Fluorescent Chemosensor for Cu(II) in Aqueous and Non-Aqueous Media. *J. Fluoresc.* **2014**, 24 (4), 1129–1136.
- (17) Wang, H.-H.; Xue, L.; Yu, C.-L.; Qian, Y.-Y.; Jiang, H. Rhodamine-Based Fluorescent Sensor for Mercury in Buffer Solution and Living Cells. *Dyes Pigments* **2011**, 91 (3), 350–355.
- (18) Ma, C.; Lin, L.; Du, Y.; Chen, L.; Luo, F.; Chen, X. Fluorescence Quenching Determination of Iron( Iii ) Using Rhodamine 6G Hydrazone Derivative. *Anal. Methods* **2013**, 5 (7), 1843–1847.
- (19) Xiang, Y.; Tong, A.; Jin, P.; Ju, Y. New Fluorescent Rhodamine Hydrazone Chemosensor for Cu(II) with High Selectivity and Sensitivity. *Org. Lett.* **2006**, 8 (13), 2863–2866.
- (20) Lee, M. H.; Kim, H. J.; Yoon, S.; Park, N.; Kim, J. S. Metal Ion Induced FRET OFF–ON in Tren/Dansyl-Appended Rhodamine. *Org. Lett.* **2008**, 10 (2), 213–216.
- (21) Roy, A.; Mukherjee, R.; Dam, B.; Dam, S.; Roy, P. A Rhodamine-Based Fluorescent Chemosensor for Al<sup>3+</sup>: Is It Possible to Control the Metal Ion Selectivity of a Rhodamine-6G Based Chemosensor? *New J. Chem.* **2018**, 42 (11), 8415–8425.

- (22) Kumar, M.; Kumar, N.; Bhalla, V.; Sharma, P. R.; Kaur, T. Highly Selective Fluorescence Turn-on Chemodosimeter Based on Rhodamine for Nanomolar Detection of Copper Ions. *Org. Lett.* **2012**, *14* (1), 406–409.

### Appendix 3: Chapter 3 Supporting Information

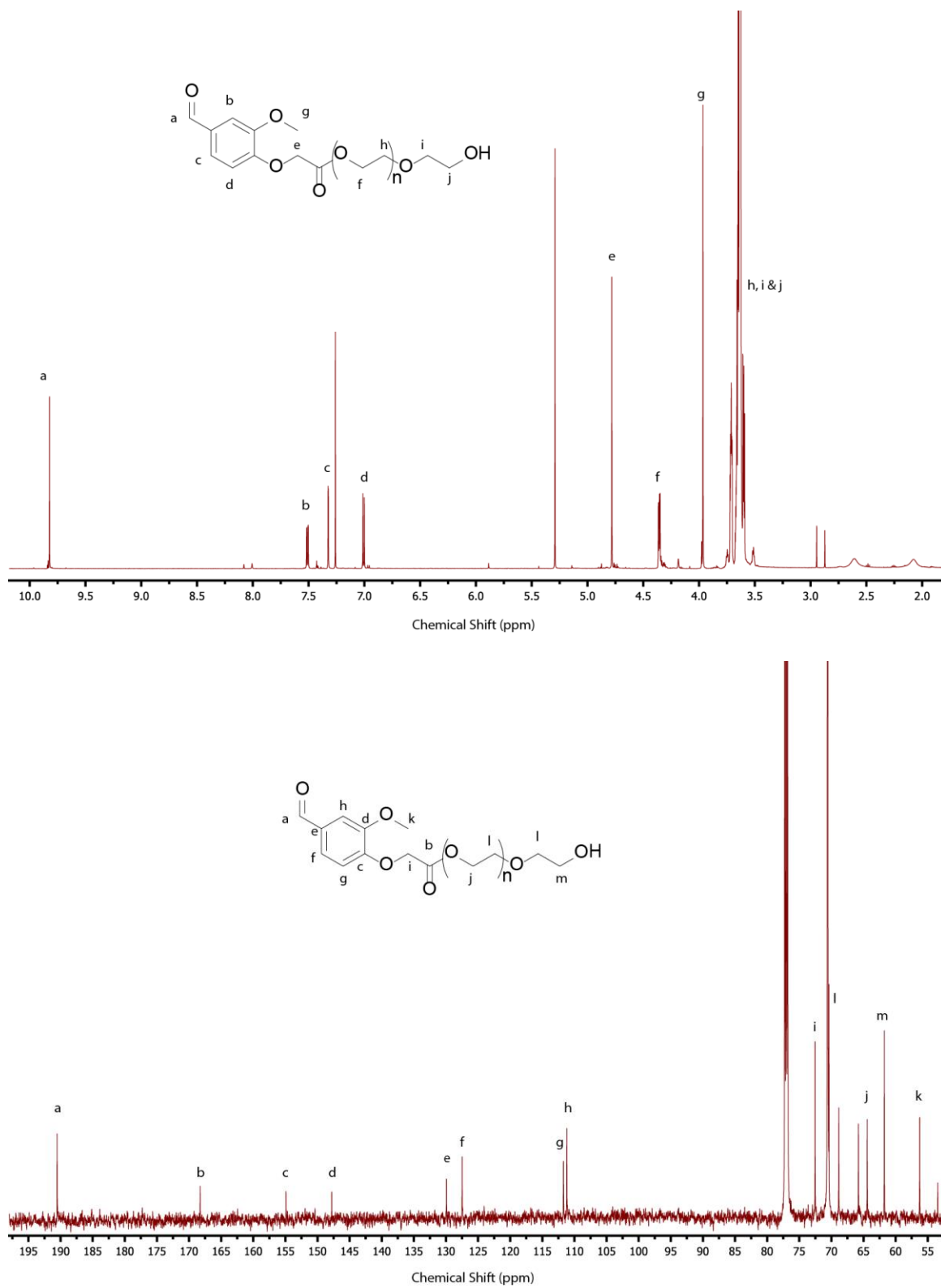


**Figure S3.1** Characterization of Rhodamine 6G hydrazide (Rh6G-NH<sub>2</sub>). Top: <sup>1</sup>H NMR spectrum; Bottom: High-resolution ESI-Q-TOF mass spectrum.

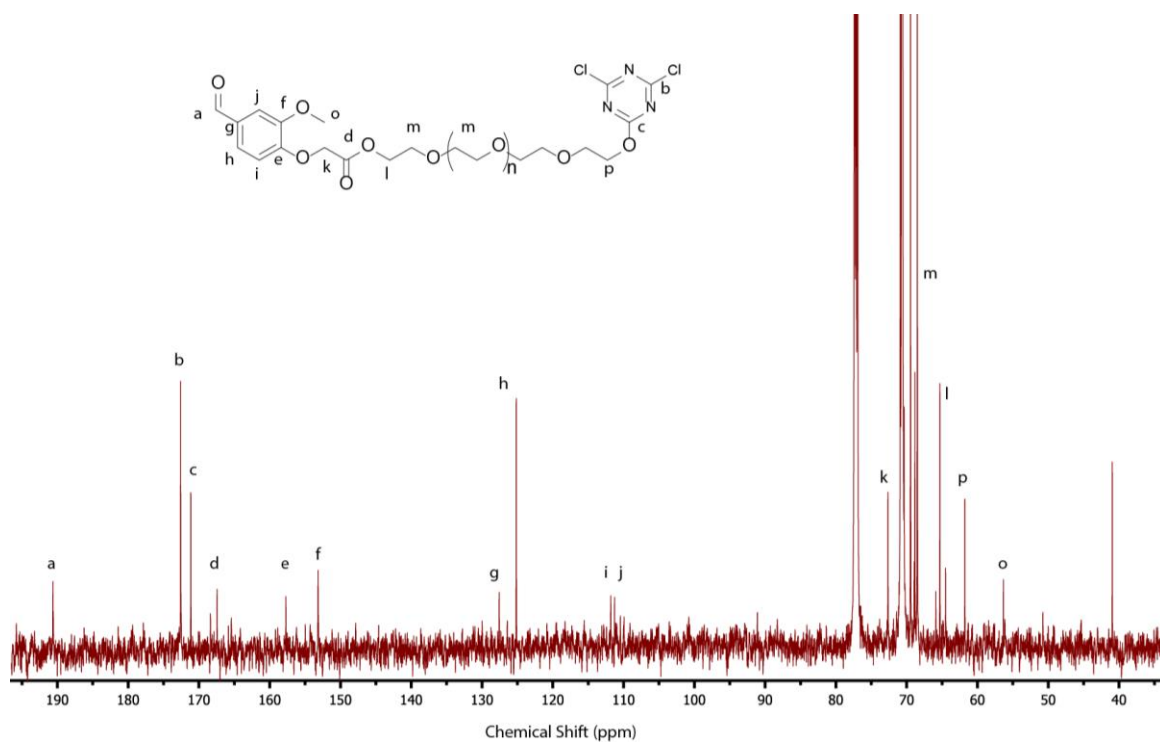


**Figure S3.2 Characterization of Thioxorhodamine 6G hydrazide (RhS6G-NH<sub>2</sub>).** Top: <sup>1</sup>H NMR spectrum; Bottom: High-resolution ESI-Q-TOF mass spectrum.

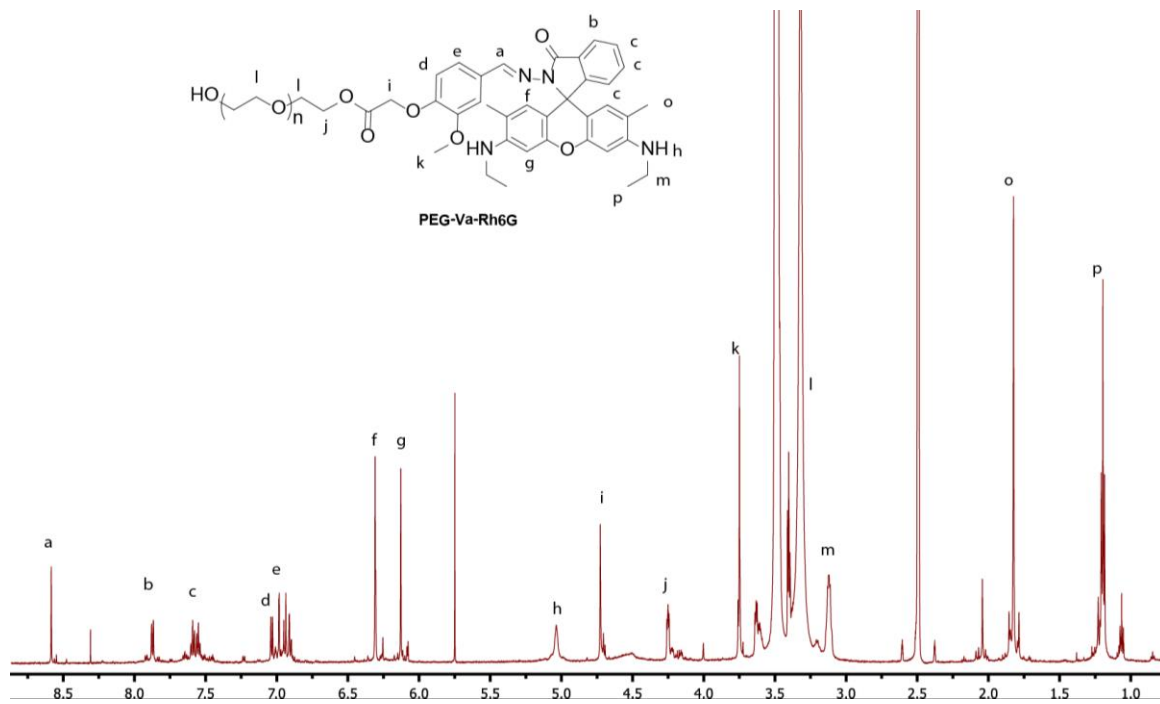




**Figure S3.3 Characterization of PEG-vanillin.** Top:  $^1\text{H}$  NMR spectrum; Bottom:  $^{13}\text{C}$  NMR spectrum.



**Figure S3.4** Characterization of 4,6-dichloro-triazinyl-polyethylene(glycol)-vanillin (Triazine-PEG-Vanillin). <sup>13</sup>C NMR spectrum.



**Figure S3.5** Characterization of Polyethylene(glycol)-vanillin-rhodamine Schiff base (PEG-Va-Rh6G).  $^1\text{H}$  NMR spectrum.

## **CHAPTER 4: Catalyst-Free Silicone Elastomers Crosslinked using Triazines\***

### **4.1 Abstract**

Silicone elastomers are a class of polymers typically created using metal-based cure chemistries. Faced with some challenges in term of cost and versatility during and after cure, the need for a simple and efficient catalyst-free system to prepare both functional and/or cross-linked silicones arise. This work describes the preparation of amino-triazinyl silicone networks, which are readily formed between commercially available aminopropyl silicones and cyanuric chloride or a synthesized, premodified tetrachloro-triazinyl silicone analog without the use of catalyst, optionally in the presence of a solvent. The presence of residual amines, and the types of residual amines, could be utilized to manipulate elastomer properties. The self-neutralizing ability of available amines for the HCl byproduct made it possible to tailor silicone mechanical properties from very soft gels to much more rigid elastomers. In addition, the neutralization facilitates the maintainance of stability of the products against hydrolytic and thermal oxidative stress. The use of nucleophilic aromatic substitution reactions of readily available chloro-s-triazines, as an alternative organic cure, is an attractive route to catalyst free silicone elastomers.

---

\* This chapter is in preparation for submission as A. Fatona, A. Osamudiamen, J. M. Moran-Mirabal and M. A. Brook. Fatona and Brook designed the experiments and analyzed the data. Fatona and Osamudiamen performed all experiments including syntheses and characterization. Fatona wrote the manuscript with additions, edits and guidance from both Moran-Mirabal and Brook.

## 4.2 Introduction

Silicone elastomers are widely used in many applications ranging from biomaterials<sup>1-3</sup> to insulators, coatings, sealants, etc.<sup>4,5</sup> The vast majority of these elastomers undergo cure using three different chemistries: radical cure at elevated temperature;<sup>6</sup> moisture driven hydrolysis condensation room temperature vulcanization<sup>7,8</sup> (RTV) or platinum-catalyzed hydrosilylation.<sup>9,10</sup> While there are many merits associated with these methods, all suffer from the need for catalysts, and the production of by-products associated with the catalysts, or residual catalysts, that may need to be addressed before the final use, particularly in sensitive technical areas such as biomaterials.<sup>11</sup> In addition, many of the cure reactions are relatively slow and their functional group intolerance in starting materials lead to premature deactivation or shelf-life limitations.<sup>12</sup>

Alternative strategies for crosslinking functional polysiloxanes using organic reactions have been shown to be advantageous in some circumstances, mostly because they can be free of catalysts and can benefit from mild conditions such as no solvents, low cure temperatures, and occur with high yields with no by-product formation.<sup>13-15</sup> Amines are particularly useful in such reactions and, using aminopropylsilicones, have been utilized in aza-Michael<sup>16</sup> and Schiff-base<sup>17</sup> reactions to afford thermoset elastomers with high modulus or thermoplastics with self-healing capabilities that can facilitate recycling and repurposing of silicone elastomers.<sup>17</sup> In the case of epoxy chemistry, such amines can act as curing agents for epoxy resins, leading to enhancements in performance, including the mechanical properties, increasing resistance to weatherability in sunlight and improved hydrophobicity.<sup>18,19</sup> The amino functionality in aminopropylsilicones has also been shown to participate in other cure systems such as vinylogous urea exchange reactions via a  $\beta$ -keto ester to create quenched vitrimers with tunable properties.<sup>20</sup>

Compounds based on triazines have found an important place in material science, mostly as reactive or fluorescent dyes grafted onto biopolymer cellulose to achieve varieties of textile color shades,<sup>21</sup> to monitor hydrolysis of crystalline cellulose,<sup>22-26</sup> to prepare antibacterial fabrics<sup>27,28</sup> or as activated polysaccharides for affinity based separations.<sup>29,30</sup> Triazines are widely used as herbicides and the compounds are perceived not to be acutely toxic to humans.<sup>31</sup> Nevertheless, one clearly wishes to avoid toxic materials. Once the

molecular weight of triazine-containing systems is increased, the biological activity significantly drops.<sup>32</sup> Even the polymer of most concern – melamine in formaldehyde resins – is approved for use as a food contacting substance.<sup>33</sup>

The efficacy of the triazinyl chemistry in macromolecular synthesis has been highlighted in the synthesis of dendrimers based on triazines decorated with pharmacophores and DNA. These materials were found to be effective and nontoxic drug delivery systems for infectious disease and anticancer management.<sup>34–36</sup> Importantly, these syntheses have been executed at scales that ranged from high milligrams to over a kilogram with different choices of nucleophiles,<sup>37</sup> demonstrating the ease with which chemoselective nucleophilic aromatic substitution reactions occur with the precursor cyanuric chloride. Covalent organic frameworks (COF) based on triazines has also been used in the form of films on metal surfaces to improve the lubricity in copper and steel systems with excellent tribological performance.<sup>38</sup> The stabilization against photodegradation in polymethyl methacrylate (PMMA) co- and ter-polymer films have been attributed to the presence of triazinyl 2,2,6,6-tetramethylpiperidine and 2-hydroxybenzo-phenone groups incorporated within the structure of the polymers.<sup>39</sup>

In view of the benefits that amine chemistry delivers to silicones in the form of accessible cure chemistries and the versatility of the triazinyl chemistry in building macromolecular architectures, we have examined the combination of these two as an alternative organic cure process with the hope that the product elastomeric properties could be readily manipulated. We report for the first time that commercial aminopropyl-modified silicones are easily crosslinked by the addition of commercially available cyanuric chloride or pre-formulated tetrachloro-triazinyl silicones, to create silicone elastomers under mild and catalyst free conditions with controlled and variable crosslink densities and predictable properties. The presence of the residual amines were shown to play a significant role in the formation of networks determining the mechanical properties of the elastomers; the self-neutralizing ability of available amines towards the HCl byproduct made it possible to tailor silicone mechanical properties from very soft gels to much more rigid elastomers.

## 4.3 Experimental

### 4.3.1 Materials

Telechelic 3-(aminopropyl)-terminated polydimethylsiloxanes (DMS-A11, MW 920 g mol<sup>-1</sup>; DMS-A21, MW 1000 g mol<sup>-1</sup>); 3-(aminopropyl)methylsiloxane-dimethylsiloxane copolymers (PDMS-NH<sub>2</sub>, Me<sub>3</sub>SiO(Me(H<sub>2</sub>N(CH<sub>2</sub>)<sub>3</sub>)SiO)<sub>n</sub>(Me<sub>2</sub>SiO)<sub>m</sub>SiMe<sub>3</sub>, AMS-132, n = 2-3 mol% (of n+m), MW 4500-6000 g mol<sup>-1</sup>; AMS 152, n = 4-5 mol%, MW 7000–9000 g mol<sup>-1</sup>; AMS 162, n = 6-7 mol%, 4000–5000 g mol<sup>-1</sup>; AMS 163, n = 6-7 mol%, 50,000 g mol<sup>-1</sup>); and (aminoethylaminopropyl)methylsiloxane-dimethylsiloxane copolymer (PDMS-NHC<sub>2</sub>NH<sub>2</sub>, Me<sub>3</sub>SiO(Me(H<sub>2</sub>N(CH<sub>2</sub>)<sub>2</sub>NH(CH<sub>2</sub>)<sub>3</sub>)SiO)<sub>n</sub>(Me<sub>2</sub>SiO)<sub>m</sub>SiMe<sub>3</sub>, AMS-233, n = 2-4 mol%, 5000 g mol<sup>-1</sup>) were obtained from Gelest. Cyanuric chloride (99%) and triethylamine (99%) were purchased from Millipore-Sigma. Silica gel (Aerosil 150) was obtained from Evonik. Tetrahydrofuran, dichloromethane (DCM), acetonitrile, ethyl acetate, chloroform, hexane and toluene were purchased from Caledon. All materials were used as received except for THF, DCM and toluene dried through an activated alumina column before use.

### 4.3.2 Characterization

**Nuclear Magnetic Resonance,** <sup>1</sup>H & <sup>13</sup>C NMR experiments were recorded at room temperature and performed on Bruker Avance 600 MHz nuclear magnetic resonance spectrometer using deuterated chloroform as solvent.

**Mass Spectrometry (MS).** Mass spectra of synthesized rhodamine derivatives were recorded on a Micromass Ultima (LC-ESI/APCI) Triple Quadrupole Mass spectrometer and Micromass Global Ultima ESI Quadrupole Time of Flight (Q-TOF) Mass spectrometer.

**Infrared Spectroscopy.** Infrared measurements of triazinyl-crosslinked silicone elastomers were conducted on a Thermo Scientific Nicolet 6700 FT-IR spectrometer equipped with a Smart iTX attenuated total reflectance (ATR) attachment.

**Thermogravimetric Analysis (TGA).** Analyses were carried out on a Mettler Toledo TGA 2 thermogravimetric analyzer. Data was collected after placing ca. 5 mg of a vacuum-dried sample in a clean alumina crucible and heating from ambient temperature to 800 °C under both argon and oxygen atmosphere (heating rate of 20 °C min<sup>-1</sup>).

**Young's modulus measurement.** Modulus data was collected 24 h after elastomer formation on 3.5 mm thick samples using a MACH-1 micromechanical testing instrument (Biomomentum) equipped with a 0.5 mm hemispherical indenter using a Poisson ratio of 0.3 and a constant indentation depth of 1.0 mm. All measurements were conducted at 22 °C and taken six times. Shore OO measurements were taken using Rex Durometer, Type OO Model 1600 from Rex Gauge Co.

**Rheometry.** Rheological measurements were taken using a TA instruments Discovery HR-3 Hybrid Rheometer equipped with 40 mm parallel plate geometry. Dynamic strain sweep experiments at frequency 1 Hz were performed for all samples to decide the linear dynamic range of the strain. All experiments were performed at 25 °C. The linear viscoelastic regime extends to oscillatory strains above 50% in both systems studied. However, at higher strains, changes in the gel structure (ruptured bonds or entanglements) resulted in a decrease in the measured moduli, as expected. For gel point determination, time sweep experiments (using the 40 mm parallel plate geometry) were performed under the single frequency of 6.28 rad/s with a constant strain of 0.5% at 25 and 60 °C.

Dispersions of pre-elastomers were mixed using a planetary centrifugal mixer “Speedmixer” (model: DAC 150.1 FVZ-K, FlackTek Inc.).

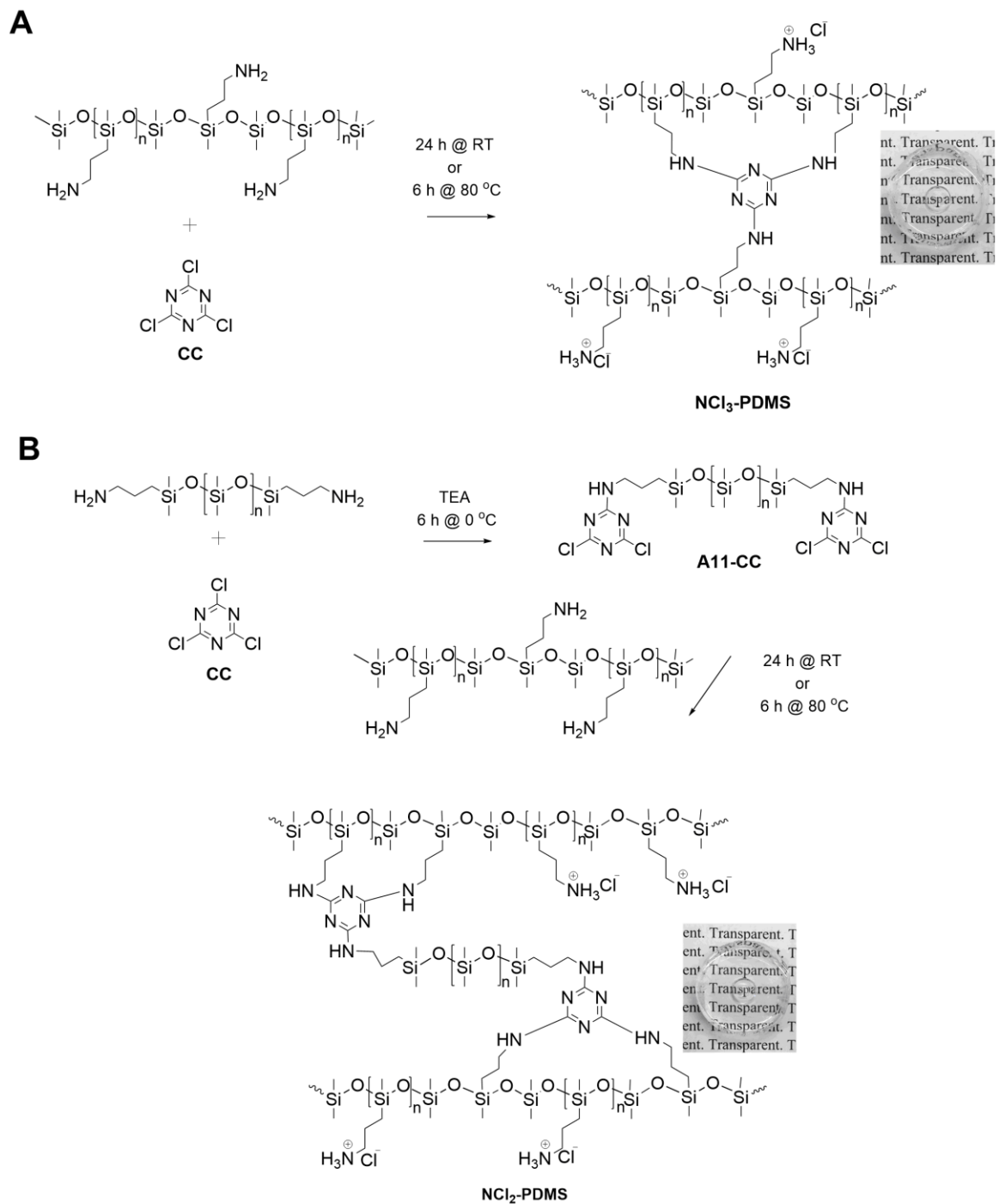
### **4.3.3 Silicone elastomer preparation using triazinyl crosslinkers**

Two different types of triazinyl crosslinkers – cyanuric chloride or its pre-modified tetrachloro-s-triazinyl silicone analog – were studied. In both types of systems, the NH<sub>2</sub>/Cl ratios (Table 1) were varied. As is discussed below, the amines serve two roles acting both as the reactive nucleophile driving the crosslinking reaction and the active base in the system to sequester the HCl byproduct (Figure 4.1). A systematic study was undertaken to establish the relationship between modulus and [NH<sub>2</sub>]/[Cl] with respect to crosslink density (average molecular weight between crosslink points) and the role of free amines and ammonium salts on properties.



#### **4.3.3.1 Preparation of aminosilicone elastomers directly with cyanuric chloride (NCl<sub>3</sub>-PDMS)**

**NCl<sub>3</sub>-PDMS** elastomers – aminotriazinyl-functional silicone networks – with various crosslink densities were fabricated. A representative curing procedure for the synthesis based on cyanuric chloride (Table 1, Figure 4.1A) is provided. AMS 162 (aminopropyl)methylsiloxane-dimethylsiloxane copolymer (PDMS-NH<sub>2</sub>, AMS 162, 1 g, 0.891 mmol of amino groups) was weighed into a polypropylene mixing cup (FlackTek, size 10, diluted with 1 mL of toluene) followed by the addition of cyanuric chloride (27.5 mg, 0.447 mmol of chloro groups) dissolved in 1 mL of toluene at an optimized 2/1 (amine:chloride) functional group ratio. After mixing using the Speedmixer (3500 rpm, 30 sec), the transparent and homogeneous silicone mixture quickly gelled (< 1 min) and was allowed to fully cure at room temperature for 24 h or at 80 °C for 6 h. Characterization of elastomers by FTIR showed installation of new functional C-N, C=N groups as curing occurred. Note: similar outcomes were obtained using THF, DCM and chloroform as solvent but the reaction without solvent in either reagent was problematic because cyanuric chloride does not dissolve or disperse well in silicone oil.



**Figure 4.1** Reaction scheme depicting catalyst-free crosslinking reaction of amino-PDMS via the triazinyl linkages. (A) using cyanuric chloride (CC) (B) using pre-grafted  $\alpha,\omega$ -Bis(4,6-dichloro)-s-triazinyl-modified aminosilicone (A11-CC). Insets show ambient light photographs of **NCl<sub>3</sub>-PDMS** and **NCl<sub>2</sub>-PDMS** elastomers, respectively.

### **4.3.3.2 Preparation of aminosilicone elastomers with pre-grafted $\alpha,\omega$ -Bis(4,6-dichloro)-s-triazine (NCl<sub>2</sub>-PDMS)**

#### **4.3.3.2.1 Synthesis of pre-grafted $\alpha,\omega$ -Bis(4,6-dichloro)-s-triazinyl-modified aminosilicone (A11-CC)**

To a solution of cyanuric chloride (400 mg, 2.17 mmol) dissolved in tetrahydrofuran (15 mL) cooled to 0 °C was added a mixture of aminopropyl-terminated polydimethylsiloxane (DMS-A11, 1g, 2.17 mmol of amino groups) and triethylamine (303  $\mu$ L, 220 mg, 2.17 mmol) in tetrahydrofuran (15 mL) dropwise over 30 min. The reaction mixture was stirred for additional 6 h (with the end of reaction monitored via TLC, silica gel, DCM) after which the precipitate formed was filtered and solvent removed under reduced pressure to afford crude bis(4,6-dichloro)-s-triazinyl-modified silicone oil. This was redissolved in ethyl acetate (30 mL), washed with saturated brine solution (3 x 10 mL) and the ethyl acetate extracts were combined, dried over anhydrous MgSO<sub>4</sub> and concentrated under reduced pressure. This was redissolved in chloroform stirred over neutral alumina for 3 h, filtered and finally concentrated to give pure product as a pale-yellow silicone oil. Yield (1.190 g, 90%, Figure S4.4 - S4.5, Appendix 4). <sup>1</sup>H NMR (600 MHz, CDCl<sub>3</sub>, ppm)  $\delta$ : 0.080 (s, 84H, Si-CH<sub>3</sub>), 0.56 (t, 4H, Si-CH<sub>2</sub>,  $J$  = 8.64 Hz), 1.65 (p, 4H, CH<sub>2</sub>,  $J$  = 8.10 Hz), 3.46 (q, 4H, CH<sub>2</sub>,  $J$  = 7.04 Hz). <sup>13</sup>C NMR (151 MHz, CDCl<sub>3</sub>, ppm)  $\delta$ : 1.00, 15.61, 23.16, 44.46, 166.15, 169.01. IR (ATR-FTIR, cm<sup>-1</sup>): 3253, 2951, 2877, 2846, 1588, 1546, 1502, 1411, 1389, 1330, 1318, 1230, 1254, 1050, 1005, 822, 780, 660.

#### **4.3.3.2.2 Elastomer formation using pre-grafted $\alpha,\omega$ -Bis(4,6-dichloro)-s-triazinyl-modified aminosilicone (A11-CC)**

A representative curing procedure for the synthesis of amino-triazinyl-functional silicone networks based on  $\alpha,\omega$ -bis(4,6-dichloro)-s-triazinyl-modified aminosilicones, is shown for AMS 162 (Table 1, Figure 4.1B). Two methods were implemented; (1) with solvent and (2) without solvent.

Method **1**, To (aminopropyl)methylsiloxane-dimethylsiloxane copolymer (PDMS-NH<sub>2</sub>, AMS 162, 1 g, 0.891 mmol of amino groups) weighed into a polypropylene mixing cup (FlackTek, size 10, diluted with 1 mL of toluene) was added a 1 mL toluene solution of A11-CC (135.41 mg, containing 0.446 mmol of chloro groups) at an optimized 2/1 (amine/chloride) functional group ratio. After mixing using the Speedmixer (3500 rpm, 30 sec), the transparent and homogeneous silicone mixture was allowed to fully cure at 80 °C for 6 h. Characterization of elastomers by FTIR showed changes in functional groups similar to **NCl<sub>3</sub>** crosslinked elastomers showing new functional C-N, C=N groups as curing occurred. Note: similar outcomes were obtained when using THF, DCM and chloroform as solvent.

Method **2**, To (aminopropyl)methylsiloxane-dimethylsiloxane copolymer (PDMS-NH<sub>2</sub>, AMS 162, 1 g, 0.891 mmol of amino groups) weighed into a polypropylene mixing cup (FlackTek, size 10, neat) was added A11-CC (135.41 mg, containing 0.446 mmol of chloro groups, neat) at an optimized 2/1 (amine/chloride) functional group ratio. After mixing using the Speedmixer (3500 rpm, 30 sec), the transparent and highly viscous homogeneous silicone mixture was allowed to fully cure at room temperature for 24 h or at 80 °C for 6 h. Characterization of elastomers by FTIR showed changes in functional groups similar to method **1** as new functional C-N, C=N groups were incorporated into the silicone networks.

#### **4.3.4 Reinforcement of triazinyl crosslinked elastomers**

Selected recipes of **NCl<sub>3</sub>-PDMS** and **NCl<sub>2</sub>-PDMS** elastomers (Table 1) were prepared with levels of 2, 5 or 10 wt % Aerosil R150 silica to determine the compatibility of triazinyl chemistry toward the addition of reinforcing fillers – silica with surfaces that are covered with a layer of hydroxyl groups and adsorbed H<sub>2</sub>O which could potentially interfere with the crosslinking reactions. The following is a representative curing procedure for the synthesis of silica-filled (at 2 wt%) **NCl<sub>3</sub>**-crosslinked functional silicone networks. To Aerosil R150 silica (20 mg) in a polypropylene mixing cup (FlackTek, size 10), was added (aminopropyl)methylsiloxane-dimethylsiloxane copolymer (PDMS-NH<sub>2</sub>, AMS 162, 0.98 g, 0.873 mmol of amino groups, diluted in 1 mL toluene). After mixing using the Speedmixer (3500 rpm, 30 sec), the crosslinker (**CC** = 26.84 mg or **A11-CC** = 132.7 mg,

containing 0.437mmol of chloro groups dissolved in 1 mL of toluene) was added, followed by additional mixing for 30 sec. The resulting transparent and homogenous silicone mixture was then allowed to fully cure at 80 °C for 6 h (Table 1).

#### 4.3.5 Hydrolytic stability of amino-triazinyl silicone elastomers

To assess the hydrolytic stability of the amino-triazinyl silicone elastomers, **NCl<sub>3</sub>-PDMS-M<sub>2</sub>** (1g, circular disk) was boiled in Milli-Q H<sub>2</sub>O (150 mL) at 95 °C for 6 h during which the pH was monitored every hour using a Corning 320 pH meter. The weight and physical appearance of the elastomers were monitored after 1, 3, and 6 h of boiling. The weight of the boiled elastomers was recorded after gentle wiping of the elastomer surfaces via kimwipe to absorb residual water droplets (Figure S4.6, Appendix 4). After 6 h of boiling, the elastomers were allowed to dry on benchtop at ambient temperature for several days.

**Table 1 Silicone triazinyl elastomer formulations**

Entry	Product name <sup>a</sup>	Crosslinker (mg)	Silicone	Silicones (g)	[NH <sub>2</sub> ] / [Cl]	Silica (mg)	Young's modulus (MPa, ±S.D.)*
1	<b>NCl<sub>3</sub>-PDMS-M<sub>1</sub></b>	C.C (55)	AMS 162	1.00	1/1	0	<sup>b</sup>
2	<b>NCl<sub>3</sub>-PDMS-M<sub>2</sub></b>	C.C (27.5)	AMS 162	1.00	2/1	0	0.65± 0.03
3	<b>NCl<sub>3</sub>-PDMS-M<sub>2.67</sub></b>	C.C (20.5)	AMS 162	1.00	2.67/1	0	0.24± 0.01
4	<b>NCl<sub>3</sub>-PDMS-M<sub>4</sub></b>	C.C (13.75)	AMS 162	1.00	4/1	0	0.06± 0.01
5	<b>NCl<sub>2</sub>-PDMS-M<sub>1</sub></b>	<b>A11-CC</b> (270.8)	AMS 162	1.00	1/1	0	0.25± 0.03
6	<b>NCl<sub>2</sub>-PDMS-M<sub>2</sub></b>	<b>A11-CC</b> (135.4)	AMS 162	1.00	2/1	0	0.31± 0.01
7	<b>NCl<sub>2</sub>-PDMS-M<sub>2.67</sub></b>	<b>A11-CC</b> (101.4)	AMS 162	1.00	2.67/1	0	0.15± 0.01
8	<b>NCl<sub>2</sub>-PDMS-M<sub>4</sub></b>	<b>A11-CC</b> (67.7)	AMS 162	1.00	4/1	0	0.02± 0.01
9	<b>NCl<sub>3</sub>-PDMS-L<sub>2</sub></b>	C.C (14.4)	AMS 152	1.00	2/1	0	0.27± 0.02
10	<b>NCl<sub>3</sub>-PDMS-H<sub>2</sub></b>	C.C (23.63)	AMS 163	1.00	2/1	0	0.93± 0.02
11	<b>NCl<sub>3</sub>-PDMS-M<sub>2S2</sub></b>	C.C (26.84)	AMS 162	0.98	2/1	20	0.75± 0.03
12	<b>NCl<sub>3</sub>-PDMS-M<sub>2S5</sub></b>	C.C (26)	AMS 162	0.95	2/1	50	0.92± 0.02
13	<b>NCl<sub>3</sub>-PDMS-M<sub>2S10</sub></b>	C.C (24.65)	AMS 162	0.90	2/1	100	2.62± 0.20

14	<b>NCl<sub>2</sub>-PDMS-M<sub>2S2</sub></b>	A11-C.C (132.7)	AMS 162	0.98	2/1	20	0.32± 0.01
15	<b>NCl<sub>2</sub>-PDMS-M<sub>2S5</sub></b>	A11-C.C (128.6)	AMS 162	0.95	2/1	50	0.58± 0.04
16	<b>NCl<sub>2</sub>-PDMS-M<sub>2S10</sub></b>	A11-C.C (121.9)	AMS 162	0.90	2/1	100	1.40± 0.06
17	<b>NCl<sub>3</sub>-PDMS-PS<sub>1</sub></b>	C.C (13.53)	AMS 233	1.00	1/1	0	0.48± 0.03
18	<b>NCl<sub>3</sub>-PDMS-PS<sub>2</sub></b>	C.C (6.77)	AMS 233	1.00	2/1	0	0.19± 0.01
19	<b>NCl<sub>3</sub>-PDMS-PS<sub>2.67</sub></b>	C.C (5.07)	AMS 233	1.00	2.67/1	0	0.07± 0.01
20	<b>NCl<sub>3</sub>-PDMS-PS<sub>4</sub></b>	C.C (3.38)	AMS 233	1.00	4/1	0	0.02± 0.01
21	<b>NCl<sub>3</sub>-PDMS-M<sub>1+</sub></b> TEA	C.C (55)	AMS 162	1.00	1/1	0	0.56± 0.03
22	<b>NCl<sub>3</sub>-PDMS-LM<sub>2</sub></b>	C.C (7.9)	AMS 132	1.00	2/1	0	0.02± 0.01
23	<b>NCl<sub>3</sub>-PDMS-T<sub>2</sub></b>	C.C (12.3)	DMS A21	1.00	2/1	0	0.10± 0.01

<sup>a</sup>Nomenclature: Crosslinker-PDMS-Amine content. Thus, **NCl<sub>3</sub>-PDMS-M<sub>2</sub>** is the unfilled (with silica) elastomer made directly from cyanuric chloride and AMS 162 in an optimized 2/1 functional group ratio. **NCl<sub>2</sub>-PDMS-M<sub>2</sub>** is the unfilled with silica elastomer made from A11-CC and AMS 162 in an optimized 2/1 functional group ratio. **NCl<sub>3</sub>-PDMS-M<sub>2S2</sub>** is the same as **NCl<sub>3</sub>-PDMS-M<sub>2</sub>** but filled with 2% silica while **NCl<sub>3</sub>-PDMS-L<sub>2</sub>** and **NCl<sub>3</sub>-PDMS-H<sub>2</sub>** are unfilled elastomers at optimized 2/1 functional group ratios having low (AMS 152) and higher (AMS 163) aminopropyl content, leading to lower and higher crosslink densities in the elastomer, thus “-L & -H”. **NCl<sub>3</sub>-PDMS-PS<sub>1</sub>** represent unfilled elastomers made from cyanuric chloride and AMS 233 comprising of aminoethylaminopropyl densities with an optimized 1/1 functional group ratio. **NCl<sub>3</sub>-PDMS-T<sub>2</sub>** is the unfilled with silica elastomer made from cyanuric chloride and telechelic aminopropyl silicone. **NCl<sub>3</sub>-PDMS-LM<sub>2</sub>** is the unfilled elastomer made from cyanuric chloride and AMS 132 (with very low aminopropyl content similar to telechelic) in an optimized 2/1 functional group ratio. <sup>b</sup>The elastomers were too soft to measure using MACH-1 micromechanical testing instrument. TEA = triethylamine, C.C = cyanuric chloride, S.D = Standard Deviation, \* = from elastomers with solvent (DCM).

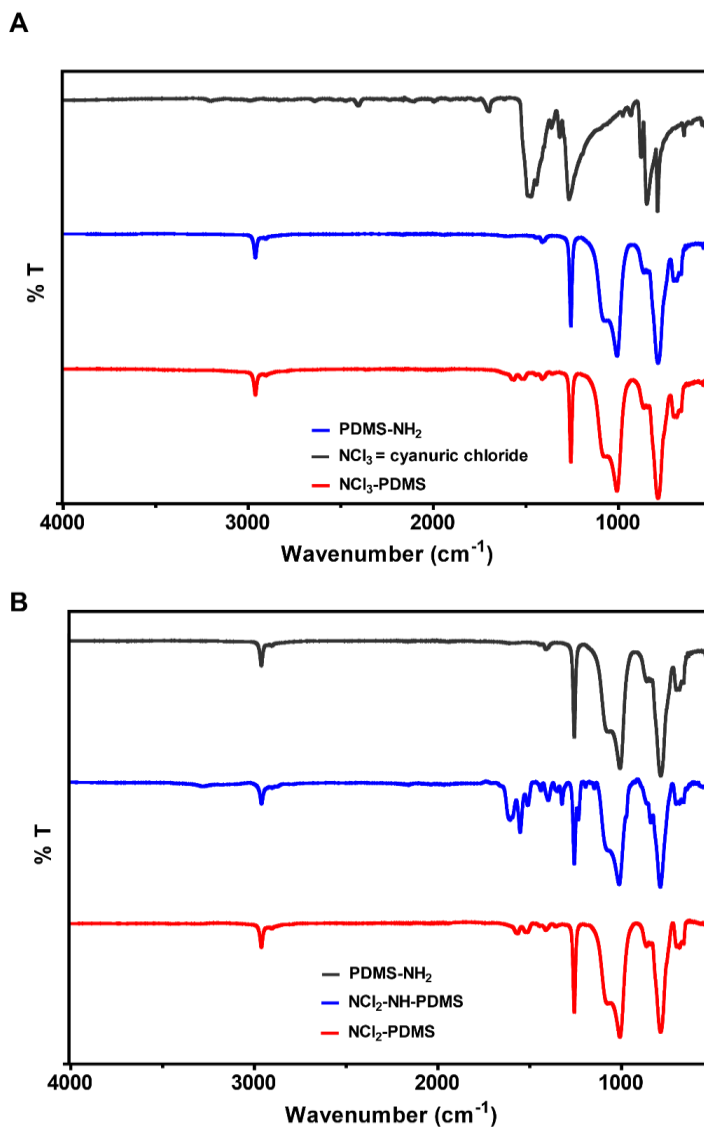
## 4.4 Results and Discussion

### 4.4.1 Formation and physical properties of amino-triazinyl silicone elastomers

At the inception of this work, we desired to develop a simple method for the preparation of silicone elastomers without the need for catalysts. Initial experiments focused on the preparation of triazine-crosslinked silicones from cyanuric chloride and telechelic or pendant aminopropyl silicones.

Cyanuric chloride does not mix or dissolve in silicones in the absence of solvents. Therefore, cyanuric chloride, dissolved in a small amount of chloroform, DCM, THF or toluene (preferred) was added to neat pendant aminopropylsilicones; gelation occurred within less than one minute. Samples were allowed to reach full cure for 24 hours at ambient temp or 6 hours at 80 °C. Physical measurement (Shore OO hardness) showed that hardening plateaued at 4 hours (Figure S4.1, Appendix 4). NMR and MS studies with small molecule models showed the displacement of the first two chlorine atoms were rapid and instantaneous while complete cure involving displacement of all three chlorine atoms, took 180 minutes under dilute conditions (Figure S4.2 – S4.3, Appendix 4).

A systematic study in which amine to cyanuric chloride ratios were varied revealed that it was possible only to use about half of the available amines as crosslinker sites (Table 1, Figure 4.1A). This is ascribed to the (beneficial) self-neutralizing ability of available amines; the nucleophilic aromatic substitution reaction between cyanuric chloride and aminosilicones was accompanied by amine quenching of the HCl produced. A combination of NMR and FTIR experiments were conducted to demonstrate that the formation of amino-triazine linkages in the presence of H<sub>2</sub>N-PDMS is optimal at a 2/1 [NH<sub>2</sub>]/[C-Cl] functional group ratio (i.e., one amine does the nucleophilic substitution, a second mops up the HCl produced). <sup>1</sup>H NMR analysis of products (NCI<sub>3</sub>-PDMS-M<sub>2</sub>) showed a shift of protons adjacent to nitrogen from 2.5 to 3.5 ppm while IR spectroscopy showed the presence of new and distinct absorption bands 1535-1487 cm<sup>-1</sup> corresponding to C=N and C-N sp<sup>2</sup> stretching vibrations present in the triazine rings tethered into the silicone networks (Figure 4.2A).



**Figure 4.2** FTIR-ATR spectra of (A) **NCl<sub>3</sub>-PDMS** and (B) **NCl<sub>2</sub>-PDMS** elastomers.

The ability to tune the network structure of resulting elastomers by varying the stoichiometry of the reaction was examined. A series of **NCl<sub>3</sub>-PDMS** elastomers was prepared using cyanuric chloride and different aminopropylsilicones with varying molecular weights and amine contents (2-7 mol %NH<sub>2</sub>; AMS 132 (**LM**), 80-120 cSt, 4500-8000 g mol<sup>-1</sup>; AMS 152 (**L**), 100-300 cSt, 7000-9000 g mol<sup>-1</sup>; AMS 162 (**M**), 80-120 cSt, 4000-5000 g mol<sup>-1</sup>; or AMS 163 (**H**), 1800-2200 cSt, 50000 g mol<sup>-1</sup>, Table 1, entries 1-4; 9-10 and 22). The crosslink density in all cases could be simply controlled by the relative



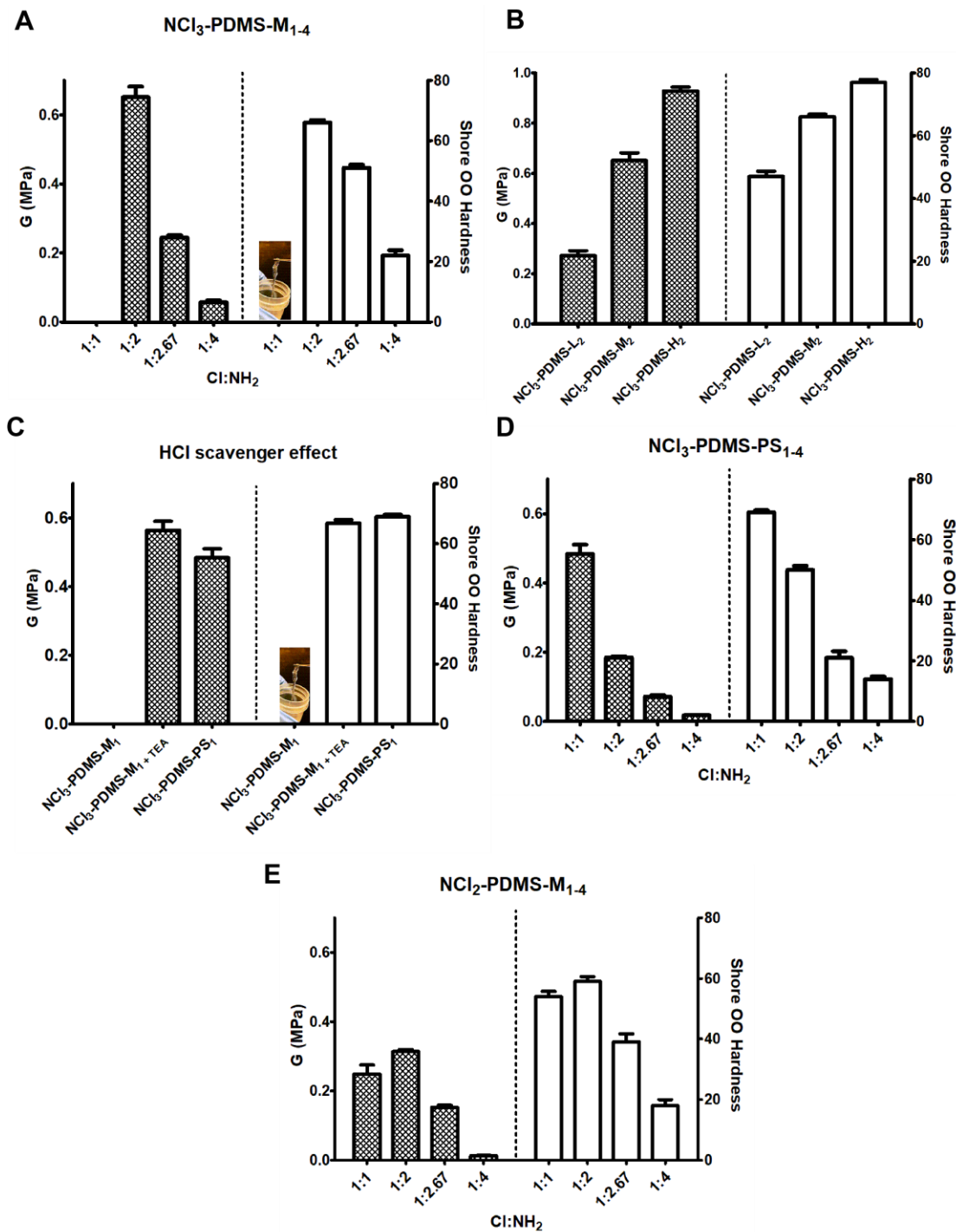
amine / cyanuric chloride concentration. For example, crosslinking at stoichiometric  $[\text{NH}_2]/[\text{C-Cl}]$  ratio (1/1) (AMS 162, 1/1  $[\text{NH}_2]/[\text{C-Cl}]$ ) led to a tacky, very soft gel-like elastomers (**NCl<sub>3</sub>-PDMS-M<sub>1</sub>**) too soft to measure using Shore OO durometer; adhesive-like properties were observed (Figure 4.3A, Table 1 entry 1). However, by increasing the ratio to 2/1  $[\text{NH}_2]/[\text{C-Cl}]$  under optimal conditions, harder elastomers were obtained (**NCl<sub>3</sub>-PDMS-M<sub>2</sub>**) with the highest Young modulus and Shore OO hardness values of 0.68 MPa and 67 reported, respectively, (Figure 4.3A, Table 1 entry 2). As noted above, for each amine involved in covalent bond formation, a second amine was required to neutralize HCl produced during the reaction.

When the same aminopropylsilicone AMS 162, was crosslinked with a lower quantities of cyanuric chloride at sub-optimal functional group ratios (2.67/1 and 4/1  $[\text{NH}_2]/[\text{C-Cl}]$  molar ratios), fewer crosslinks were produced resulting in softer elastomers (**NCl<sub>3</sub>-PDMS-M<sub>2.67</sub>** and **NCl<sub>3</sub>-PDMS-M<sub>4</sub>**, Figure 4.3A, Table 1 entries 3-4). These changes are ascribed to the presence of residual aminopropyl spaces, unreacted silicone chains or chains only tethered at one terminus within the crosslinked networks.<sup>40</sup> Switching to other silicones with different amine contents (AMS 152 and AMS 163) permitted the formation of softer (**NCl<sub>3</sub>-PDMS-L**) or harder (**NCl<sub>3</sub>-PDMS-H**) elastomers as crosslink densities were further tuned (Figure 4.3B, Table 1 entries 9-10). In all cases, the physical properties of elastomers were found to be intimately linked to the crosslink density (related to the spacing between crosslinks,  $M_c$ ). All products were transparent and defect free even though ammonium salts are homogeneously distributed within the silicone networks.

#### 4.4.2 Effect of external amino functionality on elastomer properties

In addition to changing amine / C-Cl ratios when using different silicones, it is possible to utilize different types of amines that do not participate in polymer chemistry to control crosslinking and sequester HCl. For example, the addition of 1 equivalent of  $\text{NEt}_3$  to the mixture of amino silicone/cyanuric chloride with an  $\text{NH}_2/\text{C-Cl}$  ratio of 1:1 led to elastomers. The primary amine on the silicone formed crosslinks, while the small molecule tertiary amine neutralized the HCl produced. The product elastomer was cloudy in the presence of the ammonium salt and a fourfold increase in Young modulus was observed

compared to **NCl<sub>3</sub>-PDMS-M<sub>2</sub>** (Figure 4.3C, Table 1 entry 21). Similar results were obtained despite a 3 mol% drop in amino content when AMS 233 with pendant aminoethylaminopropyl functionality (2-4 mol%, having similar molecular weight as **NCl<sub>3</sub>-PDMS-M<sub>2</sub>**) led to significant changes in the physical properties of **NCl<sub>3</sub>-PDMS-PS** elastomers (Figure 4.3D, Table 1 entries 17-20). An optimal crosslink density was achieved at a NH<sub>2</sub>/C-Cl ratio of 1:1 (Figure 4.3C, Table 1 entries 17 vs 1, 17 vs 2 and 17 vs 4); all products were transparent. The observations have been attributed to the differences in amine reactivity, which enable further control via the primary amine forming crosslinks while the secondary amine neutralized HCl.<sup>41</sup> In addition, the location of the secondary amine on the same pendant chain ensures crosslink points are not spaced out like in **NCl<sub>3</sub>-PDMS-M** elastomers.



**Figure 4.3** Physical properties of amino-triazinyl silicone elastomers. (A, B) effect of cyanuric chloride concentration on elastomer properties. (C) Effect of pendant amino group structure on elastomer properties. (D) Comparison between internal and external acid scavenger on elastomer properties at a 1:1 [NH<sub>2</sub>]/[Cl] ratio. and (E) effect of A11-CC concentration on elastomer properties.

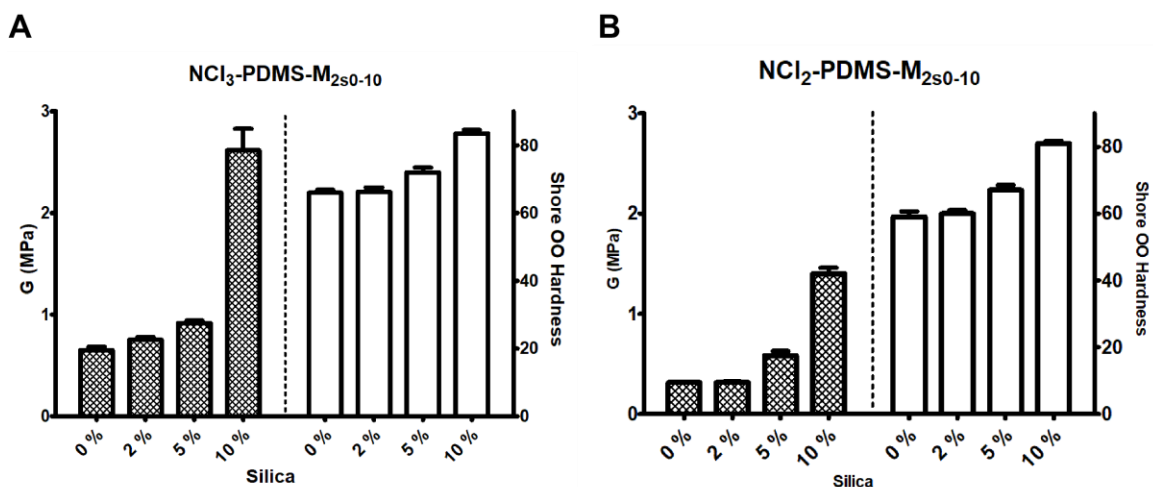
#### 4.4.3 Role of pre-grafted $\alpha,\omega$ -Bis(4,6-dichloro)-s-triazinyl-modified aminosilicone (A11-CC)

The use of solvents is disadvantageous per se, and particularly in the final step of a polymerization or rubber forming process, where solvent removal from the product becomes difficult. We therefore developed a reactive monomer based on triazine that could react without solvent to give cured rubbers in a two-step process; solvent was required in the first step but, because the product is a fluid, recapturing the solvent was facile. Telechelic polymers were first modified with triazinyl groups to create a kind of masterbatch, and then reacted with various pendant aminosilicones. Thus,  $\alpha,\omega$ -bis(4,6-dichloro)-s-triazine aminosilicone was prepared using the process described above at a  $[\text{NH}_2]/[\text{C-Cl}]$  ratio of 1/1 to give **A11-CC** (Table 1, Figure 4.1B). IR spectroscopy showed absorption bands 1542-1492  $\text{cm}^{-1}$  corresponding to C=N and C-N  $\text{sp}^2$  stretching vibrations present in the triazine rings incorporated into the **NCl<sub>2</sub>-PDMS-M<sub>2</sub>** elastomer networks similar to **NCl<sub>3</sub>-PDMS-M<sub>2</sub>** elastomers (Figure 4.2B).

Once prepared, the  $\alpha,\omega$ -bis(4,6-dichloro)-s-triazine aminosilicone (**A11-CC**) could be used to crosslink pendant aminopropyl silicones to give products analogous to those prepared from cyanuric chloride, but in a curing step that doesn't involve solvent. For example, crosslinking AMS 162 with **A11-CC** at various stoichiometric  $[\text{NH}_2]/[\text{C-Cl}]$  ratios from 1/1 to 1/4 (Figure 4.3E, Table 1 entries 5-8) showed effective control over the physical properties such that **NCl<sub>2</sub>**-elastomers had properties similar to **NCl<sub>3</sub>**-elastomers, although at lower thresholds as the crosslinked chains were further spaced out.<sup>42</sup> Several advantages accrue from this masterbatch strategy: as noted, the reagents and final product are solvent free; the viscosities of the reactive crosslinker and aminosilicone reagent are much more closely matched, which facilitates reactivity mixing/blending; and, final product moduli are chosen by mixing a single reactive crosslinker with readily available, commercial aminopropylsilicones at the desired ratio with the crosslink sites mostly reproducible and precisely known.

#### 4.4.4 Reinforcing triazinyl-based silicone elastomers

Silicone elastomers are normally rather weak. Commercial products, gels excepted, are almost universally reinforced with minerals, typically silica to improve tensile strength and elongation at break.<sup>43</sup> The elastomers described above were reinforced using formulations containing 2, 5 or 10 wt% silica, respectively, at an optimized  $[\text{NH}_2]/[\text{C-Cl}]$  ratio of 2/1. Both  $\text{NCl}_3$  and  $\text{NCl}_2$ -derived elastomers exhibited increased moduli and Shore hardness values that tracked with silica content in a predictable manner (Table 1, Figure 4.4). For example, an increase in silica from 0% to 10% in  $\text{NCl}_3$ -PDMS- $\text{M}_2$  elastomers resulted in an increase in Young's modulus from 0.65 MPa to 2.62 MPa (Table 1, Figure 4.4A). Silica loading into 1/1  $[\text{NH}_2]/[\text{C-Cl}]$  molar ratio elastomers led to products with the same trend, but the products remained tacky and soft gel-like elastomers. This result, the reinforcement of elastomers by silica therefore benefits from the chemoselectivity of the crosslinkers toward the amino functionality in aminopropylsilicones over the presence of hydroxy groups on the surface of silica.<sup>41</sup>



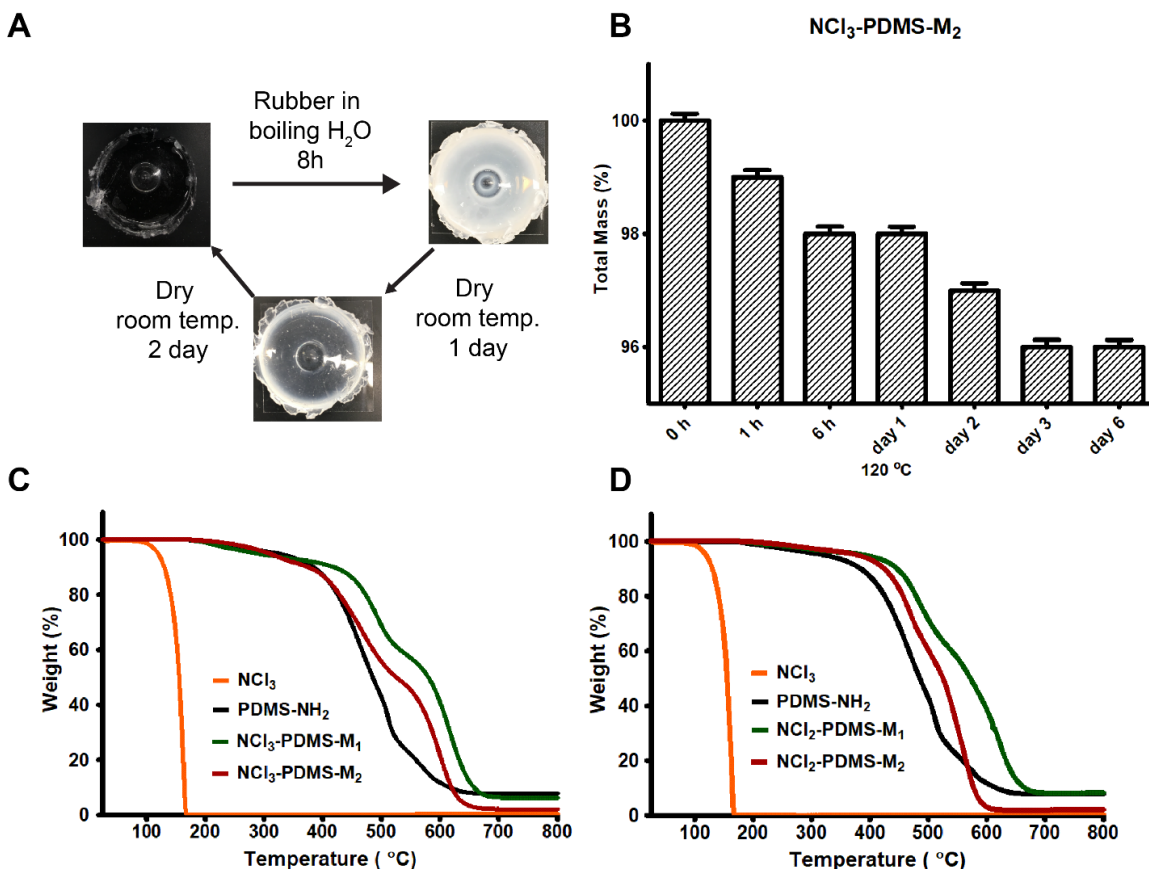
**Figure 4.4** Chemoselectivity of crosslinker and physical properties of elastomers based on filler silica content.

#### 4.4.5 Hydrolytic and thermal stability of amino-triazinyl elastomers

Silicones have an enviable reputation for thermal and hydrolytic stability.<sup>44</sup> Amino-triazinyl silicone elastomers were characterized for their hydrolytic and thermal stability

over time under these effects. Attempts to initiate hydrolytic degradation of prepared **NCl<sub>3</sub>-PDMS-M<sub>2</sub>** elastomers by boiling in water for 6-8 hours were unsuccessful. A small ingress of water (<1.4% increase in mass weight, Figure S4.6, Appendix 4) was observed, presumably as a result of the presence of hydrophilic ammonium ions within the networks. However, this was lost upon drying with no change in modulus and hardness of the elastomer (Figure 4.5A). Silicones are known to be sensitive to acids and bases, but neither the free amines nor ammonium salts present in the elastomer led to physical changes under these conditions.<sup>5</sup>

Post-cure heat treatment revealed the long-term thermal stability of the product with <4% loss in weight after 6 days heating at 120 °C. Both **NCl<sub>3</sub>-PDMS-M<sub>1-2</sub>** and **NCl<sub>2</sub>-PDMS-M<sub>1-2</sub>** elastomers, formed at 1:1 to 2:1 [NH<sub>2</sub>]/[Cl] molar ratios, respectively, were more stable to thermal decomposition under argon than the starting aminosilicone oil as the presence of both crosslink points and ammonium salts (requires phase transition) help extend the onset of thermal decomposition; while degradation temperature were comparable to those found in commercially crosslinked elastomers (Figure 4.5B-D).<sup>45</sup> These was quite sustained as degradation profiles of **NCl<sub>3</sub>-** and **NCl<sub>2</sub>- PDMS-M<sub>2</sub>** elastomers under air were similar to the starting aminosilicone oil (Figure S4.7, Appendix 4).



**Figure 4.5** Stability of amino-triazinyl elastomers. (A) hydrolytic stability (B) post-cure heat treatment of NCl<sub>3</sub>-PDMS-M<sub>2</sub> and (C, D) TGA thermograms of cyanuric chloride, NH<sub>2</sub>-PDMS, NCl<sub>3</sub>-PDMS-M<sub>1-2</sub> and NCl<sub>2</sub>-PDMS-M<sub>1-2</sub>.

## 4.5 Conclusions

Amino-triazinyl silicone networks form from nucleophilic aromatic substitution reactions between commercial aminosilicones and chloro-s-triazines. The route provides an efficient way to make catalyst and solvent free silicone elastomers. The presence of residual amines promotes reaction formation by neutralizing the HCl byproduct formed. The nature of crosslinker, type of residual amine, the use of silica filler and the amount of chemical crosslink density could be independently utilized to manipulate elastomer properties. The resulting crosslinked products showed enhanced stability to that of pure silicones cured by conventional processes.

## 4.6 Acknowledgements

We thank Prof. T. Hoare for access to equipment. We gratefully acknowledge the financial support of the Natural Sciences and Engineer Research Council of Canada. JMM is the recipient of an Early Researcher Award from the Province of Ontario and holds the Tier 2 Canada Research Chair in Micro and Nanostructured Materials.

## 4.7 References

- (1) Malpass, C. A.; Millsap, K. W.; Sidhu, H.; Gower, L. B. Immobilization of an Oxalate-Degrading Enzyme on Silicone Elastomer. *J. Biomed. Mater. Res.* **2002**, *63* (6), 822–829.
- (2) Mustoe, T. A. Evolution of Silicone Therapy and Mechanism of Action in Scar Management. *Aesthetic Plast. Surg.* **2007**, *32* (1), 82.
- (3) Künzler, J. F. Silicone Hydrogels for Contact Lens Application. *Trends Polym. Sci.* **1996**, *2* (4), 52–59.
- (4) Chen, H.; Brook, M. A.; Sheardown, H. D.; Chen, Y.; Klenkler, B. Generic Bioaffinity Silicone Surfaces. *Bioconjug. Chem.* **2006**, *17* (1), 21–28.
- (5) Brook, M. A. Chapter 9. In *Silicon in Organic, Organometallic, and Polymer Chemistry*; A Wiley-Interscience publication; John Wiley & Sons, Inc: New York, **2000**; p 256.
- (6) Moretto, H.-H.; Schulze, M.; Wagner, G. Silicones. In *Ullmann's Encyclopedia of Industrial Chemistry*; American Cancer Society, **2000**.
- (7) Cervantes, J.; Zárraga, R.; Salazar-Hernández, C. Organotin Catalysts in Organosilicon Chemistry. *Appl. Organomet. Chem.* **2012**, *26* (4), 157–163.
- (8) Weij, F. W. van D. The Action of Tin Compounds in Condensation-Type RTV Silicone Rubbers. *Makromol. Chem.* **1980**, *181* (12), 2541–2548.



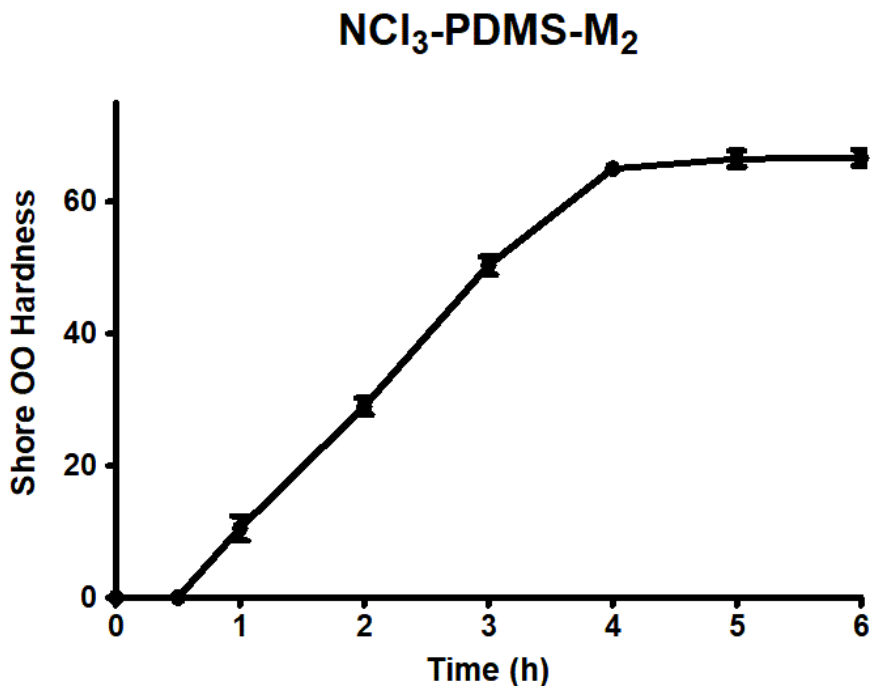
- (9) Putzien, S.; Nuyken, O.; Kühn, F. E. Functionalized Polysilalkylene Siloxanes (Polycarbosiloxanes) by Hydrosilylation—Catalysis and Synthesis. *Prog. Polym. Sci.* **2010**, *35* (6), 687–713.
- (10) Wang, C.; Nair, S. S.; Veeravalli, S.; Moseh, P.; Wynne, K. J. Sticky or Slippery Wetting: Network Formation Conditions Can Provide a One-Way Street for Water Flow on Platinum-Cured Silicone. *ACS Appl. Mater. Interfaces* **2016**, *8* (22), 14252–14262.
- (11) Boyer, I. J. Toxicity of Dibutyltin, Tributyltin and Other Organotin Compounds to Humans and to Experimental Animals. *Toxicology* **1989**, *55* (3), 253–298.
- (12) Wang, D.; Klein, J.; Mejía, E. Catalytic Systems for the Cross-Linking of Organosilicon Polymers. *Chem. – Asian J.* **2017**, *12* (11), 1180–1197.
- (13) Genest, A.; Binauld, S.; Pouget, E.; Ganachaud, F.; Fleury, E.; Portinha, D. Going beyond the Barriers of Aza-Michael Reactions: Controlling the Selectivity of Acrylates towards Primary Amino-PDMS. *Polym. Chem.* **2017**, *8* (3), 624–630.
- (14) Fawcett, A. S.; Brook, M. A. Thermoplastic Silicone Elastomers through Self-Association of Pendant Coumarin Groups. *Macromolecules* **2014**, *47* (5), 1656–1663.
- (15) Gonzaga, F.; Yu, G.; Brook, M. A. Polysiloxane Elastomers via Room Temperature, Metal-Free Click Chemistry. *Macromolecules* **2009**, *42* (23), 9220–9224.
- (16) Genest, A.; Portinha, D.; Fleury, E.; Ganachaud, F. The Aza-Michael Reaction as an Alternative Strategy to Generate Advanced Silicon-Based (Macro)Molecules and Materials. *Prog. Polym. Sci.* **2017**, *72*, 61–110.
- (17) Bui, R.; Brook, M. A. Dynamic Covalent Schiff-Base Silicone Polymers and Elastomers. *Polymer* **2019**, *160*, 282–290.
- (18) Murias, P.; Byczyński, Ł.; Maciejewski, H.; Galina, H. A Quantitative Approach to Dynamic and Isothermal Curing of an Epoxy Resin Modified with Oligomeric Siloxanes. *J. Therm. Anal. Calorim.* **2015**, *122* (1), 215–226.
- (19) Gupta, P.; Bajpai, M. Development of Siliconized Epoxy Resins and Their Application as Anticorrosive Coatings. *Adv. Chem. Eng. Sci.* **2011**, *1* (3), 720–726.

- (20) Stukenbroeker, T.; Wang, W.; Winne, J. M.; Prez, F. E. D.; Nicolaÿ, R.; Leibler, L. Polydimethylsiloxane Quenchable Vitrimers. *Polym. Chem.* **2017**, *8* (43), 6590–6593.
- (21) Lewis, D. M. Developments in the Chemistry of Reactive Dyes and Their Application Processes. *Color. Technol.* **2014**, *130* (6), 382–412.
- (22) Mu, B.; Xu, H.; Li, W.; Yang, Y. Quantitation of Fast Hydrolysis of Cellulose Catalyzed by Its Substituents for Potential Biomass Conversion. *Bioresour. Technol.* **2019**, *273*, 305–312.
- (23) Karst, D.; Yang, Y. Effect of Structure of Large Aromatic Molecules Grafted onto Cellulose on Hydrolysis of the Glycosidic Linkages. *Macromol. Chem. Phys.* **2007**, *208* (7), 784–791.
- (24) Moran-Mirabal, J. M.; Santhanam, N.; Corgie, S. C.; Craighead, H. G.; Walker, L. P. Immobilization of Cellulose Fibrils on Solid Substrates for Cellulase-Binding Studies through Quantitative Fluorescence Microscopy. *Biotechnol. Bioeng.* **2008**, *101* (6), 1129–1141.
- (25) Santa-Maria, M.; Jeoh, T. Molecular-Scale Investigations of Cellulose Microstructure during Enzymatic Hydrolysis. *Biomacromolecules* **2010**, *11* (8), 2000–2007.
- (26) Jeoh, T.; Santa-Maria, M. C.; O'Dell, P. J. Assessing Cellulose Microfibrillar Structure Changes Due to Cellulase Action. *Carbohydr. Polym.* **2013**, *97* (2), 581–586.
- (27) Ringot, C.; Saad, N.; Granet, R.; Bressollier, P.; Sol, V.; Krausz, P. Meso-Functionalized Aminoporphyrins as Efficient Agents for Photo-Antibacterial Surfaces. *J. Porphyr. Phthalocyanines* **2010**, *14* (11), 925–931.
- (28) Mbakidi, J.-P.; Herke, K.; Alvès, S.; Chaleix, V.; Granet, R.; Krausz, P.; Leroy-Lhez, S.; Ouk, T.-S.; Sol, V. Synthesis and Photobiocidal Properties of Cationic Porphyrin-Grafted Paper. *Carbohydr. Polym.* **2013**, *91* (1), 333–338.
- (29) Baird, J. K.; Sherwood, R. F.; Carr, R. J. G.; Atkinson, A. Enzyme Purification by Substrate Elution Chromatography from Procion Dye—Polysaccharide Matrices. *FEBS Lett.* **1976**, *70* (1–2), 61–66.

- (30) Sherwood, R. F.; Melton, R. G.; Alwan, S. M.; Hughes, P. Purification and Properties of Carboxypeptidase G2 from *Pseudomonas* Sp. Strain RS-16. *Eur. J. Biochem.* **1985**, *148* (3), 447–453.
- (31) Schuler, L. J.; Trimble, A. J.; Belden, J. B.; Lydy, M. J. Joint Toxicity of Triazine Herbicides and Organophosphate Insecticides to the Midge *Chironomus Tentans*. *Arch. Environ. Contam. Toxicol.* **2005**, *2* (49), 173–177.
- (32) Steffensen, M. B.; Hollink, E.; Kuschel, F.; Bauer, M.; Simanek, E. E. Dendrimers Based on [1,3,5]-Triazines. *J. Polym. Sci. Part Polym. Chem.* **2006**, *44* (11), 3411–3433.
- (33) Centre for Food Safety and Applied Nutrition, Melamine in Tableware Questions and Answers <http://www.fda.gov/food/chemicals/melamine-tableware-questions-and-answers> (accessed Aug 30, 2019).
- (34) Bell, S. A.; McLean, M. E.; Oh, S.-K.; Tichy, S. E.; Zhang, W.; Corn, R. M.; Crooks, R. M.; Simanek, E. E. Synthesis and Characterization of Covalently Linked Single-Stranded DNA Oligonucleotide–Dendron Conjugates. *Bioconjug. Chem.* **2003**, *14* (2), 488–493.
- (35) Lim, J.; Chouai, A.; Lo, S.-T.; Liu, W.; Sun, X.; Simanek, E. E. Design, Synthesis, Characterization, and Biological Evaluation of Triazine Dendrimers Bearing Paclitaxel Using Ester and Ester/Disulfide Linkages. *Bioconjug. Chem.* **2009**, *20* (11), 2154–2161.
- (36) Lo, S.-T.; Stern, S.; Clogston, J. D.; Zheng, J.; Adisheshaiah, P. P.; Dobrovolskaia, M.; Lim, J.; Patri, A. K.; Sun, X.; Simanek, E. E. Biological Assessment of Triazine Dendrimer: Toxicological Profiles, Solution Behavior, Biodistribution, Drug Release and Efficacy in a PEGylated, Paclitaxel Construct. *Mol. Pharm.* **2010**, *7* (4), 993–1006.
- (37) Chouai, A.; Simanek, E. E. Kilogram-Scale Synthesis of a Second-Generation Dendrimer Based on 1,3,5-Triazine Using Green and Industrially Compatible Methods with a Single Chromatographic Step. *J. Org. Chem.* **2008**, *73* (6), 2357–2366.
- (38) Wen, P.; Zhang, C.; Yang, Z.; Dong, R.; Wang, D.; Fan, M.; Wang, J. Triazine-Based Covalent-Organic Frameworks: A Novel Lubricant Additive with Excellent Tribological Performances. *Tribol. Int.* **2017**, *111*, 57–65.

- (39) Bojinov, V.; Grabchev, I. Synthesis and Application of New Combined 2,2,6,6-Tetramethylpiperidine–2-Hydroxybenzophenone 1,3,5-Triazine Derivatives as Photostabilizers for Polymer Materials. *J. Photochem. Photobiol. Chem.* **2002**, *146* (3), 199–205.
- (40) Fatona, A.; Moran-Mirabal, J.; Brook, M. A. Controlling Silicone Networks Using Dithioacetal Crosslinks. *Polym. Chem.* **2018**, *10* (2), 219–227.
- (41) Steffensen, M. B.; Simanek, E. E. Chemoselective Building Blocks for Dendrimers from Relative Reactivity Data. *Org. Lett.* **2003**, *5* (13), 2359–2361.
- (42) Dušek, K.; Dušková-Smrčková, M. Network Structure Formation during Crosslinking of Organic Coating Systems. *Prog. Polym. Sci.* **2000**, *25* (9), 1215–1260.
- (43) Boonstra, B. B.; Cochrane, H.; Dánnenberg, E. M. Reinforcement of Silicone Rubber by Particulate Silica. *Rubber Chem. Technol.* **1975**, *48* (4), 558–576.
- (44) Gan, L. M.; Ong, H. W. K.; Tan, T. L.; Chan, S. O. Hydrolytic Stability of Single-Package Silicone Sealant. *J. Appl. Polym. Sci.* **1986**, *32* (3), 4109–4118.
- (45) Camino, G.; Lomakin, S. M.; Lazzari, M. Polydimethylsiloxane Thermal Degradation Part 1. Kinetic Aspects. *Polymer* **2001**, *42* (6), 2395–2402.

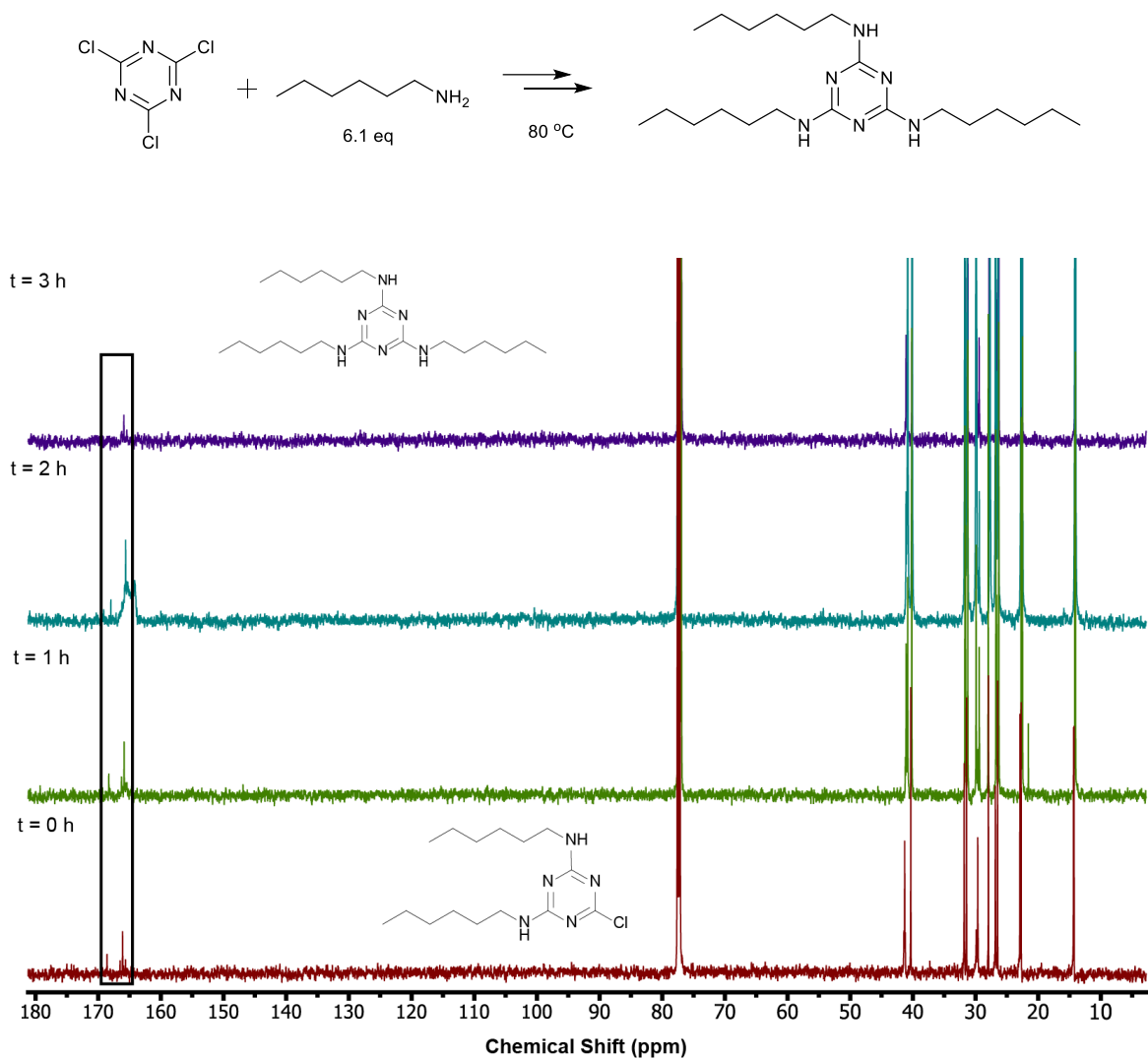
#### 4.8 Appendix 4: Chapter 4 Supporting Information



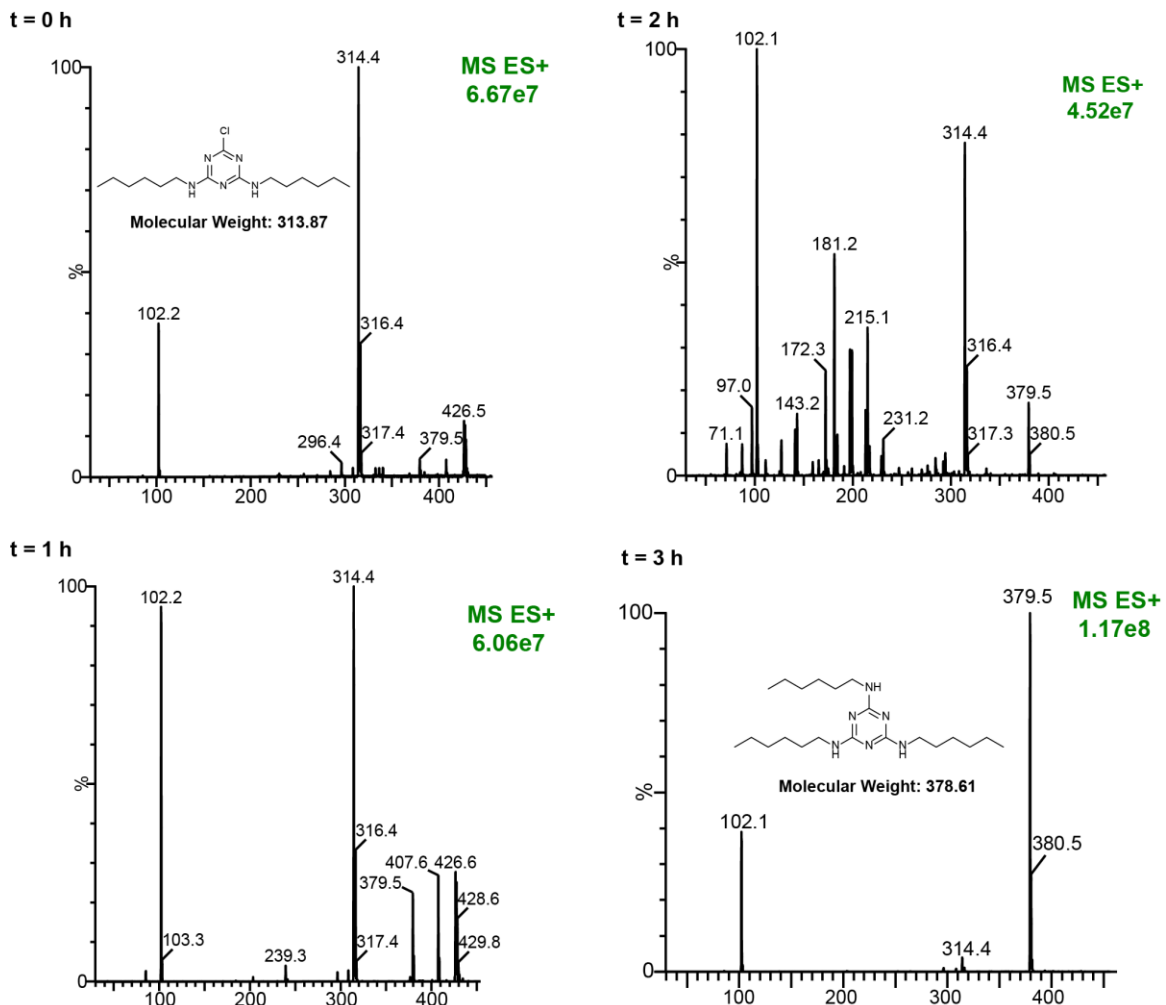
**Figure S4.1** Change in NCI<sub>3</sub>-PDMS-M<sub>2</sub> elastomer hardness as a function of cure at 80 °C over the course of 6 h.

#### **Model Reaction of hexylamine with cyanuric chloride: Preparation of trihexylmelamine (N,N,N-trihexyl-s-triazine-2,4,6-triamine)**

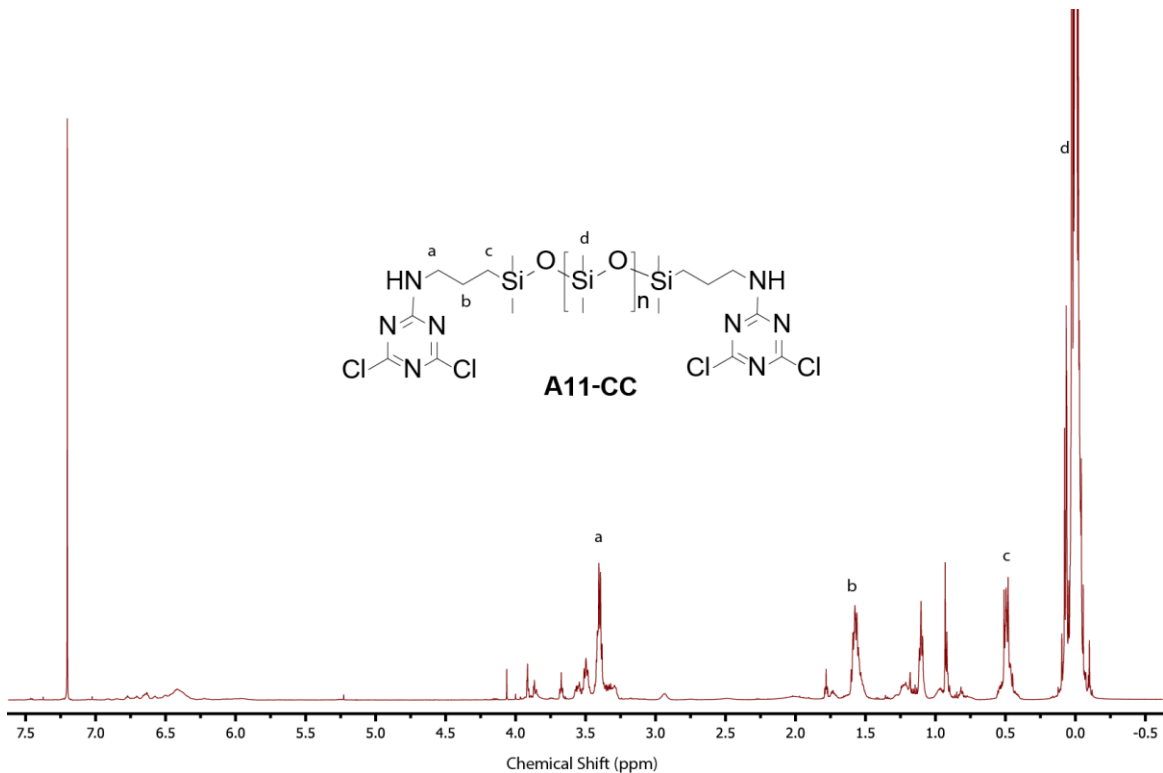
To a solution of cyanuric chloride (150 mg, 0.81 mmol) dissolved in dry toluene (2 mL) was added hexylamine (653  $\mu$ L, 500 mg, 4.94 mmol) diluted in dry toluene (1 mL). The reaction mixture was stirred (800 rpm) at 80 °C over the course of 4 h with 200  $\mu$ L aliquots taken at various time intervals and analyzed by <sup>1</sup>H and <sup>13</sup>C NMR spectroscopy in addition to mass spectrometer to track the changes in functional group concentrations and product during the nucleophilic aromatic substitution reaction.



**Figure S4.2** Stacked  $^{13}\text{C}$  NMR spectra (125 MHz,  $\text{CDCl}_3$ ) of model hexylamine/cyanuric chloride mixture at optimized stoichiometric amounts ( $[\text{NH}_2]/[\text{Cl}]$ , 2/1). Showing the characteristic disappearance of C-Cl signal ( $\delta=169.00\text{ ppm}$ ) while the C-NH melamine signal ( $\delta=165\text{ ppm}$ ) becomes dominant at  $80\text{ }^\circ\text{C}$  over the course of 3 h.

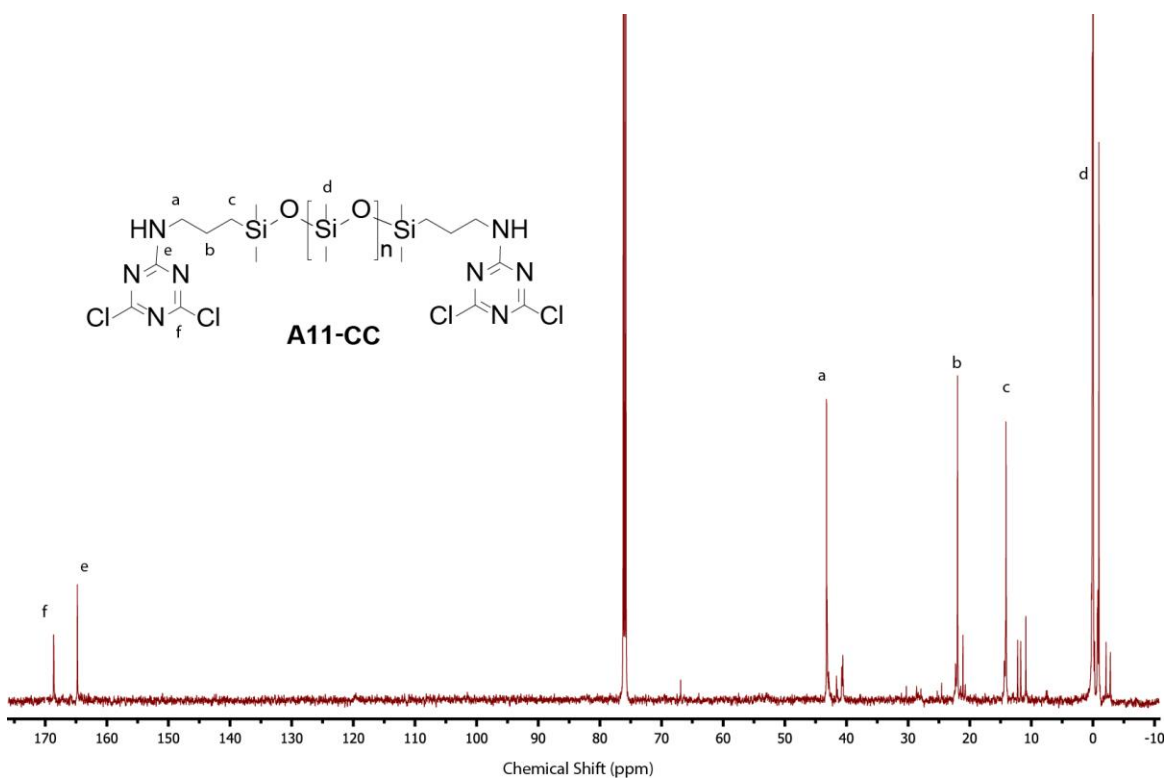


**Figure S4.3** High-resolution ESI-Q-TOF mass spectra of model hexylamine/cyanuric chloride mixture at optimized stoichiometric amounts ( $[\text{NH}_2]/[\text{Cl}]$ , 2/1). Showing the type of products formed at 80 °C over the course of 3 h. This highlights the rapid formation of the disubstituted product at room temperature (0 h) while the trisubstituted product required longer time and higher temperature for its formation.

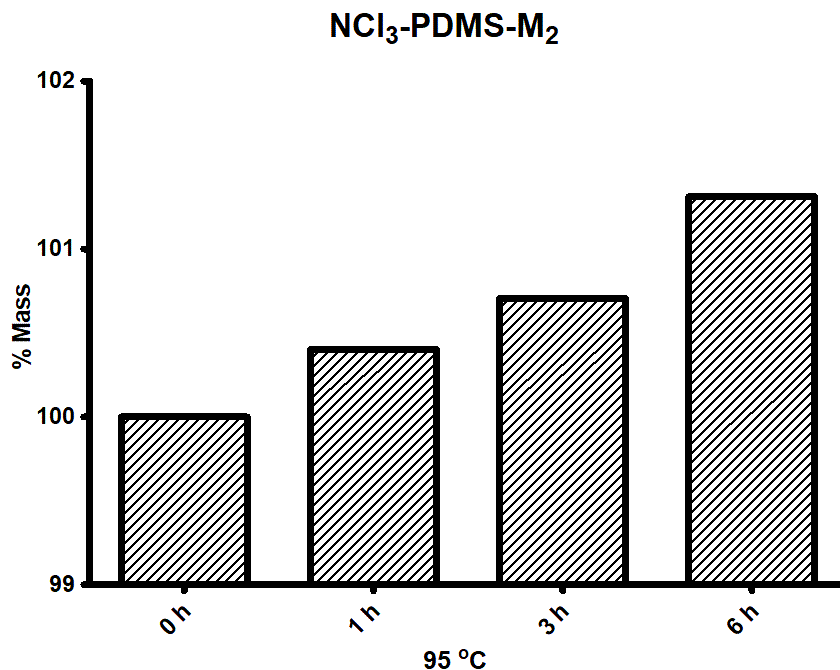


**Figure S4.4**  $^1\text{H}$  NMR spectrum (600 MHz,  $\text{CDCl}_3$ ) of pre-grafted  $\alpha,\omega$ -bis(4,6-dichloro)-s-triazinyl-modified aminosilicone (**A11-CC**). Showing the characteristic shift of protons adjacent to nitrogen from 2.5 to 3.5 ppm once the nucleophilic aromatic substitution reaction between cyanuric chloride and DMS A11 had taken place at zero degree in the presence of triethylamine, the active base.

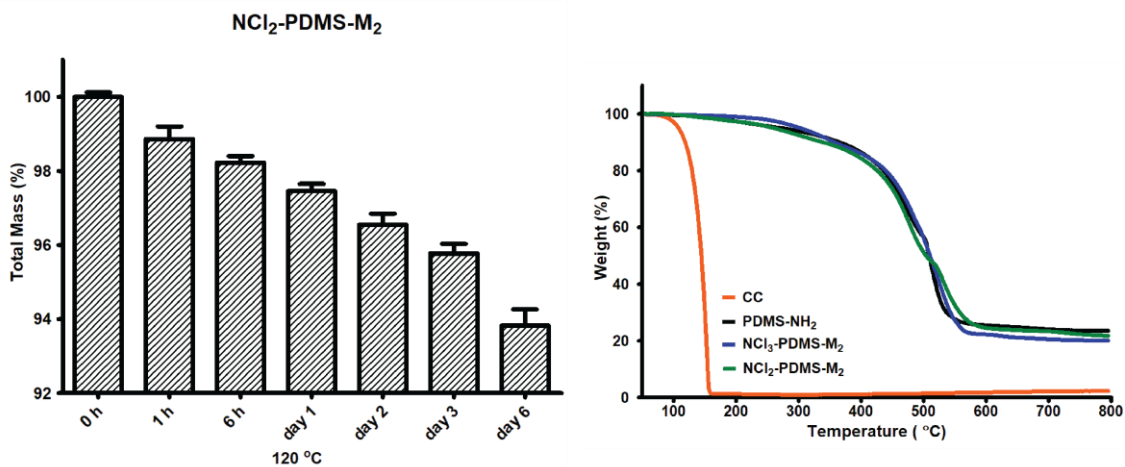




**Figure S4.5**  $^{13}\text{C}$  NMR spectrum (125 MHz,  $\text{CDCl}_3$ ) of pre-grafted  $\alpha,\omega$ -bis(4,6-dichloro)-s-triazinyl-modified aminosilicone (**A11-CC**). Showing the presence of both C-Cl signal ( $\delta=169.00$  ppm) and the C-NH melamine signal ( $\delta=165$  ppm) as DMS A11 get becomes modified with cyanuric chloride.



**Figure S4.6** Hydrolytic stability and weight increase of  $\text{NCl}_2\text{-PDMS-M}_2$  elastomers at 95 °C over the course of 6 h.



**Figure S7.** Post-cure heat treatment of  $\text{NCl}_2\text{-PDMS-M}_2$  and TGA thermograms in air of CC, PDMS-NH<sub>2</sub>,  $\text{NCl}_3\text{-PDMS-M}_2$  and  $\text{NCl}_2\text{-PDMS-M}_2$ .

## **CHAPTER 5: Controlling Silicone Networks using Dithioacetal Crosslinks<sup>§</sup>**

### **5.1 Abstract**

Traditional preparative methods for silicone elastomers center on platinum and tin-based cure chemistries. There is a need, for environmental and cost reasons, to find routes to silicones that do not require the use of heavy metals which remain in the elastomer after cure. This work describes dithioacetal silicone networks, which readily form between thiol-modified silicone monomers and polymers and aromatic aldehydes in the presence of acids, and do not require metal catalysts. Both chemical and physical crosslinks were utilized to independently manipulate elastomer properties. Subtle differences in the aromatic aldehyde used to crosslink the silicone led to large changes in modulus, due to differences in network structure. Using these associations, it was possible to tailor the silicone mechanical properties from very soft gels to much more rigid elastomers. The products were very stable to both hydrolytic and thermal stress, which was surprising given the normal susceptibility of silicones to acid-catalyzed reactions. The use of thioacetalization of readily available aromatic aldehydes as an alternative, metal free, organic cure provides an attractive route to polymer property optimization.

### **5.2 Introduction**

Silicone elastomers are high performance polymers of commercial importance because of their exceptional properties, which include: flexibility; low chemical reactivity; biocompatibility; thermal stability; and, hydrophobicity.<sup>1-3</sup> Conventionally, platinum,<sup>4</sup> tin

---

<sup>§</sup>This chapter is reproduced from A. Fatona, J. M. Moran-Mirabal and M. A. Brook, *Polymer Chemistry*, 2019, 10, 219-227 with permission from the Royal Society of Chemistry, Copyright 2019 Royal Society of Chemistry. Fatona and Brook designed the experiments and analyzed the data. Fatona performed all experiments and wrote the manuscript with additions, edits and guidance from both Moran-Mirabal and Brook.

or titanium<sup>5</sup>-catalyzed reactions are used to create commercial elastomers from silicone oils and crosslinkers. More recently, alternative routes, including the Piers–Rubinsztajn<sup>6</sup> (boron-catalyzed) condensation reaction, have been used to assemble well-defined 3D networks. Each of these strategies has limited functional group tolerance and can be challenged in certain environmental conditions.<sup>7</sup>

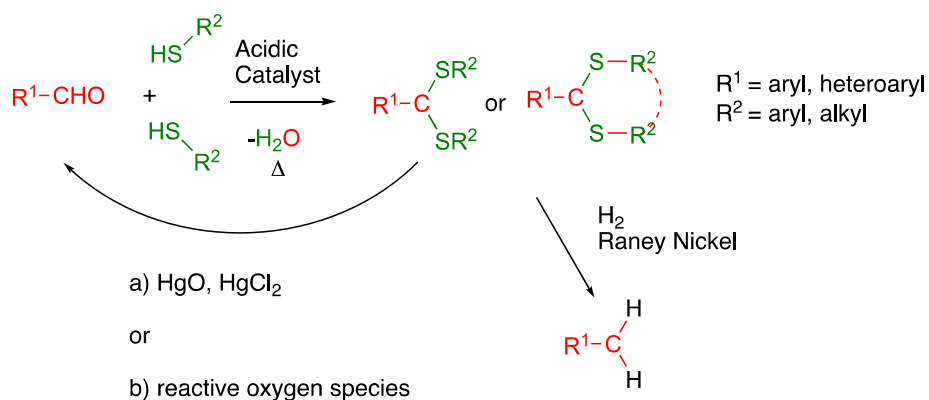
An evolving trend used to avoid these sensitivities, avoid the use of (expensive) heavy metal catalysts, and/or prepare ‘dual cure’ network structures, involves either organic cure alone, or the combination of organic cure with traditional silicone cure technologies.<sup>8</sup> The chosen organic process should not normally utilize conditions – typically acidic or basic – that can lead to reaction on the siloxane backbone.<sup>9</sup> Fortunately, many radical, ionic and pi-orbital controlled reactions fulfil these criteria. In the latter case, for example, azide alkyne click chemistry can be used to assemble silicone elastomers with interesting properties,<sup>3</sup> including tunable wettability for low protein adsorption,<sup>10</sup> or adhesion to other silicone polymers.<sup>11</sup> An alternative, efficient click process involves thiol-ene chemistry. Bowman et al. demonstrated, and beautifully reviewed,<sup>12, 13</sup> the efficacious use of thiol-ene chemistry to create silicone elastomers under relatively mild conditions.<sup>14, 15</sup> This has more recently been used for the 3D printing of silicone-based objects of various geometrical structures and containing more than one modulus.<sup>16</sup>

The dithioacetal group stands as an important complementary partner to acetals when used as a protecting group.<sup>17, 18</sup> While carbonyl groups undergo ready and reversible acetalization with alcohols, particularly 1,2- or 1,3 diols, in the presence of acid, dithioacetal formation from thiols and a carbonyl group typically requires stronger acids,<sup>19-23</sup> with the Lewis acid BF<sub>3</sub> often found to be a convenient catalyst. Dithioacetals are rather stable both in acidic and basic environments,<sup>24</sup> much more so than simple acetals, and removal to regenerate the carbonyl group usually utilizes a soft metal like mercury, although complete reduction to the methylene groups using Raney nickel and hydrogen is an alternate option (Figure 1).<sup>17, 18</sup>

The use of dithioacetals has received less attention in polymer chemistry. The main uses are as selectively degradable sites leading to thiols. For instance, Hilf and Kilbinger<sup>25</sup> reported the synthesis of a thiol-functionalized poly(norborneneimide) polymer through a

sacrificial method using alkene functionalized thioacetal monomers as end-capping agents that were later reduced to expose desired thiol groups, and efficient synthesis using ring-opening metathesis polymerization (ROMP) of a polymer containing thiol end groups has been successfully achieved; the dithioacetal in this case was prepared using  $S_N2$  reactions.<sup>25</sup> Post-polymerization modification of a vinyl ether polyphosphoester scaffold via thioacetalization was used in the study of core degradable polymer nanoparticles.<sup>26</sup> In a completely different approach, hyperbranched polythioketals have been prepared using 2-[4-(4-mercaptobutoxy)phenoxy]-9H-fluoren-9-one as an  $AB_2$  monomer.<sup>27</sup>

Polymers that contain dithioacetals have found an important place in biomaterials science. Reactive oxygen species that are released as part of the inflammatory process, for example, are able to oxidatively cleave dithioacetals, leading to regeneration of thiols.<sup>28</sup> Therefore, nanoparticles,<sup>29</sup> cements,<sup>30</sup> and polymers<sup>28, 31</sup> containing these functional groups undergo oxidative cleavage as a consequence of biological events, leading, for example, to drug delivery. The presence of the functional group in polyurethanes is particularly well developed, although other polymers containing the linkage have been described (Figure 5.1).<sup>28</sup>



**Figure 5.1** Protection of aldehydes mediated via thioacetalization reaction.

Given the benefits that sulfur chemistry delivered to silicones in the form of thiol-ene chemistry, it was of interest to examine if other sulfur-based chemistry could bring value. In particular, could the thioacetalization reaction<sup>19-23</sup> act as an alternative organic cure process to create dithioacetal silicone networks whose elastomeric properties could be readily manipulated? We report that commercial thiopropyl-modified silicones are easily

crosslinked by the addition of a variety of commercially available aromatic mono- and di-aldehyde molecules in the presence of Lewis or Brønsted acids to create silicone elastomers with controlled and variable crosslink densities and predictable properties. The structures of the aldehyde linkers were shown to play a surprisingly important role in determining the mechanical properties of the elastomers.

## 5.3 Experimental section

### 5.3.1 Materials

(Mercaptopropyl)methylsiloxane-dimethylsiloxane copolymers (HS-PDMS,  $\text{Me}_3\text{SiO}(\text{Me}(\text{HS}(\text{CH}_2)_3\text{SiO})_n(\text{Me}_2\text{SiO})_m\text{SiMe}_3$ , SMS 022  $n=2-3\%$  MW 6,000-8,000 and SMS 142  $n=13-17$  mol%, 3,000-4,000  $\text{g mol}^{-1}$ , respectively), vinyl-terminated polydimethylsiloxane (telechelic, DMS V21, MW 6,000  $\text{g mol}^{-1}$ ) and methylhydrosiloxane-dimethylsiloxane copolymer (SiH-PDMS,  $\text{Me}_3\text{SiO}(\text{Me}(\text{H})\text{SiO})_n(\text{Me}_2\text{SiO})_m\text{SiMe}_3$ , HMS 151  $n=15-18\%$  MW 1900-2000  $\text{g mol}^{-1}$ ) were obtained from Gelest. Glutaraldehyde (50wt% solution), benzaldehyde (99.5%), fluorene-2-carboxaldehyde (99%), terephthalaldehyde (99%), boron trifluoride diethyl etherate (46.5%  $\text{BF}_3$ , as determined by base titration),<sup>32, 33</sup> aluminum chloride (99.9%), *p*-toluenesulfonic acid monohydrate (*p*-TsOH, 98%), methanesulfonic acid (MsOH, 99%) and platinum(0)-1,3-divinyl-1,1,3,3-tetramethyldisiloxane (Karstedt's catalyst, Pt ~2% in xylene) were purchased from Millipore-Sigma. Silica gel (Aerosil 150) was obtained from Evonik. THF and toluene were purchased from Caledon. All materials were used as received.

### 5.3.2 Characterization

**Nuclear Magnetic Resonance:**  $^1\text{H}$  NMR experiments were recorded at room temperature and performed on Bruker Avance 600 MHz nuclear magnetic resonance spectrometer using deuterated chloroform as solvent.

**Thermogravimetric Analysis (TGA).** Analyses were carried out on a Mettler Toledo TGA 2 thermogravimetric analyzer. Data was collected after placing ca. 5 mg of a vacuum-dried sample in a clean alumina crucible and heating from ambient temperature to 800 °C under air or argon atmosphere (heating rate of 20 °C min<sup>-1</sup>).

**Differential Scanning Calorimetry (DSC).** Differential scanning calorimetry (DSC) analyses were performed on a TA Q200 calorimeter under nitrogen at purge rate of 50 mL min<sup>-1</sup> using a heat/cool/heat procedure. Samples were heated at the rate of 10 °C min<sup>-1</sup> to 200 °C from room temperature then cooled at the rate of 5 °C min<sup>-1</sup> to -40 °C before finally heating back to 200 °C.

**Ultraviolet-Visible Spectroscopy.** Absorbance measurements of fluorene-2-carboxaldehyde-crosslinked silicone elastomers were conducted on a Cary 100 Bio UV-Vis/NIR spectrophotometer (Figure S5.1 Appendix 5).

**Young's modulus measurement.** Modulus data was collected 24 h after elastomer formation within 15-well plates on 2.5 mm thick samples using a MACH-1 micromechanical testing instrument (Biomomentum) equipped with a 0.5 mm hemispherical indenter using a Poisson ratio of 0.3. Shore OO measurements were taken using a Rex Durometer, Type OO, Model 1600 from Rex Gauge Co.

**Rheometry.** Rheological measurements were taken using a TA instruments Discovery HR-3 Hybrid Rheometer equipped with 8 mm parallel plate geometry. Dynamic strain sweep experiments at frequency 1 Hz were performed for all samples to decide the linear dynamic range of the strain. All experiments were performed at 25 °C. The linear viscoelastic regime extends to oscillatory strains above 100% in both systems studied. However, at higher strains, changes in the gel structure (ruptured bonds or entanglements) resulted in a decrease in the measured moduli, as expected. For gel point determination, time sweep experiments (using the 40 mm parallel plate geometry) were performed under the single frequency of 6.28 rad/s with a constant strain of 0.5% at 60 °C.

Dispersions of pre-elastomers were mixed using a planetary centrifugal mixer “Speedmixer” (model: DAC 150.1 FVZ-K, FlackTek Inc.).

### 5.3.3 Elastomer preparation using traditional platinum cure technique

To telechelic vinyl terminated silicone (DMS V21, 1 g, 0.33 mmol of vinyl groups) weighed into a glass scintillation vial containing HMS 151 (hydromethylsiloxane-dimethylsiloxane copolymer, 0.11g, 0.33 mmol of SiH groups) was added Pt solution (30 ppm, 10  $\mu$ L taken from a stock solution, prepared by pipetting Karstedt's Catalyst (1.75  $\mu$ L, ~2% Pt in xylene) and diluting in 1 mL of hexanes). After mixing with the help of a digital Vortex mixer (3000 rpm, 1 min), the pre-cured silicone mixture was poured into a polystyrene Petri dish lined with Teflon film to cure at 60 °C for 24 hr. The Young's modulus was found to be  $0.14 \pm 0.01$  MPa.

### 5.3.4 Elastomer preparation using dithioacetal crosslinked silicones

Initial attempts to use glutaraldehyde as a crosslinker were unsuccessful. To HS-PDMS (SMS 022, 1 g, 0.3 mmol of thiol groups) weighed into a glass scintillation vial containing glutaraldehyde (neat, previously freeze-dried, 7.5mg, 0.075 mmol) was added *p*-TsOH (75  $\mu$ L of a 0.0105M solution dissolved in 50 % THF/chloroform, 0.79  $\mu$ mol). After mixing with the help of a digital Vortex mixer (3000 rpm, 1 min), the pre-cured silicone mixture was poured into a polystyrene Petri dish lined with Teflon film to cure at 60 °C for 6 h. Both thioacetal and aldol condensation reactions occurred during cure. The products were thermally unstable, as shown by facile yellowing and changes in the  $^1\text{H}$  NMR (Figures S5.2 - S5.6, Appendix 5). Aliphatic aldehydes were therefore abandoned.

A representative curing procedure for the synthesis of dithioacetal functional silicone networks based on aromatic aldehydes, is provided, as shown in Figure 5.2 (Table 1). Analogous experiments with alternative acids are noted in Table S1, Appendix 5. Lewis acid-catalyzed reactions were extremely rapid and gave elastomers with varied moduli in an irreproducible fashion, possibly due to subtle differences in the moisture present in the reaction mixture. Different acid concentrations were examined, with the 'best behaved' reported. For *p*-TsOH, low catalyst quantities (~0.25mol%) were efficacious. (Mercaptopropyl)methylsiloxane-dimethylsiloxane copolymer (HS-PDMS, SMS 022, 1 g, 0.3 mmol of thiol groups) was weighed into a polypropylene mixing cup (FlackTek, size 10) followed by the addition of *p*-TsOH (75  $\mu$ L of a 0.0105M solution dissolved in 50 %



THF/chloroform, 0.79  $\mu\text{mol}$ ). After mixing using the Speedmixer (3000 rpm, 1 min), the appropriate aromatic aldehyde (e.g., benzaldehyde (neat, 16 mg, 0.15 mmol) or terephthaldehyde (10 mg, 0.075 mmol dissolved in 300  $\mu\text{L}$  of chloroform)) were added to the transparent, homogeneous silicone/catalyst mixture while mixing continued for another 30 s. Finally, the mixture was poured into Falcon™ polystyrene microplates lined with Teflon film, and cure occurred at room temperature for 24 h or at 60 °C for 4 h.

$^1\text{H}$  NMR and FTIR data showing the functional group changes during cure is provided in Figure S5.7, S5.8 Appendix 5.

### **5.3.5 The role of silica**

Aerosil R150 silica was added to selected recipes (Table 1, Figure S5.9, Appendix) at levels of 1, 2, 5 or 10 wt% (10, 20, 50 or 100 mg), respectively. In the case of the 1 wt% silica, *p*-TsOH (0.15 mg) was pre-adsorbed to the silica to see if there was a difference in reactivity when the catalysis was nominally heterogeneous.

Table 1 Silicone dithioacetal elastomer formulations

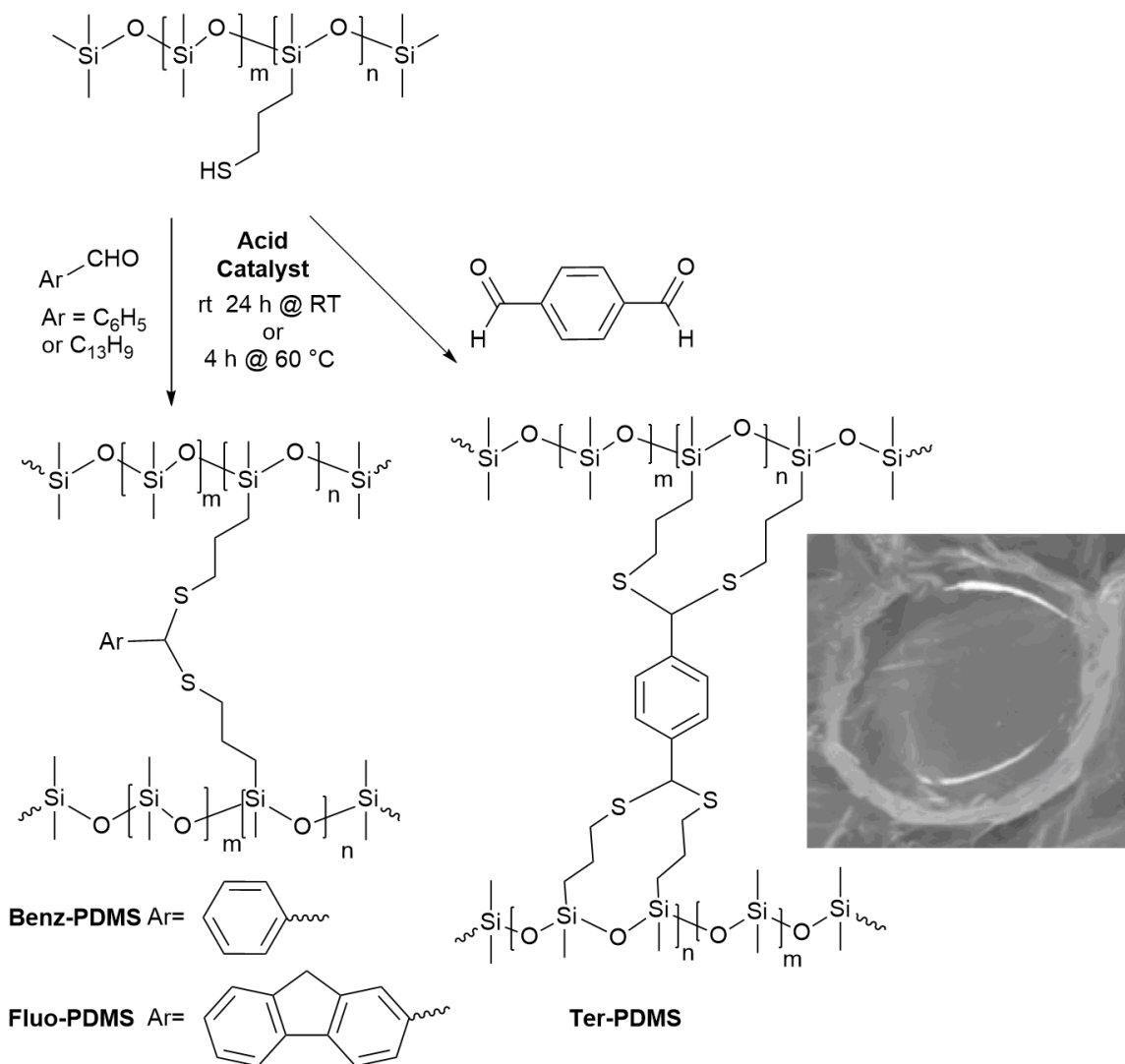
Entry	Product name <sup>a</sup>	p-TsOH μL (ppm <sup>b</sup> )	ArCHO (mg)	Silicone	Silico nes (g)	[SH]/ [CHO]	Silica (mg)	Solvent (mL)	Temp/ Reaction time (°C/h)	Young's modulus (MPa, ±S.D.) <sup>c</sup>
1		75 (150)	Benz-CHO (8)	SMS 022	1.00	4/1	0	Neat	60/4	
2	<b>Benz-PDMS</b>	75 (150)	Benz-CHO (16)	SMS 022	1.00	2/1	0	Neat	60/4	0.11±0.01
3		75 (150)	Benz-CHO (38)	SMS 142	1.00	4/1	0	Neat	60/4	0.70±0.02
4	<b>Benz-PDMS-H</b>	75 (150)	Benz-CHO (76)	SMS 142	1.00	2/1	0	Neat	60/4	2.24±0.09
5	<b>Fluo-PDMS</b>	75 (150)	Fluo-CHO (29)	SMS 022	1.00	2/1	0	CHCl <sub>3</sub> (0.2)	60/4	0.21±0.01
6	<b>Ter-PDMS</b>	75 (150)	Ter-CHO (10)	SMS 022	1.00	2/1	0	CHCl <sub>3</sub> (0.3)	60/4	0.49±0.01
7	<b>Benz-PDMS-S1</b>	75 (152)	Benz-CHO (15)	SMS 022	0.99	2/1	10	Neat	60/4	0.11±0.02
8	<b>Benz-PDMS-S2</b>	75 (153)	Benz-CHO (14.9)	SMS 022	0.98	2/1	20	Diox (0.2) <sup>d</sup>	60/4	0.15±0.01
9	<b>Benz-PDMS-S5</b>	75 (158)	Benz-CHO (14.4)	SMS 022	0.95	2/1	50	Diox (0.2)	60/12	0.23±0.03
10	<b>Benz-PDMS-S10</b>	75 (167)	Benz-CHO (13.7)	SMS 022	0.90	2/1	100	Diox (0.2)	60/12	0.46±0.06
11	<b>Fluo-PDMS-S2</b>	75 (153)	Fluo-CHO (27.2)	SMS 022	0.98	2/1	20	Diox (0.2)	60/4	0.37±0.03
12	<b>Fluo-PDMS-S5</b>	75 (158)	Fluo-CHO (26.4)	SMS 022	0.95	2/1	50	Diox (0.2)	60/12	0.58±0.06
13	<b>Fluo-PDMS-S10</b>	75 (167)	Fluo-CHO (25)	SMS 022	0.90	2/1	100	Diox (0.2)	60/12	0.93±0.08
14	<b>Ter-PDMS-S2</b>	75 (153)	Ter-CHO (9.4)	SMS 022	0.98	2/1	20	Diox (0.3)	60/4	0.99±0.07
15	<b>Ter-PDMS-S5</b>	75 (158)	Ter-CHO (9.1)	SMS 022	0.95	2/1	50	Diox (0.3)	60/12	1.36±0.05
16	<b>Ter-PDMS-S10</b>	75 (167)	Ter-CHO (8.63)	SMS 022	0.90	2/1	100	Diox (0.3)	60/12	2.0±0.2
17	<b>Glu-PDMS<sup>e</sup></b>	75 (150)	Glu-CHO (7.5)	SMS 022	1.00	2/1	0	Neat	60/6	0.20±0.02

<sup>a</sup> Nomenclature: aldehyde-PDMS-silica content. Thus, **Benz-PDMS-S1** is the elastomer made from benzaldehyde and SMS 022 in an optimized 2/1 functional group ratio and contains 1% silica. **Benz-PDMS-H** is unfilled with silica but made from a silicone with higher thiopropyl density, leading to higher crosslink densities in the elastomer, thus “-H”. <sup>b</sup> With respect to [SH]. <sup>c</sup> The elastomers were too soft to measure using MACH-1 micromechanical testing instrument. <sup>d</sup> Diox = dioxane is not the ideal solvent based on safety. We subsequently demonstrated, in one case, that toluene can also serve as diluent. <sup>e</sup> The products were thermally unstable, as shown by facile yellowing and changes in the <sup>1</sup>H NMR with heating (Figure S2-S6, ESI<sup>†</sup>). S.D = Standard Deviation.

## 5.4 Results

Initial attempts to create silicone dithioacetals from aliphatic aldehydes were discouraging. The products with glutaraldehyde were yellow, dithioacetal formation was accompanied by aldol reactions, and ready degradation occurred at elevated temperatures (Figure S5.2-S5.6, Appendix 5). By contrast, stoichiometric amounts of aromatic aldehydes and thiopropyl-silicones, in the presence of Lewis or Brønsted acids, led to silicone elastomers (Figure 5.2). Silicones are sensitive to metathesis (redistribution/ equilibration) in the presence of acids, which leads to changes in molecular weight and the production of cyclic monomers, typically D<sub>4</sub> (Me<sub>2</sub>SiO)<sub>4</sub>.<sup>9</sup> Therefore, a variety of the acids commonly used to catalyze thioacetalization<sup>19-23</sup> (AlCl<sub>3</sub>, BF<sub>3</sub>, MsOH and *p*-TsOH, Table S1, Appendix 5) were examined in a silicone environment to identify conditions that minimize this possibility. Note that AlCl<sub>3</sub> and BF<sub>3</sub> are moisture-sensitive Lewis acids that can complex with water<sup>34</sup> or react to generate Brønsted acids that can also facilitate the thioacetalization reaction. The reaction was found to be exceptionally (impractically) rapid with both of these Lewis acids, and led to irreproducible elastomers with different physical properties (Table S1, Appendix 5). While rapid cure could be advantageous (e.g., for industrial applications) further use of BF<sub>3</sub> was not explored given the sensitivity of silicon to fluoride,<sup>9</sup> nor with AlCl<sub>3</sub>, since HCl-release could cause problems with steel vessels.

*p*-Toluenesulfonic acid was selected as the best choice of acid catalyst due to several technical advantages, including ease of handling, ability to dry the catalyst reproducibly, and its consistency in leading cleanly to dithioacetal-crosslinked silicone networks. This acid also undergoes oxidative decomposition relatively easily, which is advantageous when considering the environmental impact of catalysts.<sup>35</sup> The reaction, with aromatic aldehydes under optimal conditions (Figure 5.2), gave dithioacetal silicone networks in quantitative yield after curing either at 60 °C for 4 hours or at room temperature for 24 hours (Table 1). Cured elastomers were analyzed by <sup>1</sup>H NMR, which showed characteristic dithioacetal protons (δ=4.81 ppm) and the simultaneous disappearance of aldehydic and thiol protons (Figure S5.7, Appendix 5).



**Figure 5.2** Reaction scheme depicting the crosslinking of thiol-PDMS via dithioacetal linkages using aromatic aldehydes to form **Benz-**, **Fluo-** and **Ter-PDMS** elastomers (Inset: photo of **Ter-PDMS**).

Silica is commonly used as a filler in silicone elastomers.<sup>9</sup> It is also a sorption agent for well-known reagents. Silica provides an additional advantage in these formulations in that it can absorb water produced during the thioacetalization process, thereby shifting the equilibrium towards dithioacetal formation. The impact of combining the silica with *p*-TsOH – before or after cure was initiated – was therefore examined. The reactions occurred smoothly in the presence of silica and similar products arose regardless of whether *p*-TsOH

was added directly or after pre-adsorption onto silica (Figure S5.9, Appendix 5). The Young's modulus of the elastomers increased proportionally to the amount of silica incorporated, as expected (Table 1).

#### 5.4.1 Elastomer formation: Stoichiometry controls physical properties

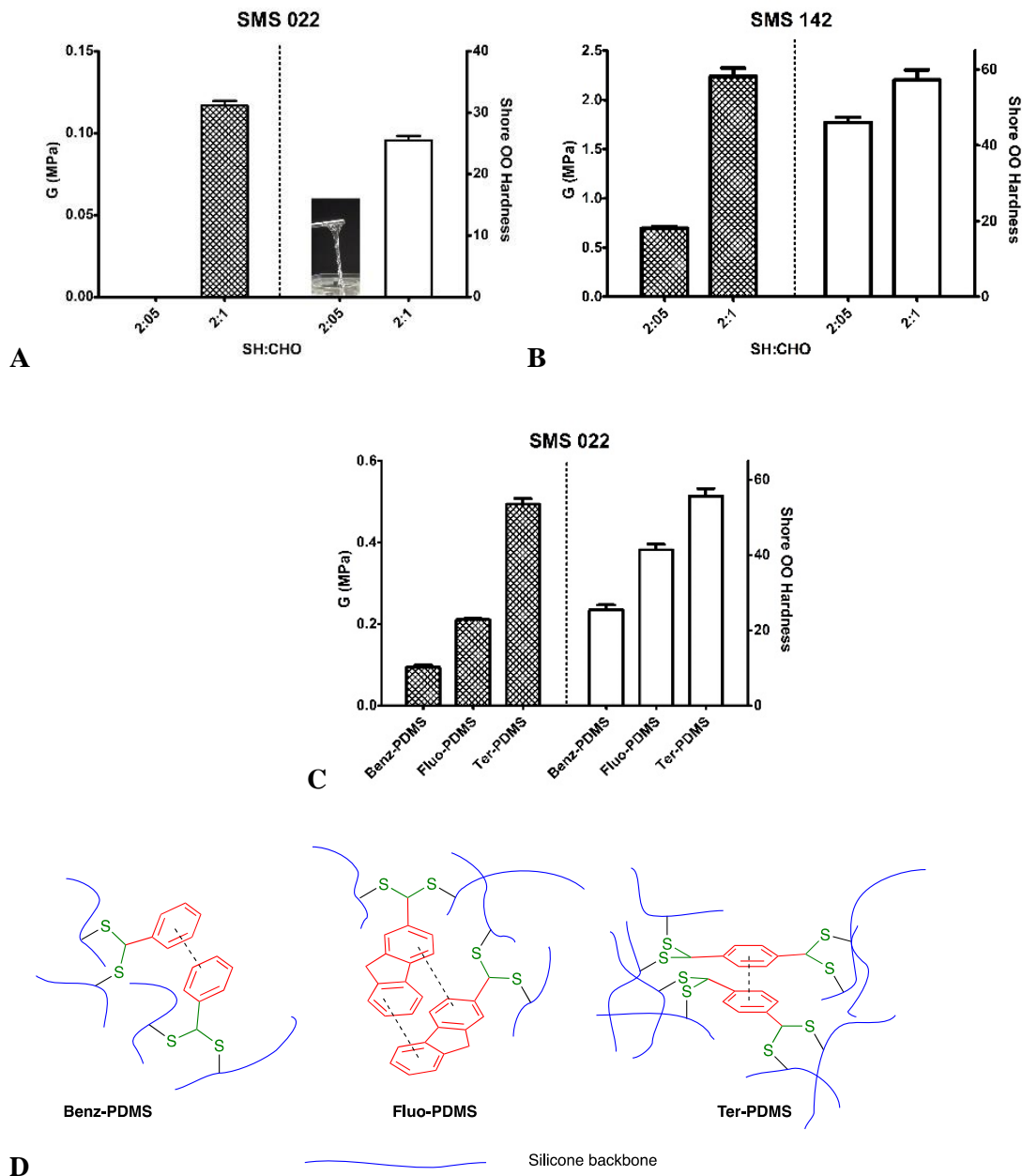
Thiopropyl-silicones containing 2-3 or 13-17 mol %SH (SMS 022 120-180 cSt, MW 6,000-8,000 g mol<sup>-1</sup> or SMS 142 100-200 cSt, MW 3,000-4,000 g mol<sup>-1</sup>), respectively, were readily crosslinked with benzaldehyde (Table 1, Entries 1-4). The process of the reaction is readily followed by eye. An initially clear mixture becomes hazy as water forms within the silicone body. Over time clarity returns as the water droplets migrate to the external elastomer surface. The crosslink density in either case was controlled both by the SH concentration and the amount of benzaldehyde added. For example, completely crosslinking (no residual SH groups) a silicone possessing longer spacers between thiopropyl groups with stoichiometric quantities of benzaldehyde (SMS 022, 2/1 [SH]/[CHO]) led to soft elastomers to give **Benz-PDMS** (Shore OO hardness 27, Figure 5.3A, Table 1, Entry 2). A reduction in the quantity of aldehyde, and thus fewer crosslinks, produced softer silicone gels; the same silicone SMS 022, crosslinked with a 4/1 [SH]/[CHO] molar ratio led to a tacky, very soft gel-like elastomer (the sample was too soft to measure using a Shore OO durometer, Figure 5.3A, Table 1 entries 2 vs 1 and 4 vs 2). Residual, thiopropyl spacers, unreacted silicone chains, or chains only tethered at one terminus, inevitably convey such adhesive gel-like, low modulus properties to the material.<sup>6</sup> Analogous behavior was observed when starting with a silicone possessing higher concentrations of thiopropyl groups along the chain. In this case (SMS 142), higher crosslink densities resulted in harder materials to give **Benz-PDMS-H**; with similar trends observed between properties and [SH]/[CHO] molar ratios; Young's moduli ranged from 0.70 to 2.24 MPa (Figure 5.3B, Table 1 Entries 3-4).

A comparison was made between thioacetal-crosslinked silicones (considering that  $2 \times \text{SH} + \text{CHO} = 1$  chemical crosslink) and platinum-cured silicones ( $\text{SiH} + \text{CH}=\text{CH}_2 = 1$  chemical crosslink). The two elastomers were formulated so that the thioacetal-crosslinked silicone

would have half the crosslink density of platinum-cured systems. When comparing the mechanical properties of the two elastomers, almost identical values were observed (elastic modulus  $G'$  24.7 vs 26.0 kPa, and loss modulus  $G''$  207.5 vs 268.6 Pa, for thioacetal vs Pt-cured, Figure S5.10, Appendix 5). This indicates that the physical interactions provided by aryl association in the thioacetal-crosslinked silicone lead to strong crosslinks.

#### 5.4.2 Role of the aromatic crosslinker

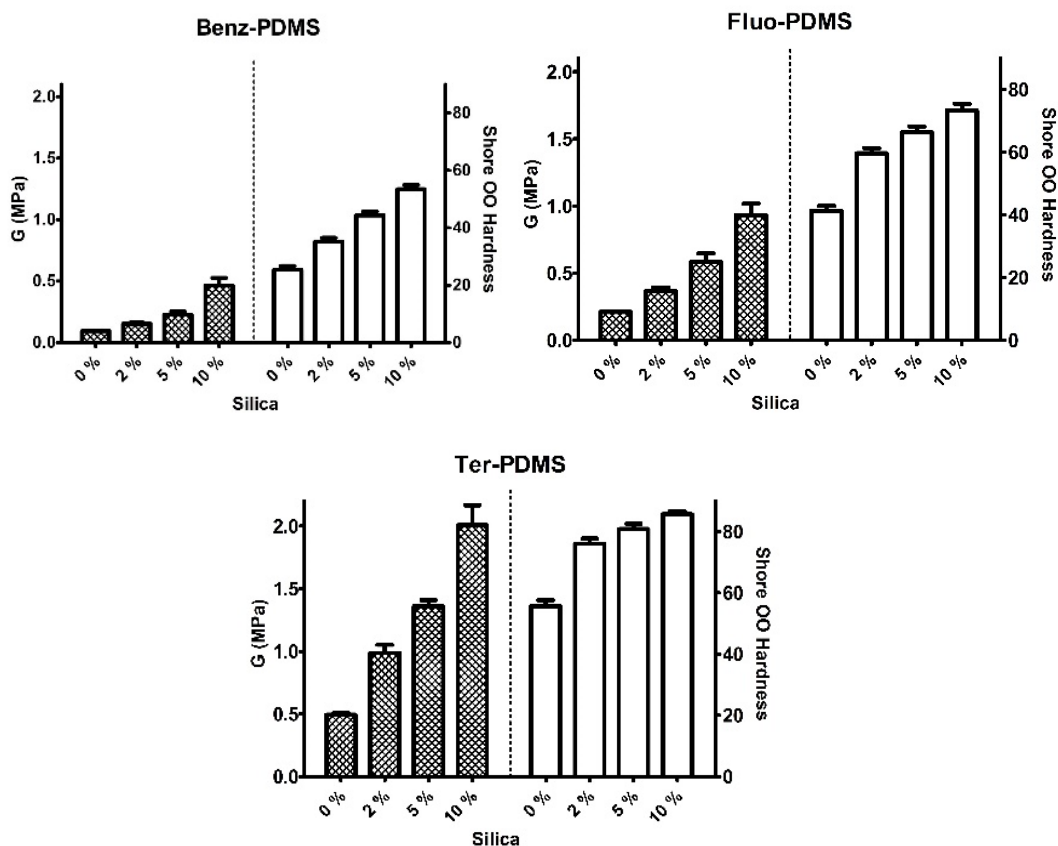
Changes in the aldehyde linkers led to significant changes in the silicone elastomer properties. The subtle change from benzaldehyde to fluorene-2-carboxaldehyde as a linker led to a surprising increase of 160% in the elastic modulus from **Benz-PDMS** v. **Fluo-PDMS** (Figure 5.3C). Similarly, the use of a dialdehyde, terephthalaldehyde, at the same  $[SH]/[CHO]$  ratio, had an even more profound impact, resulting in an increase in the mechanical modulus of 225% from **Benz-** to **Ter-PDMS**. The optical properties of the silicone elastomer were slightly affected by the nature of the aromatic aldehyde in one case. All the elastomers retained high transparency in the visible region.



**Figure 5.3** A, B: Effect of crosslinker concentration on elastomer properties. C: Effect of crosslinker structure on elastomer properties at a 2:1 SH/CHO ratio. D: Models showing dimeric self-association of aromatic crosslinkers in dithioacetal crosslinked elastomers.

### 5.4.3 Role of silica

Formulae containing 1 or 2 wt% silica cured at approximately 1.5 times longer the rate as unfilled samples, while loadings of 5 or 10 wt% required ~3 times longer (Figure S5.11, Appendix 5). As with any silicone fluid, it was much more difficult to prepare the pre-cured formulations at higher loadings because of the large increases in viscosity that arise as higher fractions of silica are added. Small amounts of solvent were added to facilitate mixing of the latter mixtures with the equipment available. The cured elastomers exhibited Shore hardnesses that correlated with silica content (Table 1, Figure 5.4).

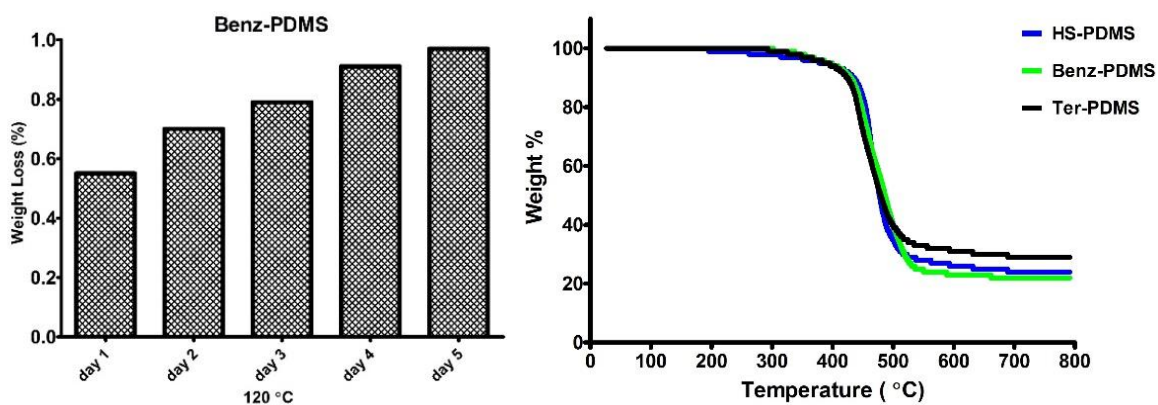


**Figure 5.4** Physical properties of elastomers as a function of aromatic crosslinker and silica filler concentration.



#### 5.4.4 Stability of the resulting products

The stabilities of the newly installed dithioacetal silicone linkages were characterized during hydrolytic and thermal challenge. Attempts to facilitate hydrolytic dithioacetal bond cleavage, by boiling the prepared elastomers in water for 8-12 hours, were unsuccessful; there was neither increase of weight due to ingress of water nor loss of weight due to hydrolysis and release of the aromatic aldehyde. The modulus of the elastomer remained unchanged following this experiment. These outcomes were somewhat surprising given that the acidic catalysts used for dithioacetal formation remains in the elastomer and would be expected to facilitate silicone degradation.



**Figure 5.5** Post-cure heat treatment of **Benz-PDMS** and TGA thermograms in air of **HS-PDMS**, **Benz-PDMS** and **Ter-PDMS** (for TGA under argon, Figure S5.15, appendix 5).

In an attempt to follow changes in acid concentration over time, a model reaction between dodecanethiol and benzaldehyde in the presence of *p*TsOH was undertaken to follow possible changes in acid concentration. The reaction proceeded rapidly to completion – no residual aldehyde was observed by  $^1\text{H}$  NMR. It was determined that there was no change in acid concentration during the reaction (Figures S5.12-S5.14, appendix 5)

Post-cure heat treatment demonstrated the long-term thermal stability of the product; there was no significant loss in weight (less than 1% after 5 days at 120 °C, Figure 5.5A). Thermal decomposition of the dithioacetal-linked silicone elastomer, measured by thermogravimetric analysis in argon, began at the temperature normally observed for a

traditional, commercial hydrosilylation crosslinked rubber (above 350 °C, Figure S5.15, appendix 5).<sup>36</sup> Surprisingly, a similar stability was observed upon heating in air (Figure 5.5B); the dithioacetals proved extremely stable to this type of oxidative stress.

## 5.5 Discussion

Dithioacetals readily formed from commercial thiopropyl-modified silicones and aromatic aldehydes. Only very small quantities of solvent were required to dissolve some of the aldehydes (e.g.,  $\text{OHCC}_6\text{H}_4\text{CHO}$ ) and/or the acid catalyst in the hydrophobic silicone matrix; the silicone otherwise acted as its own solvent. Both Lewis and Brønsted acids catalyzed the reaction – fluid silicones serve as a convenient precursor to silicone elastomers. The most robust and predictable crosslinking came from low concentrations (0.25mol%) of *p*-toluenesulfonic acid catalyst, which is a readily purified (including drying) and convenient crystalline solid. Lewis acids were less practical because they proved to be too susceptible to hydrolysis and reactions with them were too difficult to control. The acid catalyst was never removed from the silicone elastomer. Dithioacetals are known for their stability to acidic conditions,<sup>17, 37</sup> thus their stability within the silicone elastomer during storage, heating under argon and boiling in water was expected.

A more surprising consequence of residual *p*-TsOH within the elastomer was the stability of the silicone backbone itself towards acid-catalyzed depolymerization; sulfonic acids are routinely used to polymerize (or depolymerize) silicone polymers,<sup>9, 38</sup> or to incorporate functional groups using equilibration processes.<sup>6, 7, 39-41</sup> The TGA data under either argon or air showed no evidence of acid-catalyzed depolymerization (Figure 5.5B, Figure S5.15, appendix 5), the onset of which typically occurs at or below 200 °C. These TGA data mimic our observations of the hardness and surface tackiness of these materials over time, where no changes over months were observed. The absence of acid-catalyzed degradation of the polymer was surprising. Model studies showed essentially no change in the amount of available *p*TsOH during the reaction. However, the solubility of *p*TsOH in silicone oil was found to be only  $\sim 0.13 \text{ mg L}^{-1}$  ( $\sim 0.01\%$ ). We propose that the small amount of solvent initially added to facilitate the reaction evaporates, leading to (partial) precipitation of the acid, dramatically reducing the concentration of available acid, leading to the surprisingly

high level of stability over time and at higher temperatures. Regardless, the samples will remain kinetically unstable until the acid is quenched. Viable strategies to address this will be revisited with larger scale reactions.

Sulfur-based compounds, including dithioacetals, can be sensitive to oxidation. TGA data under air (for samples not filled with silica), however, showed the sulfur linkages in the silicone elastomers were not susceptible to oxidation until elevated temperatures were reached, but at a point at which the silicone backbone itself was also undergoing degradation (Figure 5.5B). The stability profile of these sulfur-cured elastomers is therefore excellent. We note that this behavior is somewhat inconsistent with the reported fragility of dithioacetals towards reactive oxygen species.<sup>28, 31</sup> In those cases, the oxidizing reagents are typically much more aggressive than air, and the active species are delivered in an aqueous or organic medium. We are currently working to develop oxidative methods to permit cleavage of the elastomers under controlled conditions.

The physical properties of elastomers were found to be intimately linked to the crosslink density (related to the spacing between crosslinks,  $M_c$ ). At sub-stoichiometric quantities of aldehyde, only partial crosslinking occurred and dangling silicone chains and unreacted thiopropyl groups led to soft, gel-like materials. When the aldehyde concentration was increased to the ideal 2/1 match of [SH]/[CHO] groups, more rigid materials resulted (Table 1 entries 2 vs 1 and 4 vs 2).

Subtle changes in the nature of the aromatic aldehyde linker led to large changes in the physical properties of the elastomer. When compared at identical [SH]/[CHO] ratios, the moduli followed the order benzaldehyde < fluorene-2-carboxaldehyde < terephthaldehyde (Figure 5.3), demonstrating the roles played by both the linker itself, and the structure of the network.

Aromatic systems are well known for their ability to self-associate, often described as  $\pi$ - $\pi$  ( $\pi$ - $\pi$ ) stacking, although this term may not accurately describe the interactions.<sup>42</sup> The range of molecular interactions that can take place has been beautifully reviewed by Persch et al.<sup>43, 44</sup> Subtle changes in aromatic structure can lead to huge changes in physical association and, thus, to the physical properties of polymers because of the secondary crosslinks these provide. For example, the combination of hydrogen bonding and aromatic

association of coumarin moieties led to increases of modulus of several orders of magnitude compared to the precursors – coumarin-free silicones.<sup>45-47</sup> In this case, simply increasing the size of the aromatic group<sup>45, 46, 48</sup> from phenyl to fluorenyl led to a notable increase in modulus. One possibility was that the larger aromatic groups more efficiently associated to give clusters that generate tighter networks. To test this, DSC experiments were performed. They did not show a thermal transition consistent with this hypothesis (Figure S5.16, appendix 5). We therefore propose that the association of aromatic dimers, trimers... leading to crosslinks is more efficient with the larger aromatic groups (Figure 5.3C,D). One may choose from the (many commercially) available aromatic aldehydes to further manipulate the silicone network properties.

The comparison of **Benz-PDMS** with a silicone cured using hydrosilylation is instructive with respect to the strength of the physical interactions in the thioacetal elastomers. When formulated with half as many chemical crosslinks, **Benz-PDMS** exhibited essentially the same elastic modulus as platinum cured systems with twice as many covalent crosslinks. That is, the physical crosslinks provided by phenyl group association contribute as much to the network structure at room temperature as a covalent crosslink. The modulus data for the **Fluo-PDMS** suggest that even stronger network contributions arise from larger aromatic moieties. Thus, one of the advantages of this system is the ability to fine tune the physical properties of the elastomer using both covalent crosslinks and physical crosslinks; starting from a specific thiopropylsilicone, the number of covalent crosslinks is fixed while the physical ones will depend on the specific arylaldehyde chosen.

Additional control over elastomer properties may be exercised by changing the network structure through proximity of the linking aldehydes.<sup>49</sup> The modulus of the terephthaldehyde-linked materials exceeded that of the benzaldehyde-linked structures at the same crosslink density (Figure 5.3C,D).

Fillers can be used to further manipulate the physical properties of elastomers. Silicone elastomers are very weak materials that exhibit poor tear strength. To improve the resilience of these polymers, fillers – typically based on silica – are added at levels up to ~30wt%.<sup>50</sup> The addition of silica to the dithioacetal-cured silicones further increased the modulus in a

programmed way, as shown for Ter-PDMS. For example, 0% → 10% silica results in 0.49 MPa → 2.0 MPa (Table 1, Figure 5.4).

Commercial silicone polymers rely on a few organic residues, typically Me, Ph and, for crosslinking, SiH and SiVinyl. While organically modified silicones are commercially available, their use remains rather limited. The benefits of metal-free click chemistry has been clearly shown in a variety of applications. We have demonstrated here that the use of dithioacetal formation, which occurs under very mild conditions, with low catalyst concentrations and without the need for heavy metal catalysts, leads to robust silicone elastomers whose properties are easily tuned by use of readily available aromatic aldehydes. The silicones produced from aromatic aldehydes maintain high transparency during and after cure, exhibit high thermal and hydrolytic stability at levels comparable to simple Pt- or tin-cured silicone systems, and can be formulated with silica fillers in to control mechanical properties in a predictable way. They thus serve as a convenient alternative to classically cured silicone elastomers when the presence of heavy metals needs to be avoided.

## 5.6 Conclusions

Aromatic dithioacetals prove exceptionally easy to form from commercial thiopropylsilicones and avoid the need for the (heavy) metal catalysts traditionally used for the preparation of silicone elastomers; the hydrophobic silicone facilitates the formation by expelling the water formed. The physical properties of the elastomers formed are readily manipulated by changing the chemical crosslink density, the nature of the aromatic aldehyde and the use of silica fillers. The resulting crosslinked products exhibit stability similar to that of pure silicones cured by traditional means.

## 5.7 Acknowledgements

We thank Prof. T. Hoare for access to equipment. We gratefully acknowledge the financial support of the Natural Sciences and Engineer Research Council of Canada. JMM is the recipient of an Early Researcher Award from the Province of Ontario and holds the Tier 2 Canada Research Chair in Micro and Nanostructured Materials.

## 5.8 References

1. M. Amjadi, K. U. Kyung, I. Park and M. Sitti, *Adv. Funct. Mater.*, 2016, **26**, 1678-1698.
2. E. Yilgör and I. Yilgör, *Prog. Polym. Sci.*, 2014, **39**, 1165-1195.
3. F. Gonzaga, G. Yu and M. A. Brook, *Macromolecules*, 2009, **42**, 9220-9224.
4. A. M. Stricher, R. G. Rinaldi, C. Barres, F. Ganachaud and L. Chazeau, *RSC Advances*, 2015, **5**, 53713-53725.
5. F. W. van Der Weij, *Makromol. Chem.*, 1980, **181**, 2541-2548.
6. A. S. Fawcett, J. B. Grande and M. A. Brook, *J. Polym. Sci., Part A: Polym. Chem.*, 2013, **51**, 644-652.
7. J. B. Grande, D. B. Thompson, F. Gonzaga and M. A. Brook, *Chem. Commun.*, 2010, **46**, 4988-4990.
8. C.-S. Lin, T. Fay-Oy Lim and J. Angus, Richard Oliver, *US Patent 6,627,672*, 2003.
9. M. A. Brook, *Silicon in Organic, Organometallic, and Polymer Chemistry*, Wiley, New York, 2000.
10. T. Rambarran, F. Gonzaga, M. A. Brook, F. Lasowski and H. Sheardown, *J. Polym. Sci., Part A: Polym. Chem.*, 2015, **53**, 1082-1093.
11. T. Rambarran, F. Gonzaga, A. Fatona, M. Coulson, S. Saem, J. Moran-Mirabal and

- M. A. Brook, *J. Polym. Sci., Part A: Polym. Chem.*, 2018, **56**, 589-597.
12. C. E. Hoyle and C. N. Bowman, *Angew. Chem. Int. Edit.*, 2010, **49**, 1540-1573.
13. M. J. Kade, D. J. Burke and C. J. Hawker, *J. Polym. Sci., Part A: Polym. Chem.*, 2010, **48**, 743-750.
14. M. A. Cole and C. N. Bowman, *J. Polym. Sci., Part A: Polym. Chem.*, 2012, **50**, 4325-4333.
15. Y. Zuo, Z. Gou, J. Zhang and S. Feng, *Macromol. Rapid Comm.*, 2016, **37**, 597-604.
16. S. Zheng, M. Zlatin, P. R. Selvaganapathy and M. A. Brook, *Add. Manuf.*, 2018, **24**, 86-92.
17. P. Kocienski, *Protecting Groups* Thieme, Stuttgart, 3rd edn., 2005.
18. P. G. M. Wuts and T. W. Greene, *Greene's Protective Groups in Organic Synthesis*, Wiley-Interscience, New Jersey, 4th edn., 2006.
19. T. Nakata, S. Nagao, N. Mori and T. Oishi, *Tetrahedron Lett.*, 1985, **26**, 6461-6464.
20. H. Tani, K. Masumoto, T. Inamasu and H. Suzuki, *Tetrahedron Lett.*, 1991, **32**, 2039-2042.
21. V. Kumar and S. Dev, *Tetrahedron Lett.*, 1983, **24**, 1289-1292.
22. C. Djerassi and M. Gorman, *J. Am. Chem. Soc.*, 1953, **75**, 3704-3708.
23. S. K. De, *Adv. Synth. Catalysis*, 2005, **347**, 673-676.
24. M. H. Ali and M. Goretti Gomes, *Synthesis*, 2005 (8), 1326-1332.
25. S. Hilf and A. F. M. Kilbinger, *Macromolecules*, 2009, **42**, 4127-4133.
26. Y. H. Lim, G. S. Heo, Y. H. Rezenom, S. Pollack, J. E. Raymond, M. Elsbahy and K. L. Wooley, *Macromolecules*, 2014, **47**, 4634-4644.
27. W. Sinananwanich and M. Ueda, *J. Polym. Sci., Part A: Polym. Chem.*, 2008, **46**,

2689-2700.

28. J. R. Martin, M. K. Gupta, J. M. Page, F. Yu, J. M. Davidson, S. A. Guelcher and C. L. Duvall, *Biomaterials*, 2014, **35**, 3766-3776.
29. J. S. Kim, S. D. Jo, G. L. Seah, I. Kim and Y. S. Nam, *J. Ind. Eng. Chem.*, 2015, **21**, 1137-1142.
30. M. A. P. McEnery, S. Lu, M. K. Gupta, K. J. Zienkiewicz, J. C. Wenke, K. N. Kalpakci, D. A. Shimko, C. Duvall and S. A. Guelcher, *RSC Advances*, 2016, **6**, 109414-109424.
31. Y. Lu, A. A. Aimetti, R. Langer and Z. Gu, *Nature Rev. Mater.*, 2016, **2**, 16075.
32. L. Wuke, Z. Weijiang, X. Jiao and Z. Lei, *J. Coord. Chem.*, 2014, **67**, 1530-1540.
33. N. Yoneda, K. Aomura and H. Ohtsuka, *Bull. Japan Petrol. Inst.*, 1966, **8**, 19-26.
34. C. A. Wamser, *J. Am. Chem. Soc.*, 1951, **73**, 409-416.
35. L. Zhang, Y. R. Yang, H. Y. Yang, Z. X. Chang and D. L. Li, *Asian J. Chem.*, 2013, **25**, 1609-1612.
36. G. Camino, S. M. Lomakin and M. Lazzari, *Polymer*, 2001, **42**, 2395-2402.
37. P. G. M. Wuts and T. W. Greene, *Greene's Protective Groups in Organic Synthesis*, Wiley, 4th edn., 2007.
38. J. Chojnowski, in *Siloxane Polymers*, eds. S. J. Clarson and J. A. Semlyen, Prentice Hall, Englewood Cliffs, NJ, 1993, ch. 1, pp. 1-71.
39. J. Cella and S. Rubinsztajn, *Macromolecules*, 2008, **41**, 6965-6971.
40. M. A. Hoque, Y. Kakihana, S. Shinke and Y. Kawakami, *Macromolecules*, 2009, **42**, 3309-3315.
41. J. Chojnowski, S. Rubinsztajn, W. Fortuniak and J. Kurjata, *J. Inorg. Organomet. Polym. Mat.*, 2007, **17**, 173-187.



42. C. R. Martinez and B. L. Iverson, *Chem. Sci.*, 2012, **3**, 2191-2201.
43. L. M. Salonen, M. Ellermann and F. Diederich, *Angew. Chem. Int. Ed.*, 2011, **50**, 4808-4842.
44. E. Persch, O. Dumele and F. Diederich, *Angew. Chem. Int. Ed.*, 2015, **54**, 3290-3327.
45. A. S. Fawcett and M. A. Brook, *Macromolecules*, 2014, **47**, 1656-1663.
46. A. S. Fawcett, T. C. Hughes, L. Zepeda-Velazquez and M. A. Brook, *Macromolecules*, 2015, **48**, 6499-6507.
47. W. Hayes and B. W. Greenland, in *Supramolecular Polymer Networks and Gels*, ed. S. Seiffert, Springer, 2015, vol. 268, pp. 143-166.
48. S. Burattini, B. W. Greenland, D. H. Merino, W. Weng, J. Seppala, H. M. Colquhoun, W. Hayes, M. E. Mackay, I. W. Hamley and S. J. Rowan, *J. Am. Chem. Soc.*, 2010, **132**, 12051-12058.
49. K. Dušek and M. Dušková-Smrčková, *Prog. Polym. Sci.*, 2000, **25**, 1215-1260.
50. B. B. Boonstra, H. Cochrane and E. M. Dánenberg, *Rubber Chem. Tech.*, 1975, **48**, 558-576.

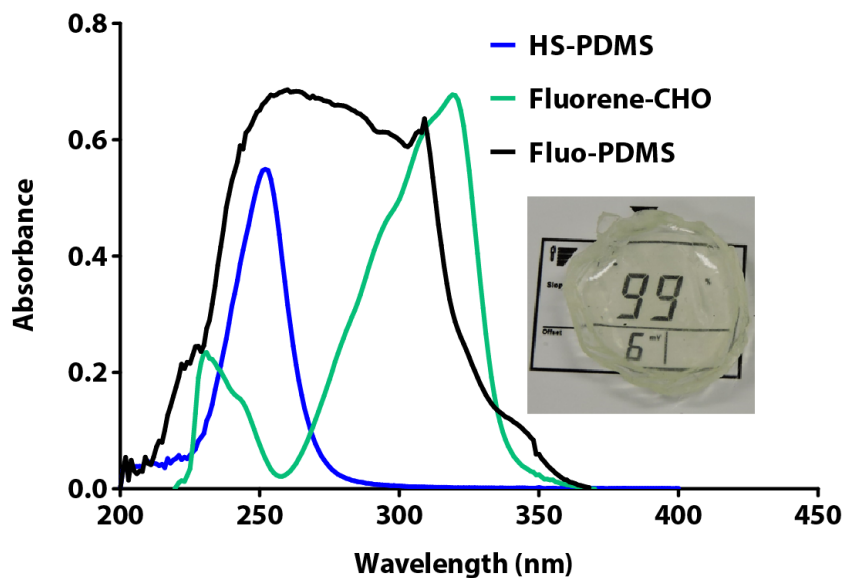
## 5.9 Appendix 5: Chapter 5 Supporting Information

### Effect of different acids on the thioacetalization process

Table S1. Efficacy of acidic catalyst and optimization of the thioacetalization reaction

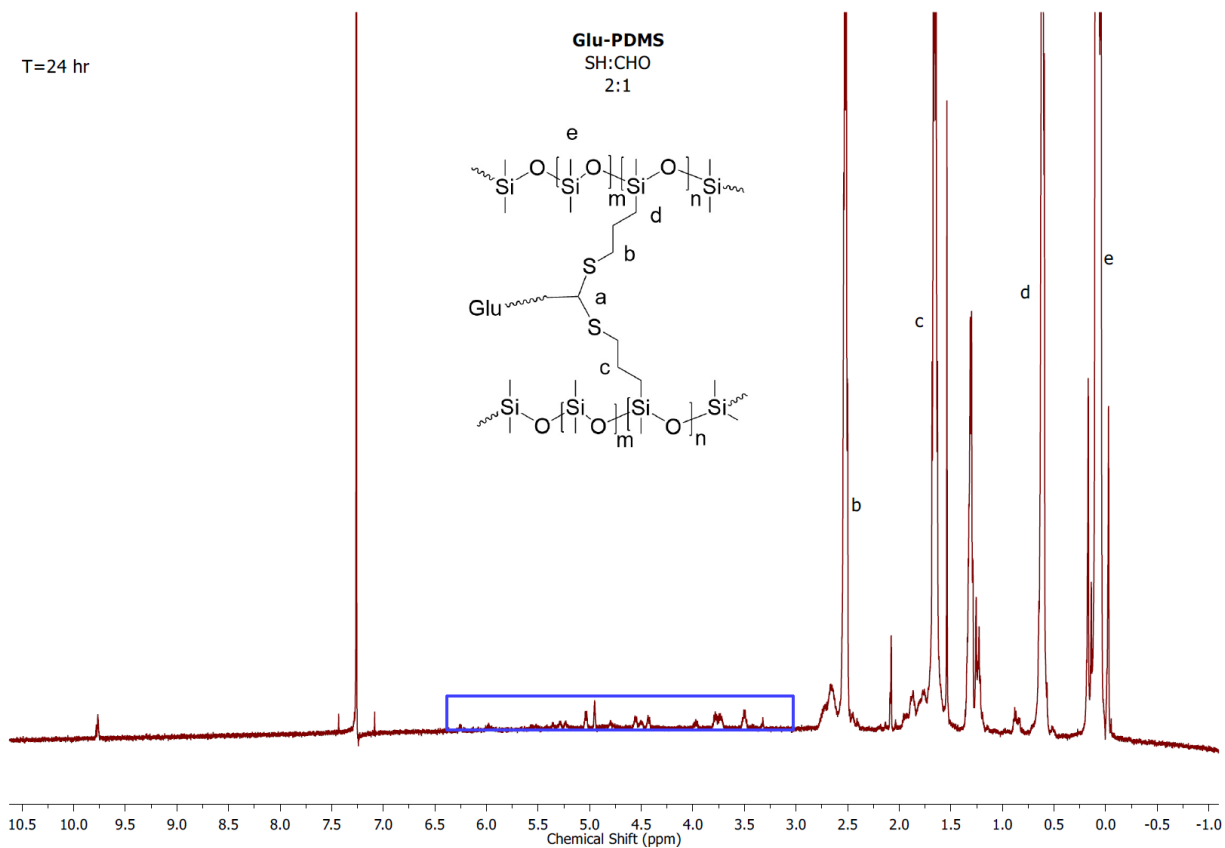
Entry	Catalyst (ppm)	Observation
1	BF <sub>3</sub> ·OEt <sub>2</sub> (50 ppm)	reaction too fast, irreproducible (does not disperse efficiently in PDMS), transparent elastomer,
2	AlCl <sub>3</sub> (200 ppm)	reaction too fast, irreproducible (long induction time then extremely rapid reaction), transparent elastomer
3	MsOH (150 ppm)	reaction controllable, reproducible (dispensing less convenient), transparent elastomer
4	p-TsOH (150 ppm) (~0.25mol% vs HS-PDMS)	reaction controllable, reproducible, flexible, transparent elastomer

Changes in UV-Visible Absorption during cure of silicones using Fluorene-CHO

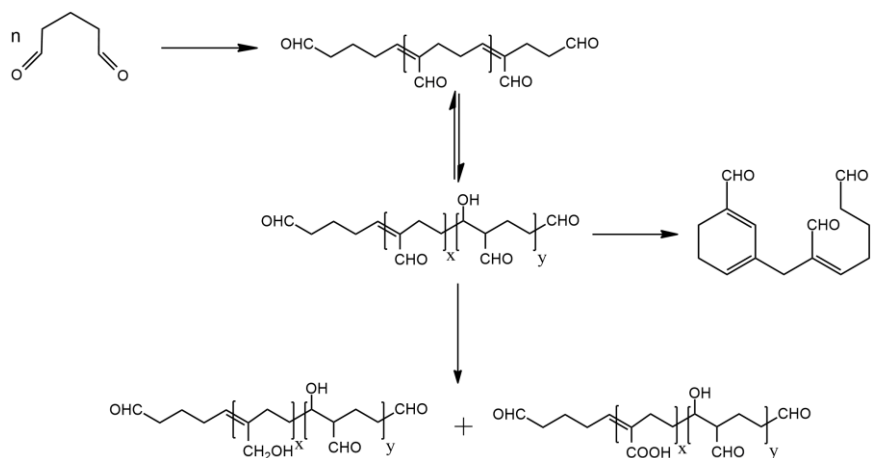


**Figure S5.1** UV-vis absorption spectra of (a) **SMS 022**; (b) Fluorene-2-carboxaldehyde and (c) **Fluo-PDMS**, where **Fluo-PDMS** shows a blue shift upon the consumption of the aldehyde functionality during dithioacetal formation. Photo (inset) of **Fluo-PDMS**.

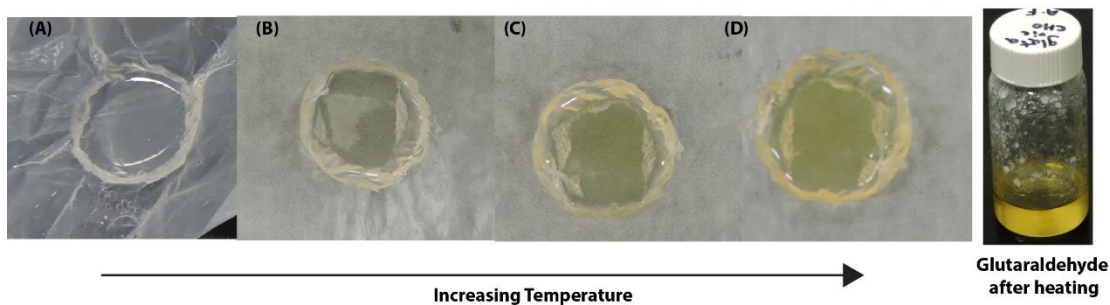
**Differences between glutaraldehyde and aromatic aldehydes as crosslinkers.**



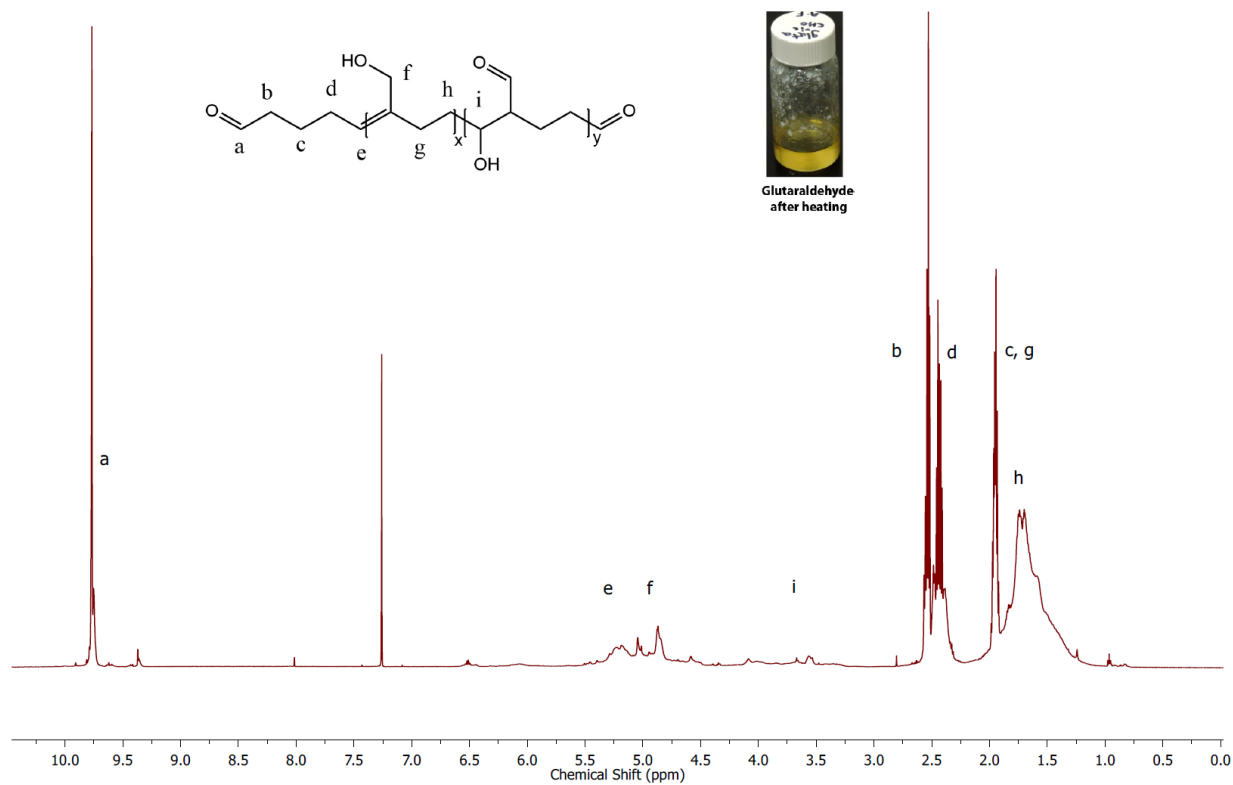
**Figure S5.2** <sup>1</sup>H NMR spectrum (600 MHz, CDCl<sub>3</sub>) of **Glu-PDMS** elastomer at 60 °C after 24 h reaction (above) showing the inefficiency of aliphatic aldehydes for the formation of silicone dithioacetals. The blue box shows characteristic dithioacetal protons ( $\delta=4.81$  ppm) accompanied by aldol products.



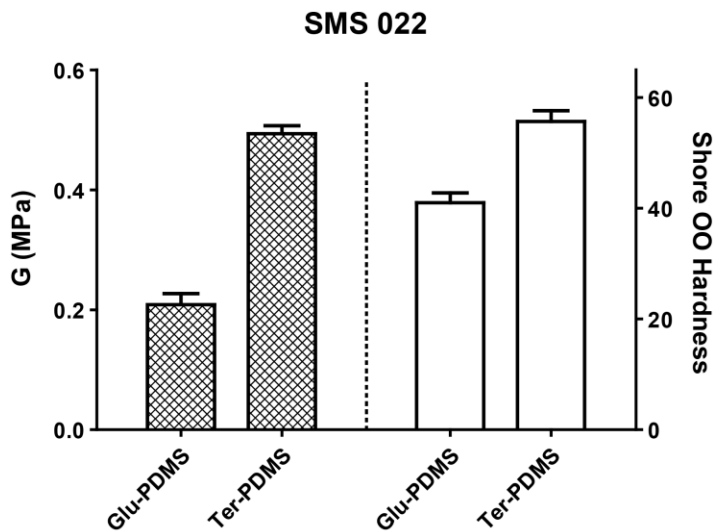
**Figure S5.3** Possible structures of poly(glutaraldehyde)-derived components found in the mercaptopropylsilicones cured using glutaraldehyde.<sup>1, 2</sup>



**Figure S5.4** Thermal stability of **Glu-PDMS** (A) room temperature (B) 80 °C (C) 100 °C and (D) 130 °C. To the right, glutaraldehyde after heating at 80 °C.

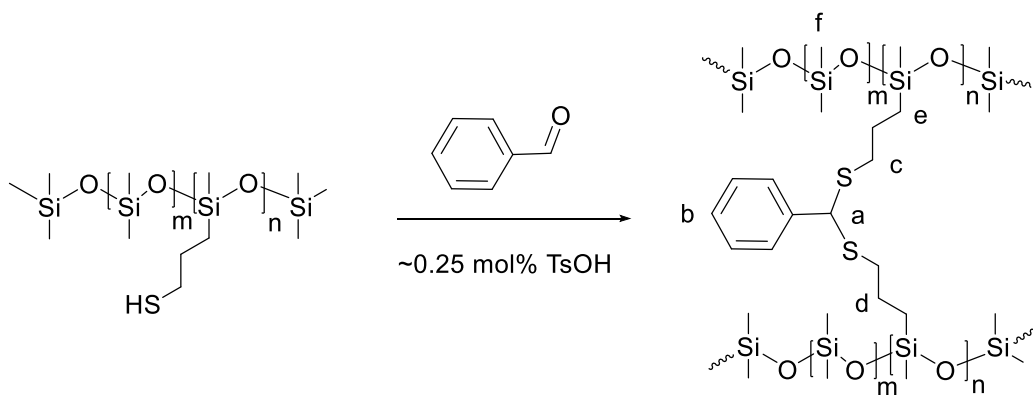


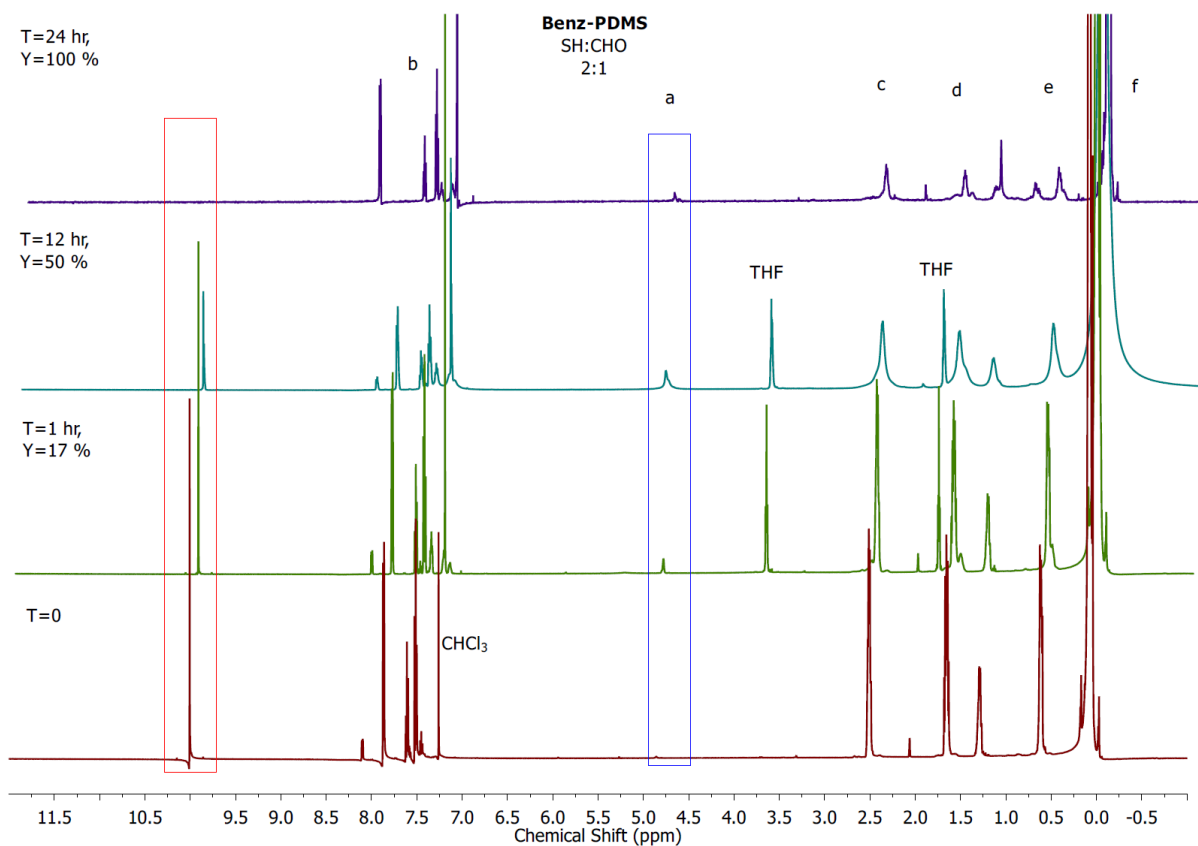
**Figure S5.5**  $^1\text{H}$  NMR spectrum (600 MHz,  $\text{CDCl}_3$ ) of glutaraldehyde after heating overnight at 80  $^\circ\text{C}$ .



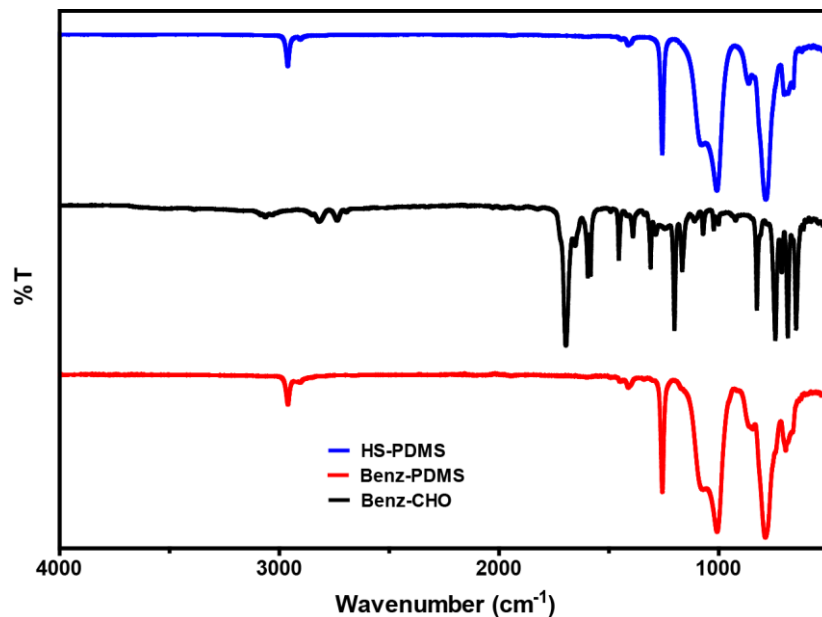
**Figure S5.6** Comparison of stoichiometric amounts of aliphatic and aromatic aldehydes in the formation of silicone dithioacetals (products with glutaraldehyde were accompanied by aldol reactions, see above).

**Curing of silicone dithioacetals using benzaldehyde**



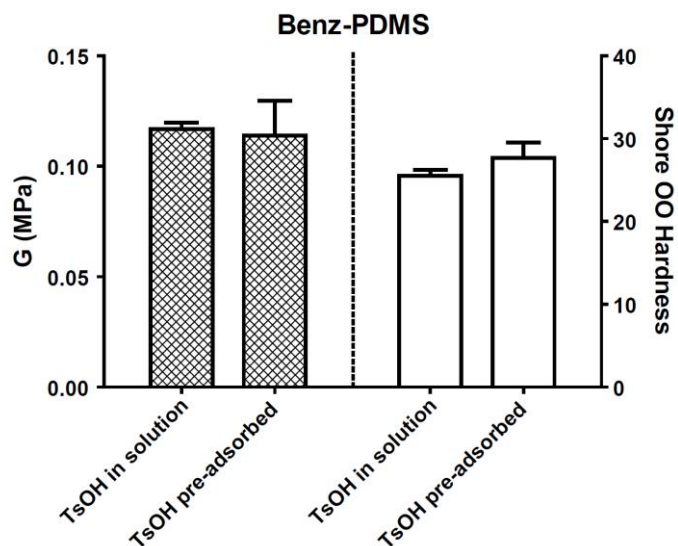


**Figure S5.7** Stacked <sup>1</sup>H NMR spectra (600 MHz, CDCl<sub>3</sub>) of benzaldehyde/HS-PDMS mixture in stoichiometric amounts and corresponding elastomers at room temperature over the course of 24 h. The blue box shows characteristic dithioacetal protons ( $\delta=4.81$  ppm) while the red box shows disappearance of aldehydic protons ( $\delta=10.00$  ppm).



**Figure S5.8** FTIR-ATR spectra of HS-PDMS, Benzaldehyde and Benz-PDMS.

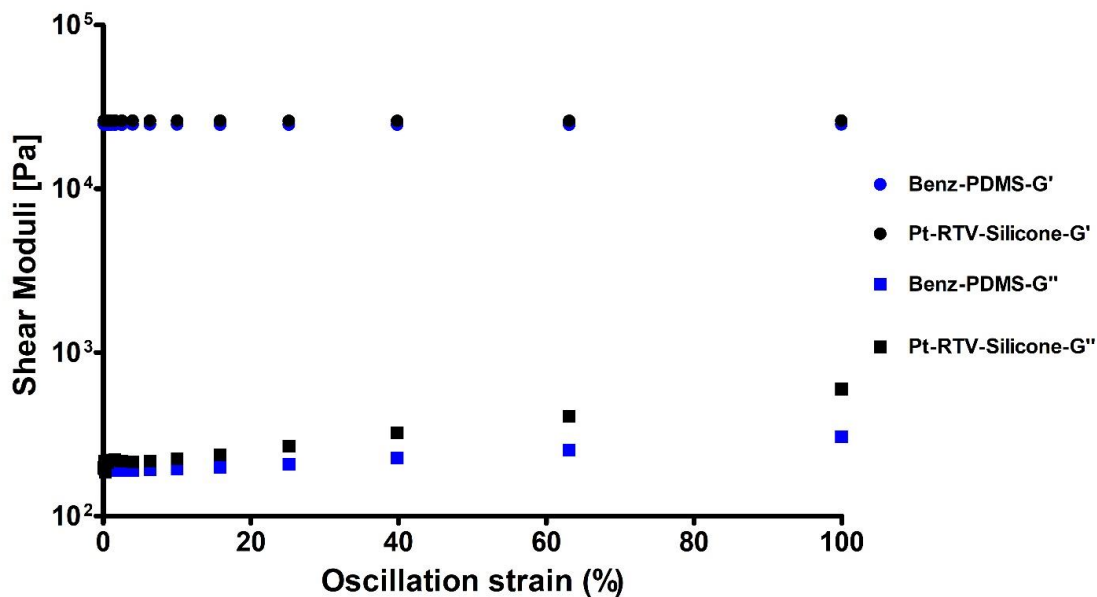
#### Pre-adsorption of *p*-TsOH on silica



**Figure S5.9** Comparison of elastomer outcomes of *p*-TsOH addition with and without pre-adsorption onto silica (1 wt%). Reactions occurred smoothly. Young's moduli tracked well with silica incorporation.

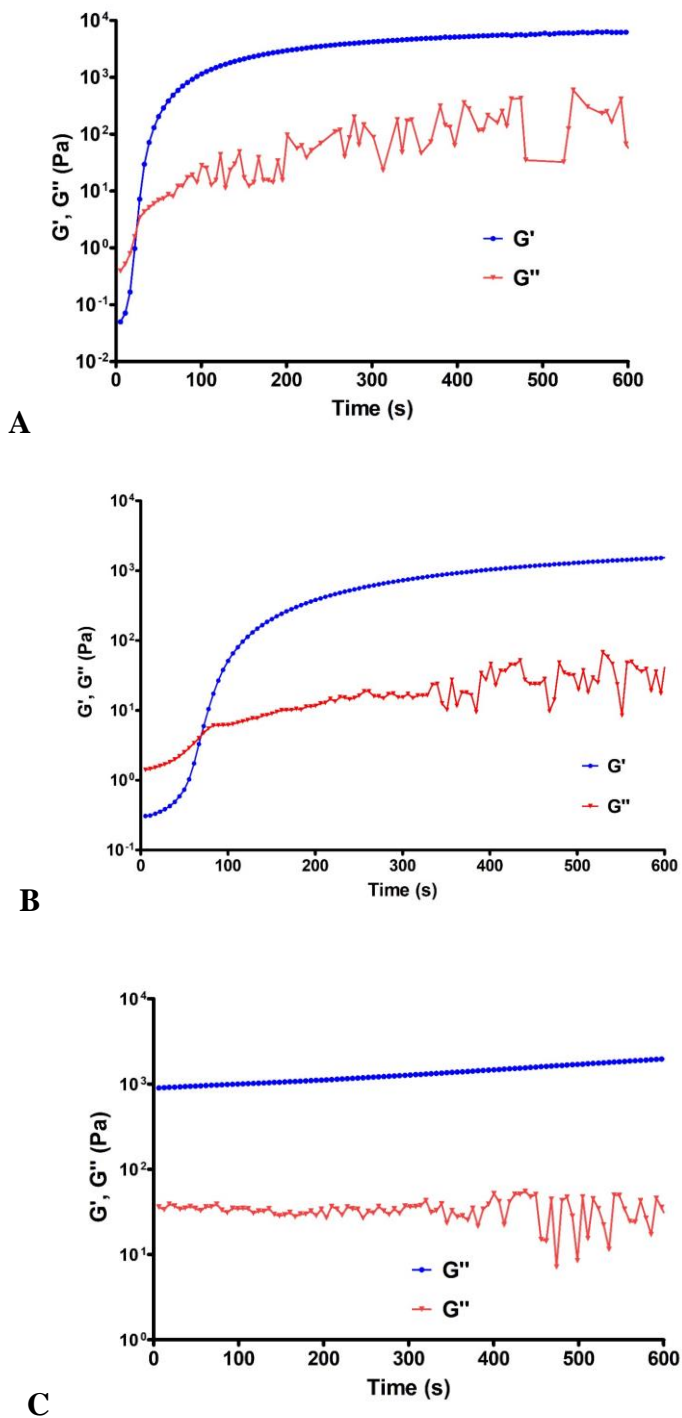


**Physical property similarities between thioacetal cured and traditional hydrosilylation cured silicones.**



**Figure S5.10** Shear modulus of **Benz-PDMS** and platinum-cured silicone rubber (logarithmic scale) with increasing shear strain, showing the different cure chemistries result in elastomers with similar properties. Neither silicone contained silica fillers.

### Critical gel point determination

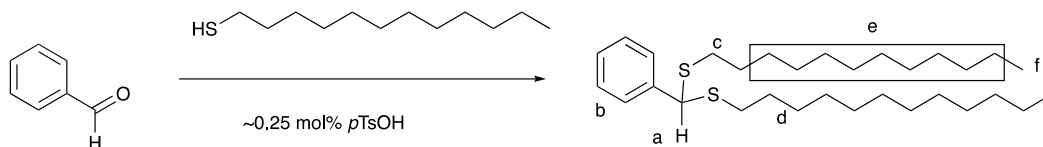


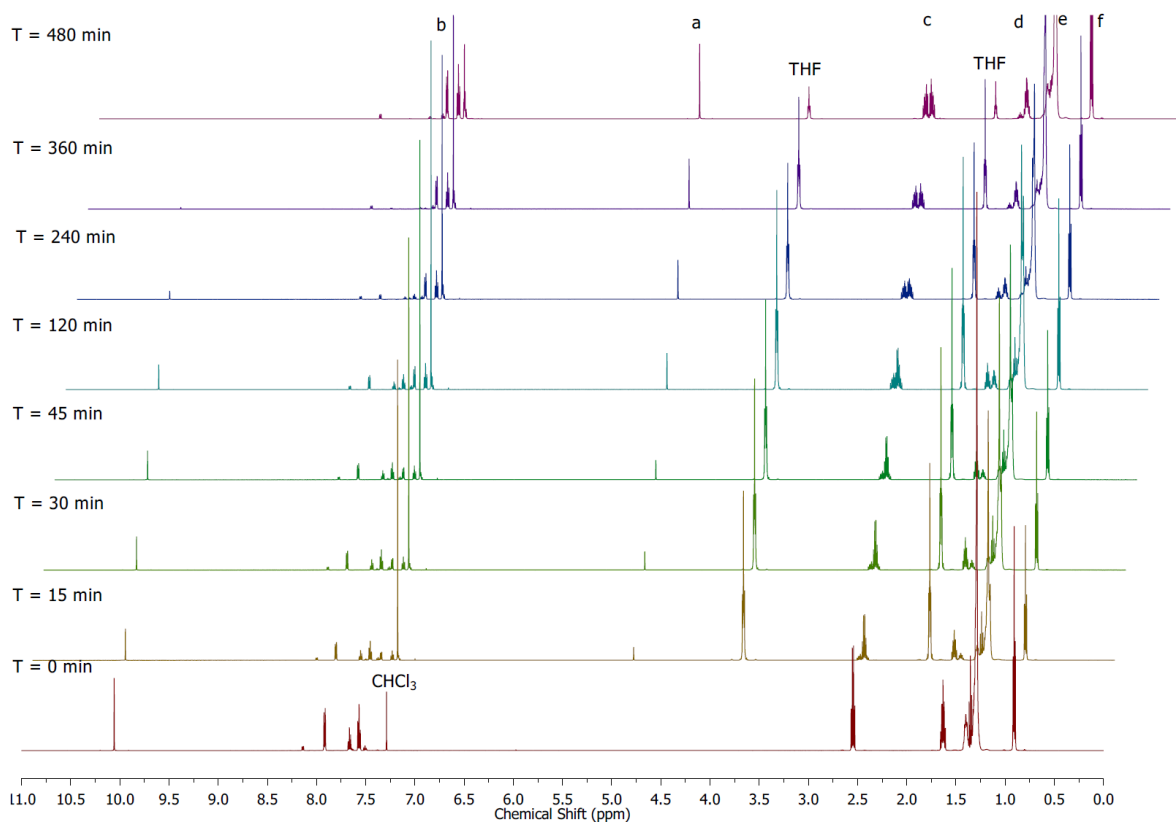
**Figure S5.11** Shear moduli as a function of time during crosslinking reaction of Benz-PDMS under  $6.28 \text{ rad} \cdot \text{s}^{-1}$  for 600s at  $60^\circ \text{C}$ . A: (unfilled); B: (1% silica); and C: (5% silica).

**Model Reaction of dodecanethiol with benzaldehyde: Preparation of (phenylmethylene)bis(dodecylsulfane)**

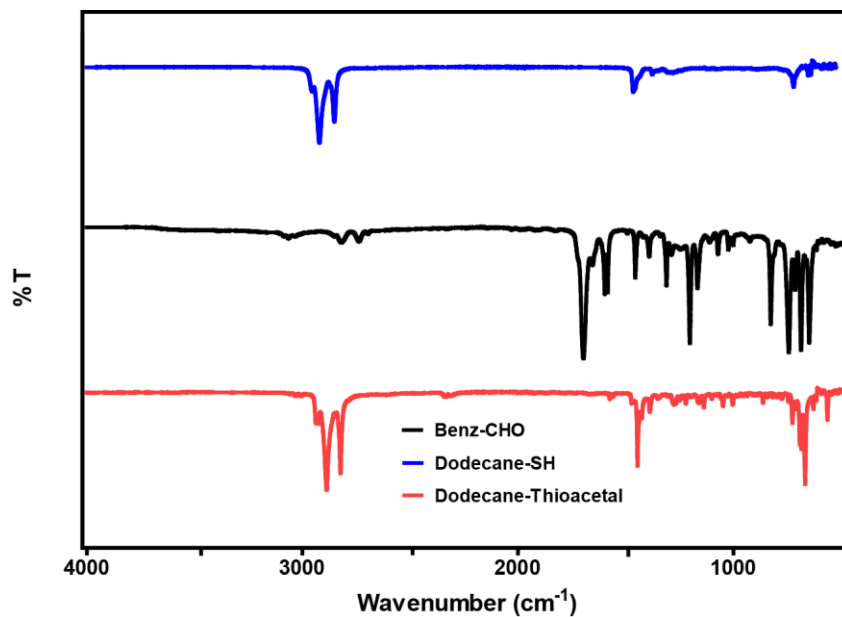
To 1-dodecanethiol (1g, 4.94 mmol, 1.183 mL) weighed into a glass scintillation vial containing benzaldehyde (0.262g, 2.47 mmol, 0.251 mL) was added *p*-TsOH (1.262 mL of a 0.0105M solution dissolved in 50 % THF/chloroform, 0.0132 mmol). The reaction mixture was stirred (1000 rpm) at room temperature over the course of 8 h with 100  $\mu$ L aliquots taken at various time intervals and analyzed by  $^1\text{H}$  NMR spectroscopy to permit on to track the changes in functional group concentrations during dithioacetal formation.

To track pH changes during the reaction, the reaction mixture (200  $\mu$ L) at  $t = 0$  (pipetted immediately after adding the catalyst) was added to 10 mL of milliQ  $\text{H}_2\text{O}$  and the pH measured to be 4.04; at  $t = 8$  h ( at the end of the reaction) 200  $\mu$ L of reaction mixture was added to 10 mL of milliQ  $\text{H}_2\text{O}$  and the pH measured to be 4.01. Thus, there was no change in the acid concentration during thioacetalization.

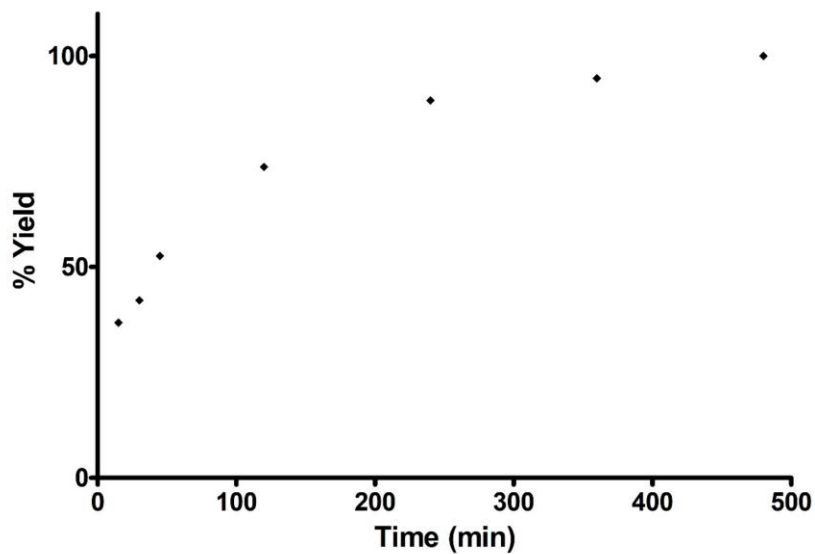




**Figure S5.12** Stacked <sup>1</sup>H NMR spectra (600 MHz, CDCl<sub>3</sub>) of model benzaldehyde/dodecane-thiol mixture in stoichiometric amounts. Showing characteristic dithioacetal protons ( $\delta=4.81$  ppm) with the disappearance of aldehydic protons ( $\delta=10.00$  ppm) at room temperature over the course of 8h.

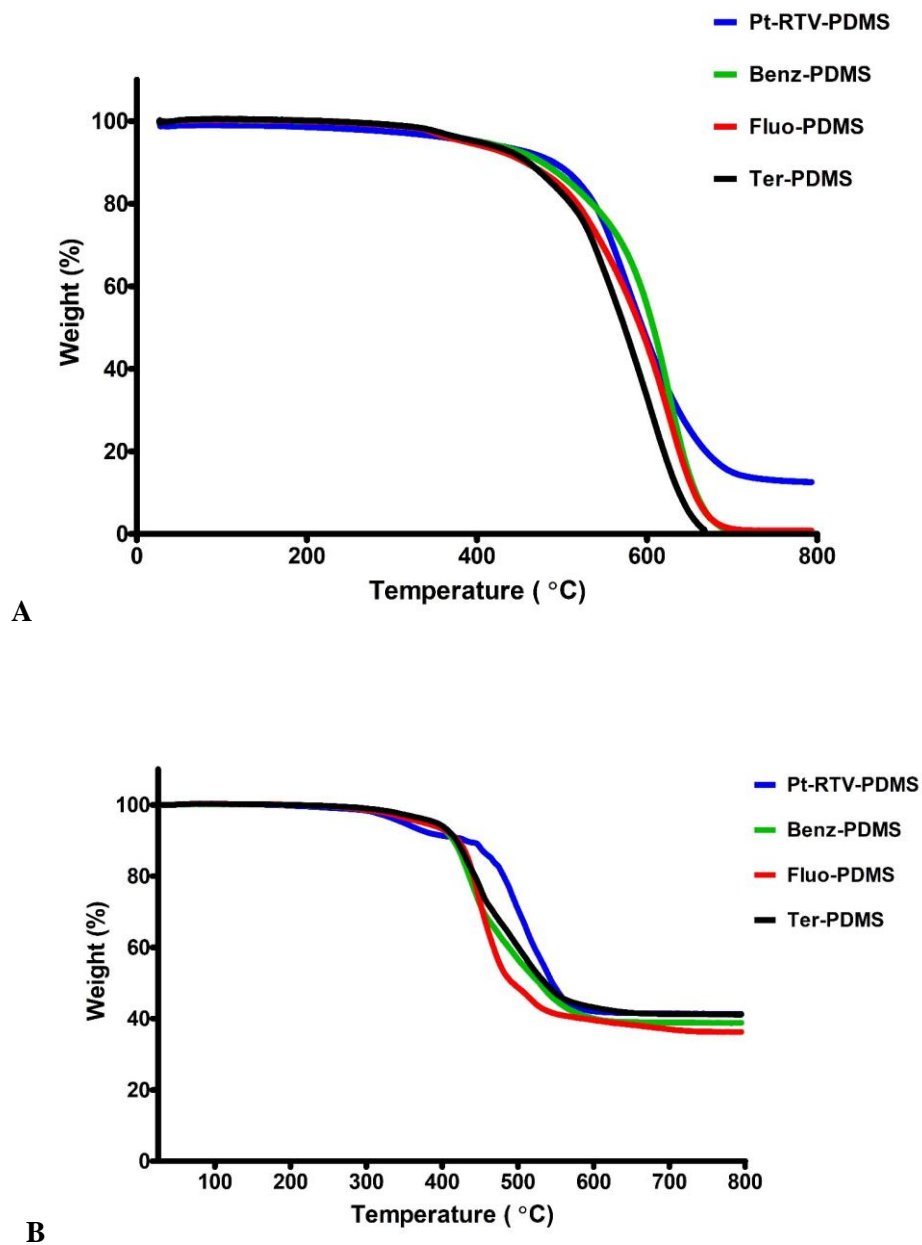


**Figure S5.13** FTIR-ATR spectra of dodecanethiol, benzaldehyde and dodecanethioacetal.



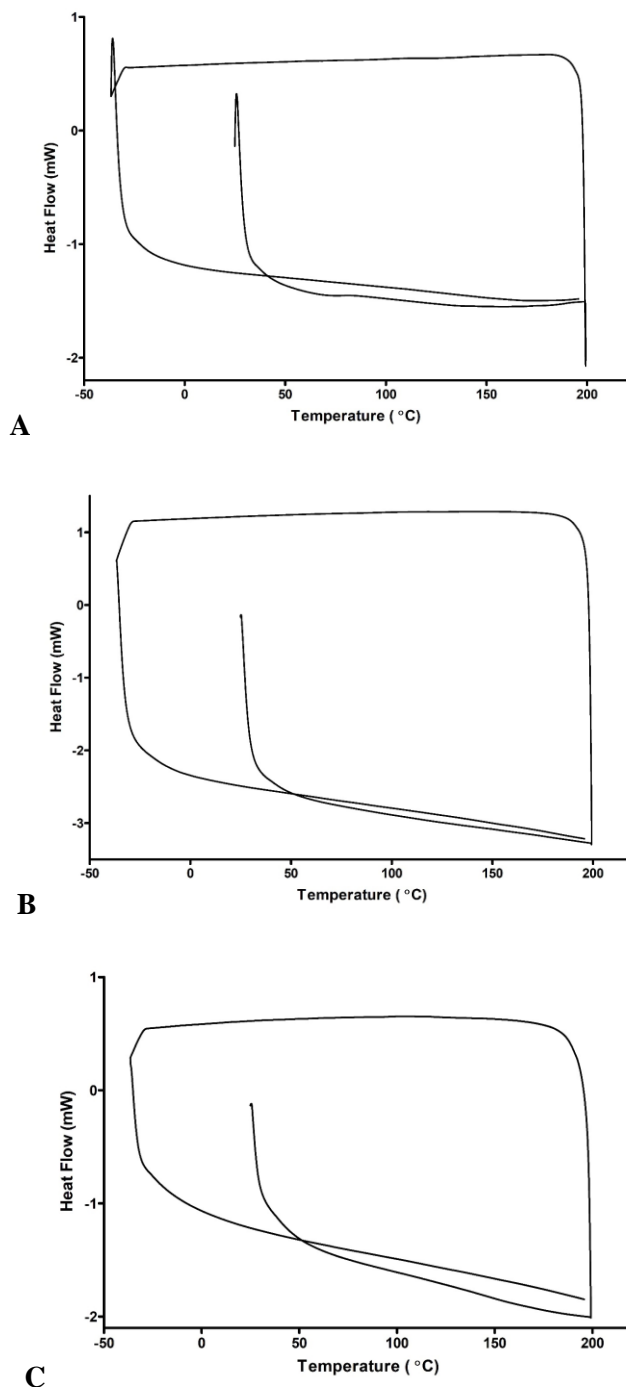
**Figure S5.14** Formation of dithioacetal as a function of reaction time for the dodecanethiol-benzaldehyde model study based on the overall conversion of benzaldehyde and dodecanethiol.

TGA data in argon demonstrating thermal stability of thioacetal linkages



**Figure S5.15** TGA thermograms of **Fluo-PDMS**, **Benz-PDMS**, **Ter-PDMS** and **Pt-RTV-PDMS**. A: under argon, B: in air (the samples did not contain silica fillers).

### Heat flow data of dithioacetal crosslinked silicones



**Figure S5.16** DSC thermograms of A: **Benz-PDMS** (unfilled); B: **Fluo-PDMS** (unfilled); and C: **Ter-PDMS** (unfilled).

## References

1. S. Margel and A. Rembaum, *Macromolecules*, 1980, **13**, 19-24.
2. C. Isabelle Migneault, *BioTechniques*, 2004, 37.



## **CHAPTER 6: One-step in-mould Modification of PDMS Surface and its Application in the Fabrication of Self-driven Microfluidic Channels\***

### **6.1 Abstract**

Poly(dimethylsiloxane) (PDMS) has become the material of choice for fabricating microfluidic channels for lab-on-a-chip applications. Key challenges that limit the use of PDMS in microfluidic applications are its hydrophobic nature, and the difficulty in obtaining stable surface modifications. Although a number of approaches exist to render PDMS hydrophilic, they suffer from reversion to hydrophobicity and, frequently, surface cracking or roughening. In this study, we describe a one-step in-mould method for the chemical modification of PDMS surfaces, and its use to assess the ability of different surfactants to render PDMS surfaces hydrophilic. Thin films of ionic and non-ionic surfactants were patterned into an array format, transferred onto silicone pre-polymer, and subsequently immobilized onto the PDMS surface during vulcanization. The hydrophilicity of the resulting surfaces was assessed by contact angle measurements. The wettability was observed to be dependent on the chemical structure of the surfactants, their concentration and interactions with PDMS. The morphology of modified PDMS surfaces and their change after wetting and drying cycles were visualized using atomic force microscopy. Our results show that while all surfactants tested can render PDMS surfaces hydrophilic through the in-mould modification, only those modified with PEG-PDMS-PEG copolymer surfactants were stable over wetting/drying cycles and heat treatments. Finally, the in-mould functionalization approach was used to fabricate self-driven microfluidic devices that

---

\* This chapter is reproduced from A. Fatona, Y. Chen, M. Reid, M. A. Brook and J. M. Moran-Mirabal, *Lab Chip*, 2015, 15, 4322-4330 with permission from the Royal Society of Chemistry, Copyright 2015 Royal Society of Chemistry. Fatona and Moran-Mirabal designed the experiments and analyzed the data. Fatona performed all experiments using surfactants provided by Chen while Reid helped with all AFM measurements. Fatona wrote the manuscript with additions, edits and guidance from both Brook and Moran-Mirabal.

exhibited steady flow rates, which could be tuned by the device geometry. It is anticipated that the in-mould method can be applied to a range of surface modifications for applications in analytical separations, biosensing, cell isolation and small molecule discovery.

## 6.2 Introduction

Advances in the microfabrication of microfluidic and biochip devices have made PDMS the material of choice for biomedical, analytical and biotechnological applications. The inherent properties of PDMS such as optical transparency, biocompatibility, gas permeability, widespread availability, low cost, and ease of fabrication have made it particularly attractive in lab-on-a-chip applications for biomedical diagnostics<sup>1-4</sup>. The biggest drawback in the use of PDMS for these applications is adsorption of proteins and small molecules<sup>5</sup>. Significant efforts have been made to introduce reactive chemical functionalities its hydrophobic nature, which prevents aqueous solutions from filling micron and nanometer-sized channels through capillary action and promotes device fouling through the non-specific onto PDMS surfaces to render them hydrophilic. Such strategies include the use of high-energy treatments in the form of ion plasma<sup>6,7</sup>, UV-O<sub>3</sub><sup>8,9</sup> and corona discharge<sup>10</sup> to introduce hydroxyl groups on the surface of PDMS, coating of PDMS surfaces with polar functionalities using chemical vapour deposition<sup>11</sup>, silanization<sup>12, 13</sup>, phospholipid bilayer<sup>14, 15</sup> or polyelectrolyte multilayer<sup>16, 17</sup> modifications, and more recently grafting of hydrophilic polymers to or from the surface of PDMS via ultraviolet/atom transfer radical polymerization<sup>18-21</sup>, hydrosilylation<sup>22</sup> and click chemistry<sup>23</sup>. While these interventions have proved successful, they can be limited in applications, have limited chemical stability, are hard to direct to specific sites within microfluidic channels, or involve multiple steps that make the process cumbersome or difficult to achieve within microdevices. More recently, a strategy was reported to make permanently wettable silicone elastomers, but the chemical steps necessary preclude its utilization in microfluidic channels<sup>24</sup>. Additional issues reported with some of these modifications include surface cracking and increased roughness, increased opacity, loss of elasticity and reversion to hydrophobicity over time<sup>25, 26</sup>. These issues limit the usefulness of modified PDMS surfaces and can prevent the subsequent immobilization of biomolecules or cause issues of biocompatibility. To address some of the challenges and

provide a simple solution to stable PDMS surface modifications, we have turned to silicone-based molecules as direct functionalization agents that preserve the inherent attributes of silicone elastomers.

In this manuscript, we present a one-step in-mould PDMS functionalization approach, where patterned moulds define the surface sites to be modified and the surface functionalization occurs during the PDMS vulcanization step. Using this method, arrays were prepared where ionic and non-ionic surfactants were applied to the elastomer surface during the curing process, leading to the spatial tethering of uncharged and charged alkyl/polymer chains on PDMS. This method allowed us to directly compare small molecule and block co-polymer surfactant modifications of PDMS surfaces. We investigated the effect of surfactant chemical structure, surfactant-PDMS interaction, drop-casting concentration, and morphology of the modified surface on the wetting properties of the modified surfaces. Through these experiments, we have identified treatments that render the PDMS surface hydrophilic even after repeated wetting/drying cycles and thermal treatment, and further show that the one-step in-mould surface modification approach can be used to produce hydrophilic microfluidic channels that can be filled through capillary action. We anticipate that similar surface modification strategies can be used to spatially pattern channels with functional groups for lab-on-a-chip devices used in analytical separations, biosensing, cell targeting and isolation, or small molecule discovery.

## **6.3 Experimental section**

### **6.3.1 Materials**

Seven ionic and non-ionic surfactants were used to modify PDMS surfaces: Sodium dodecyl sulphate (SDS), cetyl trimethylammonium bromide (CTAB) and Tween 20 were from Sigma-Aldrich (Oakville, ON), Silsurf A008-UP was from Siltech Corp (Toronto, ON), poly(ethyleneglycol)-silicone-poly(ethyleneglycol) (PEG-PDMS-PEG) non-ionic triblock copolymers with alkyl (o-Wet) and siloxane terminal functionalities (n-Wet and a-Wet, where a-Wet has a more highly branched siloxane) were provided by EnRoute Interfaces, Inc. (Hamilton, ON). Isopropyl alcohol was purchased from Caledon and all materials were used as received.

### **6.3.2 Fabrication of surface functionalized PDMS arrays**

In this study, the fabrication approach used soft lithography with masks made by xurography. Self-adhesive Teflon masks (Bytac® surface protection laminate, Sigma-Aldrich) defining 5 mm diameter, 220µm depth sample wells were designed by computer aided design (CAD) software and patterned using a blade cutter (Graphtec ROBOPRO CE5000, Irvine, CA). The Teflon masks were lifted off and adhered to clean polystyrene dishes. Thin surfactant films were formed inside the sample wells by drop casting either 8 µl of ionic (2, 5 and 10% wt/v in 7:3 IPA/water) or non-ionic (2, 5, and 10% wt/v in IPA) surfactant solutions into each well and allowing them to dry overnight. Silicone pre-polymer (10:1 wt% elastomer:hardener, Sylgard 184, Dow corning) was applied with a syringe around the Teflon mask and allowed to flow over the sample wells. This was left to cure at room temperature (RT) for 48 h on a level surface. The modified PDMS arrays were gently peeled off the Teflon mask and further cured at 60°C for 4 h. The arrays were then rinsed with isopropyl alcohol (IPA) to remove excess surfactant and returned to the oven to dry at 60°C for an additional 4 h. Finally, the modified surfaces were soaked in water for 20 h at RT and dried under a nitrogen stream.

### **6.3.3 Elastomer preparation using traditional platinum cure technique**

The wettability of the functionalized PDMS surfaces was assessed through static contact angle measured by the sessile drop method using an OCA 20 Future Digital Scientific system (Garden City, NY). Briefly, 1 µl of 18.2 MΩ/cm water (A10-Merck-Millipore system, Darmstadt, Germany) was dropped onto the modified PDMS surface and digital images were acquired. The average of measurements taken from 40 replicate surfaces is reported as the mean contact angle for the functionalized PDMS.

The morphology of the functionalized surfaces was visualized through Atomic Force Microscopy (AFM) using an Asylum Research MFP-3D Classic™ Scanning Probe Microscope (Santa Barbara, CA). The images were taken in tapping mode with aluminium reflex coated silicon cantilevers (Veeco AC240TS-R3, Olympus) with nominal spring constant of 2 N/m and resonant frequency of 70 kHz.

### **6.3.4 Fabrication of surface-modified microfluidic devices**

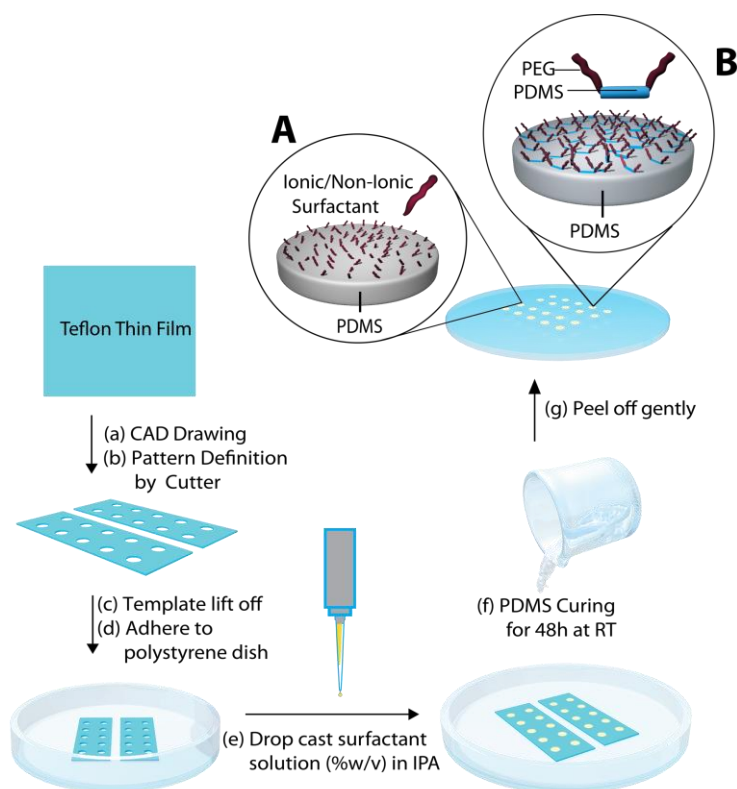
Self-adhesive vinyl film (80 $\mu$ m thickness, FDC-4300, FDC graphic films, South Bend, IN) was used in the fabrication of microfluidic channel moulds. Vinyl films were patterned into both linear and serpentine channel templates (0.1, 0.5, 1 mm width  $\times$  50 mm length) using a blade cutter (Graphtec ROBOPRO CE5000). These templates were lifted off with the aid of transfer tape and adhered to a clean polystyrene dish. Vinyl masks 0.1 mm wider than the microfluidic templates were also patterned and adhered around each template, leaving a space between the mask and the template. Each of the vinyl templates was coated with a thin film of a-Wet by drop casting 30  $\mu$ l of 10% solution (wt/v in IPA) over the template and allowing it to dry overnight at RT. The vinyl masks were then carefully removed. 1.2 cm Masterflex<sup>®</sup> Silicone tubing (1/16"  $\times$  0.189", Cole-Parmer Canada Inc.) was placed over each reservoir on the vinyl template to define inlet and outlet ports. Silicone prepolymer (10:1 wt% elastomer base:curing agent, Sylgard 184) was applied with a syringe around the coated vinyl and allowed to flow slowly over the template. After curing at RT for 24 h, the surface-modified modified microfluidic channel was cut using a scalpel, rinsed with IPA to remove excess surfactant, dried under nitrogen and adhered to a 75 mm  $\times$  25 mm microscope slide by applying even pressure.

## **6.4 Results and Discussion**

### **6.4.1 In-mould modification of PDMS surfaces**

A one-step in-mould modification process for the controlled spatial tethering of surfactant molecules at the PDMS surface was developed as a simple and cost-effective alternative to conventional surface grafting and modification approaches (Figure 6.1). The key concept behind the one-step modification is that exposure of the pre-polymer to surfactants during the vulcanization process can entrap the surfactant molecules through adsorption, hydrophobic binding, and/or entanglement at the PDMS interface and confer to it the surfactant's functionality (Figure 6.1, inset A). Furthermore, we hypothesized that by

choosing the right chemical structure of the surfactant molecules (*i.e.*, copolymers containing a PDMS block), they would be irreversibly entrapped by forming an interpenetrating network with the crosslinking polymer, yielding stable functional PDMS surfaces (Figure 6.1, inset B). The one-step in-mould functionalization process was used to produce arrays of PDMS surfaces modified with a range of surfactants. These arrays allowed us to compare the ability of the immobilized surfactants to convey a stable hydrophilic character to the PDMS surface.



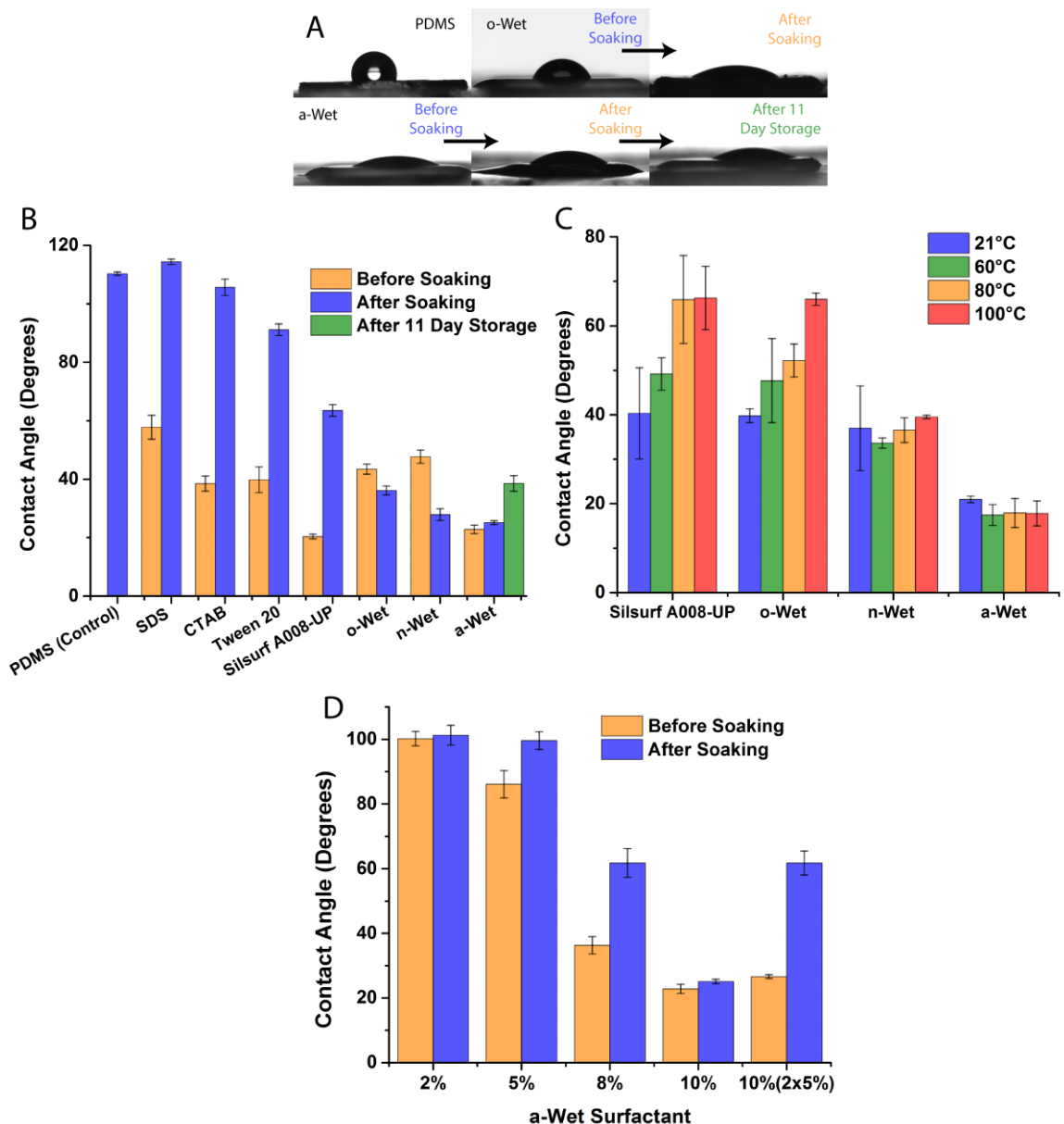
**Figure 6.1** Hydrophilic PDMS arrays: a schematic of the fabrication technique for immobilizing surfactant molecules onto PDMS surface. Insets: Schematics of proposed molecular conformation of adsorbed and/trapped surfactant molecules at the PDMS-air interface.

Seven sets of ionic and non-ionic surfactants were spatially patterned onto PDMS as illustrated in Figure 6.1. First, xurography was used to pattern individual wells into Teflon adhesive sheets. Then, the surfactant solutions were drop cast into each well and allowed to dry into thin films, after which the PDMS pre-polymer solution was applied and cured. The dry thin films made from non-ionic surfactant solutions appeared optically clear

(Figure S6.1). Such morphology was expected, as the non-ionic surfactants have been reported to form ordered reverse micelle multilayers upon drying.<sup>27</sup> In particular, non-ionic PEG-PDMS-PEG block co-polymer surfactants were expected to form multilayers, where the PEG moiety would reside at the core and the hydrophobic PDMS would be exposed at the air interface, which would allow them to become entrapped in the interpenetrating network of the cured PDMS material. On the other hand, films deposited from ionic surfactant solutions were opaque (Figure S6.1, Appendix 6), since the ionic surfactants crystallized as the solvent was removed. The observed thin film morphology was transferred to the PDMS surface during the curing/moulding process and was visible under the optical microscope after the PDMS surfaces were peeled off from the Teflon moulds (Figure S6.2, Appendix 6). Extensive rinsing of the modified surfaces with water produced optically clear areas for all surfactant treatments (Figure S6.3, Appendix 6). This indicated that immersion in water or rinsing could change the surface properties and/or topography.

#### **6.4.2 Wettability of modified PDMS surfaces**

The efficiency and reproducibility of the one-step modification method in producing stable hydrophilic surfaces was assessed by measuring sessile water droplet contact angles (WCA) on the surfactant-modified surfaces and comparing them against unmodified PDMS. It was observed that all surfactant films were stable and able to withstand the drag force of the uncured prepolymer mixture during the PDMS casting step. After peeling from the Teflon template, the one-step modification produced surfaces that exhibited uniform droplet spreading and wetting behaviour over the modified areas. This suggested the homogeneous transfer as well as full coverage of surfactant molecules within each of the circular modified areas.



**Figure 6.2** Water contact angle (WCA) measurements of surfactant functionalized PDMS surfaces. A) Representative images of WCA measurements performed on PDMS surfaces as prepared before soaking, after soaking and after 11 days of storage in air. B) Quantification of WCA measurements for all surfactant-modified PDMS surfaces. C) Quantification of WCA measurements for surfactant modified PDMS surfaces at different temperatures. D) WCA measurements of PDMS surfaces functionalized with thin films produced by a-Wet solutions cast at different concentrations. Error bars represent the standard error ( $n > 7$ ).



Figure 6.2 depicts the wettability of PDMS surfaces functionalized by each of the surfactant molecules. All seven surfactants tested led to hydrophilic surfaces after the one-step in-mould modification, with contact angles significantly below that of unmodified PDMS ( $109^\circ$ ). Surfaces that were functionalized by trapping/adsorbing ionic surfactants SDS and CTAB yielded WCA of  $57^\circ$  and  $38^\circ$  respectively. Tween 20 (a non-ionic PEG(20)sorbitan monolaurate surfactant) and Silsurf A008-UP (a non-ionic, low molecular weight ethoxylated PDMS surfactant commercially available as a silicone super-wetter) also demonstrated a significant drop in the hydrophobicity of the treated PDMS surfaces, as they were hydrophilic with WCA of  $39^\circ$  and  $20^\circ$ , respectively. Finally, surfaces functionalized with PEG-PDMS-PEG triblock co-polymers o-Wet, n-Wet and a-Wet were all hydrophilic with WCA  $43^\circ$ ,  $47^\circ$  and  $22^\circ$ , respectively. The contact angle measurements show that all the surfactant-functionalized surfaces were rendered hydrophilic through the one-step in-mould PDMS functionalization process.

The stability of the hydrophilicity of modified surfaces and the strength of PDMS-surfactant interactions were tested by soaking the treated PDMS surfaces in  $18.2\text{ M}\Omega$  water for 20 hours. Figure 6.2B shows that in most cases, soaking the treated surfaces led to a drastic change in the contact angle. As expected, there were weak interactions between PDMS and the ionic surfactants, which were solvated as the modified surfaces were soaked in water. Thus, soaking the surfaces left behind bare PDMS surfaces that were hydrophobic in nature (WCA of  $114^\circ$  and  $106^\circ$  for SDS and CTAB, respectively). Similar scenarios were observed after soaking Tween 20 and Silsurf A008-UP modified surfaces, but with milder effects (they exhibited WCA of  $91^\circ$  and  $63^\circ$ ). The incomplete reversion toward hydrophobicity can be explained as the result of an increased interaction of non-ionic surfactants with the hydrophobic PDMS surface. Nevertheless, prolonged exposure to an aqueous environment or fluid flow has been observed to lead to full reversion of surfaces treated with Tween 20 or the Silsurf A008-UP silicone super-wetter (data not shown). On the other hand, surfaces treated with the three PEG-PDMS-PEG block copolymers o-Wet, n-Wet and a-Wet remained hydrophilic after soaking (Figures 6.2A-B). This suggests that the triblock copolymers were effectively entrapped in the silicone network at the PDMS interface during the polymerization step. Furthermore, it was observed that after soaking, o-Wet and n-Wet treated surfaces exhibited a drop in contact angle values to  $36^\circ$  and  $27^\circ$ ,

respectively. This observation suggests a rearrangement of the surfactant molecules at the surface mediated by hydration. The third triblock copolymer a-Wet showed highly stable hydrophilic behaviour, as it only exhibited a slight increase in contact angle from 22° to 25° after soaking and remained hydrophilic (WCA of 40°) even after 11-day storage in dry conditions on the bench top.

The impact of temperature on the hydrophilicity of triblock copolymer and Silsurf-modified PDMS surfaces was also investigated. The treated surfaces were soaked for two hours, dried with nitrogen and incubated at different temperatures for one hour prior to measuring their WCA. Figure 6.2C shows that surfactants Silsurf A008-UP and o-Wet exhibit an increase in contact angle as the temperature is increased, indicating a loss of the exposed surfactant or a collapse of the hydrophilic moieties in the surfactant as the modified surface is dried at higher temperatures. On the other hand, triblock copolymer surfactants n-Wet and a-Wet showed stable wettability under the temperature conditions tested. It must also be noted that at temperatures higher than 21°C the o-Wet treated surfaces required a couple of minutes incubation time with the water droplet for the contact angle to stabilize to the values reported in Figure 6.2C, indicating that rehydration of the dry surfactant on the surface is important for it to display its hydrophilic properties. These experimental results demonstrate that all surfactants tested can be used in the one-step in-mould modification protocol to produce hydrophilic PDMS surfaces, but that only the triblock copolymers that are entrapped at the interface show stability against wetting/drying cycles. The retention of hydrophilicity after washing/drying cycles, prolonged storage and temperature treatment shows that a-Wet modified surfaces do not readily undergo reversion to hydrophobicity, as many other PDMS surface modifications do, making it an excellent candidate for the permanent modification of silicone surfaces.

### **6.4.3 Effect of surfactant concentration on wettability**

Since the surfactant a-Wet showed promising results for the production of stable hydrophilic PDMS surfaces, we further studied how the concentration of the surfactant impacted the wettability. To this end, a series of a-Wet solutions with 2-10% concentration were used and the WCA of the modified PDMS surfaces was assessed (Figure 6.2D). It

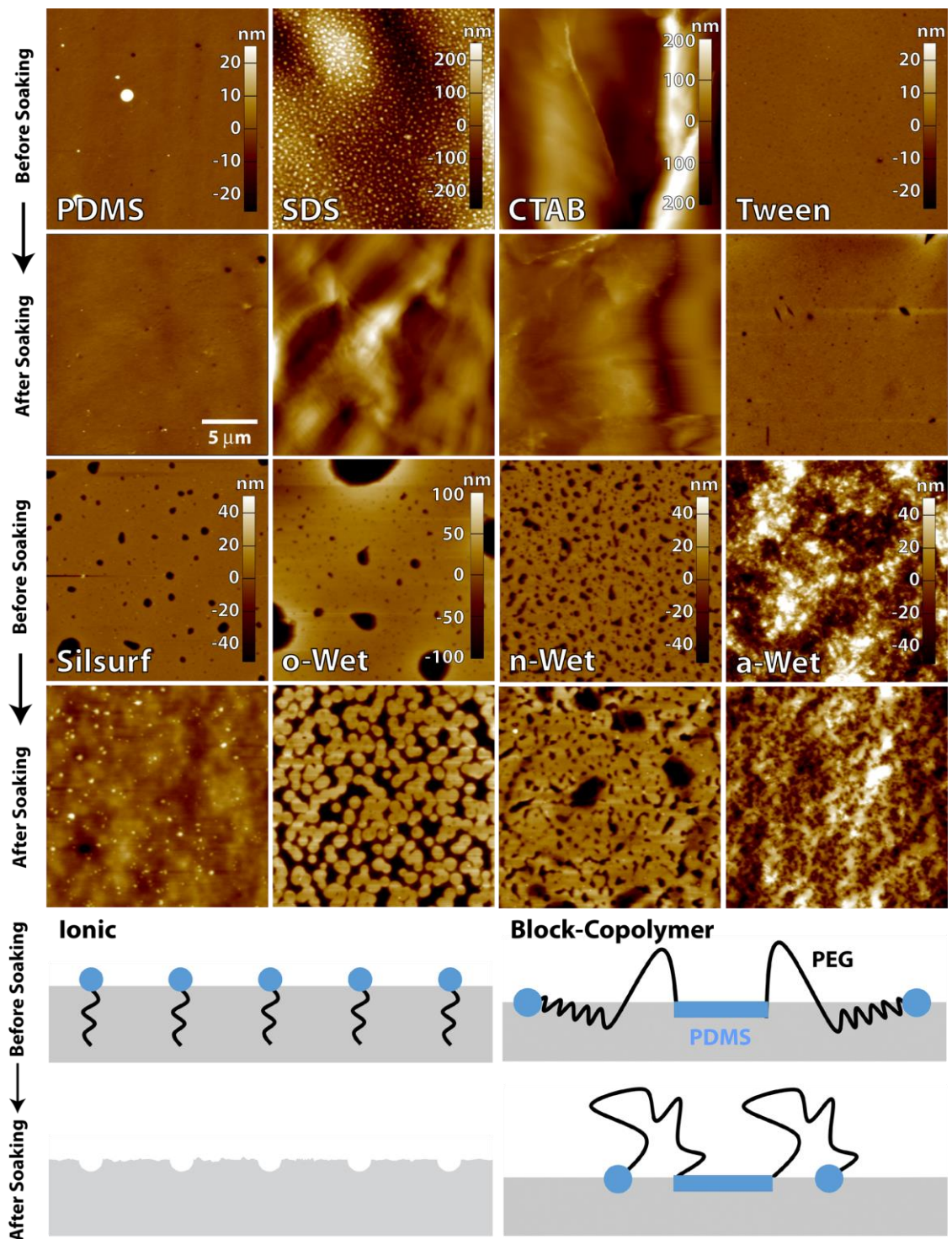
was observed that films produced with concentrations  $> 2\%$  readily increased the wettability of PDMS, with the most hydrophilic surfaces achieved by using 10% surfactant films. This suggests that a minimum amount of surfactant is needed to completely cover the 5 mm diameter sample wells cut into the mask used in the modification process. In addition, it was observed that some treatments (5 & 8%) exhibited significant increases in WCA after soaking. This can be attributed to insufficient surfactant immobilized in the well, which results in a fraction of the surfactant molecules that are not trapped within the interpenetrating network of PDMS and can thus be washed away in the soaking step leading to increased WCA values. Nevertheless, it is important to note that surface coverage and total surfactant mass are not the only requirements for a successful and stable surface modification. This was demonstrated by casting a 5% solution twice, which resulted in a film with the same mass of surfactant as one produced from a 10% solution and using the resulting film in the in-mould modification (Figure 6.2D). While the hydrophilicity before soaking resembled that of the 10% modification ( $23^\circ$ ), the contact angle after soaking underwent a drastic increase to  $\sim 60^\circ$ . This behaviour is attributed to the layer-by-layer deposition of the thin film, where the micellar arrangement of the first surfactant film was disrupted by the second surfactant application. Thus, to obtain a stable hydrophilic surface it was important to optimize the concentration of the surfactant solution used in the one-step in mould modification process.

#### **6.4.4 Surface morphology of functionalized PDMS surfaces**

To gain a better understanding of the surface chemistry of functionalized PDMS, AFM imaging was done on the surfactant-modified surfaces before and after soaking in water. This probed the dependency of the morphology of the modified surface on the chemical structure of the surfactant and its hydration state. All surfactant-modified surfaces were rougher than unmodified PDMS and exhibited changes in surface roughness before and after soaking (representative images shown in Figure 6.3). SDS and CTAB-modified PDMS showed roughened surfaces consistent with crystalline aggregates before soaking, which dissolved after soaking leaving behind highly structured, hydrophobic PDMS surfaces. Tween20 formed a highly uniform film on the PDMS surface and exhibited the

lowest surface roughness of all surfactants before soaking. After soaking, this surface remained relatively smooth with only a few depressions forming. This observation, coupled with the WCA measurements of Tween20-modified surfaces, suggest that this surfactant forms uniform ordered layers that can be dissolved during the soaking step, leaving behind a smooth hydrophobic PDMS surface. PDMS modified with the Silsurf super-wetter showed surfaces presenting small dimples with a narrow size distribution before soaking. However, after soaking the morphology was drastically changed, leaving behind structured surfaces with protruding spherical aggregates. The changes in morphology observed for ionic and non-ionic surfactants can be explained by a limited interaction between the curing PDMS and the surfactant molecules, which can be solvated upon exposure to the aqueous medium leaving behind an imprint that resembles the structure of the dried thin film of surfactant (schematic in Figure 6.3).

Surfaces functionalized with PEG-PDMS-PEG block copolymers displayed morphologies that are consistent with polymer entrapment and polymer chain rearrangement upon hydration. Before soaking, o-Wet and n-Wet functionalized surfaces showed relatively smooth surfaces with depressions that ranged in size from large (microns wide, o-Wet) to small (sub-micron wide, n-Wet). These morphologies underwent significant changes upon soaking in water. For o-Wet, the surface showed discrete sub-micron circular domains closely packed or fused together, which suggests that the exposed polymer chains self assembled into hydrophilic-hydrophobic domains. This is consistent with the structure of o-Wet, which has a long alkyl group pendant from the end of each PEG block. For n-Wet the changes were less pronounced, with the small depressions merging into larger ones and the depression size becoming more heterogeneous. On the other hand, the morphology of a-Wet-functionalized PDMS surfaces showed small random features that remained largely unchanged after soaking. This is consistent with the structure of the a-Wet surfactant, where the more highly branched pendant groups at the end of the PEG blocks are not large enough to become segregated upon soaking and remain randomly distributed on the surface, producing a uniformly hydrophilic surface. The topographical images before and after soaking agree with the spreading patterns observed during the WCA measurements. The change in morphology for o-Wet and n-Wet treated surfaces justifies the drop in contact angle upon soaking, as polymer chain rearrangement would swell the PEG blocks



**Figure 6.3** Representative atomic force microscopy height images of functional PDMS surfaces before and after soaking in aqueous solution. Below: Schematic of proposed molecular conformation of adsorbed and/trapped surfactant and triblock copolymer surfactant molecules at the PDMS-air interface before and after soaking.

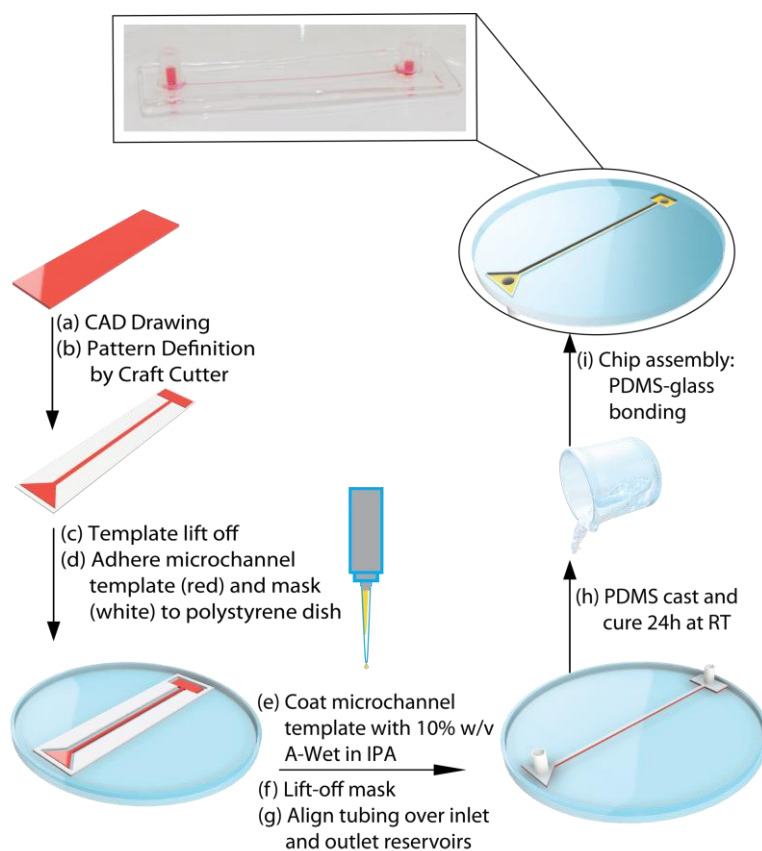
and leave them exposed towards the aqueous solution, rendering the surface more hydrophilic. Similarly, the limited change in a-Wet-treated surfaces mirrors the small change in WCA value, supporting the notion that due to the limited branching of siloxane pendants groups, the polymer is randomly distributed on the surface. The morphologies of surfaces functionalized with triblock copolymer surfactants are also similar to those reported for the chemical grafting of PEG onto PDMS.<sup>28, 29</sup>

Based on the wettability and AFM data we propose the following model for the surface functionalization with PEG-PDMS-PEG block copolymers through the one-step in-mould approach. The casting and drying of surfactant solutions within the mould produces ordered multilayers composed of reverse micelles where the PDMS blocks are exposed on the film surface. These blocks then interact with the silicone pre-polymer mixture during the crosslinking step, which breaks up the micelle aggregates and leads to the physical entrapment of the triblock surfactant molecules at the PDMS-air interface. This interaction produces a surface-confined interpenetrating polymer network with a fraction of the PEG blocks that, although in a partially collapsed state, remain exposed at the PDMS surface as the silicone substrate is lifted off the Teflon mask. The exposed PEG blocks confer to the modified PDMS surface the hydrophilicity observed before the soaking step. Upon soaking the modified surfaces in an aqueous solution, the PEG blocks swell in water, can adopt stretched conformations and interact with each other, leading to changes in the surface morphology (schematic in Figure 6.3). The extent of the rearrangement is strongly dependent on the nature of the functional groups appended to the end of the PEG blocks. The outcome of the in-mould surface functionalization approach coupled to the chemical structure of the surfactant used leads to hydrophilic PDMS surfaces that are highly stable over time.

#### **6.4.5 Fabrication of self driven microfluidic devices**

Having demonstrated the successful hydrophilization of PDMS surfaces using in-mould modification with a-Wet surfactant, we pursued the application of a similar approach for the fabrication of hydrophilic PDMS microfluidic devices. The fabrication process, shown in Figure 6.4, utilized xurography to create vinyl moulds (red) in the shape of the

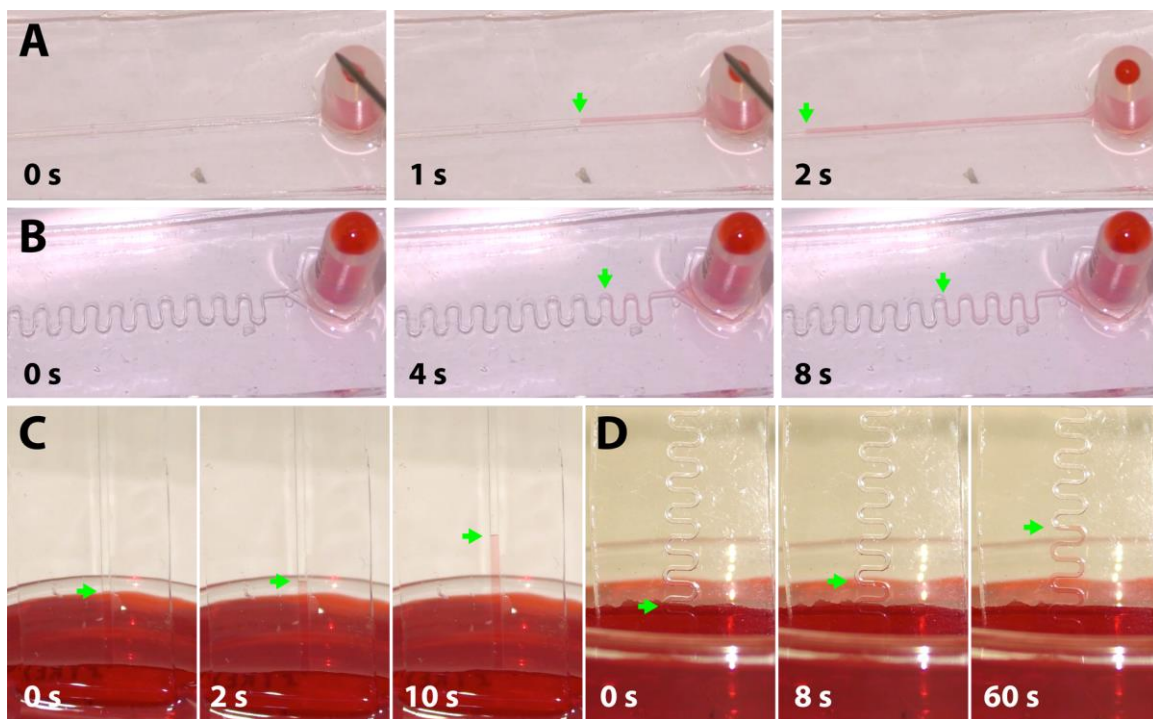
microfluidic channel. An additional layer was added as a surrounding mask (Figure 6.4, white) to confine



**Figure 6.4** Self-driven microfluidic device: a schematic of the fabrication technique for immobilizing surfactant molecules onto microfluidic channel surfaces via a one-step in-mould method.

the surfactant film applied and achieve the functionalization of the sidewalls of the microfluidic channel. This mask was removed after surfactant thin film deposition and prior to casting PDMS. The absence of this surrounding mask during the surfactant application caused the surfactant to flow over the mould and spread preferentially over the polystyrene dish, resulting in a loss in efficiency of the functionalization and decreased hydrophilicity (SV6.1, Appendix 6). A total of six microfluidic channel designs were fabricated including 3 linear and 3 serpentine channels with varied geometries (0.1, 0.5 and 1 mm widths, 80

$\mu\text{m}$  height, and 50 mm length). These were rendered hydrophilic using the in-mould modification process. The functionalized PDMS microfluidic layers were adhered to commercial glass slides that were not cleaned to avoid any capillary flow due to a hydrophilic glass surface. All the fabricated devices were shown to fill through steady capillary action even against gravity (Figure 4.5, SV6.2-6.4, Appendix 6), while unmodified PDMS control devices failed to fill at all (SV6.5, Appendix 6). The advantage of the fabrication technique presented here is that hydrophilic PDMS microfluidic channels that fill uniformly can be fabricated in one step through inexpensive bench-top methods.



**Figure 6.5** Capillary-driven filling of hydrophilic PDMS channels with aqueous solutions. Still frames of filling process of A) 0.5 mm wide linear and B) 0.1 mm wide serpentine channels filled horizontally, and 0.5 C) linear and D) serpentine channels filled vertically against gravity. Arrows indicate advancing fluid meniscus position.

Given that the flow rate within microfluidic channels is dependent on channel geometry, liquid viscosity, total flow resistance, and pressure differential, we compared the flow rates



generated experimentally within a-Wet modified microfluidic channels with those calculated theoretically. The flow rate  $Q$  in a capillary system is governed by the expression:

$$Q = \frac{1 \Delta P}{\eta R_F}, \quad (1)$$

where  $\eta$  is the viscosity of the liquid,  $\Delta P$  can be taken as the capillary pressure  $P_C$ , and  $R_F$  is the total flow resistance along the flow path. For our system,  $P_C$  at the liquid-air interface within the channel can be calculated from equation<sup>30</sup>

$$P_C = -\gamma \left[ \left( \frac{\cos \alpha_t + \cos \alpha_b}{h} \right) + \left( \frac{\cos \alpha_l + \cos \alpha_r}{w} \right) \right] \quad (2)$$

where  $\gamma$  is the surface tension of the liquid, while  $\alpha_{t,b,l,r}$  are the contact angles on the top, bottom, left and right walls of the channel. For top and sidewalls of the channel we used the contact angle measured for a-Wet-modified surfaces before soaking, while for the bottom wall we used an experimentally measured contact angle for non-cleaned glass slides of 54°. Furthermore, for the microfluidic channels used in this study the total flow resistance in rectangular channels was approximated by<sup>31</sup>

$$R_F = \left[ \frac{1}{12} \left( 1 + \frac{5h}{6w} \right) \frac{hwR_H^2}{L} \right]^{-1} \quad (3)$$

where  $h$  is the height (80  $\mu\text{m}$ ),  $w$  is the width (0.1, 0.5 or 1 mm),  $L$  is the length and  $R_H$  is the hydraulic radius of the microchannel, which was calculated as the ratio of the cross-sectional area by half the wetted perimeter,

$$R_H = \frac{A}{P/2} = \frac{hw}{h+w} \quad (3)$$

Using these equations, we estimated theoretical flow rates of 270, 1080 and 2530  $\text{nl s}^{-1}$  for linear functionalized microfluidic channels with widths of 0.1, 0.5 and 1 mm. The experimental flow rates measured were 40, 430 and 450  $\text{nL s}^{-1}$  for linear microfluidic channel with 0.1-, 0.5- and 1-mm widths respectively (cf. Figure 6.5, SV6.2, Appendix 6). The experimental flow rates were expected to be lower than the theoretical ones because they are influenced by reservoir geometry as well as any inhomogeneity in the fabricated device. Similarly, serpentine microfluidic channels had experimental flow rates of 2.4, 36 and 91  $\text{nL s}^{-1}$  for channel widths of 0.1, 0.5 and 1 mm respectively (cf. Figure 6.5, SV6.3, Appendix 6). These results show that the capillary flow rate can be tuned by changing the dimensions and channel morphology of hydrophilic PDMS microfluidic devices fabricated via the one-step in-mould modification using surfactant a-Wet. In addition, the observed flow rates are comparable to those reported in the literature for hydrophilic microfluidic devices fabricated by other methods<sup>30, 31</sup>. This highlights the ability of the developed method for generating self-driven microfluidic devices with steady flow rates in a simple and cost-effective manner.

## 6.5 Conclusions

This work introduces in-mould modification as a simple one-step fabrication method to spatially graft surfactant chains onto unstructured and structured PDMS surfaces. An array format was used to directly compare the hydrophilic nature of surfaces modified with ionic, non-ionic and block co-polymer surfactants. It was shown that although all surfactants tested could produce hydrophilic surfaces, only PEG-PDMS-PEG block co-polymer surfactants were stable against repeated wetting/drying cycles. Furthermore, surfaces modified with the a-Wet surfactant retained their hydrophilicity even after prolonged storage at the bench top. Changes in morphology of the modified surfaces support the notion that the entrapped surfactant chains can rearrange upon exposure to aqueous media, leading to potential changes in surface hydrophilicity. In addition, this work demonstrates the ability to fabricate hydrophilic PDMS microfluidic devices that can be self-driven by capillary force using a modified in-mould functionalization approach. We anticipate that similar strategies can be used to spatially pattern PDMS surfaces and microfluidic devices

Ayodele Fatona – Ph.D. Thesis McMaster University – Chemistry and Chemical Biology

with functional groups attached to molecules containing a PDMS moiety as a surface anchor. Despite the time required to fabricate the modified surfaces (~48 hours) and the need for masking techniques to confine the modifications to the inner walls of microfluidic channels, we believe this method holds potential as a simple and direct way to modify PDMS surfaces with functionalities for applications such as analytical separations, biosensing, cell targeting and isolation, or small molecule discovery.

## 6.6 Acknowledgements

We thank Dr. Emily Cranston for access to AFM equipment. This research was supported through the Natural Sciences and Engineering Research Council (RGPIN/418326) and a Canada Foundation for Innovation Leaders Opportunity Fund. A.F. is partially supported by the BioInterfaces CREATE grant. J.M.M. is the recipient of an Early Researcher Award through the Ontario Ministry of Research and Innovation. We thank EnRoute Interfaces for providing the silicone-based wetting agents.

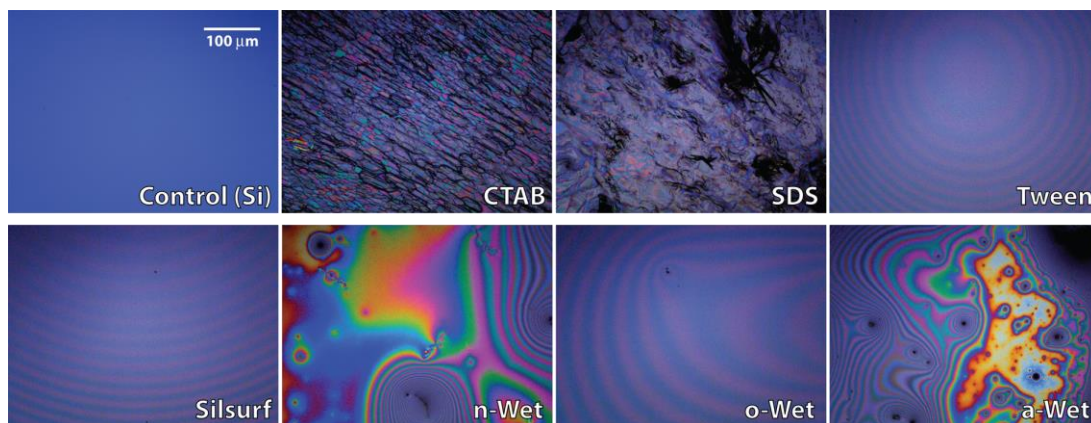
## 6.7 References

1. J. Zhou, D. A. Khodakov, A. V. Ellis and N. H. Voelcker, *Electrophoresis*, 2012, **33**, 89-104.
2. W. Zhang, D. S. Choi, Y. H. Nguyen, J. Chang and L. Qin, *Sci. Rep.*, 2013, **3**.
3. V. Sharma, M. Dhayal, Govind, S. M. Shivaprasad and S. C. Jain, *Vacuum*, 2007, **81**, 1094-1100.
4. M. Y. a. J. Fang, *Journal of Micromechanics and Microengineering*, 2012, **22**, 025012.
5. K. Boxshall, M.-H. Wu, Z. Cui, Z. Cui, J. F. Watts and M. A. Baker, *Surface and Interface Analysis*, 2006, **38**, 198-201.

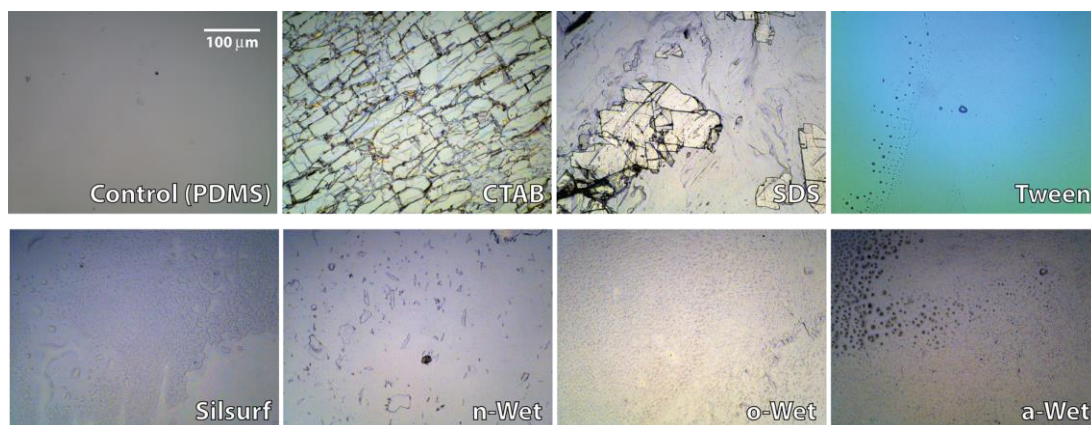
6. J. A. Vickers, M. M. Caulum and C. S. Henry, *Analytical chemistry*, 2006, **78**, 7446-7452.
7. J. Zhou, A. V. Ellis and N. H. Voelcker, *Journal of nanoscience and nanotechnology*, 2010, **10**, 7266-7270.
8. K. Efimenko, W. E. Wallace and J. Genzer, *Journal of Colloid and Interface Science*, 2002, **254**, 306-315.
9. Y. Berdichevsky, J. Khandurina, A. Guttman and Y. H. Lo, *Sensors and Actuators B: Chemical*, 2004, **97**, 402-408.
10. V. Di Virgilio, S. Bermejo and L. Castañer, *Langmuir*, 2011, **27**, 9614-9620.
11. J. Xu and K. K. Gleason, *Chemistry of Materials*, 2010, **22**, 1732-1738.
12. C. Séguin, J. M. McLachlan, P. R. Norton and F. Lagugné-Labarthe, *Applied Surface Science*, 2010, **256**, 2524-2531.
13. Z. Zhang, X. Feng, Q. Luo and B.-F. Liu, *Electrophoresis*, 2009, **30**, 3174-3180.
14. H. Mao, T. Yang and P. S. Cremer, *Analytical chemistry*, 2001, **74**, 379-385.
15. T. Yang, S.-y. Jung, H. Mao and P. S. Cremer, *Analytical chemistry*, 2000, **73**, 165-169.
16. H. Makamba, Y. Y. Hsieh, W. C. Sung and S. H. Chen, *Analytical chemistry*, 2005, **77**, 3971-3978.
17. Y. Liu, J. C. Fanguy, J. M. Bledsoe and C. S. Henry, *Analytical chemistry*, 2000, **72**, 5939-5944.
18. D. Xiao, H. Zhang and M. Wirth, *Langmuir*, 2002, **18**, 9971-9976.
19. S. Tugulu and H.-A. Klok, *Macromolecular Symposia*, 2009, **279**, 103-109.
20. L. K. Fiddes, H. K. Chan, B. Lau, E. Kumacheva and A. R. Wheeler, *Biomaterials*, 2010, **31**, 315-320.

21. C.-Y. Liao and Y.-C. Su, *Biomed Microdevices*, 2010, **12**, 125-133.
22. H. Chen, L. Wang, Y. Zhang, D. Li, W. G. McClung, M. A. Brook, H. Sheardown and J. L. Brash, *Macromolecular bioscience*, 2008, **8**, 863-870.
23. Z. Zhang, X. Feng, F. Xu, X. Liu and B.-F. Liu, *Electrophoresis*, 2010, **31**, 3129-3136.
24. M. A. Brook, Y. Wang and Y. Chen, *US 8,648,211*, (to McMaster University) 2014.
25. J. Zhang, Y. Chen and M. A. Brook, *Langmuir*, 2013, **29**, 12432-12442.
26. S. Hu, X. Ren, M. Bachman, C. E. Sims, G. P. Li and N. Allbritton, *Electrophoresis*, 2003, **24**, 3679-3688.
27. L. Song and Y. M. Lam, *Journal of nanoscience and nanotechnology*, 2006, **6**, 3904-3909.
28. A. Synytska, E. Biehlig and L. Ionov, *Macromolecules*, 2014, **47**, 8377-8385.
29. A. Synytska, E. Svetushkina, D. Martina, C. Bellmann, F. Simon, L. Ionov, M. Stamm and C. Creton, *Langmuir*, 2012, **28**, 16444-16454.
30. P. B. Lillehoj, F. Wei and C.-M. Ho, *Lab on a Chip*, 2010, **10**, 2265-2270.
31. M. Zimmermann, H. Schmid, P. Hunziker and E. Delamarche, *Lab on a Chip*, 2007, **7**, 119-125.

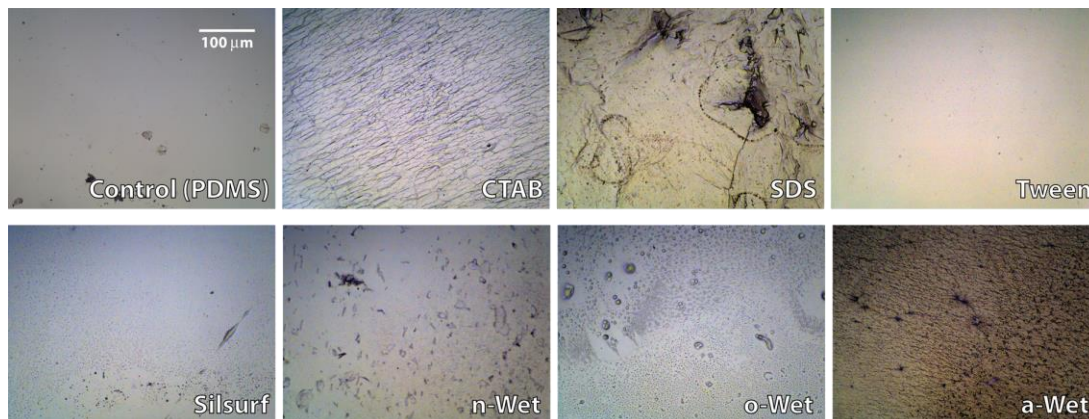
## 6.8 Appendix 6: Chapter 6 Supporting Information



**Figure S6.1** Optical microscopy images of surfactant thin films cast onto Teflon moulds adhered to silicon wafers. Small defects were observed on the surfactant surfaces due to dust particles in the environment.



**Figure S6.2** Optical images of surfactant films transferred onto PDMS array surfaces during the vulcanization step. The surfaces evidence structuring due to ionic surfactant crystal and non-ionic surfactant multilayer transfer.



**Figure S6.3** Optical microscopy images of surfactant modified PDMS surfaces after soaking in water for 20 hours. Changes in morphology are observed on the surfaces after soaking due to hydration and solvation of films or surfactant chain rearrangement.

**\*SV 6.1** Demonstration of operation of a microfluidic channel fabricated using the one-step in-mould approach without the use of a bounding mask during the a-Wet surfactant casting. Note that a “streak” is observed across the PDMS, which represents the surfactant flow during the prepolymer application. Also note that there is leakage through the end reservoir due to the hydrophilic nature of the flat surface outside the channel, which was functionalized by the flowing surfactant.



Supplemental\_Video\_1\_-\_Microchannel\_made\_without\_bounding\_mask\_-\_small2.mp4

**\*SV 6.2** Demonstration of the capillary force-driven filling of linear PDMS microfluidic channels modified with a-Wet surfactant using the one-step in-mould approach.



Supplemental\_Video\_2\_-\_Linear\_Microfluidics\_-\_small2.mp4

**\*SV 6.3** Demonstration of the capillary force-driven filling of serpentine PDMS microfluidic channels modified with a-Wet surfactant using the one-step in-mould approach.



Supplemental\_Video\_3\_-\_Serpentine\_Microfluidics\_-\_small2.mp4

**\*SV 6.4** Demonstration of the capillary force-driven filling against gravity of PDMS microfluidic channels modified with a-Wet surfactant using the one-step in-mould approach.



Supplemental\_Video\_4\_-\_Filling\_against\_gravity\_-\_small2.mp4

**\*SV6.5** Demonstration of lack of capillary force-driven filling of unmodified PDMS microfluidic channels.



Supplemental\_Video\_5\_-\_Unmodified\_Microfluidics\_-\_small2.mp4

Note \* : link to the videos can be found online using;

<https://pubs.rsc.org/en/content/articlelanding/2015/lc/c5lc00741k#!divAbstract>



## CHAPTER 7: General Conclusions

The unique properties of cellulose are attributed to the molecular construct of the glucan chains. The intra- and inter-molecular hydrogen bonding, in addition to van der Waals interactions within or along the glucan chains, allow for the establishment of hierarchical structures in cellulose. However, despite its surface hydroxyl groups, amphiphilic and moisture responsive nature, cellulose remains largely insoluble in water and in most common organic solvents or polymer matrices. The first half of this thesis focused on the modification of cellulose in order to tune its interfacial properties and reactivity and to improve our understanding of how small structural changes along the glucan backbone translate to (frequently substantial) changes in materials properties. The second half of the thesis demonstrated the development of a new class of cure technologies based on organic chemistry designed to further tune the physical properties of dimethylsiloxanes. These changes in properties, including interfacial property, permit these materials to be used for Lab-on-a-Chip and micro total analysis system applications.

In Chapter 2 the chemical grafting of a variety of 4,6-dichloro-s-triazinyl derivatives onto cellulose fibres and cellulose nanocrystals led to large changes in wettability of modified cellulosic materials. Instead of having colloidal suspension in water alone, the presence of octadecyl, mono-allyl-PEG, benzyl and propargyl functionalities at the surface of CNCs led to colloidal suspensions that were stable both in polar and non-polar organic solvents through both electrostatic and steric interactions. These stabilities showed a correlation between the polarity of solvent and polarity of grafted surface functionality. The degree of substitution was shown to be directly dependent on the size and chain length of derivatizing molecule; molecules with larger sizes and chain lengths (octadecyl and mono-allyl-PEG) gave lower degree of substitution compared to benzyl and propargyl. The morphologies of modified CNCs were found to be unaffected by the modification (compared to unmodified), as modification occurred only at the CNC surface while the bulk crystalline core remained unmodified. As a consequence, all triazinyl-modified materials showed enhancement in thermal stability, indicative that the sulfate half-ester groups on the backbone of the crystalline cellulose were further protected by the modification. Overall, the reactive nature

of propargyl-modified cellulose was demonstrated by the successful grafting of an azido-fluorescein dye via copper-catalysed Huisgen 1,3-dipolar cycloaddition reaction onto cellulose. The triazinyl chemistry described in this chapter thus presents a low cost and versatile route for tuning the interfacial properties of nanocellulose, with the possibility of post-modification for applications that require the conjugation of molecules onto cellulose through bio-orthogonal chemistries.

In Chapter 3, based on the efficient nature of the triazinyl-cellulose interactions examined in Chapter 2, further investigation into the installation of hydrophilic rhodamine chemosensors onto cellulose for heavy metal sensing was exploited. Although quite difficult, this was accomplished using cyanuric chloride to generate a triazine-PEG-vanillin compound, which was grafted onto cellulose. The aromatic aldehyde-functionalized cellulose was then treated as a platform to graft both rhodamine 6G hydrazide and thioxorhodamine 6G hydrazide to give their cellulose-PEG-rhodamine Schiff base counterparts. In an attempt to understand the sensitivity and selectivity of these compounds, they were tested against different metal ions in water. The colorimetric and fluorescent assay of these chemosensors were observed. Initially, the hydrophilic nature of the chemosensor as a result of the attachment of PEG spacer molecule onto the Schiff base framework in water was assessed. Data for the pregrafted PEGylated vanillin-rhodamine Schiff base showed complete dissolution in water (without the aid of any organic solvent unlike its non-PEGylated analog) with sensitivity and selectivity towards  $\text{Cu}^{2+}$  ions amongst a host of other metal ions. This suggests the  $\text{Cu}^{2+}$  ions may be able to induce a ring opening reaction of the spiro lactam rhodamine ring upon metal ion complexation reactions. Similar effects in term of wettability, selectivity and sensitivity were observed for all cellulose immobilized chemosensors with a switch in selectivity towards  $\text{Hg}^{2+}$  ions once the carbonyl in rhodamine was changed to thiocarbonyl. That is, the grafting of chemical receptors was required before significant changes in the physical and optical properties of cellulose could occur; changes in color from colorless to pink with enhancement in fluorescent emission was established on exposure to  $\text{Cu}^{2+}$  and  $\text{Hg}^{2+}$  ions. Thus, the use of triazinyl chemistry to install hydrophilic chemical probes onto cellulose creates a unique paper-based lab-on-a-molecule system, which may have use in many applications, including heavy metal sensing and sequestering for biomedical and

Ayodele Fatona – Ph.D. Thesis McMaster University – Chemistry and Chemical Biology  
environmental diagnostics.

The reactivity of cyanuric chloride towards other nucleophiles or functional polymer system was also examined. Chapter 4 capitalizes on the covalent interactions between amines and cyanuric chloride. By controlling the stoichiometry of reaction between reactive amines, the type of crosslinker and the structure/number of residual amines, a variety of silicone elastomers can be synthesized. Taking advantage of the aromatic nucleophilic substitution reaction between commercially available aminopropylsilicones and cyanuric chloride/triazines allows for tuning the synthesis of silicone elastomers and their properties. Telechelic or pendant aminopropyl silicone with cyanuric chloride or pre-functionalize triazinyl-aminosilicone made silicone elastomers with crosslink densities varying from 2 to 7% aminopropyl content. The Young's modulus and Shore hardness were found to track linearly as the crosslink density was increased. The properties associated with elastomers prepared using the triazinyl chemistry are similar to elastomers prepared with traditional cure technologies, however, the main benefit to using this system is in the fact that it is catalyst and solvent free as the case may. Hence the process offers a variety of advantages including low cost, ease of preparation, control of crosslink density, as well as the presence of residual amines within the elastomer that can be repurposed for further reactions such as  $S_N2$ , Michael addition or ring opening chemistries.

Following in the direction of silicone crosslinking technologies, Chapter 5, examines the use of a new cure system for functional silicones using the thioacetalization reaction to create novel silicone elastomer with unique properties. Here, readily available thiopropyl silicones were reacted with series of aromatic aldehydes in the presence of catalytic amounts of acids to yield thioacetal-crosslinked silicone elastomers. Early on, a combination of Brønsted and Lewis acids was demonstrated to be efficient in catalysing the thioacetalization reaction in silicones with toluenesulfonic acid found to be milder, easy to handle and best behaved Brønsted acid of those tested. The fact that the byproduct (water) is immiscible and easily phase separates and then evaporates, as well as the ability to modify the structure of the crosslinker, allows one to tune the synthesis of silicone elastomers and their resulting properties. Reactions of pendant thiopropylsilicone with benzaldehyde, fluorene-aldehyde and terephthalaldehyde permitted the synthesis of

silicone elastomers with crosslink densities varying from 4 to 13% thiopropyl content. The Young's modulus and Shore hardness were found to increase as the crosslink density was increased. The moduli of elastomers prepared using the thioacetal chemistry were surprisingly high, as a consequence of physical interactions between aromatic moieties along the crosslinked silicone chains; the moduli are much higher than analogous elastomer prepared by platinum-cured hydrosilylation. The moduli could be controlled simply by changing the structure of the crosslinker; a six-fold increase in mechanical properties was observed going from benzaldehyde to terephthalaldehyde. Even more interesting, the thioacetal groups in the prepared elastomers were very stable to both hydrolytic and oxidation stress in the presence of residual acid catalyst.

Lastly, Chapter 6 examined the interfacial properties of silicones when thin films of surfactants were attached at the silicone-air interface. It was discovered that the design of a new in-mould modification method for the chemical modification of PDMS surface allowed one to assess relationships between the structural effects of different surfactants and their ability to render PDMS surfaces hydrophilic. Thin films of ionic and non-ionic surfactants were patterned into an array format, transferred onto silicone pre-polymer, and subsequently immobilized at the PDMS surface during vulcanization. The wettability was observed to be dependent on the chemical structure of the surfactants, their concentration and interactions with PDMS. The morphology of modified PDMS surfaces and their changes after wetting and drying cycles were visualized using atomic force microscopy. It was determined that, while all surfactants tested can render PDMS surfaces hydrophilic through the in-mould modification, only those modified with PEG-PDMS-PEG copolymer surfactants were stable over wetting/drying cycles and heat treatments. Surfaces functionalized with PEG-PDMS-PEG block copolymers displayed morphologies that are consistent with polymer entrapment and polymer chain rearrangement upon hydration. Finally, the in-mould functionalization approach was used to fabricate self-driven microfluidic devices that exhibited steady flow rates, which could be tuned by the device geometry. It is anticipated that the in-mould method can be applied to a range of surface modifications for applications in analytical separations, biosensing, cell isolation and small molecule discovery.

In conclusion, the body of work presented in this thesis accomplishes its intended goal; to demonstrate the ability to tune the interfacial and physical properties of cellulose and silicones using a variety of approaches and represents a foundation of knowledge towards polymer property optimization. While the work began with the use of triazinyl chemistry as a versatile route to the surface modification of cellulosic materials, creating functional and reactive cellulosic materials processible in a wide range of solvents and applications such as heavy metal sensing, it was subsequently shown also to have potent activity in the crosslinking of amino-functional silicones.

With respect to silicones, it was possible to manipulate the physical properties of silicone elastomers under catalyst free conditions. We demonstrated that small changes in the amine-triazine reaction, in the presence of residual amines, can completely change how polymer chains will covalently interact with one another. This allows one to form elastomers with tunable properties. We further demonstrated that using physical interactions between aromatic moieties through thioacetal linkages, as well as covalent crosslinks, provided an ancillary mode for polymer manipulation. Expanding our understanding of the bulk polymers was then extended to interfaces, including the creation of surface-confined interpenetrating polymer network with a fraction of hydrophilic polymers, which led to self-driven silicone microfluidic devices.

Future work will continue to build on the developed techniques for surface modification of nanocellulose material using triazinyl chemistry, by creating a library of nanocelluloses grafted with a variety of Bis-triazinyl-linked surface functionalities particularly PEG-acrylates/PEG-biotin, PEG-furfuryl/PEG-maleimide and Azido-PEG/Alkyne-PEG systems that can be used either as standalone components or as building blocks for secondary modifications via bioorthogonal chemistries. The incorporation of these reactive functionalities onto nanocellulose will allow post modification utilization of modified nanocellulose in creating cross-linkable nanocellulose structures with tunable mechanical properties and surface functionalities. These could find application in the development of printable materials, hierarchical scaffolds or hydrogels for tissue engineering, cell or drug encapsulation. We anticipate ongoing work will open new application areas in printable electronics, bioremediation, biomedical and packaging materials.